Toegepaste arteriële mechanica: van theorie tot klinische praktijk

Applied Arterial Mechanics: from Theory to Clinical Practice

Sebastian Vermeersch

Promotoren: prof. dr. ir. P. Segers, prof. dr. ir. P. Verdonck, prof. dr. P. Boutouyrie
Proefschrift ingediend tot het behalen van de graad van
Doctor in de Ingenieurswetenschappen: Biomedische Ingenieurstechnieken

Vakgroep Civiele Techniek
Voorzitter: prof. dr. ir. J. De Rouck
Faculteit Ingenieurswetenschappen
Academiejaar 2008 - 2009

UNIVERSITEIT
GENT

ISBN 978-90-8578-291-9
NUR 954, 870
Wettelijk depot: D/2009/10.500/49

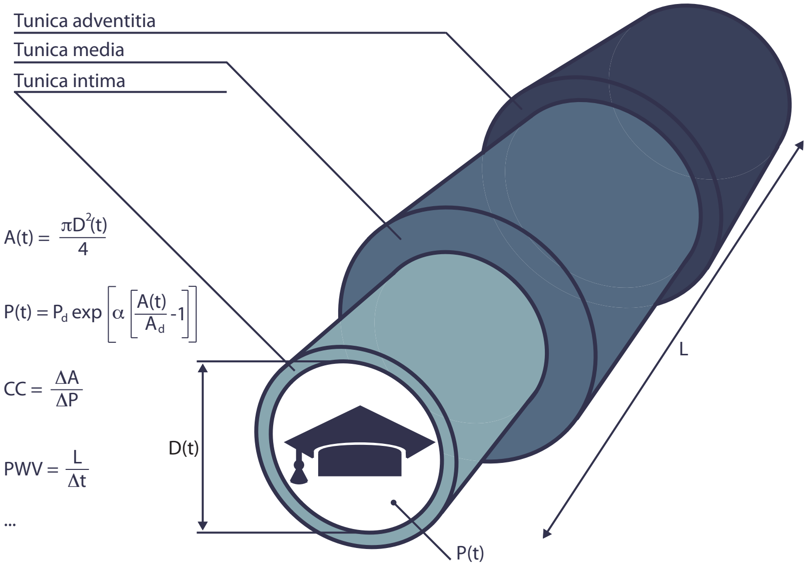
Tunica adventitia
Tunica media
Tunica intima
D(t)
P(t)
L

$$A(t) = \frac{\pi D^2(t)}{4}$$

$$P(t) = P_d \exp\left[\alpha\left[\frac{A(t)}{A_d} - 1\right]\right]$$

$$CC = \frac{\Delta A}{\Delta P}$$

$$PWV = \frac{L}{\Delta t}$$

...

Supervisors:

Prof.dr.ir. Patrick Segers
Prof.dr.ir. Pascal Verdonck
Prof.dr. Pierre Boutouyrie

Research lab:

Institute Biomedical Technology
Biofluid, Tissue and Solid Mechanics for Medical Applications
Ghent University
De Pintelaan 185 - Blok B
B–9000 Gent
BELGIUM

Members of the exam committee:

Chairman:	
Prof.dr.ir. Ronny Verhoeven	Faculty of Engineering, UGent
Secretary:	
Prof.dr. Stefaan Vandenberghe	Faculty of Engineering, UGent
Reading committee:	
Prof.dr.ir. Alberto Avolio	Australian School of Advanced Medicine, Sydney, Australia
Prof.dr.ir. Naomi Chesler	University of Wisconsin at Madison, USA
Dr.ir. Tom Claessens	Hogeschool Gent, Belgium
Prof.dr. Stefaan Vandenberghe	Faculty of Engineering, UGent
Prof.dr.ir. Patrick Segers	Faculty of Engineering, UGent
Other members:	
Prof.dr. Pierre Boutouyrie	Université Paris Descartes, France
Dr.ir. Sandrine Millasseau	AtCor Medical
Prof.dr. Luc Van Bortel	Faculty of Medicine, UGent
Prof.dr.ir. Pascal Verdonck	Faculty of Engineering, UGent

This research was funded by F.W.O. (Fonds voor Wetenschappelijk Onderzoek) research grants G.0055.05 and G.02427.03 (Asklepios study)

To Lieve, and the unborn promise she carries

Preface

THE STUFF YOU WRITE AT THE END TO PUT IN THE BEGINNING

Six years ago, almost to the date, I was writing the introduction to my Master Thesis. It was, like many of my written projects before and since, a last-minute job, having spent a frantic week desperately trying to finish a year's work by writing a somewhat coherent text before an ever closing deadline looming at the horizon. Time was a precious commodity, I was tired and fed up with it, but still, I remember taking the time to write that introduction, a small piece of text likely read by practically no-one, with no particular academic merit but vast personal meaning. Because I was on the exit.

Over the course of one's life, few people have a truly lasting influence. The head teacher of my first year in secondary school was one of them. His name was Luc Desseyn and next to French, history and religion, he taught Life Lessons. Twelve year olds have especially malleable minds, being at a crossroads between starting to let go of the influence of their parents and looking for the influence of new role models to cling to, and I was no exception. There are many things I will remember vividly for the rest of my life from what he taught me, but the Life Lesson that stuck most was his comparison of life to a highway. Life, he said, was a highway, and we were the cars going down it. Most of our lives would be spent trying to go as fast as possible on the third lane, overtaking whoever and whenever we could, trying to get to wherever we were going. That's fine, he said, and it is why you should learn as much as you can, to be better equipped for this everlasting race. But equally important is to remember to go down an exit once in a while, to take time to look at the distance travelled and figure out if you still know where you are going and how you are going to get there. I was only twelve, going on thirteen but I still knew what he said was a True Thing.

That is why six years ago, I spent so much time on the introduction to my Master Thesis. Because it was a moment to take the exit and look back at what I had done. I was a young, cocky student, set to graduate as a Computer Science Engineer (which by then I had figured out was not a real engineering degree, but still the most interesting one) and looking for direction. I was arrogant (because that's one of the things they teach you how to be in that engineering building) and I had no idea what I was going to do with my life. I had taken the highway exit, and was feeling particularly nostalgic about the five years I had spent at the Engineering Faculty, looking forward to where I would be going next.

So here I am, six years later, and in a way, much has remained the same. I'm still young and probably even a little more arrogant (though nowadays I like calling it self-assured). I'm again very much fed up with this whole writing a thesis business, and a nice lady from the rectorate has just reminded me the deadline for submitting a pdf copy for my first print proof is exactly one hour and eighteen minutes away. I'm on the exit of the highway again, looking back, and feeling particularly nostalgic.

Over the course of the past six years, it has been my honor and privilege to work with a number of exceptional men and women. The first I heard of Pascal Verdonck was back at the end of my second year at university, when all of the Engineering options try to lure as many students as possible by organizing information afternoons. Pascal had been drafted to convince us young folk of the value of being a true Civil Engineer. He did this by telling us that it really didn't matter what engineering specialty we chose, we were all supposed to be able to do everything anyway. He said civil engineers were by far the most up to the task however, because they were the most flexible. He then talked a little about his own career, explaining how all of his career choices had seemed to occur by happenstance: he never thought he would do a PhD, but somehow got lured into it, never assumed he would then pursue an academic career, favoring a business degree, but still was now head of a lab. Despite a lifelong affinity with everything computer, to this day, his speech that day makes me doubt if I did the right thing choosing Computer Science and not Civil Engineering. This taught me that Pascal Verdonck is a Damn Good Salesman. He is also more than likely an excellent chess-player and a visionary. The last of course, being exemplified by hiring me.

If Pascal was the visionary hiring me, Patrick Segers is the unlucky fellow who actually had to manage me on a day to day basis. Back when

I started, Patrick was still a post-doc, his promotion to professor imminent and research was (and to some degree still is), his life. He now is the head of our lab, managing over twenty people and if I had as much research feeling as his little toe, I'd be a very happy man. Patrick is one of those rare exceptional people that despite rising swiftly through the ranks, still feels like he's just one of the guys who you can go grab a beer with after work and just talk to. I think he is an outstanding people manager with a rarely seen openness to criticism and differing points of view. I have the utmost respect for him, and I would not have been here if it wasn't for his guidance. Being a PhD student sometimes sucks bigtime, and it helps if you can just walk into the office of your boss and tell him that, basically implying everything he works for is rubbish. I will remember these open conversations and value the opportunity of having had them.

Even twenty-three year olds, much like their twelve year old counterparts, need role-models. When I started in the lab, Fadi Glor was mine. Introductions like these are of course places of hyperbole, but in my mind, he is a legend. If Pascal is a Good Salesman, Fadi is an Excellent One. His laid back attitude to work made my first year feel like I was getting paid to still live the life of a student. He's the guy who taught me to how to cantus by evening (I never would have dreamt it possible to do all of them the year after I graduated), and check the journal impact factor of a newly accepted article by night. Most importantly, I think his sharp, witty sense of humor somehow rubbed off on me.

I should mention all of the colleagues I worked with, since of course, they are what makes the lab tick (I've always liked the people I worked with in the lab even better than the work I did). I would like to mention in particular Tom Claessens, the only guy who managed to stick around as long as I have, Kris Dumont, who showed me that the lab also meant actually getting work done, Ilse Van Tricht, who illustrated beautifully that sometimes you have to stick to your guns if you want to get things done the right way and Sunny Eloot, who I always valued as a sounding board – not of work but of PhD-life in general, by far the more salient topic. Guy Mareels and Lieve Lanoye both started with me at the same time I did, and them I would like to thank in particular for finishing at least two years sooner than I have and showing me just how much slower I really am. (Lieve gets a special mention a little further down this introduction). A big thumbs up to my all my current colleagues, especially Thomas De Schryver, Bram Trachet, Jan Kips and

Koen Van Canneyt for being there. You guys still have a long way to go. Not all of it's fun :) (Ooh, that actually felt a little good, I must be ready for getting my degree). Special mention to my French connection: Ingrid Masson for putting up with me and my two screens, Cédric Collin for teaching me the meaning of French coffee breaks, Céline Fassot for being a sounding board abroad, Thanh for guiding us through foreign cities, and my two supervisors in Paris, Stéphane Laurent and Pierre Boutouyrie.

If I were a wood sculpture, I would be responsible myself for my finishing touches. But my true beauty, the wood I'm made of and its grain, I can take no credit for. I am the man I am today thanks to the never faltering support of my parents. Nadine and Marnix, mom and dad, you have instilled me with all that people love about me. For that, I am infinitely grateful. It is no doubt difficult to let go of something you nurtured so dearly for so long and give it the freedom to find its own way and for that, I thank you too. I hope to make you proud. Thank you to my brother, Joachim. You have always been there for me. This, I will not forget.

Lieve, you are my soulmate. I consider myself immeasurably fortunate to be able to spend my life with not just a drop-dead gorgeous woman, but a kindred spirit. You accept me just the way I am (well, almost anyway ;)) and with you, I never face any challenge alone. I love you more than words can say, and feel connected in a way I never thought possible. Thank you. I'm looking forward to sharing the life you carry with you (Hi Juniorette!!! – you're daddy's girl!) and much more :)

My PhD has taken me on a ride never to forget. I've worked in Paris, presented in Yaoundé, I've exchanged ideas with some of the greatest minds on the planet, I've learned and had the freedom to explore my own way of doing things and gotten better for it. These are all topics you will not find in the rest of this book, but perhaps they are what truly marks the main achievement of my work. How does one measure success? Standing here, on the exit of my highway, I can see my car may very well have gotten faster by what I gained in knowledge and experience. But the true reasons why I feel happy today are not these cosmetic changes. They are the heaps of other cars standing by me, supporting me and giving me a reason to go on. They are the old friends that have raced with me and the new ones that have joined me on the way.

Time to get back on that highway and find out what's behind the horizon.

Sebastian Vermeersch
Gent, 28 May 2009

Samenvatting
Summary

Samenvatting

INLEIDING

De inhoud van dit manuscript vat vijf jaar onderzoek samen, uitgevoerd aan twee universiteiten, met als rode draad het toepassen van 'theoretische' arteriële mechanica concepten op klinische data. De tekst bestaat uit 5 onderdelen.

Het eerste onderdeel bevat achtergrondinformatie relevant voor de onderwerpen die later in het boek aan bod komen. Dit deel bestaat uit een enkel hoofdstuk waarin een korte samenvatting gegeven wordt van een aantal basisconcepten in de anatomie en fysiologie van het cardiovasculair systeem die van essentieel belang zijn om de werkwijze en resultaten van de verschillende studies uitgevoerd in de loop van het voorgestelde onderzoek te begrijpen. De middelste drie delen zijn een neerslag van alle originele onderzoek dat in de loop van het doctoraatsonderzoek werd uitgevoerd. De inhoud van deze drie onderdelen wordt hieronder in meer detail voorgesteld. Het laatste hoofdstuk, tenslotte, vat alle conclusies gemaakt in de verschillende deelonderzoeken nogmaals samen en vormt de algemene conclusie van het werk voorgesteld in dit manuscript.

De opbouw van dit werk, waarin elk hoofdstuk een op zichzelf staande studie voorstelt die in vele gevallen in een vorm worden voorgesteld die nauw aansluit bij de vorm van een wetenschappelijk artikel, maakt het soms moeilijk om de samenhang van het werk correct in te schatten. Niettegenstaande het feit dat dit werk niet tot doel heeft om op een enkele specifieke onderzoeksvraag een antwoord te bieden, is er toch een duidelijke rode draad aanwezig, waarbij geprobeerd wordt door het beantwoorden van een aantal gerichte onderzoeksvragen de kennis rond en toepasbaarheid van arteriële mechanica in de klinische praktijk te vergroten. Deze rode draad wordt geïllustreerd in figuur 1, die u best in het achterhoofd kunt houden bij het lezen van de rest van deze samenvatting.

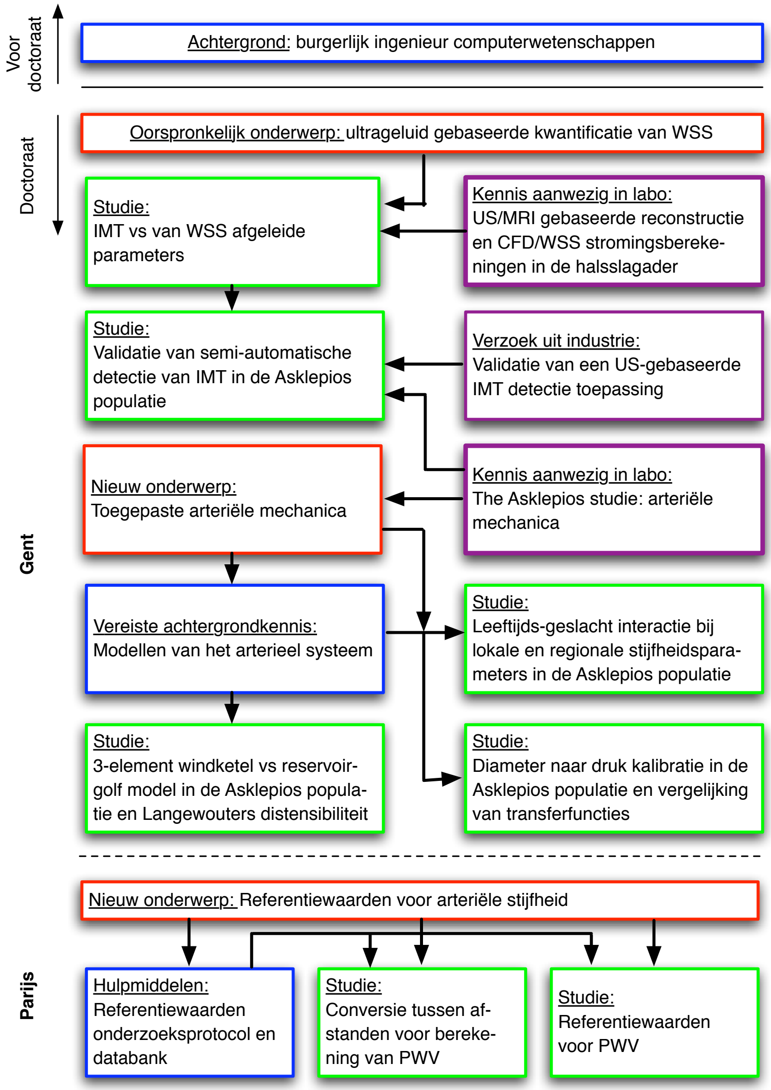
Voor doctoraat
Achtergrond: burgerlijk ingenieur computerwetenschappen
Doctoraat
Oorspronkelijk onderwerp: ultrageluid gebaseerde kwantificatie van WSS
Studie: IMT vs van WSS afgeleide parameters
Kennis aanwezig in labo: US/MRI gebaseerde reconstructie en CFD/WSS stromingsberekeningen in de halsslagader
Studie: Validatie van semi-automatische detectie van IMT in de Asklepios populatie
Verzoek uit industrie: Validatie van een US-gebaseerde IMT detectie toepassing
Gent
Nieuw onderwerp: Toegepaste arteriële mechanica
Kennis aanwezig in labo: The Asklepios studie: arteriële mechanica
Vereiste achtergrondkennis: Modellen van het arterieel systeem
Studie: Leeftijds-geslacht interactie bij lokale en regionale stijfheidsparameters in de Asklepios populatie
Studie: 3-element windketel vs reservoir-golf model in de Asklepios populatie en Langewouters distensibiliteit
Studie: Diameter naar druk kalibratie in de Asklepios populatie en vergelijking van transferfuncties
Parijs
Nieuw onderwerp: Referentiewaarden voor arteriële stijfheid
Hulpmiddelen: Referentiewaarden onderzoeksprotocol en databank
Studie: Conversie tussen afstanden voor berekening van PWV
Studie: Referentiewaarden voor PWV

FIGURE 1: Stroomdiagram van de verschillende studies uitgevoerd tijdens mijn onderzoek.

INTIMA MEDIA DIKTE

Het eerste onderdeel van dit manuscript gaat dieper in op twee studies die uitgevoerd werden in de beginfase van mijn doctoraatsonderzoek. Deze studies behandelen meetmethodes voor het bepalen van de intima-media dikte (IMT) in de halsslagader (carotis) en onderzoeken mogelijke verbanden tussen deze gemeten IMT waarden en aan wandschuifspanning gerelateerde parameters berekend aan de hand van numerieke stromingssimulaties.

Eerder onderzoek heeft aangetoond dat een verhoogde dikte van de intima-media laag gelinkt kan worden aan een verhoogd risico op overlijden aan een beroerte of hartinfarct. In de Europese richtlijnen voor het behandelen van hypertensie opgesteld door het Europese Hypertensie en het Europese Cardiologie Comité, wordt een drempelwaarde van 0,9 mm vooropgesteld, waarboven een verhoogde IMT een aanwijzing is van subklinische orgaanschade. De IMT van de carotis is een parameter die routinematig wordt gemeten in de klinische praktijk en wordt vaak mee opgenomen als parameter in klinisch onderzoek.

Een verdikking van de IMT is een van de eerste tekenen van het optreden van atherosclerose. Hoewel atherosclerose in principe kan voorkomen in elk bloedvat, zijn bepaalde locaties in het vaatstelsel gevoeliger dan andere voor het optreden van deze aandoening. Deze voorkeurslocaties zijn typisch gesitueerd in de buurt van vertakkingen of in bloedvaten die een uitgesproken curvatuur vertonen. Kenmerkend voor deze locaties is het optreden van complexe stromingspatronen die gelinkt zijn aan het voorkomen van specifieke patronen van wandschuifspanningen. Verschillende studies hebben gesuggereerd dat deze specifieke wandschuifspanningspatronen—in het bijzonder het voorkomen van lage wandschuifspanningen of afschuifsnelheden, sterke oscillaties in wandschuifspanningen en wandschuifspanningshoekgradiënten—gelinkt zijn aan de mechanismen die aan de basis liggen van het verdikken van de intima-media laag.

Hoofdstuk 3 beschrijft de resultaten van een pilootstudie waarin bestaande wandschuifspanningswaarden, eerder bepaald met numerieke stromingssimulaties (CFD), in een kleine populatie gelinkt pogen te worden aan IMT metingen op basis van zwart bloed (black blood, BB) magnetische resonantie beeldvorming (MRI). Onze onderzoeksgroep heeft een ruime ervaring in patiënt-specifieke reconstructie van de halsslagader vertakking voor het berekenen van stroming en wandschuifspanning gerelateerde parameters op basis van numerieke stromingssimulaties. In vorige studies uitgevoerd door Glor *et al.* werden de nauwkeurigheid en reproduceerbaarheid van deze reconstructie techniek aangetoond. Voor verschillende proefpersonen waren binnen de onderzoeksgroep zowel de gereconstrueerde geometrie, de berekende stroming en wandschuifspanning parameters als de originele beelden op basis waarvan de geometrie was gereconstrueerd ter beschikking. Het pilootproject omvatte drie onderdelen: (1) het creëren van een software tool om het manueel aflijnen van de IMT op BB MRI beelden mogelijk te maken; (2) een intra- en inter-observer variabiliteitsstudie uitvoeren op de nieuw voorgestelde techniek voor IMT aflijning; en (3) de gemeten IMT waarden koppelen aan de eerder bepaalde wandschuifspanning (WSS) gerelateerde parameters om te onderzoeken of in deze populatie een verband tussen beide kon vastgesteld worden. Het hoofddoel van de studie was het nagaan of de BB MRI beelden een voldoende hoge resolutie hadden om op betrouwbare en reproduceerbare manier IMT vast te stellen en na te gaan of een verband tussen IMT en de WSS gerelateerde parameters gevonden kon worden.

De studie toonde aan dat de specifiek ontwikkelde omgeving voor het manueel aflijnen van de IMT op BB MRI beelden IMT metingen gaf met goede inter- en intra-observer variabiliteit. Desalniettemin was de beeldkwaliteit van de BB MRI beelden nauwelijks goed genoeg om betrouwbare IMT metingen op uit te voeren. BB MRI beelden geven niet dezelfde beeldresolutie als ultrageluid beelden, en zijn bovendien minder toegankelijk. Ondanks deze beperkingen werd in de studie populatie toch een zwakke correlatie gevonden tussen gemeten IMT waarden en berekende wandschuifspanningsparameters. Het verband tussen deze wandschuifspanningsparameters en de IMT waarden was sterker in de carotis communis dan in de carotis interna voor alle wandschuifspanning gerelateerde parameters. Daarnaast waren de gemeten IMT waarden sterk gecorreleerd aan de plaats waar ze gemeten werden: de correlatie tussen IMT en de afstand tot de bifurcatie was groter dan voor om het even welke wandschuifspanningsparameter. Het toevoegen van deze parameters aan een model waarin de afstand tot de bifurcatie was opgenomen verhoogde de performantie van het model niet of nauwelijks.

Hoofdstuk 4 beschrijft de resultaten van een validatiestudie waarin een nieuw softwarepakket voor het semi-automatisch bepalen van de IMT van de halsslagader op basis van ultrageluid beelden werd vergeleken met manueel gemeten IMT op dezelfde beelden. Binnen het Asklepios studie protocol had 1 operator in een populatie van meer dan

2 500 mensen manueel de IMT gemeten in de halsslagader. Gezien de beschikbaarheid van deze uitgebreide en betrouwbare dataset, werd een onderzoeksproject voorgesteld waarin een nieuw softwarepakket, dat ter beschikking gesteld werd door GE Healthcare Ultrasound, gevalideerd werd op de beschikbare data. Het project omvatte drie onderdelen (1) het opnieuw uitvoeren van de manuele metingen op een deel van de Asklepios populatie om de inter-observer variabiliteit van de manuele meetmethode vast te stellen; (2) de geautomatiseerde metingen uitvoeren op dezelfde dataset; en (3) inter- en intra-observer variabiliteit en verschil in absolute waarde van IMT metingen uitgevoerd met de manuele en semi-automatische methodes vergelijken.

Modellen van het arterieel systeem

Het tweede deel van dit manuscript is gewijd aan modellering van het arterieel systeem. Zoals duidelijk wordt na de wiskundige achtergrond die aan de oppervlakte komt bij het bestuderen van de fysiologie van het cardiovasculair systeem in hoofdstuk 1, voldoen druk en stroming in het arterieel systeem, net zoals in elk netwerk van buizen, aan een aantal basiswetten die gebruikt kunnen worden om inzicht te krijgen in de werking van het arterieel systeem.

Modellen van het arterieel systeem zijn het werkstuk bij uitstek van de theoreticus om de verbanden tussen verschillende eigenschappen van de bloedvaten bloot te leggen. Modellen, gaande van zeer eenvoudige tot uitermate complexe versies, bieden de mogelijkheid om beter inzicht te krijgen in de oorzaken van een bepaald geobserveerd gedrag. Ze bieden de mogelijkheid om te voorspellen wat zal gebeuren als de werkingsparameters van het systeem door een ingreep veranderd worden. Daarnaast bieden modellen ook de practicus een duidelijke meerwaarde. Zonder een grondige kennis van de manier waarop verschillende arteriële eigenschappen interageren en de manier waarop die eigenschappen de vorm van de druk- en stroomgolfvormen in de arteriën bepalen, kan een behandeling slechts gebaseerd zijn op een 'trial-and-error' aanpak waarbij zonder overleg ingrepen gebeuren in de hoop een bepaald effect te verkrijgen.

In hoofdstuk 6 worden de belangrijkste manieren om het arterieel systeem te modelleren voorgesteld. De twee basis aanpakken—de voorstelling van het arterieel systeem als een gecondenseerd (windketel) model en als golfsysteem—worden toegelicht, deze laatste zowel in het tijds- als het frequentiedomein. Het doel van dit hoofdstuk is de lezer vertrouwd maken met een aantal belangrijke concepten die noodzakelijk zullen zijn voor het kwantificeren van arteriële stijfheid in deel 4 van dit manuscript.

Gecodenseerde windketel modellen en golfmodellen stellen twee op het eerste zicht tegenstrijdige, maar in werkelijkheid elkaar aanvullende, manieren voor om het arterieel systeem conceptueel voor te stellen. Beiden hebben hun sterktes en zwaktes en geen van beide is consistent beter dan de andere voor alle mogelijke toepassingen. Recentelijk hebben een aantal onderzoeksgroepen pogingen ondernomen om deze twee tegentrijdig lijkende concepten samen te voegen in een nieuwe modelaanpak. In deze 'hybride' modellen wordt de drukgolfvorm opgesplitst in een 'reservoir'-druk en een golfcomponent. Deze aanpak lijkt qua concept sterk op het reeds bestaande drie-element windketel model, dat ook een onderdeel toevoegt dat binnen het gecondenseerd model golf-aspecten in rekening brengt.

In *hoofdstuk 7* worden deze gelijkenissen onderzocht door zowel het reservoir-golf model als het drie-element windketel model toe te passen op data afkomstig van de Asklepios populatie. Het hoofddoel van deze studie was om (1) de toepasbaarheid van het nieuwe reservoir-golf model te testen op de Asklepios data; (2) reservoir drukken berekend aan de hand van het reservoir-golfmodel en het drie-element windketel model met elkaar te vergelijken om te zien in hoeverre ze overeenstemmen; en (3) de evolutie van de reservoir pulsdruk berekend met het reservoir-golfmodel en drie-element windketel model met stijgende leeftijd voor mannen en vrouwen te onderzoeken in de Asklepios populatie.

In dit hoofdstuk tonen we aan dat het recent voorgestelde reservoir-golf concept grote overeenkomsten vertoont met het klassieke drie-element windketel model, met name in personen waarvan het arterieel systeem een hoge reflectiecoëfficiënt vertoont en een hoog 'windketelgehalte' heeft. Hoe sterker het arterieel systeem gekenmerkt wordt door golfreflecties, en dus hoe beter het systeem lijkt op een echte windketel, hoe beter het reservoir-golf concept met de werkelijkheid overeenkomt. Het lijkt dus dat, eerder dan dat het reservoir-golf concept elementen van het klassieke windketelmodel en het golfmodel overbrugt, het reservoir-golfconcept niet meer is dan een tijdsdomein voorstelling van het drie element windketel concept. Ondanks deze sterke gelijkenissen blijven er kleine kwantitatieve verschillen in de reservoir drukken berekend met het drie-element windketel model en het reservoir-golf model. Beide modellen tonen daarentegen aan dat in de Asklepios populatie de toename van pulsdruk met de leeftijd voornamelijk verklaard kan worden door een stijging van de reservoir druk, en niet louter door verhoogde golfreflecties.

ARTERIËLE STIJFHEID

Dit onderdeel bevat het grootste deel van het werk uitgevoerd binnen het kader van mijn doctoraatsonderzoek. Alle hoofdstukken van dit deel hebben op de een of andere manier te maken met verschillende maatstaven voor arteriële stijfheid en de manieren waarop deze kunnen worden bepaald.

De stijfheid van de (grote) slagaders is een uiterst belangrijke parameter die in grote mate de werking van het cardiovasculair systeem mee bepaalt. Verschillende studies uitgevoerd in verschillende populaties hebben aangetoond dat arteriële stijfheid een voorspellend karakter heeft voor klinische aandoeningen. Verhoogde arteriële stijfheid heeft een onafhankelijk voorspellende waarde voor mortaliteit, zowel ten gevolge van cardiovasculaire als andere aandoeningen. Parameters voor de kwantificatie van arteriële stijfheid worden dan ook meer en meer gebruikt binnen de klinische praktijk en worden sinds lang opgenomen in het kader van klinisch onderzoek.

Gezien de heterogeniteit van het arterieel systeem, dat zowel zeer kleine als zeer grote bloedvaten bevat met sterk verschillende eigenschappen, is het niet verwonderlijk dat arteriële stijfheid gekwantificeerd kan worden aan de hand van een groot aantal verschillende parameters. Vele stijfheidsparameters zijn daarbij gelinkt aan een bepaalde modelleringsaanpak van het arterieel netwerk; deze modellen werden vroeger besproken in hoofdstuk 6.

Hoofdstuk 9 geeft een overzicht van de meest voorkomende parameters voor het kwantificeren van arteriële stijfheid. Deze omvatten zowel systemische, regionale en lokale parameters en parameters gebaseerd op het kwantificeren van golfreflecties. Verschillende parameters die in dit hoofdstuk besproken worden vereisen de kennis van de centrale bloeddruk, dit is de bloeddruk ter hoogte van de aorta. Aangezien deze bloeddruk enkel invasief verkregen kan worden, door het inbrengen van een katheter, bestaan verschillende alternatieve aanpakken om deze centrale bloeddrukken te benaderen. Er bestaan twee soorten aanpakken: ofwel worden drukken lokaal gemeten ter hoogte van de halsslager aan de hand van tonometrie, ofwel worden drukken gemeten op een referentielokatie—meestal ter hoogte van de radialis—die vervolgens wiskundig getransformeerd worden tot centrale drukken.

Beide aanpakken hebben voor- en nadelen. Carotis drukgolven komen goed overeen met invasief centraal gemeten bloeddrukken, maar carotis tonometrie is soms moeilijk uit te voeren bij bejaarden of obesen. Er is ook de bezorgdheid dat door het drukken op de arterie bij mensen met uitgesproken plaque vorming, deze plaque kan scheuren en een thrombus kan gevormd worden. Transfer functies anderzijds, werden bepaald op een specifieke populatie en zijn dus niet patient-specifiek.

Hoofdstuk 10 bespreekt nog een tweede probleem met het gebruik van transfer functies. In het verleden werden verschillende transfer functies voorgesteld, bepaald in verschillende populaties. In vele gevallen is het type transfer functie dat gebruikt wordt gebonden aan het toestel dat aangewend wordt om de centrale bloeddrukken en hemodynamische parameters te bepalen, en de impact van het gebruik van een andere transfer functie is niet altijd duidelijk. Deze studie had als doel om te onderzoeken of twee gekende transfer functies inwisselbaar zijn voor het berekenen van centrale systole bloeddruk en augmentatie index (AIx) in een deel van de Asklepios populatie.

De resultaten van deze studie toonden aan dat centrale systole bloeddruk en augmentatie index verschillen naargelang de transfer functie die gebruikt werd om de perifere drukken om te rekenen tot centrale drukken. Resultaten bekomen door toepassing van verschillende transfer functies zijn dan ook niet inwisselbaar: parameters afgeleid van centrale drukken zijn afhankelijk van de eigenschappen van de transfer functie die gebruikt werd om ze te berekenen, met name voor het berekenen van de augmentatie index.

Hoofdstuk 11 onderzoekt een mogelijk alternatief voor het gebruik van carotis tonometrie voor het bepalen van lokale carotis drukken. Deze studie had als doel te onderzoeken of drukken ook afgeleid konden worden van geschaalde diametermetingen verkregen aan de hand van ultrageluidmetingen ter hoogte van de carotis. Afhankelijk van het gebruikte model voor het verband tussen druk en diameter van een arterie kunnen verschillende calibratieschema's voorgesteld worden. Wij onderzochten twee calibratieschema's, een gebaseerd op een lineare druk-diameter relatie, en een gebaseerd op een exponentiële druk-diameter relatie. Voor beide calibratie-aanpakken werden systole bloeddrukken en AIx vergeleken met systole bloeddruk en AIx bepaald op basis van tonometrie-metingen.

We vonden dat exponentieel geschaalde diametermetingen een goed alternatief vormen voor het bepalen van lokale carotis drukken. In tegenstelling tot linear gekalibreerde diametergolven zijn systole bloeddrukken bepaald aan de hand van exponentieel geschaalde diameters niet afhankelijk van de pulsdruk. Systole bloeddrukken bepaald op basis van exponentieel geschaalde diametergolven onderschatten systole bloeddrukken bepaald op basis van tonometriemetingen met 1.9 mmHg. Voor augmentatie-index benaderen linear geschaalde diametergolven beter de augmentatie index afgeleid van tonometriecurves dan exponentieel geschaalde diametergolven. Het verschil tussen beide is echter wel systematisch voor exponentieel geschaalde diametercurves, wat niet zo is voor linear geschaalde diametercurves. Op basis van de resultaten van deze studie vonden we het gebruik van geschaalde diametergolven voor het bepalen van de augmentatie-index minder geschikt, ongeacht de schalingstechniek die gebruikt werd.

Hoofstuk 12 is een uitloper van de studie voorgesteld in hoofdstuk 11. Zowel de exponentiële druk-diameter relatie als de lineaire druk-diameter relatie zijn niet meer dan benaderingen van de echte druk-diameter relatie, die binnen het fysiologische drukgebied van de mens een relatief goede benadering vormen van deze laatste. Een veel beter benadering voor de echte druk-diameter relatie wordt gegeven door de Langewouters relatie, die bepaald werd door de druk-diameter verbanden op te meten over een ruim drukgebied in gedissecteerde menselijke aorta's. Een tweede voordeel van het gebruik van de Langewouters relatie is dat deze gebruikt kan worden om een druk-afhankelijke stijfheidsparameter voor te stellen. De meeste indices van arteriële stijfheid geven ofwel een waarde voor de stijfheid geldig op een bepaald moment van de hartcyclus, of een gemiddelde waarde over de hele cyclus. Zoals uiteengezet in hoofdstuk 1 is de structuur van de arteriële wand echter dusdanig dat zijn stijfheid inherent druk-afhankelijk is, en dus verandert gedurende de hartcyclus. Een druk-afhankelijke index biedt dus een veel betere benadering van de echte arteriële stijfheid. De stijfheidsindex voorgesteld door Langewouters *et al.* is echter geometrie-afhankelijk, wat vergelijking tussen individuen bemoeilijkt. Het doel van de studie voorgesteld in dit hoofdstuk is om (1) een geometrie-onafhankelijke, druk-afhankelijke stijfheidsindex voor te stellen gebaseerd op de geometrie-afhankelijke stijfheidsindex voorgesteld door Langewouters *et al.*; (2) deze index te gebruiken om de evolutie van arteriële stijfheid met leeftijd en geslacht te onderzoeken binnen de Asklepios studie; en (3) deze evolutie te vergelijken met de evolutie met leeftijd en geslacht van een stijfheidsindex gebaseerd op het exponentiële druk-diameter verband.

In dit hoofdstuk wordt een statische distensibiliteit afgeleid van een naar geometrie genormaliseerd langewouters druk-oppervlakte verband. Deze statische distensibiliteit is druk-afhankelijk. Indien deze wordt geëvalueerd op de gemiddelde arteriële druk, vertoont deze statische distensibiliteit een goede overeenkomst met de α index afgeleid van een exponentieel druk-oppervlakte verband. Beide indices tonen aan dat, binnen het leeftijdsbereik gedekt door de Asklepios populatie, de carotis stijver wordt in vrouwen dan in mannen rond de leeftijd van 45 jaar.

Arteriële stijfheidsparameters gemeten op verschillende locaties binnen het arterieel netwerk zijn niet inwisselbaar en geven complementaire informatie over de stijfheid van het arterieel systeem. *Hoofdstuk 13* onderzoekt verschillen in leeftijds-geslacht interactie tussen lokale stijfheidsindices bepaald op de carotis en femoralis (liesslagader) en carotis-femoralis golfsnelheid (PWV) in de Asklepios populatie.

De resultaten voorgesteld in dit hoofdstuk tonen aan dat, in de gezonde Asklepios populatie, de veranderingen met de leeftijd van de lokale arteriële carotis en femoralis stijfheid en carotis-femoralis golfsnelheid verschillen tussen mannen en vrouwen. Over het beschikbare leeftijdsgebied van 35–55 jaar, stijgt de carotis stijfheid sneller in vrouwen dan in mannen. Dit patroon wordt niet teruggevonden bij PWV, waar geen verschil in stijfheidstoename met leeftijd tussen mannen en vrouwen gevonden werd. Hoewel er op heden geen aanwijzingen zijn dat het verschil in stijfheidstoename opgepikt door de lokale stijfheidsparameters ook klinische relevantie heeft, is het belangrijk om deze verschillen in gedachten te houden bij het interpreteren of analyseren van resultaten van stijfheidsonderzoek. Speciale aandacht is vereist wanneer verschillende parameters met elkaar vergeleken worden, vooral omdat binnen het toepassingsgebied van arteriële stijfheid nog weinig meetstandaarden bestaan en vooralsnog geen referentiewaarden beschikbaar zijn.

Ondanks de prognostische waarde van arteriële stijfheid en zijn groeiende aanvaarding binnen de klinische praktijk, wordt het algemeen gebruik van stijfheidsparameters gehinderd door het ontbreken van referentiewaarden. Het 'Referentiewaarden voor Arteriële Stijfheid' project heeft als doel dit euvel te verhelpen door het ter beschikking stellen van een zeer uitgebreide databank waartoe alle deelnemende centra bijdragen teneinde een voldoende grote en representatieve dataset ter beschikking te hebben voor het bepalen van referentiewaarden. Tijdens mijn doctoraatsonderzoek was ik verantwoordelijk voor het verzamelen van de data en het ontwerpen van de databank voor dit referentiewaarden project, en voerde ik de eerste analyses op de verzamelde data uit.

Hoofdstuk 14 stelt de referentiewaarden databank voor, met zijn deelnemende centra en de manier waarop de databank opgesteld werd.

In eerste instantie werd de data uit de databank gebruikt voor het onderzoeken van referentiewaarden voor PWV, gezien dit de huidige gouden standaard is voor het opmeten van centraal arteriële stijfheid. PWV kan echter op verschillende manier gedefinieerd worden, waardoor vergelijking tussen centra en samennemen van data onmogelijk is. Tot op heden bestonden geen conversieformules tussen de verschillende waarden van PWV.

Hoofdstuk 15 stelt een studie voor waarin een conversieformule werd onderzocht voor het converteren tussen de verschillende PWV definities. In een deel van de referentiewaarden databank waarin alle elementen aanwezig waren voor de berekening van PWV volgens de verschillende definities werd een populatie-gebaseerd statistisch model voorgesteld dat gebruikt kan worden voor de conversie tussen de verschillende definities.

Door gebruik te maken van deze conversieformules was het mogelijk om de PWV waarden in de referentiewaarden databank te homogenizeren tot een enkele PWV definitie. In *hoofdstuk 16* tenslotte, werd de invloed van klassieke risicofactoren, leeftijd en bloeddruk op de PWV waarden in de referentiewaarden databank onderzocht om tenslotte normaal- en referentiewaarden voor PWV voor te stellen, geldig in een Europese populatie.

Summary

INTRODUCTION

The present manuscript is a summary of five years of research performed at two institutions, all related to the application of 'theoretical' arterial mechanics. The manuscript is subdivided into 5 topical parts.

The first part, background, contains a single chapter discussing the basics of cardiovascular anatomy and physiology, introducing a number of concepts which are important to understanding the contents of the following chapters. The middle three parts bundle all of the actual research performed over the course of my PhD. The contents of each of these parts is briefly summarized in the following sections. Finally, all conclusions are summarized in the final section, representing the overall conclusion of this manuscript.

INTIMA MEDIA THICKNESS

The first section of this manuscript focusses on two studies that were performed during the early stages of my PhD related to the measurement of carotid artery intima-media thickness (IMT) and its relationship to wall shear stress (WSS) related parameters.

Increased carotid artery intima-media thickness has been shown to be a predictor of both stroke and myocardial infarction, with a threshold value of 0.9 mm being indicative of subclinical organ damage, as outlined in the 2007 European Society of Hypertension and Cardiology (ESH and ESC) guidelines for the management of hypertension. As such, carotid artery IMT is a parameter that is relatively routinely assessed in clinical practice and often reported in clinical research.

Thickening of the intima-media layer is one of the first signs of the onset of atherosclerosis. Though atherosclerosis can appear at any arterial location, some points in the arterial tree appear especially susceptible. These regions are typically found near bifurcations or arterial sections with pronounced curvature. Those sites are characterized by the occurrence of complex blood flows, which are coupled to specific types of wall shear stress patterns. It has been proposed that the mechanisms of intima-media thickening are linked to areas influenced by these wall shear stress patterns, notably those areas which are subjected to low wall shear rates or WSS, oscillating levels of WSS or large wall shear stress angle gradients (WSSAG).

Chapter 3 details the results of a pilot study leveraging existing numerically calculated WSS parameters in a small study population by investigating whether in this population a relationship could be found with IMT measured with black blood MRI (magnetic resonance imaging) images. Our research group has extensive experience in the reconstruction of patient-specific carotid artery bifurcations based on MRI and ultrasound imaging for the calculation of flow and WSS related parameters. In previous studies performed by Glor *et al.*, the accuracy and reproducibility of the MRI based reconstruction had been established. For several subjects, the reconstructed geometry and calculated flow and WSS patterns were available in conjunction with the original image sets that had been used for the reconstruction. The pilot project consisted of three components: (1) construct a tool to aid in the manual delineation of IMT on black blood (BB) MRI images; (2) perform an intra-and inter-observer variability study on the manual IMT delineation; and (3) match the measured IMT values to the previously obtained WSS related parameters and investigate whether a relationship between both could be identified. Its main goal was to determine whether the black blood MRI images provided sufficient resolution for the reliable determination and see whether in this small data set we could link certain types of WSS to measured IMT levels.

We found the manual delineation using the custom-developed tool for manual delineation on BB MRI images to show good intra- and inter-observer variability. Nevertheless, image quality in general is only barely acceptable for the purpose of defining IMT. BB MRI images cannot compete with the superior resolution and accessibility of ultrasound. In spite of this, the tentative results of the analysis outlined in chapter 3 have shown that in the study population a weak, but significant correlation is found between IMT and measured WSS. The relationship between IMT and WSS related parameters was stronger in the CCA than in the ICA regardless of the WSS parameter under consideration. In contrast, measured IMT values were strongly correlated to the site of measurement; taking the distance to the carotid bifurcation into account has more predictive power than any of the investigated WSS related parameters. Furthermore, including WSS related parameters in a model taking into account the distance to the carotid bifurcation did not significantly improve model performance.

Chapter 4 outlines the results of a validation study in which a new semi-automated tool for the measurement of carotid IMT based on ultrasound images was compared to manually measured IMT on the same ultrasound images. As part of the Asklepios study protocol, one expert operator manually processed the ultrasound images of over 2,500 subjects to determine carotid IMT. Since IMT is a measure increasingly used in clinical practice over the past few years, several tools have emerged to aid in the detection of carotid IMT by providing (semi-) automated delineation of the intima-media and media-adventitia interfaces. Given the extensive, reliable data set of manual IMT measurements available in the Asklepios population, a research project was proposed to validate a new semi-automated tool provided by GE Healthcare Ultrasound, on a subset of the Asklepios data. The project consisted of three components (1) re-perform the manual measurements on a subset of the Asklepios data to assess the inter-observer variability of the manual measurements; (2) perform the automated measurements; and (3) compare inter- and intra-observer variability of and the difference between the manual and automated IMT measurements.

We found the automated IMT measurement to deliver a reliability at least as good as the manual measurements in a fraction of the time, without the need for extensive training of operators. Given these properties, the automated IMT detection algorithm tested in this study seems an excellent tool for routine assessment of IMT in clinical practice.

Models of the arterial tree

The second part of this manuscript is dedicated to modeling aspects of the arterial network. As evident from the mathematical background of arterial physiology discussed in chapter 1, pressure and flow in the arterial tree—like in any other tube network—obey a set of basic laws which can be used to gain knowledge of what makes the arterial system tick.

Arterial models are the theoreticist's tools for dissecting the inner workings of the arterial tree. From the simple to the extremely complex, models are used to understand what lies at the cause of certain observed behavior and what happens if the boundary conditions of the system change. Yet models also have real practical use. Only by a thorough understanding of how different properties of the arterial tree interact and how these properties influence the shape of the pressure and flow waveforms can approaches for treating unwanted behavior be defined without having to resort to random 'trial and error' testing. They are also, to a certain degree, required for the quantification of arterial stiffness, a topic that will be the subject of part 4 of this manuscript.

Chapter 6 therefore introduces the most important models of the arterial tree. The two basic paradigms of the arterial tree—its representation as a lumped parameter (windkessel) or wave system—are discussed, the latter both in the frequency and the time domain. The goal of this chapter is to familiarize the reader with the concepts that will be required for the quantification of arterial stiffness in part 3 of this manuscript.

Lumped parameter and wave (transmission line) models represent two contradictory, yet complimentary views of how the arterial tree should be viewed. Both have their strengths and weaknesses, but neither is sufficiently superior over the other in all application domains. Recently, efforts have been made to marry the windkessel and wave reflection views of the arterial tree in 'hybrid' models by separating the pressure wave in the time domain in a reservoir and wave reflection component. This approach however seems to have a lot in common with the established three element windkessel model.

Chapter 7 investigates these similarities by applying both the 3-element windkessel and the reservoir-wave separation model to the Asklepios study population data. The main goal of this study was to (1) evaluate the performance and applicability of the reservoir-wave separation model in the Asklepios population; (2) compare reservoir pressure derived using the three element windkessel to reservoir pressures derived using the reservoir-wave separation models to see to which extent they are different; and (3) examine the evolution of the three element windkessel and reservoir-wave separation reservoir pulse pressure with age and gender in the Asklepios population.

We have shown that the recently proposed (time domain) reservoir pressure concept shows large similarities to the classical (frequency domain) 3-element windkessel model, especially in subjects characterized by a high reflection magnitude and high 'windkesselness' of their arterial system. The more wave reflections are present in the system, and the more the arterial tree behaves like a windkessel, the better the reservoir pressure concept seems to hold. Hence, rather than unify the lumped parameter and wave reflection model views, the reservoir-wave concept thus seems to merely represent a time-domain wave propagation analogy of the classic three element windkessel model, albeit yielding slightly different quantitative results. When both models are applied to the Asklepios population, both show the increase of pulse pressure with age to be largely due to increasing reservoir pressures, rather than changes in wave pressures.

ARTERIAL STIFFNESS

The material in this section covers the bulk of the work performed during my PhD research. All of it is related in some way to different measures of arterial stiffness and tools for their assessment. The stiffness of the arteries is a critical parameter for the function of the cardiovascular system. Arterial stiffness has been shown to be predictive for clinical outcome in numerous populations and an elevated stiffness has been shown to be an independent predictor for all-cause and cardiovascular mortality. As such, measurements of arterial stiffness are increasingly used in clinical practice and have since long found their way in research and clinical trial settings.

Given the heterogeneity of the arterial system, with its wide range of different-sized arteries with differing structures, it should come as no surprise that arterial stiffness can be quantified using a similarly large set of different stiffness measures. Many arterial stiffness measures are related to certain models of the arterial network; these models are discussed in chapter 6.

Chapter 9 gives an overview of the most commonly used measures of arterial stiffness. These include systemic, regional and local measures and measures based on the quantification of wave reflections. Several of the arterial stiffness parameters discussed in this chapter require the measurement of central (aortic) pressure signals. Since true aortic pressure waveforms can only be obtained invasively through the use of catheters, alternatives have been developed to approximate central arterial pressure using some other waveform. Two main approaches exist: either pressures can be measured at the carotid artery, which due to its proximity to the aorta has pressure waveforms that match closely to invasively measured aortic pressures, or pressures measured at a different location—usually the radial artery—can be transformed into central pressures using a radial-to-aortic transfer function.

Both approaches have strengths and drawbacks. Carotid tonometry can be difficult to perform in the elderly, particularly obese subjects or in the presence of carotid artery plaques, and the transfer function is non-patient specific, being a population based function.

Chapter 10 examines another potential problem with the use of transfer functions. Over the course of the years, different transfer functions (TFF) have been proposed, determined on different populations. Often, the type of transfer function used is tied to the device used to determine the central hemodynamics and arterial stiffness, and the impact of using different types of transfer functions is not always clear. The aim of this study was to investigate whether two established transfer functions could be used interchangeably for the calculation of central systolic blood pressure and augmentation index in a subset of the Asklepios population.

We found central systolic blood pressure and augmentation index to differ depending on the transfer function used to calculate the central pressure waveform from the measured peripheral waveform. Data obtained with different TFF are not interchangeable: derived parameter values are determined by the specifics of the TFF, especially for AIx (augmentation index).

Chapter 11 investigates a possible alternative to carotid tonometry for measuring carotid artery pressures. Instead of determining carotid pressures directly from the tonometry readings, this study aimed to ascertain whether calibrated diameter distension waveforms, obtained using ultrasound, could be used as a surrogate pressure signal. Depending on the assumed pressure-diameter relationship, different calibration schemes can be proposed. We investigated two calibration techniques, based on an assumed linear and exponential pressure-diameter relationship. For both relationships, the model parameters can be determined based on pressures obtained at a reference location (in our case, the brachial artery). The aim of the study was to compare systolic blood pressures and augmentation indices determined on linearly and exponentially scaled diameter waveforms to systolic blood pressures and augmentation indices determined on carotid artery tonometry readings in the Asklepios population.

We found exponentially calibrated diameter waveforms offered a valid alternative for local pressure assessment at the carotid artery. Unlike linearly calibrated waveforms, systolic blood pressure assessed by exponential diameter calibration is independent of the level of pulse pressure. Systolic blood pressure derived from exponentially calibrated diameter curves underestimate pressures obtained by carotid tonometry by 1.90 mmHg. AIx determined from exponentially calibrated diameter waveforms yields values which differ more from AIx derived from tonometry waveforms than when linear calibration is used, though in contrast to the linear calibration, the bias is systematic and should thus easily be corrected for. Nevertheless, the use of scaled carotid diameter waveforms for the assessment of AIx might be less appropriate as a direct alternative for carotid applanation tonometry.

Chapter 12 is a corollary to chapter 11. Both the exponential and linear pressure-diameter relationships are an approximation of the true pressure-diameter relationship that give good approximations of the true arterial pressure-diameter relationships in the largest part of the physiological pressure range. A far better approximation of the true arterial pressure-diameter relationship is given by the Langewouters relationship, which was determined by studying the diameter changes for a broad pressure range on excised human aortas. A second advantage to the sigmoidal langewouters pressure-area relationship is that it can be used to define a pressure dependent stiffness index. Most stiffness indices give some value of arterial stiffness which is either valid for a specific point in the cardiac cycle, or an average value over the complete cardiac cycle. As explained in chapter 1 however, the structure of the artery implies that its stiffness is inherently pressure dependent and thus changes over the course of the cardiac cycle. A pressure dependent index is thus a better representation of the real-life arterial behavior. The pressure dependent index proposed by Langewouters *et al.*, however, is geometry dependent, which makes comparing the stiffness index between subjects difficult. The goals of the study outlined in this chapter were (1) to propose a geometry independent, pressure dependent stiffness index based on the geometry dependent index proposed by Langewouters *et al.*; (2) to use this index to investigate the evolution of arterial stiffness with age and gender in the Asklepios population and (3) to compare this evolution with the evolution with age and gender of a different stiffness index, derived from the exponential pressure-diameter relationship.

The static distensibility proposed in chapter 12, which was derived from a geometry-normalized Langewouters P-A relationship shows results in good agreement with the α stiffness index derived from an exponential pressure-area relationship. Both indices demonstrate that over the studied age-range, the carotid artery becomes stiffer in women than in men around the age of 45.

Arterial stiffness indices measured at different locations do not necessarily match and may yield complementary information on the arterial system. *Chapter 13* investigates differences in age-gender interaction in local arterial stiffness determined on the carotid and femoral arteries and carotid-femoral pulse wave velocity in the Asklepios population.

The data presented in chapter 13 demonstrate that, in an apparently healthy middle-aged population, the evolution with age of local carotid and femoral stiffness and pulse wave velocity (PWV) is not the same in men and women. While carotid stiffness shows a more rapid increase with age in women than in men (over the measured age range of 35–55 years), this pattern is not reflected in aortic PWV, which increases to a similar extent in men and women. Other central arterial stiffness parameters do show an age-gender effect similar to the one observed at the carotid artery. Though the differences in evolution of different stiffness parameters with age and gender have not yet proven to be of clinical significance, the fact that these differences exist is important to keep in mind when analysing or interpreting results from arterial stiffness investigations. Special care is needed when different parameters are compared, especially in a field where proposed measurement standards are not yet widely adopted and reference values are lacking.

Despite its prognostic value and its growing use in clinical practice, the widespread use of arterial stiffness is hampered by the lack of reference values. The reference values for arterial stiffness' collaboration aims to remedy this issue by providing a large database to which participating centers contribute in order to obtain a representative and sufficiently large dataset on which reference values can be determined. During my PhD I performed the data collection and construction of the reference value database and performed the analysis leading to the reference values for pulse wave velocity.

Chapter *14* introduces the reference values for arterial stiffness' collaboration set-up and database.

In a first stage, the data from the reference value database were leveraged to investigate reference values for PWV, which is the current gold-standard method for assessing central arterial stiffness. PWV measures do however suffer from important methodological issues: a number of different definitions of PWV exist, and up to now no conversion factors between both had been investigated, making comparisons between or pooling of data from different centres impossible.

Chapter *15* presents a study in which an approach was investigated to convert between PWV definitions. In a subpopulation of the reference value database—consisting of the Asklepios and Hôpital Européen Georges Pompidou databases—in which all elements were available for the calculation of PWV according to either definitions, a population based statistical model is proposed which can be used for the conversion between definitions. Though ideally all distances should be measured when measuring PWV so that exact conversion between the different distance definitions is always possible, for those cases in which only one type of measurement is available, the proposed conversions equations based on distance and body height offer a viable alternative, which can be used to convert between distance measurements—and thus PWV types.

Using these conversion formulae, the PWV values in the reference value database were homogenized to a single PWV definition.In *Chapter 16* the influence of classic risk factors, age and blood pressure on PWV is investigated in the reference value population and finally, reference values and normal values for PWV are presented.

Contents

Preface **v**
The stuff you write at the end to put in the beginning v

Samenvatting
Summary **xi**

Samenvatting **xiii**
Inleiding xiii
Intima media dikte xv
Modellen van het arterieel systeem xvii
Arteriële stijfheid xix

Summary **xxv**
Introduction xxv
Intima media thickness xxv
Models of the arterial tree xxvii
Arterial stiffness xxix

Contents **xxxiv**

List of Figures **xlii**

List of Tables **xlvii**

Abbreviations and Symbols **xlix**

Introduction **liii**

Introduction **lv**

The flow of a PhD lv
Structure lix
List of publications lx
First author lx
Accepted for publication lxi
Submitted for publication lxi
To be submitted lxi
Co-author lxi
Accepted for publication lxii
To be submitted lxii

I Background 1

1 The cardiovascular system 3
1.1 Anatomy of the cardiovascular system 3
1.1.1 The circulatory system 3
1.1.2 The heart 4
1.1.3 The vessels 5
1.2 Cardiovascular physiology 9
1.2.1 Homeostasis and the cardiovascular system . 9
1.2.2 Functional arrangement of the cardiovascular system 11
1.2.3 Blood flow physics 13
1.2.4 The heart pump 16
1.3 The arterial pulse 18
1.3.1 Components of the arterial pulse 18
1.3.2 Measuring the arterial pulse 19
Direct methods 19
Indirect methods 19
1.3.3 Determinants of the arterial pulse 20
1.3.4 The arterial pulse waveform 22
1.4 Cardiovascular risk 22

II Carotid artery intima media thickness 27

2 Outline 29

3 Carotid intima media thickness and wall shear stress 33
3.1 Introduction 33

3.2 Methods 34
3.2.1 Study population 34
3.2.2 MRI imaging 34
3.2.3 Geometry reconstruction and calculation of WSS parameters 35
3.2.4 IMT measurements 37
3.2.5 Matching IMT measurements to WSS parameters 38
3.2.6 Statistical analysis 39
3.3 Results 39
3.3.1 Intra- and inter-observer variability 40
3.3.2 IMT and WSS related parameters 40
3.4 Discussion 44
3.5 Conclusions 48

4 Validation of an automated ultrasound-based IMT detection tool 49
4.1 Introduction 49
4.2 Methods 49
4.2.1 Ultrasonography 49
4.2.2 Manual IMT assessment 50
4.2.3 Automated IMT assessment 50
4.2.4 Study protocol 51
4.2.5 Data analysis and statistics 52
4.3 Results 54
4.3.1 Manual IMT assessment 54
4.3.2 Automated IMT assessment 54
4.3.3 Automated versus manual assessment 56
4.4 Discussion 57
4.5 Conclusions 58

III Models of the arterial tree 59

5 Outline 61

6 Modeling the arterial system 63
6.1 Introduction 63
6.1.1 On the use and limitations of models 63
6.1.2 Models and the arterial system 64
6.2 Windkessel models 65

6.2.1 Two-element windkessel model 66
6.2.2 Three- and four-element windkessel models . 71
6.3 The arterial tree as a wave system – frequency domain 72
6.3.1 Fourier decomposition of pressure and flow waves 72
6.3.2 Separation of pressure and flow in forward and backward waves 73
6.3.3 (Characteristic) impedance of the arterial tree 75
6.3.4 Reflection coefficient 75
6.4 The arterial tree as a wave system – time domain . . . 77
6.4.1 Pressure and flow decomposition in wavefronts 77
6.4.2 Wave intensity 79
6.4.3 Separation of forward and backward waves in the time domain 80
6.4.4 Reservoir-wave separation 81

7 The reservoir-wave pressure concept and the 3-element windkessel model 85
7.1 Introduction 85
7.2 Methods 87
7.2.1 Study population 87
7.2.2 Basic clinical data 87
7.2.3 Measurement of local carotid pressure 87
7.2.4 Measurement of aortic outflow 88
7.2.5 Determination of reservoir pressure by pressure wave separation ($P_{res,WS}$) 89
7.2.6 Determination of reservoir pressure using a 3-element windkessel model 89
7.2.7 Statistical analysis 90
7.3 Results 91
7.3.1 Fitting performance 91
7.3.2 Evolution of carotid pulse pressure and reservoir pressure with age in men and women and model comparisons 92
7.4 Discussion 94
7.5 Conclusions 102

IV Arterial stiffness 105

8 Outline 107

9 Arterial stiffness 111

9.1 Introduction 111

9.2 Arterial stiffness and models of the arterial tree 112

9.3 Lumped parameter view — systemic parameters . . . 114

9.3.1 Time decay method 114

9.3.2 Area method 115

9.3.3 Pulse pressure method 116

9.3.4 Clinical applications of systemic arterial stiffness parameters 116

9.4 Direct measures of arterial stiffness — local parameters 116

9.4.1 Compliance and distensibility coefficient . . . 116

9.4.2 Clinical applications of local stiffness measures 118

9.5 Direct measures of arterial stiffness — regional parameters 118

9.5.1 Pulse wave velocity definition 118

9.5.2 Transit time: detection of the foot of the waveform 120

9.5.3 Measurement sites and distance measurements 120

9.5.4 Clinical applications of PWV 122

9.6 Indices quantifying wave reflections 123

9.6.1 Central pressure wave analysis 123

9.6.2 Clinical applications of pressure wave analysis 124

10 Comparison of two transfer functions 127

10.1 Introduction 127

10.2 Methods 129

10.2.1 Study population 129

10.2.2 Measurement of carotid, radial and central pressures 129

10.2.3 Augmentation index 130

10.2.4 Statistical analysis 131

10.3 Results 131

10.3.1 Blood pressures 131

10.3.2 Augmentation index 132

10.4 Discussion 132

10.5 Conclusions 137

11 Carotid diameter distension versus applanation tonometry 139

11.1 Introduction 139

11.2 Materials and methods 140

11.2.1 Study population 140
11.2.2 Basic clinical data 141
11.2.3 Measurement of local pressure by tonometry . 141
11.2.4 Measurement of local arterial diameter 142
11.2.5 Calibration of diameter waveforms 142
11.2.6 Comparison of scaled diameter and pressure waveforms 144
11.2.7 Statistical analysis 145
11.3 Results 145
11.3.1 Root mean squared error 145
11.3.2 Carotid systolic blood pressure 146
11.3.3 Carotid augmentation index 147
11.4 Discussion 151
11.5 Conclusions 155

12 A new pressure dependent, geometry independent stiffness index? 157
12.1 Introduction 157
12.2 Methods 158
12.2.1 Arterial stiffness indices 158
12.2.2 Study population 159
12.2.3 Data acquisition and signal processing 159
12.3 Results 160
12.4 Discussion 163
12.5 Conclusions 163

13 Local vs regional stiffness in the Asklepios population 165
13.1 Introduction 165
13.2 Methods 166
13.2.1 Study population 166
13.2.2 Basic clinical data 167
13.2.3 Measurement of local blood pressure 167
13.2.4 Measurement of local arterial diameter 168
13.2.5 Carotid-femoral pulse wave velocity 169
13.2.6 Local arterial stiffness 169
13.2.7 Local arterial stiffness: derived parameters . . 169
13.2.8 Statistical analyses 170
13.3 Results 170
13.3.1 Basic clinical data and hemodynamics 170
13.3.2 Carotid-femoral pulse wave velocity (PWV_{ao}) 171

13.3.3 Local arterial stiffness - carotid artery 171
13.3.4 Local arterial stiffness - femoral artery 172
13.4 Discussion 176
13.5 Conclusions 180

14 The Reference Values for Arterial Stiffness' Collaboration 181
14.1 The reference value project 181
14.2 Overview of the reference value database 183

15 Distance conversion for PWV calculation 189
15.1 Introduction 189
15.2 Methods 190
15.2.1 Study population 190
15.2.2 Basic clinical data and PWV measurements . 191
15.2.3 Statistical analyses, model development and validation 191
15.3 Results 192
15.3.1 Population 192
15.3.2 Model development 192
15.3.3 Model validation 193
15.4 Discussion 200
15.5 Conclusions 202

16 Reference values for carotid-femoral pulse wave velocity 203
16.1 Introduction 203
16.2 Methods 204
16.2.1 Participating centers 204
16.2.2 Study population 204
16.2.3 PWV: methodological considerations 205
16.2.4 Factors influencing PWV in the study population 206
16.2.5 Reference and normal values in the study population 206
16.2.6 Statistical analyses 207
16.3 Results 207
16.3.1 Study population 207
16.3.2 Risk factors and observed PWV 207
16.3.3 Reference and normal values for PWV 208
16.4 Discussion 221
16.4.1 Limitations of the study 224
16.5 Conclusions 225

V Conclusions **227**

17 Conclusions **229**
17.1 Carotid artery intima-media thickness 229
17.2 Models of the arterial tree 230
17.3 Arterial stiffness 231

Appendices **235**

Appendix A.1: Reference values for arterial stiffness research proposal **237**
Introduction 237
Population issues 237
Methodological issues — pulse wave velocity 238
Signal used 238
Path length 238
Algorithm 238
Methodological issues — Carotid artery stiffness . . . 239
Aim of the study and objectives 239
Project management 239
Promoters and scientific head 239
Research committee 240
Data access and benefits 240
Data management 241
Tentative list of parameters to be collected 241
Inclusion/exclusion criteria 241
Confidentiality 241
Security 242
Database access 242

Appendix A.2: Parameters for the reference value project **243**

Bibliography **247**

List of Figures

1 Stroomdiagram van de verschillende studies uitgevoerd tijdens mijn onderzoek. xiv

2 PhD flowchart lvii

1.1 The human blood circulatory system. 3
1.2 Front view of heart and lungs 5
1.3 Schematic anterior (front) view of the open heart. 6
1.4 Section of the heart showing the four heart valves obtained by removal of the atria. 7
1.5 Structure of the arterial wall 8
1.6 Functional view of the cardiovascular system indicating the distribution of the cardiac output in an average resting individual. 12
1.7 Factors influencing blood flow through a tube. 14
1.8 Cardiac cycle of the left heart and pressure-volume loop of the left ventricle 17
1.9 Main components of an arterial pressure waveform 18
1.10 The UGent tonometry hard- and software platform 20
1.11 Pressure amplification of the arterial pulse from the central to the peripheral arteries 23
1.12 Stratification of CV risk according to the 2007 ESC/ESH guidelines 25

3.1 Typical black blood MRI image of an aorta 35
3.2 OSI distribution over a reconstructed geometry before (left) and after (right) patching 39
3.3 Bland-Altman plots of intra-observer variability study for operator FG (top) and SV (bottom) 41
3.4 Bland-Altman plots of inter-observer variability study . . 42

3.5 Top: Scatter plot of IMT versus WSS. Bottom: scatter plot of $\frac{1}{IMT}$ versus $ln(WSS)$ 43
3.6 Distribution of WSS before (top) and after (bottom) transformation 44
3.7 Regression analysis of $\frac{1}{IMT}$ vs $abs(z)$ in the CCA (top) and ICA (bottom) 46

4.1 Example of IMT detection using the new IMT detection algorithm 51
4.2 Bland-Altman plots of the intra-variability study for the manual (top) and automated (bottom) IMT detections. . . 55
4.3 Bland-Altman plots of the inter-variability study for the manual (top) and automated (bottom) IMT detections. . . 56
4.4 Bland-Altman plot of manual versus automated IMT . . . 57

6.1 Schematic summary of the major elements of cardiovascular physiology playing a role in the windkessel models. 67
6.2 Hydraulic and electric representations of the two-, three, and four-element windkessel models 68
6.3 Example of aortic input impedance plotted with impedances predicted from a two-, three- and four element windkessel model 71
6.4 Decomposition of a pressure waveform into its harmonics 73
6.5 Schematic representation of the frequency domain method 76
6.6 Separation of an aortic pressure waveform in sequential wavefronts 78
6.7 Measurement of wave intensity in the ascending aorta . . 79
6.8 Separation of a measured pressure (top panel) and flow (bottom panel) into its forward and backward components 82
6.9 Separation of a measured pressure (top panel) and flow (bottom panel) into its forward and backward components using the reservoir-wave hypothesis 84

7.1 Representative example of the fittings to a carotid pressure waveform using the reservoir pressure and windkessel model approach 91
7.2 Stacked bar representation of the evolution of carotid pulse pressure and the contribution of the reservoir pressure determined by a wave separation model and a three-element windkessel model 93

7.3 Top panel: regression of $PP_{res,WS}$ and $PP_{res,WK}$. Bottom panel: Bland-Altman plot of $PP_{res,WS}$ and $PP_{res,WK}$ 95
7.4 Regression of parameters b (from wave separation model) and 1/RC (from windkessel model) 98
7.5 Case study for A-type (left panel) and C-type (right panel) waveform showing measured pressure (P; full line), flow (Q; dotted line) and reservoir pressure ($P_{res,WS}$, dashed line). 99
7.6 Case study for A-type (left panel) and C-type (right panel) waveform showing the relation between Q versus P_{ex} (excess pressure: the difference between measured pressure and $P_{res,WS}$). 100
7.7 Top panel: Difference between reservoir pulse pressures derived using the wave separation ($PP_{res,WS}$) and windkessel ($PP_{res,WK}$) models versus reflection magnitude. Bottom panel: area enclosed by Q–P_{ex} versus reflection magnitude 101

9.1 Measurement of carotid-femoral pulse wave velocity . . . 119
9.2 Different algorithms used to identify a specific reference point on a waveform 121
9.3 Overview of different approaches for defining the path length for PWV calculation 122
9.4 Carotid pressure waveform recorded by applanation tonometry and definition of augmentation index 124
9.5 Calibration method to obtain central pressure waveforms from carotid tonometry readings 125

10.1 Graphical representation of the transfer functions of Karamanoglu and Chen 130
10.2 Principle behind the automated detection of the shoulder point based on the 4th derivative of the pressure signal . . 131
10.3 Regression analysis of $SBP_{sao,1}$ and $SBP_{sao,2}$ versus SBP_{ca} (top) and $AIx_{sao,1}$ and $AIx_{sao,2}$ versus AIx_{ca} (bottom) . . . 133
10.4 Bland-Altman plot of $SBP_{sao,1}$ versus SBP_{ca} (top) and $SBP_{sao,2}$ versus SBP_{ca} (bottom) 134
10.5 Bland-Altman plot of $SBP_{sao,1}$ versus $SBP_{sao,2}$ (top panel) and $AIx_{sao,1}$ versus $AIx_{sao,2}$ (bottom panel). 135
10.6 Bland-Altman plot of $AIx_{sao,1}$ versus AIx_{ca} (top) and $AIx_{sao,2}$ versus AIx_{ca} (bottom) 136

11.1 SBP and AIx from calibrated diameter waveforms compared to SBP and AIx from tonometry waveforms 146

11.2 Bland-Altman plots of SBP_{car} from calibrated diameter distension and tonometry waveforms . . . 148
11.3 Influence of brachial artery pulse pressure on estimated calibrated diameter distension systolic blood pressure . . 149
11.4 Bland-Altman plots of carotid AIx from calibrated diameter distension and tonometry waveforms . . . 150
11.5 Measured pressure (a) and diameter (b) at the carotid artery; different pressure-area relationships (c) and their performance in comparison to measured data in the physiological pressure range (d); comparison of different diameter to pressure scaling techniques with carotid tonometry (e) 156

12.1 α stiffness index and static distensibility evaluated at mean arterial pressure . . . 161
12.2 Static distensibility evaluated over a broad pressure range per age quartile for men and women . . . 162

13.1 Evolution of carotid-femoral PWV with age and gender in the Asklepios population . . . 171
13.2 Evolution of carotid and femoral stiffness indices with age and gender in the Asklepios population . . . 173

14.1 Geographic distribution of the centers participating in the reference value project . . . 183
14.2 Overal mean (SD) of key subject characteristics in the reference value database and distribution of average values per center . . . 185
14.3 Percentage of subjects in which the listed parameters were available in March 2008 . . . 187

15.1 Comparison of estimated direct distance to measured direct distance . . . 196
15.2 Comparison of estimated subtracted distance to measured subtracted distance . . . 197
15.3 Comparison of estimated to measured pulse wave velocities for PWVs calculated using direct distance . . . 198
15.4 Comparison of estimated to measured pulse wave velocities for PWVs calculated using subtracted distance . . . 199

16.1 Flowchart illustrating the different subpopulations used throughout the study. . . . 209

16.2 PWV versus age in the reference value population 212
16.3 PWV versus SBP in the reference value population 213
16.4 Boxplots showing the distribution of PWV per age decade in the reference value population 215
16.5 Boxplots showing the distribution of PWV per blood pressure category in the reference value population 216
16.6 Average PWV [m/s] in the reference population according to age and blood pressure categories. 217
16.7 Average PWV per age decade in the normal values population. 220

List of Tables

1.1 Structural characteristics of the vascular system 6

3.1 Age and blood pressures in the study population 40
3.2 Common box-cox transformations 42
3.3 Summary of regression analysis of transformed IMT and WSS parameters in the common and internal carotid arteries 45
3.4 Summary of the stepwise forward linear regression for $\frac{1}{IMT}$ versus each of the WSS parameters in the CCA and ICA . 47

4.1 Available datasets (top) and protocol for the intra- and inter-operator variability study and comparison of manual to automated measurements (bottom) 53
4.2 Intra- and inter-observer variability study for manual and automated measurements 54

6.1 Analogy between electrical circuit elements and physiological properties for the windkessel models 69

7.1 Overview of general population parameters of the study population 92
7.2 Overview of fitting parameters for the reservoir-wave and three-element windkessel models obtained by fitting them to the measured carotid pressure data. 92

10.1 Results of regression analysis of SBP and AIx derived from synthesized aortic pressure waves and carotid tonometry . 132
10.2 Mean differences between SBP and AIx derived from synthesized aortic pressure waves and carotid tonometry. . . 133

11.1 General description of the study population 145

13.1 Basic clinical data of the study population 174

13.2 Hemodynamic and arterial parameters 175

14.1 Subjects included per center in the reference value database 184

15.1 Results of the forward stepwise regression analysis for the selection of model parameters for the subtracted to direct conversion sense 193
15.2 Basic body size and clinical parameters of the Asklepios, HEGP, model and validation populations 195

16.1 Basic body size and general clinical parameters of the complete, reference value and normal value populations 210
16.2 Influence of gender and risk on observed PWV values . . 211
16.3 Regression equations for PWV versus age and SBP according to blood pressure category and age category in the reference value population 214
16.4 Distribution of PWV values in the reference value population according to age and blood pressure categories . . . 218
16.5 Number of subjects included in each of the age and blood pressure categories used for determination of the reference values 219
16.6 Distribution of PWV according to age categories in the normal values population 222

1 List of minimal and optional parameters for inclusion in the reference value database 244
2 List of minimal and optional documentation for inclusion in the reference value database 245

Abbreviations and Symbols

Abbreviations

AIx	Augmentation index
BB	Black blood
CCA	Common carotid artery
CFD	Computational fluid dynamics
CO	Cardiac output
CV	Coefficient of variation
CVP	Central venous pressure
DBP	Diastolic blood pressure
DICOM	Digital imaging and communications in medicine
ECA	External carotid artery
HR	Heart rate
ICA	Internal carotid artery
IMT	Intima-media thickness
LVOT	Left ventricular outflow tract
MAP	Mean arterial pressure
MRI	Magnetic resonance imaging
OSI	Oscillatory shear index
PC	Phase contrast
PhD	Doctor of philosophy
PP	Pulse pressure
PWV	Pulse wave velocity
RC	Repeatability coefficient
SBP	Systolic blood pressure
SD	Standard deviation
SV	Stroke volume
SVR	Systemic vascular resistance
US	Ultrasound
WSS	Wall shear stress

WSSAG	Wall shear stress angle gradient
WSSGs	Spatial wall shear stress gradient
WSSGt	Temporal wall shear stress gradient

Symbols

C	Capacitance	[F]
c	Wave speed	[m/s]
dP	Pressure wavelet	[Pa]
dU	Flow velocity wavelet	[m/s]
η	Dynamic viscosity	[Pa.s]
E	Young's modulus	[Pa]
Φ	Phase angle	[rad]
f	Frequency	[Hz]
Γ	Reflection coefficient	
Γ_M	Reflection magnitude	
h	Wall thickness	[m]
I	Current	[A]
L	Length	[m]
μ	Dynamic viscosiy	[Pa·s]
ω	Angular frequency	[rad/s]
P	Pressure	[mmHg]
Q	Electric charge	[C]
Q	Flow rate	[m^3/s]
ρ	Density	[kg/m^3]
R	Radius	[m]
R	Resistance (electrical)	[Ω]
R	Resistance (hydraulic)	[mmHg.s/m^3]
τ	Instantaneous wall shear stress	[Pa]
τ	Time constant	
T	Heart cycle	[s]
U	Flow velocity	[m/s]
U	Potential	[V]
Z	Impedance	

Operators

Δ	Difference
∂	Partial derivative
d	Derivative

Subscripts

dia	During diastole
es	End-systolic
sys	During systole

Superscripts

Units

A	ampère
C	coulomb
cm	centimeter
dm	decimeter
F	farad
g	gram
Hz	hertz
kg	kilogram
km	kilometer
l	liter
m	meter
MHz	Megahertz
min	minute
ml	milliliter
mmHg	millimeter of mercury
Ω	ohms
Pa	pascal
rad	radian
s	second
V	volt
Wb	weber

Introduction

Introduction

THE FLOW OF A PHD

As I'm writing this introduction, I am looking at a PDF copy of the latest brochure on the ins and outs of doing a PhD at Ghent University. Past the puzzled looking face on the cover and the usual required promo-talk on the first couple of pages, the brochure gets down to business by listing the 'formal aspects' of a PhD, starting by the choice of the PhD subject. This is how the brochure lists it:

> '*Before* you start a PhD, it is important to properly define your ideas into a solid research proposal. During a number of years—*I like how they stay nice and vague in this bit*—you will focus intensively on this specific topic in order to contribute to science.'

Hence probably comes the common misconception among my not-in-academia-working friends that when you start out on your quest for 'contributing to science', you more or less know what you are going to be working on for the next four years or so. Reality is different. It certainly was in my case.

When I started my PhD on a sunny Monday morning in the fall of 2003, with a lot of theoretical background on computer science engineering and *no* background in biomedical engineering, all I had to cling to were my 'properly defined ideas', suitably formulated in a 'solid research proposal', stating that as far as the engineering faculty was concerned, I would be devoting all my attention on *'the development and validation of an ultrasound-based tool for the quantification of wall shear stress in routine clinical practice'*. What I did not know was that this research proposal was little more than a rite of passage, a hurdle required to pass before starting on a whirlwind of research topics, all of them only having in common that they were in varying degrees *not* related to this initial research project.

The manuscript lying before you represents my best attempt at bundling most of what I have done during the past few years, as far as research is concerned, into a single volume of text, combining a relative disparity of topics. I feel very strongly that in order to properly appreciate the link between all these different topics, it is important I spend some time explaining how they fit in the broad picture of five years of research, before formally stating the goals and structure of the present document. To this extent, figure 2 on page lvii gives a kind of flowchart, listing the different research topics I have tackled, and how each of them follows from previously explored ones.

Investigating wall shear stress (WSS), as per my initial PhD project proposal, was of course not a randomly chosen subject. One of my predecessors in the lab, dr.ir. Fadi Glor, had for his PhD worked on the reconstruction of carotid geometries based on magnetic resonance imaging (MRI) and ultrasound (US) images for flow reconstruction and calculation of WSS parameters. His approach was solid, though time-consuming, and I was to continue his work to attempt to streamline and expedite the calculation of WSS for real-time analysis in clinical practice. First though, I had to get to know his work. To do so, my first research project 'IMT versus WSS derived parameters' was drafted.

While I was working on this topic, I was exposed to what would become the staple of the first half of my PhD research: the Asklepios study database. For this large-scale population database, our lab was responsible for analyzing the arterial mechanics. At that time, the first round of data collection had just recently been finished and a wealth of data was available for research purposes. With my background in computer science engineering, I took it upon myself to try and organize this data into a database.

At about the same time as I was working on the MRI IMT measurements and the Asklepios database, our lab was asked to participate in a validation study of a new automated ultrasound-based IMT detection algorithm by comparing its measurements to manual IMT measurements performed on the Asklepios subjects. As I had been working on IMT and had gotten familiar with the Asklepios data, I was the logical go-to man to perform this study.

My IMT and WSS investigating days, however, would soon be over. The brunt of the Asklepios research, as far as our lab is concerned, lies on the arterial mechanics and arterial stiffness parameters to be calculated from the Asklepios data. As I had been working on the Asklepios

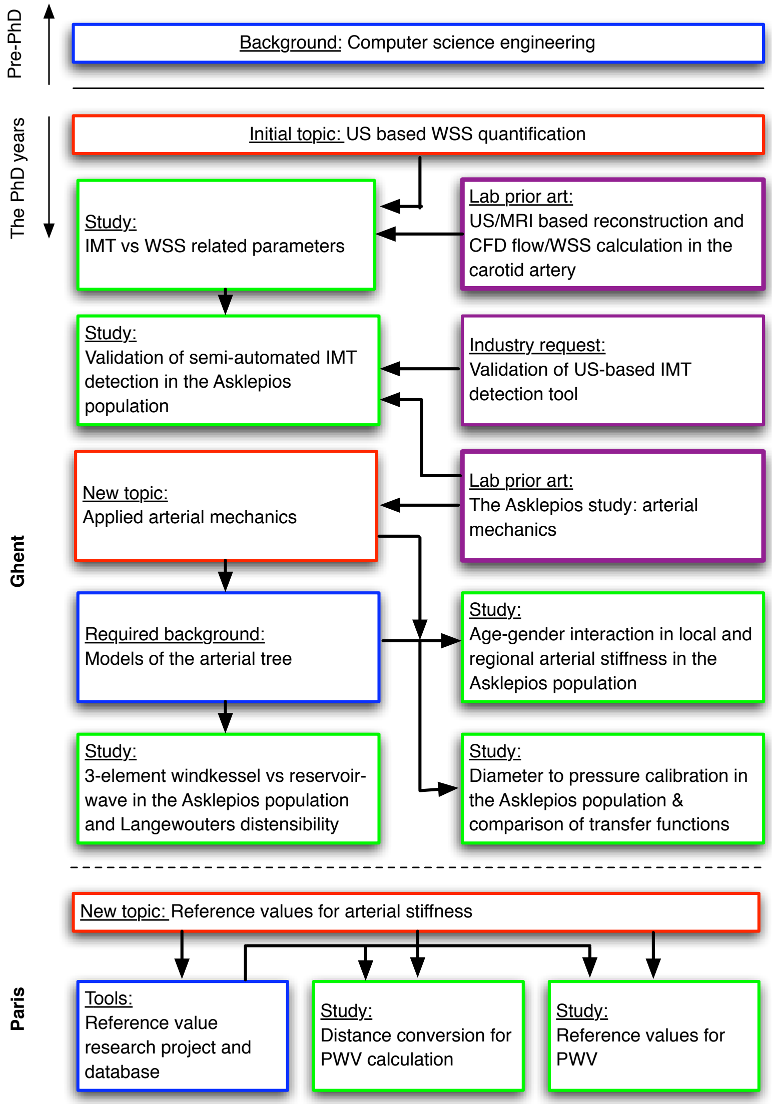
Pre-PhD
The PhD years
Ghent
Paris
Background: Computer science engineering
Initial topic: US based WSS quantification
Study: IMT vs WSS related parameters
Lab prior art: US/MRI based reconstruction and CFD flow/WSS calculation in the carotid artery
Study: Validation of semi-automated IMT detection in the Asklepios population
Industry request: Validation of US-based IMT detection tool
New topic: Applied arterial mechanics
Lab prior art: The Asklepios study: arterial mechanics
Required background: Models of the arterial tree
Study: Age-gender interaction in local and regional arterial stiffness in the Asklepios population
Study: 3-element windkessel vs reservoir-wave in the Asklepios population and Langewouters distensibility
Study: Diameter to pressure calibration in the Asklepios population & comparison of transfer functions
New topic: Reference values for arterial stiffness
Tools: Reference value research project and database
Study: Distance conversion for PWV calculation
Study: Reference values for PWV

FIGURE 2: PhD flowchart

database and had by then at least seen lots of arteries on MRI and ultrasound images, I was lured into working on the Asklepios database and would never look back. The first study my promotor suggested, was to exploit the tonometry and diameter distension tracings at the carotid artery to investigate whether we could calibrate diameter curves into surrogate pressure curves. In parallel, as the pressure-diameter relationships all have some stiffness parameter included, I was looking into differences in these local carotid stiffness parameters with the regional 'gold standard' stiffness measure of PWV, and into gender effects of their changes with age.

Working on these topics, it was soon pretty obvious that having looked at lots of arteries, or more specifically at lots of images of arteries, would not be enough to properly investigate the issues at hand. If I was to get to the bottom of the age-gender and pressure-diameter studies, I would have to get down and dirty into arterial mechanics and arterial models. Fortunately, this happens to be my promotor's area of expertise. Unfortunately, being a good-for-nothing computer science engineer, mechanics were (and probably still are) not my strong suit. I thus spent considerable time learning the finer points of windkessel, wave and other models of the arterial tree. So much time in fact, it had to be justified by a proper study of its own, examining the difference between the three-element windkessel and reservoir-wave separation model on the Asklepios study database.

In the meantime, I was deemed sufficiently coherent to go present my work at various conferences. On a balmy summer day in June, having just used my 'PhD student's prerogative', skipping the morning sessions of the 2006 European Society of Hypertension conference to visit the Picasso exhibit at the Prado museum, fate would take its turn to determine the final leg of my PhD research. Joining my promotor somewhere in between the chocolate fountain and the Japanese sushi section of the scrumptious noon buffet, I was told two researchers in Paris were looking for a PhD-level student, preferably with some background in computer science and vascular mechanics, to help run a European project that was to set up a database for the determination of reference values for arterial stiffness. Of course, I had to go. During the final two years of my PhD research, I thus helped formalize the research proposal and data collection for this European database and got to work on the largest project presented in this manuscript: the determination of reference values for pulse wave velocity, which for all intents and purposes represents my crowning achievement.

Perhaps it is a flaw of mine, or maybe it is related to my limited biomedical background at the start of my research career, in any case one of my major disappointments over the course of the past years has been that I always felt I lacked some well defined end-goal. I never did feel like there was some master plan to all I was doing, with well-defined landmark steps I was set to take on the way to scientific enlightenment. Now, having the advantage of hindsight, I'm not so sure I was right to question the existence of this well-defined end goal so fiercely. If one thing should be clear from the 'historical' outline of my PhD research, it is that while I may have never felt there was a master plan, there always was some sort of natural flow of what to do next, in no small part due to the gentle (and sometimes not so gentle) prods of my supervisors along the way, putting me on the right track. As such, almost to my own surprise, I now truly feel the present manuscript represents a coherent block of research, of which its constituent parts do not just represent individual research questions but also essential building blocks I needed to pick up along the way.

STRUCTURE

To help structure the different topics broached in this manuscript, and more importantly, to facilitate writing it, the present manuscript has been subdivided into five parts. The first part contains a single chapter discussing the basics of cardiovascular anatomy and physiology, introducing a number of concepts which are important to understand the contents of the following chapters. The middle three parts bundle all of the actual research performed over the course of my PhD. Each of these parts contains an introduction, introducing important concepts specific to that part, one or more chapters representing an individual study answering some research question and an outline linking the different research questions together. Finally, all conclusions are summarized in the final part, representing the overall conclusion of this manuscript.

For the casual reader, I suggest glancing over the first chapter to see if any of the concepts introduced are completely new, before reading the 'outline' chapters of each of the three middle parts. These chapters briefly summarize the main objectives of all of the studies performed over the course of my PhD, allowing you to quickly identify which are of interest to you. Finally, if you're the kind of person that reads books memento-style, starting with who's done it and gradually working your way backward to see why, feel free to peruse the final part summarizing all of the conclusions made throughout this manuscript. Then read up on those chapters whose conclusions you disagree with.

LIST OF PUBLICATIONS

When my supervisor told me at the beginning of my research career about this whole 'publish or perish' thing, I thought he was being literal. So from early on, I was very motivated to write down as much as possible and get it out there. Unfortunately, I'm a slow starter and I don't like writing papers very much. Also, it turns out many of this world's publishers would just as much like seeing me perish, as they kept sending back my initial paper submissions. I'm fairly sure the problem was not quality related, as each and every editor answered me personally, ensuring me that my work was indeed of considerable interest, but that they had just run out of trees for making paper that very month and could not possibly fit me in with all the other equally worthy submissions they had already accepted before I even submitted my manuscript. They went on, practically begging me to try resubmit something else at a later date, and to please, please, please attempt submitting the manuscript somewhere else, even going so far as to include lengthy lists of changes they thought would increase my odds at getting in.

The tree shortage lasted over a year, and even then I had to shorten my first paper to a technical note for someone to have enough paper to spare to publish it. Nevertheless, submit I did, and since no PhD manuscript would be complete without a proper listing of everything I leave for posterity at this stage, I include here a listing of all published and accepted papers, as well as those currently under review or in process of getting submitted.

First author

- Vermeersch SJ, Rietzschel ER, De Buyzere ML, Van Bortel LM, D'Asseler Y, Gillebert TC, Verdonck PR, Segers P. *Validation of a new automated IMT measurement algorithm.* J Hum Hypertens, 21(12):976–8, 2007.

- Vermeersch SJ, Rietzschel ER, De Buyzere ML, De Bacquer D, De Backer G, Van Bortel LM, Gillebert TC, Verdonck PR, Segers P. *Age and gender related patterns in carotid-femoral PWV and carotid and femoral stiffness in a large, healthy, middle-aged population.* J Hypertens, 26(7):1411–9, 2008.

- Vermeersch SJ, Rietzschel ER, De Buyzere ML, De Bacquer D, De Backer G, Van Bortel LM, Gillebert TC, Verdonck PR, Segers P. *Determining carotid artery pressure from scaled diameter waveforms: comparison and validation of calibration techniques in 2026 subjects.* Physiol Meas, 29(11):1267–80, 2008.

Accepted for publication

- Vermeersch SJ, Rietzschel ER, De Buyzere ML, Van Bortel LM, Gillebert TC, Verdonck PR, Segers P. *The reservoir pressure concept: the 3-element windkessel model revisited? Application to the Asklepios population study.* Accepted for publication in J Eng Math.

Submitted for publication

- Vermeersch SJ, Rietzschel ER, De Buyzere ML, Van Bortel LM, Gillebert TC, Verdonck PR, Laurent S, Segers P, Boutouyrie P. *Influence of distance measurements on the assessment of carotid to femoral pulse wave velocity.* Submitted to J Hypertens.

To be submitted

- The Reference Values for Arterial Stiffness' Collaboration. *Reference values for carotid-femoral pulse wave velocity.*

Co-author

- Claessens TE, Georgakopoulos D, Afanasyeva M, Vermeersch SJ, Millar HD, Stergiopulos N, Westerhof N, Verdonck PR, Segers P. *Nonlinear isochrones in murine left ventricular pressure-volume loops: how well does the time-varying elastance concept hold?* Am J Physiol Heart Circ Physiol, 290(4):H1474–83, 2006.

- Segers P, Rietzschel ER, De Buyzere ML, Vermeersch SJ, De Bacquer D, Van Bortel LM, de Backer G, Gillebert TC, Verdonck PR, Asklepios investigators. *Noninvasive (input) impedance, pulse wave velocity, and wave reflection in healthy middle-aged men and women.* Hypertension, 49(6):1248–55, 2007.

- Boutouyrie P, Vermersch S, Laurent S, Briet M. *Cardiovascular risk assessment through target organ damage: role of carotid-femoral pulse wave velocity.* Clin Exp Pharmacol Physiol, 35(4):530-3, 2008.

- Boutouyrie P, Briet M, Collin C, Vermeersch S, Pannier B. *Assessment of pulse wave velocity.* Art Res, 3(1): 3–8, 2009.

Accepted for publication

- Segers P, Kips J, Trachet B, Swillens A, Vermeersch SJ, Mahieu D, Rietzschel ER, De Buyzere ML, Van Bortel LM. *Limitations and pitfalls of non-invasive measurement of arterial pressure wave reflections and pulse wave velocity.* Accepted for publication in Art Res.

To be submitted

- Rietzschel ER, De Buyzere ML, Gillebert TC, De Bacquer D, De Backer G, De Meyer T, Bekaert S, Cassiman P, Langlois M, Verdonck PR, Vermeersch SJ, Segers P. *Long term oral contraceptive use is an independent risk factor for arterial stiffening in the Asklepios population.*

One

Background

CHAPTER 1

The cardiovascular system

1.1 ANATOMY OF THE CARDIOVASCULAR SYSTEM

1.1.1 The circulatory system

The human circulatory system comprises the heart, blood, blood vessels and lymphatic system. For descriptive purposes the lymphatic system, consisting of the lymphatic nodes and vessels transporting the lymph, can be viewed seperately from the cardiovascular system, comprising the blood, heart, arteries and veins, though in reality both are intimately connected.

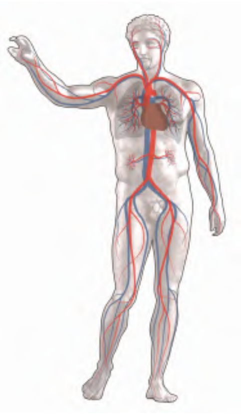

FIGURE 1.1: The human blood circulatory system.

At the center of the cardiovascular system lies the heart which works as a pump that pumps blood to the organs, tissues and cells scattered throughout the body. An average adult contains roughly 5 litres of blood, which consists of plasma, red blood cells, white blood cells and platelets. To reach every corner of the human body, the blood is transported from the heart through an intricate network of arteries, arterioles and capillaries to deliver oxygen and nutrients to every cell and to remove the carbon dioxide and waste productes generated from those cells. Finally, it is transported back to the heart by a network of venules and veins. From the arteries over the arterioles to the capillaries, venules and veins, the cardiovascular system provides a huge and fine-grained network with enormous ramifications in size. If all the vessels in the human body were to be laid end-to-end, they would on average extend for more than 96,500 km—or more than twice the circumference of the planet earth. Figure 1.1 on the previous page illustrates the human cardiovascular system: blue lines indicate the venous system; red lines the arterial system.

The circulatory system can be further subdivided into the systemic and pulmonary circulations. The systemic circulation transports blood from the heart to all organs in the body except the lungs and returns deoxygenated blood to the heart. The pulmonary circulation on the other hand, carries oxygen-depleted blood from the heart to the lungs, where it is reoxygenated and then carries the newly oxygenated blood back to the heart. Though arteries are often defined as those vessels carrying oxygenated blood and veins as those vessels carrying deoxygenated blood, this is not the case for the pulmonary circulation. Arteries must therefore more correctly be defined as those vessels carrying blood *from* the heart, while veins are those vessels returning blood *to* the heart.

1.1.2 The heart

The heart is a hollow muscle roughly the size of a human fist, measuring in the adult about 12 cm in length, 8 to 9 cm in breadth at its broadest part and 6 cm in depth. In a normal, healthy inidivual it weighs about 280 to 340 g in men and 230 to 280 g in women. By the end of a long life, the heart may have pumped about 7,600 l of blood through the circulation, and in doing so averages about 100,000 beats per day potentially adding up to over 3.5 billion heart beats in a lifetime.

The heart lies in the chest cavity between the lungs and is enclosed by a double-walled sac, the pericardium. It lies asymetrically behind the sternum (breast bone) and rib cartilages, projecting further into the left half of the thorax than the right, so that about two thirds of its mass is situated on the left half of the median plane, and one third on the right half (figure 1.2 on the facing page).

The human heart consists of four chambers. It is divided into right and left halves by septa and each half is further subdivided into two cavities: the upper parts called the atria and the lower parts called the

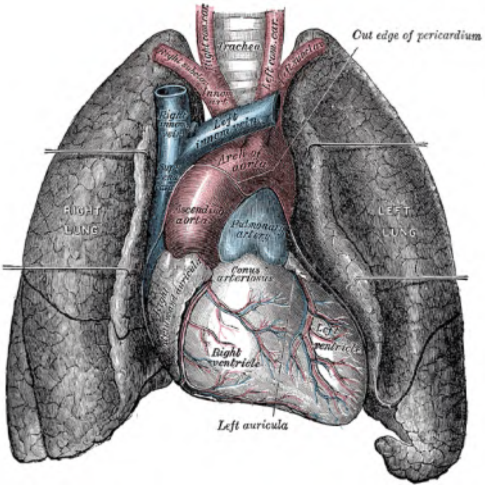
Cut edge of pericardium
Trachea
Right com. car.
Left com. car.
Right subclav.
L. subclav.
Innom. art.
Right innom. vein
Left innom. vein
Arch of aorta
Ascending aorta
Pulmonary artery
RIGHT LUNG
LEFT LUNG
Conus arteriosus
Right auricula
Right ventricle
Left ventricle
Left auricula

FIGURE 1.2: Front view of heart and lungs [1].

ventricles. The right half of the heart contains the venous or deoxygenated blood, the left part the arterial or oxygenated blood. Blood arriving from the systemic or pulmonary circulation is received in the atria and distributed to the arteries by the ventricles. The direction of blood flow through the four chambers of the heart is illustrated in figure 1.3 on the next page.

For the heart to function properly, it is of vital importance that flow through the heart chambers is unidirectional. To achieve this unidirectional flow, the heart is equipped with four heart valves: two atrioventricular valves, preventing blood from flowing from the ventricles into the atria and two semilunar valves, preventing blood flow from the arteries back into the heart. The veins injecting blood into the heart are not equipped with valves. Figure 1.4 on page 7 shows the location of the four heart valves in the human heart.

1.1.3 The vessels

The vessels transporting blood from the heart to the various organs in the body and back to the heart undergo tremendous changes in both size and composition throughout the arterial tree. Depending on their size, structure and function, vessels are categorized as arteries, arterioles, capillaries, venules and veins. Some physical characteristics of the vessels in each of these categories are summarized in table 1.1. It

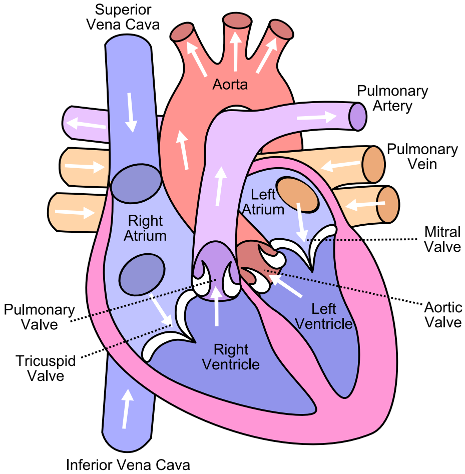
Superior Vena Cava
Aorta
Pulmonary Artery
Pulmonary Vein
Left Atrium
Right Atrium
Mitral Valve
Aortic Valve
Pulmonary Valve
Left Ventricle
Tricuspid Valve
Right Ventricle
Inferior Vena Cava

FIGURE 1.3: Schematic anterior (front) view of the open heart. White arrows indicate normal blood flow.

should be pointed out that there are no clear-cut boundaries in the arterial tree where one vessel type stops and another begins. In reality the vasculature gradually evolves from one type to the next.

TABLE 1.1: Structural characteristics of the vascular system[2, 3]

	Arteries		Arterioles
	Elastic	Muscular	
Internal diameter	1.5 cm	6.0 mm	37.0 μm
Wall thickness	1.0 mm	1.0 mm	6.0 μm
Number	~160		$\sim 5 \cdot 10^7$
Total cross-sectional area	~25 cm^2		~400 cm^2
	Capillaries	Venules	Veins
Internal diameter	9.0 μm	20.0 μm	5 mm
Wall thickness	0.5 μm	1.0 μm	0.5 mm
Number	$\sim 10^{10}$	$\sim 10^8$	~200
Total cross-sectional area	~4,500 cm^2	~4,000 cm^2	~60 cm^2

In spite of these vast differences in size, structure and function, arteries and veins have the same basic three-layered structure. Viewed from this three-layered structure, the main difference between arteries and veins lies in the relative weakness of the middle layer in the latter

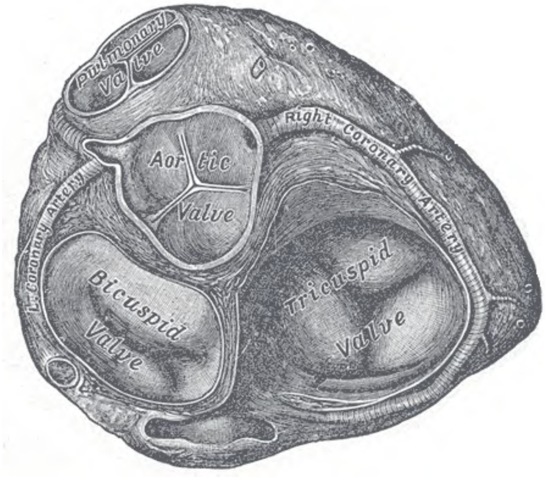

FIGURE 1.4: Section of the heart showing the four heart valves obtained by removal of the atria [1].

(figure 1.5 on the next page). These three layers of the arterial and venous vessels walls are:

- The *tunica intima* or internal or endothelial layer consisting of a single layer of endothelial cells and subendothelial layer of connective tissue interlaced with a number of circularly arranged elastic bands called the elastic lamina.
- The *tunica media* or middle or muscular layer. This layer accounts for most of the vessel wall thickness and consists of elastic fibres interlaced with vascular smooth muscle cells arranged in lamellae and disposed circularly around the vessel. With increasing size of the vessel, the number of layers of lamellae increase with the smallest arteries having only a single layer while slightly larger arteries have three or four layers. In the largest arteries the amount of elastic tissue is considerable, extending over multiple layers. The vascular smooth muscle cells influence the diameter of the vessel.
- The *tunica adventitia* or external layer consisting mostly of connective tissue. In all but the smallest of arteries this layer also contains elastic tissue. Finally, this layer also contains the nerves supplying the vascular smooth muscle cells of the tunica media as well the blood vessels supplying nutrients to the larger vessels, the vasa vasorum.

Capillaries consist of a single layer of endothelium and occasional connective tissue.

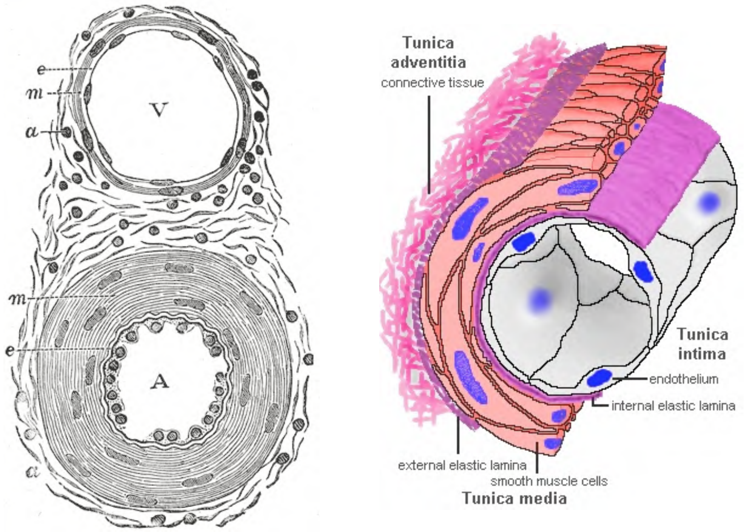

Figure 1.5: Left: Transverse section through a small artery and vein. A: artery; B. vein, both consisting of *e*: the tunica intima consisting of an layer of endothelial cells; *m*: the tunica media showing the nuclei of the vascular smooth muscle cells; *a*: the tunica adventitia [1]. Right: detail of the three layers of the arterial wall.

Arteries are thick-walled vessels, containing next to a substantial amount of smooth muscle, primarily elastin and collagen fibers. Arteries are further subdivided into elastic and muscular arteries. The elastic arteries are found closest to the heart and have the largest diameters. Their vascular smooth muscle is relatively inactive, so elastic arteries do not show much vasoconstriction. Primarily due to the large amount of elastin fibers, which can stretch under load to twice their unloaded length, elastic arteries can expand to temporarily store some of the blood ejected during systole. During diastole, this 'extra' blood is delivered to the organs by passive recoil of the elastic arteries. As such these arteries 'cushion' the arterial pulse and transform the pulsatile blood flow from the heart to a more continuous blood flow downstream. The aorta is the largest elastic artery, with a diameter of about 25 mm at the root to about 10 mm further downstream.

Further down the arterial tree, elastic arteries give way to the muscular arteries. These have the thickest media of all vessels, containing relatively the most smooth muscle cells and are much more active in vasoconstriction. Their internal diameter ranges from about 10 mm to 0.3 mm. The size of the arteries drops with every branching. At the same time, the consecutive branching pattern makes for an exponential increase in the number of arteries found further downstream. This means that while individual vessel diameters get increasingly smaller, the total cross-sectional area of all arteries also increases exponentially.

Arterioles are the smallest arteries and have a different structure. Their diameters range from 0.3 mm down to 10 μm. Proportionally, arterioles have much thicker walls than arteries, with more smooth muscle cells and less elastic material. The high number of muscle cells enables arterioles to actively regulate their diameter to change blood flow through the organs.

Capillaries are the smallest vessels in the arterial tree. Their diameters are so small, that even a single red blood cell (typical size about 7 μm) must deform to pass through them. Contrary to the other arterial vessels, capillaries do not contain smooth muscle cells and thus cannot change their diameter to regulate blood flow. They are also the most abundant of all vessels, with the total cross-sectional area of all capillaries typically exceeding by about 1,000 times the cross-sectional area of the root of the aorta.

Compared to arteries, venous blood vessels have very thin walls in proportion to their diameters. The walls of the venous vessels contain smooth muscle cells, so their diameters can actively change. Venous vessels are subdivided into venules and veins. The venules are the smallest, with diameters ranging from 8 to 100 μm. The complete venous system typically contains over 50% of the total blood volume and changes in venous volume play an important role in controlling cardiac output.

1.2 CARDIOVASCULAR PHYSIOLOGY

1.2.1 Homeostasis and the cardiovascular system

In 1865 the French physician Claude Bernard[1], often referred to as the father of physiology, wrote: *"La fixité du milieu intérieur est la condition d'une vie libre et indépendante"*, thus establishing the concept of biological homeostasis. In short, homeostatis implies that all organisms constantly strive to maintain the optimal internal condition required for survival of the organisms and to prevent external conditions from upsetting them. To do so, a range of dynamic equilibrium adjustment and regulation mechanisms are continously actively regulating all important biological parameters, be it blood pressure, core temperature, pH levels and many others, in order to maintain them at stable, constant levels. The cardiovascular system provides the body with a transport network by which these processes are maintained.

---

[1] Claude Bernard (°July 12, 1813 – †February 10, 1878)

In the body of an average human weighing 70 kg about 60% of the total body weight—or about 45 l—is accounted for by watery fluids. The sum of all the watery fluids present in the human body is called the total body water. The total body water is distributed over three compartments: the intracellular, interstitial and plasma compartment. Of these compartments, by far the most important is the intracellular compartment, alone accounting for 2/3 of the total body water, or about 30 l. Of the remaining fluids, only a small fraction is contained within the cardiovascular system, on average amounting to about 3 l. The remaining fluids, totalling about 12 l, are the interstitial fluids. These form the immediate environment in which the cells of the body live. The cells in our body, in maintaining their internal homeostatis, draw the nutrients required for their functioning directly from this interstitial fluid and in return dump their waste products into it. The transport mechanisms between the cells and their environment responsible for this exchange are mostly diffusion driven and thus depend on the concentration gradients across the cell membranes. To maintain cellular homeostatis therefore it is of vital importance to maintain the composition of the insterstitial fluid compartment.

If the interstitial fluid compartment were sufficiently large compared to the intracellular compartment to be seen as a virtually endless supply of nutrients and to be able to absorb virtually endless amounts of waste products without changing its composition, the diffusion mechanism between the cell and its environment would suffice for maintaining homeostasis. As stated before, however, the amount of interstitial fluids is actually about half the amount of intracellular fluids, so eventually the continuous uptake of nutrients from and the release of waste products into the interstitial compartment will alter its composition. This implies the interstitial fluids in turn need to somehow be kept at a constant composition by some other mechanism. Furthermore, since the process of diffusion is really only efficient at small distances, and given the fact that the exchange of nutrient components and waste products only happens at well defined locations like the lungs and intestines which typically are a large distance away from most of the cells in the human body, a system for transport of nutrients and waste products over these large distances is required. This transport task is performed by the cardiovascular system. Transfer between the interstitial fluid and the cardiovascular system is again mostly diffusion driven and occurs in the capillaries. In the vessels of the cardiovascular system, nutrients and waste products are transported by convection, i.e. as solutes in the blood, allowing to travel much greater distances than would be possible by diffusion alone. Since the transfer between capillaries and interstitial fluid is again diffusion and thus concentration driven, the interstitial fluid will strive to reach the composition of the incoming blood in the capillaries. To maintain homeostasis therefore, the composition of the incoming blood needs to be closely monitored to be that which is optimal for the interstitial fluid—and by extension for each individual cell. Furthermore, there must also be a sufficient amount of blood flow through the capillaries to ensure that the continuous uptake of nutrients and deposition of waste products does not alter the composition of the blood to the point where it disrupts homeostasis.

1.2.2 Functional arrangement of the cardiovascular system

In order to better understand how the cardiovascular system performs its task of transporting the nutrients and waste products between different sites in the body, figure 1.6 on the following page shows a schematic overview of the functional arrangement of the cardiovascular system. Note that the heart as an organ is represented by three different entities in this diagram: once as the left and right heart pumps and once as the heart muscle tissue since the heart itself of course also needs a constant supply of blood. The section of the diagram between right and left heart passing over the lungs represents the pulmonary circulation, the other section represents the systemic circulation, as previously defined.

Though figure 1.6 is a rather crude representation of the cardiovascular system, it does illustrate a number of its most important properties. First, note that the systemic and pulmonary circulations are arranged in series. This means that the blood volumes pumped by the left and right hearts must at all times be equal. The amount of blood pumped by the heart per minute is called the *cardiac output* (CO). The normal cardiac output of an average resting person usually lies somewhere between 5 and 6 l/min. The other organs in contrast, are arranged in parallel. This parallel structure of the organs of the body has two important implications. Firstly, this organisation ensures that all

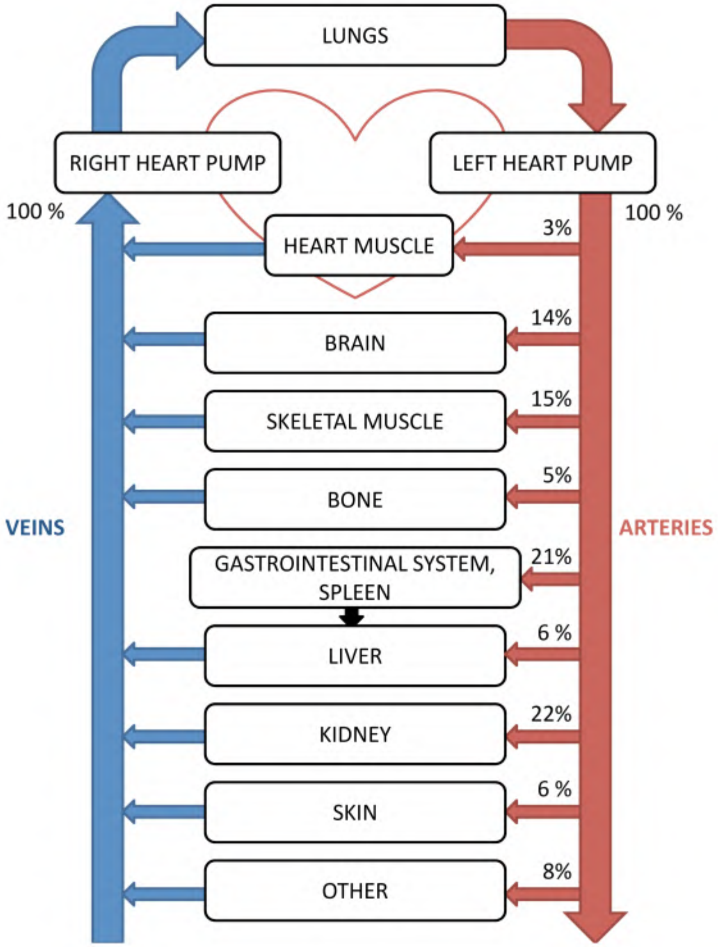
LUNGS
RIGHT HEART PUMP
LEFT HEART PUMP
100 %
100 %
HEART MUSCLE
3%
BRAIN
14%
SKELETAL MUSCLE
15%
BONE
5%
VEINS
ARTERIES
GASTROINTESTINAL SYSTEM, SPLEEN
21%
LIVER
6 %
KIDNEY
22%
SKIN
6 %
OTHER
8%

Figure 1.6: Functional view of the cardiovascular system indicating the distribution of the cardiac output in an average resting individual.

organs receive blood of equal composition. Were the arrangement in series, the organs at the end of the chain would receive blood in which a potentially significant amount of nutrients had been depleted and/or a significant amount of waste products deposited. This in turn could affect the homeostatic state of the cells at the end of the chain, as explained above. Secondly, it also means that blood flow through any organ can be regulated independently of all other organs. The blood flow requirements of the organs are not constant, and depend on a number of factors like the physical activity of a person. If the organs were arranged in series, restricting or increasing blood flow through a single organ would imply an equal increase or decrease in all other organs.

Many organs mentioned in figure 1.6 serve to recondition the blood. The most important organs involved in reconditioning blood are those which are in contact with the environment, especially the lungs. As illustrated in figure 1.6 after each passage of the blood through one of the systemic organs, it is returned to the lungs for reconditioning. The blood gas composition is thus constantly kept constant. Other organs, like the kidneys, also recondition the blood, yet are arranged in such a way that not all the blood passes through them each time it completes a complete circuit. Nevertheless, since the blood components move freely in the blood and through the vessel walls to the interstitial and intracellular environment, they still contribute to keeping the internal environment in homeostasis. This is only possible if they receive a sufficiently large part of the blood at each passage through the cardiovascular system. Note for instance the relative importance of the percentage of cardiac output passing through the kidneys, which in normal circumstances amounts to about one fifth of the total cardiac output. Since blood conditioning organs typically receive much more blood than is strictly required for their functioning, they are very resistant to large temporary reductions in blood flow through them. This means that for instance in extreme circumstances like severe cold or during exercise, flow can be reduced to conserve body heat or redirected to other organs.

Next to blood conditioning organs there are also organs which only receive blood flow for their functioning, like the skeletal muscles or the brain. In general, these organs are much more susceptible to reductions in blood flow. In fact, any flow reduction in these organs will lead to loss of function. For the heart and brain for instance, normal blood flow is only slightly in excess of the minimal blood flow required for their function. Reduction of flow and loss of function can for these organs quickly be fatal. The cardiovascular system therefore puts a very high priority in preserving blood flow to these organs.

1.2.3 Blood flow physics

The human body constantly needs to adapt to the changing blood flow requirements in its organs and tissues, be it due to changes in its environment or changes in physical activity. To do so, it can either increase the total cardiac output, or change the way in which the blood flow is distributed over the body. To understand which factors the body can influence to adapt blood flow, it is helpful to consider the basic physics of blood flow through a straight tube.

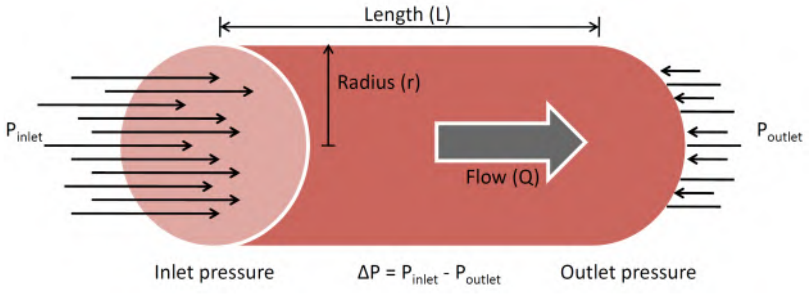

Figure 1.7: Factors influencing blood flow through a tube.

Figure 1.7 illustrates the different elements influencing blood flow through a straight tube. For any given tube segment of length L with radius r experiencing a pressure difference $\Delta P = P_{inlet} - P_{outlet}$ between the inlet and outlet planes, the flow (Q) through the tube is given by the *basic blood flow equation*:

$$Q = \frac{\Delta P}{R} \tag{1.1}$$

where

Q: Flow rate $[\frac{\mathrm{m}^3}{\mathrm{s}}]$
ΔP: Pressure difference [mmHg]
R: Resistance $[\frac{\mathrm{mmHg.s}}{\mathrm{m}^3}]$

For blood vessels, the resistance (R) is caused by the friction exerted by the stationary vessel walls on the moving fluid and is a measure of how difficult it is for the fluid to move through the tube. In the case of blood vessels, this resistance is also called the *vascular resistance*. It is worth noting that the use of equation 1.1 is not limited to flow through a single tube, but can by extension also be used to describe flow through complex networks of tubes: for any given combination of interconnected tubes, the total flow through the tubes is determined by the ratio of the pressure difference over the network over the resistance extexted by the total network.

Equation 1.1 illustrates a number of very important characteristics of flow through a tube. First and foremost: flow is only possible if a pressure difference exists between the in- and outlet planes of the tube. Additionally, equation 1.1 also clearly shows that increasing flow in any part of the arterial tree is only possible in one of two ways: either by increasing the pressure difference over that particular segment of the arterial tree, or by changing the vascular resistance of the segment in question.

The resistance exerted on a homeogeneous incompressible fluid by a circular straight tube is determined by a number of factors, including the radius (r) and length (L) of the tube and the dynamic viscosity of the fluid flowing through it (η):

$$R = \frac{8L\eta}{\pi r^4} \tag{1.2}$$

with

r: inner radius of the tube [m]
L: tube length [m]
η: fluid dynamic viscosity [Pa.s]

Note in particular the large influence of tube size on the resistance exerted by the tube. The presence of a fourth power on the radius term means that even small changes in tube diameter can have a large impact on total resistance.

Equations 1.1 and 1.2 combined yield the Hagen-Poiseuille[2] equation:

$$Q = \Delta P \frac{\pi r^4}{8L\eta} \tag{1.3}$$

describing all terms that influence flow of a incompressible homogeneous fluid through a straight cylindrical vessel.

Even though not all conditions for use of equation 1.3 (incompressible fluid, non-tapering tubes,...) are strictly met in the cardiovascular system, it does provide a useful approximation from which general conclusions regarding blood flow and pressure can be drawn. As for any complex network of tubes, the basic flow law remains valid in the cardiovascular system: flow is only possible under the influence of a pressure difference. Translated to the cardiovascular system the generation of this pressure difference is clearly the responsability of the heart: if the heart is unable to maintain a sufficiently large pressure difference over the arterial tree, flow through the organs will be compromised. Under normal circumstances, mean pressure in the arteries is about 100 mmHg, while mean pressure in the systemic veins is close to 0 mmHg. Blood flow through the organs can be approximated by the Hagen-Poiseuille equation (equation 1.3). This means that the only ways to change blood flow are to change blood pressures (increasing or decreasing the blood pressure difference) or by changing vascular resistance through (parts of) the cardiovascular system. Due to the parallel structure of the organs in the systemic circulation however, blood pressure differences across all organs are, in a crude approximation, about the same. This fact, coupled with the large influence of vessel diameter on vascular resistance indicates flow regulation through the organs is mostly achieved by changing the vascular resistance of the arterial network in the organs. Since blood flow, much like most PhD students, follows the path of least resistance, blood flow is the largest in organs with the lowest vascular resistance.

---

[2] named after Jean Louis Marie Poiseuille (°April 22, 1799 – †December 26, 1869), a French physician and physiologist and Gotthilf Heinrich Ludwig Hagen (°March 3, 1797 – †February 3, 1884), a German physicist and hydraulic engineer.

1.2.4 The heart pump

As outlined above, blood flow through the cardiovascular system is a passive process, which is completely driven by the pressure difference between the arteries and veins maintained by the pumping heart. This is true for both the systemic and pulmonary circulations: the left heart is responsible for maintaining flow in the systemic circulation, the right heart for maintaining flow in the pulmonary circulation.

The amount of blood pumped by the heart per minute, the cardiac output—which is identical for the left and right heart pumps—depends on the blood volume pumped per beat (stroke volume) and the number of heart beats per minute (heart rate):

$$CO = SV \times HR \tag{1.4}$$

with

CO: Cardiac output $[\frac{\mathrm{l}}{\mathrm{min}}]$
SV: Stroke volume [l]
HR: Heart rate [1/min]

This relationship shows that cardiac output can only change either due to a change in stroke volume, heart rate, or both.

The workings of the human heart when viewed as a simple pump can accurately be described by looking at the pressure, flow and volume changes within the heart during a complete cardiac cycle, defined as a complete contraction and subsequent relaxation of the heart muscle. The left hand panel of figure 1.8 illustrates these changes during one cycle for the left heart in a so-called Wigger's[3] diagram. The figure shows left ventricular pressure and volume, left atrial pressure and aortic pressure. The right hand panel of figure 1.8 shows a different representation of what happens during the cardiac cycle in a left ventricular pressure-volume diagram. Pressure-volume loops of the left ventricle are often used to study ventricular function. Pressure and volume changes for the right heart (right atrium and ventricle and pulmonary artery), while not depicted, are qualitatively very similar to those of the left heart. Furthermore the timings of the mechanical events in the right heart are also similar. The main difference between left and right heart is that the pressures in the left heart reach much higher levels than those in the right heart.

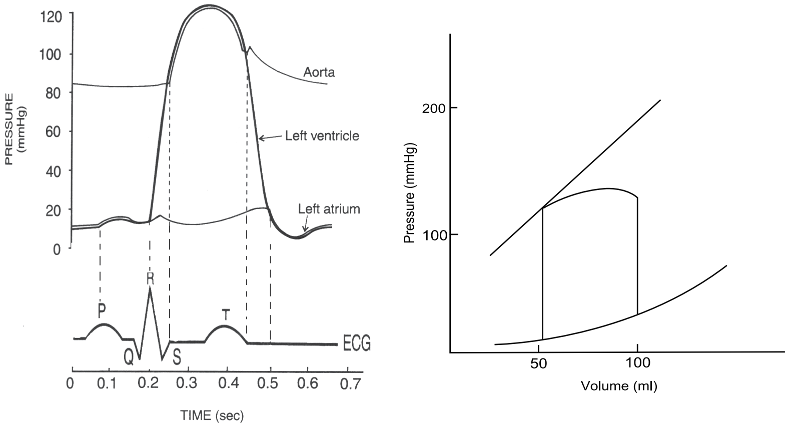

Figure 1.8: Left: Cardiac cycle of the left heart. Right: Pressure-volume loop of the left ventricle

The cardiac cycle can be subdivided into two different parts: systole and diastole. Systole refers to the contraction of the heart and accompanying ejection of blood from the ventricles. The remaining part of the cardiac cycle is the diastole which includes ventricular relaxation and filling.

---

[3] Carl J. Wiggers (°1883 – †1963), an American cardiovascular physiologist

1.3 THE ARTERIAL PULSE

1.3.1 Components of the arterial pulse

As the heart pumps blood into the aorta, the aortic pressure rises. The arterial pulse begins with the opening of the aortic valve at the time the left ventricle ejects its contents into the aorta. In the first stage of the arterial pulse, the aortic pressure rises quickly, as blood enters the aorta more quickly than it flows to the peripheral arteries. This rapid-rising section of the arterial pressure curve is called the *anacrotic limb*. The maximal aortic pressure following this ejection phase is called the *systolic blood pressure* (SBP).

After reaching this peak value, aortic pressure starts to decline, as the ejection of blood from the heart into the aorta slows down, and the outflow of blood to the peripheral vessels continues. The lowest pressure in the aorta, occurring just before the next release of blood from the heart into the aorta is called the *diastolic blood pressure* (DBP). The difference between the systolic and diastolic blood pressures is called the *pulse pressure*. The *mean arterial pressure* (MAP) is the geometric mean of the pressure over the entire cardiac cycle.

Blood pressures, which are a measure of lateral force per unit area of vascular wall are usually quantitated in *millimeters of mercury* (mmHg). One mmHg corresponds to about 133.3 Pa. Normal systolic blood pressures are below 120 mmHg and normal diastolic blood pressures 80 mmHg or less. Pulse pressures thus typically range between 40 and 50 mmHg. The different elements of the arterial pulse are illustrated in figure 1.9.

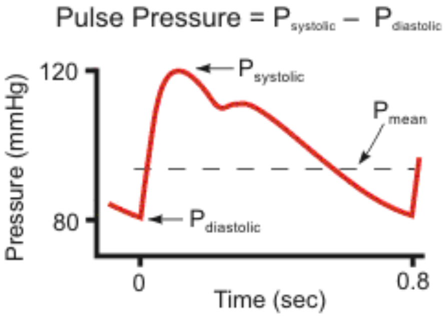

FIGURE 1.9: Main components of an arterial pressure waveform

1.3.2 Measuring the arterial pulse

Direct methods

The first direct measure of the arterial pulse was performed by Stephen Hales[4] in 1733. He cannulated a horse and used a blood-filled glass column to observe the rise and fall of the arterial pressure over the course of the cardiac cycle. Invasive measurements of arterial blood pressure remain the most accurate, and only direct means of measuring the arterial pulse. Rather than use a blood-filled glass column however, modern pressure transducers can either directly be inserted into arteries or veins or connected to the circulation through the use of catheters.

For the latter option, the catheters are filled with a saline solution, mechanically coupling the circulation to the arterial manometer. The pressure transducers record pressures by converting mechanical energy into an electric signal, which can be monitored. Pressures are calibrated using the atmospheric pressure as the zero-level and are referenced to the level of the heart by addition or subtraction of a gravitation factor. This gravitation factor is calculated as

$$gravitation\ factor = \rho g h \tag{1.5}$$

with

ρ: the density of blood
g: gravity constant, 9.8 m/s^2
h: the vertical distance between the transducer and the horizontal plane of the heart

Miniaturized manometers can also directly be attached to an intravascular catheter or needle, reducing the possibility of measurement errors linked to the indirect connection of the manometer to the circulation through the fluid-filled catheters.

Indirect methods

For routine clinical practice, arterial pressures are most commonly measured non-invasively. Since the invention of the pneumatic cuff manometer (Riva-Rocci, 1896) and the subsequent discovery and use of the so-called arterial sounds for detection of the systolic and diastolic blood pressures using this cuff manometer (Korotkoff, 1905), sphygmomanometry has become the most often used measure of arterial blood pressure. The indirect measurement of blood pressures through sphygmomanometry can introduce a number of measurement errors, linked to either improper calibration of the equipment used, inaccurate detection of the Korotkoff sounds or observer techniques, and can introduce an operator-dependence in the measurements. Furthermore, special care should be taken to use a proper cuff size depending on the arm circumference of the subject in which pressures are to be measured. Nevertheless, studies correlating direct and indirect blood pressures in the arm have, in general, shown good correlation between direct and indirect measurements.

---

[4] Stephen Hales (°September 17, 1677 – †January 4, 1761), an English physiologist

Sphygmomanometry is further limited to the requirement of being able to occlude the vessel in which pressure is to be measured. More recently therefore, an alternative technique for measuring local pressures has emerged. Arterial tonometry measures local pressure changes by flattening (applanating) the vessel in which the pressure is to be measured. The tonometer is equipped with a micromanometer at its tip, which measures the pressure changes in the flattened artery. Absolute pressure waveforms can be obtained from these relative pressure changes by proper calibration [4]. Figure 1.10 illustrates the tonometry setup used for the Asklepios study protocol at Ghent University.

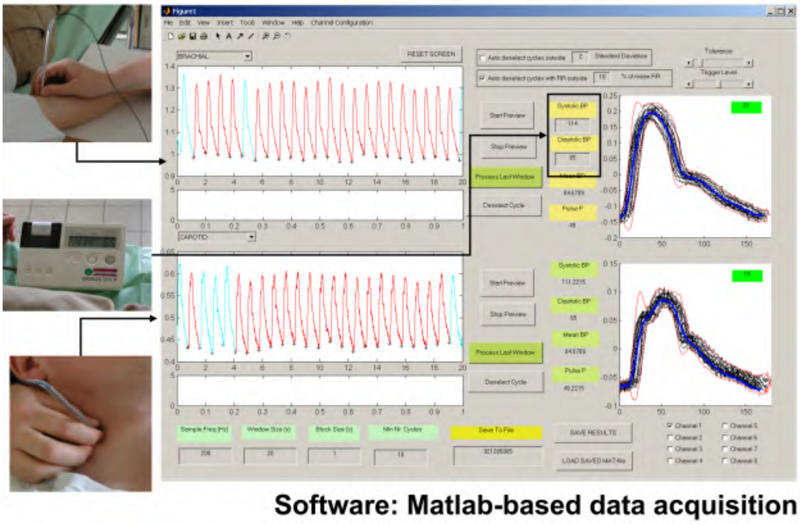
Figure1
File Edit View Insert Tools Window Help Channel Configuration
BRACHIAL
RESET SCREEN
CAROTID
Start Preview
Stop Preview
Process Last Window
Deselect Cycle
Systolic BP
Diastolic BP
Mean BP
Pulse P
Sample Freq (Hz)
Window Size (s)
Block Size (s)
Min Nr Cycles
Save To File
SAVE RESULTS
LOAD SAVED MAT-file
Software: Matlab-based data acquisition

Figure 1.10: The UGent tonometry hard- and software platform

1.3.3 Determinants of the arterial pulse

The pressure and flow in the arteries result from the interaction between the heart and the arterial system. Blood is pumped into the aorta by a driving force, the heart, against several forces that impede the flow of blood from the heart, which are all related in some way to each other. The driving force exerted by the heart depends on the contractility of the heart muscle, the size and shape of the left ventricle, the heart rate and the cardiac preload (the filling of the heart). The opposing forces impeding blood flow from the heart include resistance, inertia and compliance factors, all linked to properties of the arterial system.

As explained before, resistance is related to the blood viscosity and geometry of the vessels by the Hagen-Pouiseille equation. It is not affected by heart rate. Inertial effects and compliance (through viscoelastic behavior) however, are dependent on the heart rate. The dependence on heart rate of the inertia and compliance introduces phase shifts between pressure and flow waves in the system.

The properties of the heart and arterial system have a direct influence on the characteristics of the arterial pulse. Mean arterial pressure is determined by the cardiac output, the systemic vascular resistance (SVR) and the central venous pressure (CVP) by:

$$MAP = CO \cdot SVR + CVP \tag{1.6}$$

The central venous pressure is usually assumed to be zero or near to zero, so equation 1.6 can be simplified to:

$$MAP \approx CO \cdot SVR \tag{1.7}$$

For a given cardiac output, mean arterial pressure is thus mostly determined by the vascular resistance.

Pulse pressure is determined by the compliance of the aorta as well as the stroke volume. As stated above, during systole, the volume of blood expelled by the heart is initially larger than can immediately be drained to the distal parts of the arterial tree. As the heart is pumping this excess blood into the arterial tree, this excess blood is stored by an expansion in lumen diameter of the aorta. As the aorta expands, the increase from diastolic to systolic blood pressure is determined by the compliance of the aorta: a stiff aorta causes the pressure to rise quickly and markedly, as it offers more resistance to storing the excess blood, while a compliant aorta results in a smaller pressure increase. For a given stroke volume, the aortic stiffness is thus a major determinant of pulse pressure. Vice versa, for a given compliance, a larger ejected volume (stroke volume) will cause pressures to rise more markedly than for a smaller ejected volume [5].

1.3.4 The arterial pulse waveform

The pulse waveform observed at any site of the arterial tree is in fact the result of the composition of an incident wave, coming from the heart, and a reflected wave, which itself consists of the summation of a number of reflected waves originating at the different points of impedance mismatch along the arterial tree [6]. Typical discrete points of impedance mismatch are bifurcations, though the continuous increase of arterial stiffness along the arterial tree results in a continuous generation of reflected waves all along the arterial tree [7]. The speed with which the wave is moving from the heart to the periphery and back to the heart is called the pulse wave velocity, and is dependent on the stiffness of the arterial tree through the Bramwell-Hill equation. The stiffer the vessels, the faster the waveform will propagate. For stiffer vessels and higher pulse wave velocities, the reflected wave will return in systole, augmenting to the pressure of the incident wave, resulting in a higher systolic pressure. For compliant vessels, the reflected wave will only return in late systole to early diastole.

To study the effects of wave reflection, the arterial pulse waveform can be examined in the time domain or the frequency domain. For the latter, the pulse waveform is decomposed in a number of sinusoidal waves (called harmonics) using Fourier theory. These individual harmonics can than be used to calculate the impedance of the arterial tree, which is the measure of resistance of the system to arterial flow.

The shape of the arterial pulse is not constant throughout the entire arterial network. From central to peripheral vessels, the shape of the pulse waveform changes depending on for instance the stiffness and size of the arteries and the location of the measurement point with respect to the reflection sites. In general, arterial stiffness increases from the central to the peripheral vessels, causing the ascending limb of the pulse wave to become steeper and the systolic pressure to become higher.

1.4 CARDIOVASCULAR RISK

Cardiovascular disease is, in the Western world, still the number one cause of death. While any individual may develop cardiovascular disease, it has long been known that the presence of certain conditions or behavior increases the likelihood of its development. Any condition that is associated with an increased risk of developing cardiovascular disease is called a *cardiovascular risk factor*. The relationship between

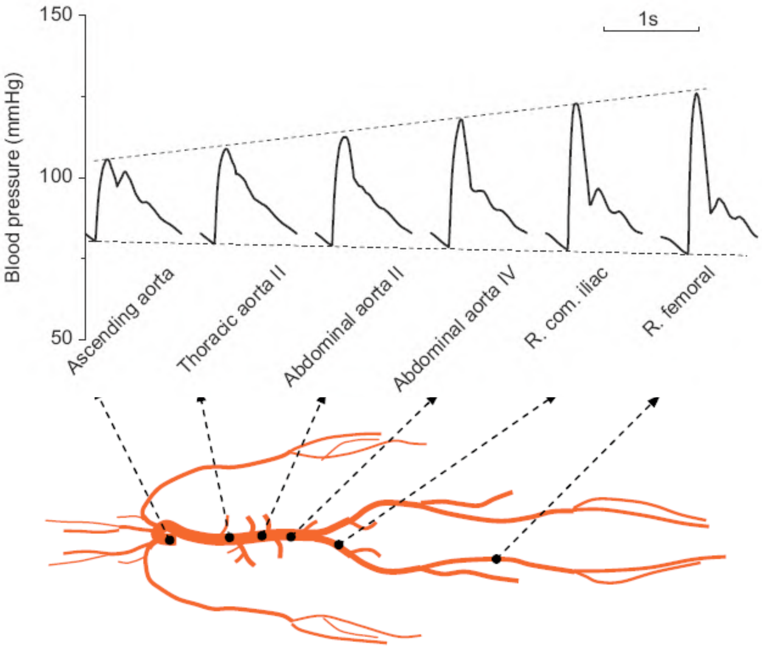

FIGURE 1.11: Pressure amplification of the arterial pulse from the central to the peripheral arteries [8].

these risk factors and cardiovascular disease is almost always a statistical one, which means that the mere fact of having one or more cardiovascular risk factors does not necessarily imply a certainty of developing cardiovascular disease. Conversely, not having any cardiovascular risk factor does not mean that one is safe from developing cardiovascular disease, just that the probability of developing cardiovascular disease is lower.

The decision of which factors are 'eligible' to be taken into account as a cardiovascular risk factor is based on the outcome of population studies. These are specially designed studies in which a group of people, whose composition is chosen to be representative of the population in which the risk factor is to be observed, is followed over time, to investigate whether in the long term a relationship can be found between the presence of a certain factor and the occurrence of cardiovascular disease (cfr. Framingham study, Rotterdam study, Asklepios study, etc…). To investigate the independent effect of the factors under consideration, the parameters are investigated using 'multivariate statistical analysis' techniques. Some risk factors are dichotomous: they are either present or absent. Examples of dichotomous variables are gender or family history of cardiovascular disease. Most parameters are, however, continuous: above a certain minimal threshold, the cardiovascular risk level rises as the strength or severity of the risk factor increases. For some continuous variables, cardiovascular risk increases only slightly or moderately below some threshold value, and increases sharply once the threshold value has been surpassed. Based on the results of these studies, guidelines can be drafted recommending treatment or lifestyle changes for subjects that are subjected to one or more cardiovascular risk factors.

While basing the decision to treat on these established threshold values for each of the cardiovascular risk factors separately certainly improves the odds of not getting cardiovascular disease, over the past decade, it has been recognized that often cardiovascular risk factors tend to cluster. This means that individual risk factors are rarely seen without the presence of one or more other risk factors. Coupled to the observation that the impact of multiple risk factors is at least additive and possible even multiplicative, this has lead to the concept of *total cardiovascular risk*. Rather than evaluate the risk for each of the risk factors separately, the concept of total cardiovascular risk takes into account that the true risk for getting cardiovascular disease for any given individual is in part determined by the number of risk factors present, as well as the level of each individual risk factor. This means that, for instance, someone suffering from mild hypertension and moderately elevated hypercholesterolemia, may be at greater risk than someone with an even higher blood pressure but normal serum cholesterol.

The most important risk factor for the development of cardiovascular disease is hypertension. There is a continuous relationship between blood pressure and the likelihood of developing cardiovascular or cerebrovascular disease. In addition, several intervention studies have shown that proper anti-hypertensive treatment significantly reduces the risk of the development of cardiovascular or cerebrovascular disease. Which other risk factors to take into account and how to use them to assess an individual's total cardiovascular risk varies between different guidelines. For the present manuscript, we will be working with the 2007 European Society of Cardiology / European Society of Hypertension guidelines for the management of hypertension [9]. These guidelines subdivide patients in terms of an approximate

10-year added risk of cardiovascular disease as low, medium, high or very high, according to the blood pressure levels and the presence of other cardiovascular risk factors, subclinical target organ damage or associated clinical conditions (figure 1.12).

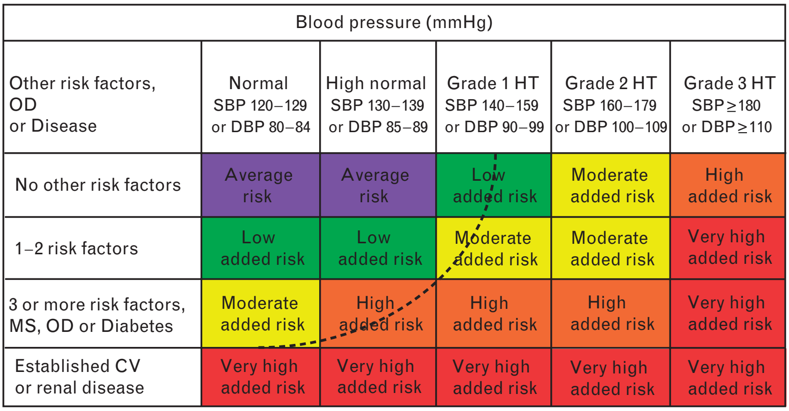

	Blood pressure (mmHg)				
Other risk factors, OD or Disease	Normal SBP 120–129 or DBP 80–84	High normal SBP 130–139 or DBP 85–89	Grade 1 HT SBP 140–159 or DBP 90–99	Grade 2 HT SBP 160–179 or DBP 100–109	Grade 3 HT SBP ≥ 180 or DBP ≥ 110
No other risk factors	Average risk	Average risk	Low added risk	Moderate added risk	High added risk
1–2 risk factors	Low added risk	Low added risk	Moderate added risk	Moderate added risk	Very high added risk
3 or more risk factors, MS, OD or Diabetes	Moderate added risk	High added risk	High added risk	High added risk	Very high added risk
Established CV or renal disease	Very high added risk	Very high added risk	Very high added risk	Very high added risk	Very high added risk

FIGURE 1.12: Stratification of CV risk according to the 2007 ESC/ESH guidelines. SBP: systolic blood pressure, DBP: diastolic blood pressure, CV: cardiovascular, HT: hypertension. Low, moderate, high, and very high risk refer to 10 year risk of a CV fatal or non-fatal event. The term 'added' indicates that in all categories risk is greater than average. OD: subclinical organ damage, MS: metabolic syndrome. The dashed line indicates how the definition of hypertension may be variable, depending on the level of total CV risk [9].

The consequences of cardiovascular disease are evident from the damage it causes to certain organs, like the kidneys or eyes. Subclinical target organ damage indicates the presence of damage in one of these target organs, before it would be considered a 'clinical case'. For instance, for the kidney, subclinical target organ damage could be the reduction of glomural filtration rate to a level which is not yet indicative of renal disease, but still lower than normal levels. One measure of target organ damage worth mentioning is the thickness of the carotid artery wall, usually expressed as the thickness of the intima-media layer (IMT). There is also a tendency to include arterial stiffening, as measured by carotid-femoral pulse wave velocity, as a measure of target organ damage.

Two

Carotid artery intima media thickness

Chapter 2

Outline

The first section of this manuscript focuses on two studies that were performed during the early stages of my PhD related to the measurement of carotid artery intima-media thickness (IMT) and its relationship to wall shear stress (WSS) related parameters.

Increased carotid artery intima-media thickness has been shown to be a predictor of both stroke and myocardial infarction [10–13], with a threshold value of 0.9 mm being indicative of subclinical organ damage, as outlined in the 2007 European Society of Hypertension and Cardiology (ESH and ESC) guidelines for the management of hypertension [9]. As such, carotid artery IMT is a parameter that is relatively routinely assessed in clinical practice and often reported in clinical research.

Thickening of the intima-media layer is one of the first signs of the onset of atherosclerosis. Though atherosclerosis can appear at any arterial location, some points in the arterial tree appear especially susceptible. These regions are typically found near bifurcations or arterial sections with pronounced curvature [14]. Those sites are characterized by the occurrence of complex blood flows, which are coupled to specific types of wall shear stress patterns. It has been proposed that the mechanisms of intima-media thickening are linked to areas influenced by these wall shear stress patterns, notably those areas which are subjected to low wall shear rates [15] or WSS [16], oscillating levels of WSS [17] or large wall shear stress angle gradients (WSSAG) [18].

Chapter 3 details the results of a pilot study leveraging existing numerically calculated WSS parameters in a small study population by investigating whether in this population a relationship could be found with IMT measured on black blood MRI (magnetic resonance imaging) images. Our research group has extensive experience in the reconstruction of patient-specific carotid artery bifurcations based on MRI and ultrasound imaging for the calculation of flow and WSS related parameters. In previous studies performed by Glor *et al.* [19–23], the accuracy and reproducibility of the MRI based reconstruction had been established. For several subjects, the reconstructed geometry and calculated flow and WSS patterns were available in conjunction with the original image sets that had been used for the reconstruction. The pilot project consisted of three components: (1) construct a tool to aid in the manual delineation of IMT on black blood (BB) MRI images; (2) perform an intra-and inter-observer variability study on the manual IMT delineation; and (3) match the measured IMT values to the previously obtained WSS related parameters and investigate whether a relationship between both could be identified. Its main goal was to determine whether the black blood MRI images provided sufficient resolution for the reliable determination and see whether in this small data set we could link certain types of WSS to measured IMT levels.

Chapter 4 outlines the results of a validation study in which a new semi-automated tool for the measurement of carotid IMT based on ultrasound images was compared to manually measured IMT on the same ultrasound images. As part of the Asklepios study protocol, one expert operator manually processed the ultrasound images of over 2,500 subjects to determine carotid IMT. Since IMT is a measure increasingly used in clinical practice over the past few years, several tools have emerged to aid in the detection of carotid IMT by providing (semi-) automated delineation of the intima-media and media-adventitia interfaces. Given the extensive, reliable data set of manual IMT measurements available in the Asklepios population, a research project was proposed to validate a new semi-automated tool provided by GE Healthcare Ultrasound, on a subset of the Asklepios data. The project consisted of three components (1) re-perform the manual measurements on a subset of the Asklepios data to assess the inter-observer variability of the manual measurements; (2) perform the automated measurements; and (3) compare inter- and intra-observer variability of and the difference between the manual and automated IMT measurements. The results of this study were published in:

S.J. Vermeersch, E.R. Rietzschel, M.L. De Buyzere, L.M. Van Bortel, Y. D'Asseler, T.C. Gillebert, P.R. Verdonck, P. Segers. *Validation of a new automated IMT measurement algorithm.* J Hum Hypertens, 21(12):976-8, 2007.

Chapter 3

Carotid intima media thickness and wall shear stress

3.1 Introduction

The combined thickness of the intima and media layers (see section 1.1.3 on page 5) of an artery is generally called the intima-media thickness (IMT). Increased carotid artery intima-media thickness has been associated with cardiovascular disease and is regarded as an early marker of atherosclerosis as shown in cross-sectional and longitudinal studies [13, 24–27]. As a consequence there has been considerable interest in IMT measurements on arteries, especially in the carotids, both based on magnetic resonance imaging (MRI) as well as ultrasound imaging (US). Concurrently, pathological studies have shown that IMT thickening is linked in some way to a number of hemodynamic parameters. It has for instance been shown that intimal hyperplasia occurs preferentially in zones with 'disturbed' wall shear stress (WSS), particularly those zones with low and oscillatory wall shear stress [28].

In this study we will investigate potential relationships between carotid artery intima media thickness and wall shear stress related parameters. Intima media thickess will be assessed by manual delineation on black blood (BB) MRI images; WSS and WSS related parameters had previously been calculated through numerical computation based on MRI image-based reconstructed geometries.

3.2 METHODS

3.2.1 Study population

Subjects were drawn from a database previously established for a different protocol [19] in which reconstructed geometries had been established and flow and WSS related parameters had been calculated. A total of eight patients (five men / three women) with untreated hypertension (office systolic blood pressure 150-200 mmHg and/or diastolic blood pressure 90-120 mmHg) were included in the present analysis. Subjects did not have atherosclerotic plaque in the carotid artery.

3.2.2 MRI imaging

Black blood MRI images had been obtained in all included subjects. Black blood MRI is an imaging technique specifically designed to eliminate the signal of (fast flowing) blood in an MRI image. In a typical MRI image, flowing blood is bright and is poorly differentiated from the surrounding tissue. The BB MRI imaging sequence has been described by Song *et al.* [29] and is based on a specific sequence of spin inversion pulses prior to the imaging pulse. A first pulse is emitted throughout the volume of interest, inverting all the spins within that volume. A second slice selective pulse is emitted immediately after the first pulse and realigns the magnetization vector in a specific slice of interest. In the rest of the imaged volume, the spins remain inverted. Within the slice of interest blood that has been realigned by the second pulse will gradually be replaced by blood that has only been affected by the first pulse. For stationary tissue, the net magnetization however remains aligned. When an image is finally made, the blood in the imaged slice will appear black, while the vessel wall is bright. A typical example of a BB MRI image is shown in figure 3.1 on the facing page.

The imaging protocol has previously been described [19, 30]. Briefly, subjects were scanned while lying supine in a Siemens Magnetom Sonata 1.5 T scanner. A head/neck supporting device was used to maintain consistent position. For each subject, ECG-gated images were acquired at mid-to-late diastole. Each image acquisition sequence took 3 to 5 minutes, depending on the subject's heart rate.

Next to the BB MRI images, cine phase contrast (PC) images were also obtained at the in- and outlet of the imaged section of the carotid arteries. The term 'cine PC imaging' refers to a family of MRI imaging techniques specifically designed to have a controlled sensitivity to flow. Using velocity encoding techniques blood velocities in voxels in

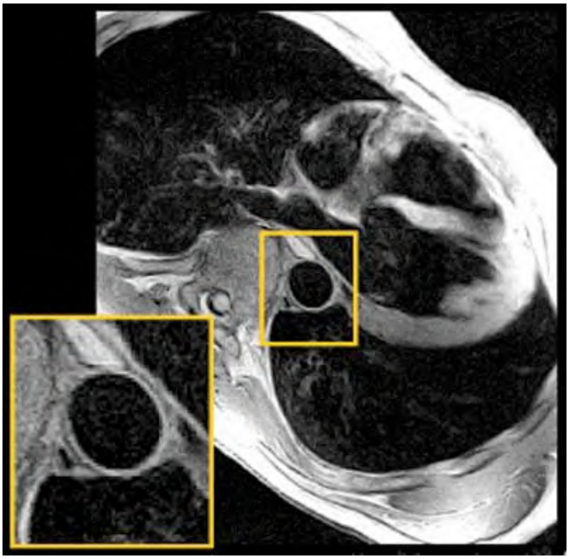

FIGURE 3.1: Typical black blood MRI image of an aorta

an entire cross-section of the artery can be obtained in all three dimensions. The term 'cine' refers to the fact that a number of images can be obtained during one cardiac cycle. When these images are displayed consecutively, they give the impression of a moving fluid.

3.2.3 Geometry reconstruction and calculation of WSS parameters

The obtained MRI images were used both to reconstruct the subject's carotid artery geometry for processing in a CFD package and, at a later stage, for manual IMT delineation. Carotid arteries had previously been reconstructed and flow and WSS parameters had been calculated, using an approach previously published [19, 30]. Briefly, the obtained BB MRI images were segmented semi-automatically in three steps. First, an initial contour was generated with the region growing method described by Long *et al.* [31] for time-of-flight MRI images. Next, a so-called snake model was used to deform and smooth the initial contour. Finally, the semi-automatically generated contour was visually checked and manually adjusted where appropriate. The serial 2D contours issuing from this first step were then aligned and smoothed to produce a 3D vessel surface geometry. This 3D volume was meshed using a custum built mesh generator [19, 30].

The measured flow at in- and outlet planes and the reconstructed geometry were then used to calculate pressure and flow in the reconstructed geometries using a numeric solver (CFX4, AEA Technology). A detailed description of the CFD methodology and the accuracy and reproducibility of reconstructed geometries and calculated flow has previously been described [19–23, 30, 32–34].

Based on the calculated flow profiles, the following WSS parameters were calculated:

Wall Shear Stress (WSS) As blood flows through a vessel, it exerts a physical force on the vessel wall. This force can be decomposed into two principal vectors. The tangential component of this force is the wall shear stress. It represents the frictional force exerted by the flowing blood at the endothelial surface of the vessel wall.

Mathematically, the instantaneous shear stress in laminar flow can be defined as:

$$\vec{\tau} = \mu \frac{\partial \vec{v}}{\partial y} \; [Pa] \tag{3.1}$$

with $\vec{v}$ the velocity vector, y the distance normal to the vessel wall and μ the dynamic viscosity

Oscillatory Shear Index (OSI) The oscillatory shear index is defined as follows:

$$OSI = \frac{1}{2} \left(1 - \frac{\left| \int_0^T \vec{\tau}\, \mathrm{d}t \right|}{\int_0^T |\vec{\tau}|\, \mathrm{d}t} \right) \; [-] \tag{3.2}$$

with T the duration of the cardiac period and $\vec{\tau}$ the instantaneous WSS as defined by equation 3.1. The OSI is zero when flow is unidirectional. For oscillating flow, the OSI will be between 0 and 0.5. Physically the OSI can be regarded as a weighted fraction of a cardiac cycle during which the instantaneous wall shear stress is in a different direction than the average direction of the WSS during that cycle. In other words the OSI is a shear stress-based measure that describes directional variation of blood flow. The higher the value of the OSI the more the direction of blood flow and thus shear stress varies.

Spatial Wall Shear Stress Gradient (WSSGs) The spatial wall shear stress gradient consists of the WSS components derived in space and averaged over a cardiac cycle:

$$WSSGs = \frac{1}{T} \int_0^T \sqrt{\left(\frac{\partial \tau_m}{\partial m} \right)^2 + \left(\frac{\partial \tau_n}{\partial n} \right)^2} \, \mathrm{d}t \; [Pa] \tag{3.3}$$

where τ_m and τ_n are the time-dependent components of the wall shear stress in the *mnl* coordinate system, where m is the temporal mean wall shear stress direction and n is the tangential to the surface and perpendicular to m.

Temporal Wall Shear Stress Gradient (WSSGt) The temporal wall shear stress gradient can be defined as:

$$WSSGt = \frac{1}{T}\int_0^T \left|\frac{\partial \vec{\tau}}{\partial t}\right| \mathrm{d}t \tag{3.4}$$

The WSSGt is simply the magnitude of the time-derived instantaneous WSS averaged over a cardiac cycle.

Wall Shear Stress Angle Gradient (WSSAG) Mathematically, the wall shear stress angle gradient can be defined as:

$$WSSAG = \frac{1}{T}\int_0^T \left|\frac{1}{A_i}\int_S \frac{\partial \phi}{\partial x}\,\mathrm{d}A_i\,\vec{i} + \frac{1}{A_i}\int_S \frac{\partial \phi}{\partial y}\,\mathrm{d}A_i\,\vec{j} + \frac{1}{A_i}\int_S \frac{\partial \phi}{\partial z}\,\mathrm{d}A_i\,\vec{k}\right| \mathrm{d}t \tag{3.5}$$

S represents the complete surface of the vessel wall and A_i is the surface of a cell face i. The WSSAG is calculated in an arbitrary coordinate system *ijk*. The scalar field of angular differences ϕ is defined as:

$$\phi = arccos\left(\frac{\vec{\tau}_i \cdot \vec{\tau}_j}{|\vec{\tau}_i|\,|\vec{\tau}_j|}\right) \tag{3.6}$$

where $\vec{\tau}_i$ refers to the wall shear stress vector at the location of interest and $\vec{\tau}_j$ represents the surrounding wall shear stress vectors. The WSSAG represents the magnitude of the wall shear stress angle deviation. Large WSSAG tend to occur in regions of dysfunctional endothelial cells, and hence sites of intimal hyperplasia.

3.2.4 IMT measurements

The black blood MRI images were also used for manual delineation of the IMT along the carotid arteries. BB MRI allows for more or less straightforward delineation of the lumen-intima and media-adventitia boundaries. For the manual delineation a custom software program was developed in Matlab R14SP2 (The Mathworks Inc, Natick, USA).

The user can load a set of BB MRI images obtained from a single subject as an AVI file in which each frame is one image in the image sequence. The contrast in these images is enhanced by transforming the grayscale of the original image to a colorscale. The user can specify a zoomed region of interest in each image, which is then blown up and again contrast enhanced. In each image the user can then select points where he or she believes the lumen-intima and intima-adventitia boundaries are located. Points must be placed in pairs (one on each boundary). The number of points to be set is not specified, though more points generally result in more accurate IMT measurements. If a user deems the quality of an image to be insufficient for placing points the slice can be skipped and will not be taken into account for further analysis. Finally the selected points can be exported in several data formats for further processing. Exported points can also be imported, for instance to continue working on a previously unfinished image set. Due to image quality constraints, IMT measurements were only performed in the common carotid artery (CCA) and internal carotid artery (ICA).

IMT is calculated from the selected data points during export and saved in a separate file. First the pixel distance between the set points is calculated and scaled to actual distances using scaling data obtained from the original DICOM images. In order to assign IMT values over the entire circumference of the vessel in a particular slice the actual measured IMT data are extrapolated. Each IMT measurement is assigned a polar coordinate in a polar axis system with origin in the center of the vessel and the IMT is calculated in fixed coordinates using spline interpolation of the measured values. These calculated IMT values are used for further analysis.

3.2.5 Matching IMT measurements to WSS parameters

To match the different WSS parameters to the calculated values for the IMT, the hemodynamic parameters and IMT values have to be known at the same location to allow for a point-by-point analysis. In order to match IMT values to hemodynamic parameter values a ‘patching’ technique was applied, as described by Thomas [35]. The patching technique is comprised of four steps. First, the carotid bifurcation is split into CCA, ICA and external carotid artery (ECA) sections. As we did not perform IMT measurements in the ECA, the WSS parameter values in the ECA were discarded. Then, the vessel is virtually ‘cut open’ and ‘unwrapped’, thus obtaining a flat irregular shape. Finally, this irregular shape is transformed into rectangles.

Using this approach, the vessel wall was divided into small rectangular patches along each slice. Each patch is assigned the average value of the shear stress parameter across its surface. Figure 3.2 shows a graphical representation of the result of the patching for the values of the OSI for one of the study subjects. A similar approach was applied to the measured IMT values. Extrapolated IMT values were averaged over the same patches and matched to calculated WSS parameter values. The segmented vessel was patched into nine evenly spaced (circumferentially) patches between each pair of measured slices. Interslice distance was 2 mm.

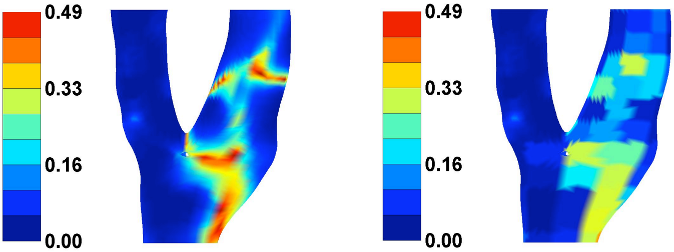

FIGURE 3.2: OSI distribution over a reconstructed geometry before (left) and after (right) patching

Values for the hemodynamic parameters had previously been calculated for each geometry. The manual IMT delineation was performed by two operators, each performing the same measurements on the same images twice.

3.2.6 Statistical analysis

Data are presented as mean (standard deviation). The relationship between each of the presented wall shear stress parameters and measured IMT will be investigated by regression analyses. Correlations will be determined for each of the parameters with IMT separately and taking into account age, systolic blood pressure (SBP), mean arterial pressure (MAP), pulse pressure (PP) and geometric parameters as co-variates. Data will be analyzed separately for the CCA and ICA. Additionally, the intra- and inter-observer variability of the manual IMT detection will be investigated by regression analysis and visually presented by Bland-Altman plots. The threshold for statistical significance was chosen as $P<0.05$ unless indicated otherwise. All statistical analyses were performed in SPSS 12.0 (SPSS Inc., Chicago, Illinois, USA).

3.3 RESULTS

General population descriptives are summarized in table 3.1

TABLE 3.1: Age and blood pressures in the study population

Age (years)	43 (35–52)
SBP (mmHg)	151 (14)
DBP (mmHg)	97 (10)
MAP (mmHg)	115 (11)
PP (mmHg)	55 (6)

3.3.1 Intra- and inter-observer variability

Figure 3.3 on the next page shows the Bland-Altman plot of repeated measurements for operator 1 (top panel) and operator 2 (bottom panel). Mean difference between measurements was -0.06 (0.12) mm and 0.02 (0.12) mm for operators 1 and 2, respectively.

Figure 3.4 on page 42 shows the Bland-Altman plot comparing measurements in the same subjects performed by operator 1 and 2. Mean difference between measurements was -0.02 (0.13) mm.

3.3.2 IMT and WSS related parameters

The top panel of figure 3.5 on page 43 shows a scatterplot of IMT versus WSS in the CCA. The data points shown represent the pooled data of all IMT measurements and calculated WSS values for all patches in the 8 included subjects. While the relationship between IMT and WSS is significant ($P<0.001$), its correlation coefficient is quite small ($R=0.23$). Furthermore, the scatterplot suggests neither IMT nor WSS to be normally distributed. As an illustration, figure 3.6 on page 44 (top panel) shows the distribution of WSS calculated in the CCA. Many different statistical tests—among which ANOVA—assume normally distributed data.

To correct for the non-normality of the data, and to potentially improve the regression analysis, data transformations can be applied to both IMT and WSS. Transforming the data means applying an appropriate transformation function to the data in order to change its distribution. One commonly applied transformation family is the family of power transformations, characterized by:

$$Y' = Y^{\lambda} \tag{3.7}$$

The proper value of the λ parameter can be determined by a procedure developed by George Box and David Cox [36]. The box-cox procedure

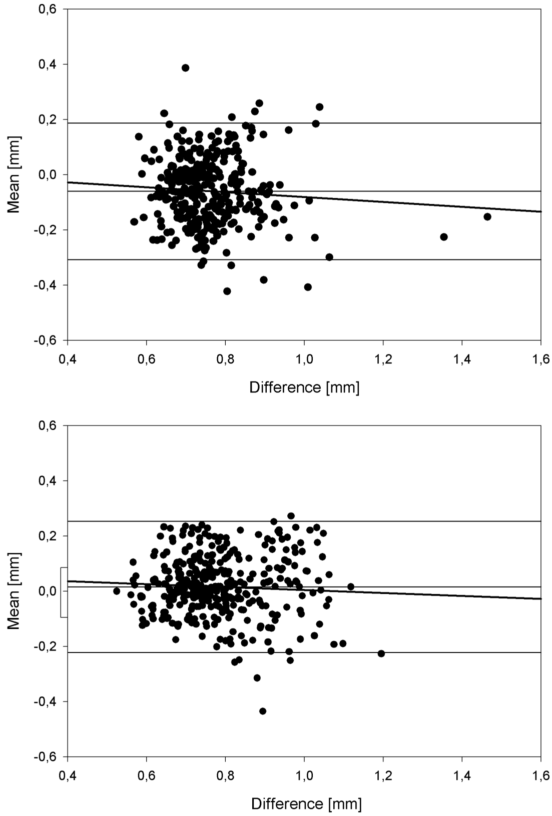

FIGURE 3.3: Bland-Altman plots of intra-observer variability study for operator FG (top) and SV (bottom). The indicated trends are not signficant.

calculates the correlation coefficient of a normal probability plot for a number of different values of the λ parameter. The better the transformation succeeds in 'normalizing' the dataset, the closer the correlation coefficient will be to one. Usually, the box-cox transformation procedure considers λ values between -5 and 5. Some common values for λ and their assocated transformations are given in table 3.2 on the next page.

The box-cox procedure was applied to all WSS parameters and the measured IMT values. It was found that for all WSS parameters, the best performing transformation was $ln(Y)$, while for IMT, the optimal transformation was given by $\frac{1}{Y}$. Figure 3.6 (bottom panel) illustrates the distribution of $ln(WSS)$, the bottom panel of figure 3.5 shows the scatter plot of $\frac{1}{IMT}$ versus $ln(WSS)$.

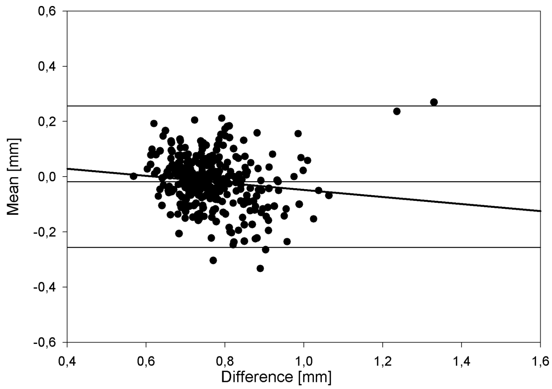

Figure 3.4: Bland-Altman plots of inter-observer variability study. The indicated trend is not significant.

Table 3.2: Common box-cox transformations

λ	Y'
2	Y^2
0.5	$\sqrt{Y}$
0	$ln(Y)$
-0.5	$\frac{1}{\sqrt{Y}}$
-1.0	$\frac{1}{Y}$
-2	$\frac{1}{Y^2}$

The results of the linear regression analyses of transformed IMT versus the transformed WSS parameters in the CCA and ICA are summarized in table 3.3 on page 45. For all of the WSS related parameters, the relationship of transformed IMT to the transformed parameter was found to be significant ($P<0.001$), though R-values were small. The strongest relationships were found in the CCA, with the R-values in the CCA being consistently higher than in the ICA, for all investigated parameters.

In our population, IMT values were not significantly related to age or blood pressure (SBP, MAP or PP). Including these variables in an ANOVA analysis of IMT versus any of the WSS related parameters, both for CCA and ICA, did not improve model performance.

Finally, we investigated the relationship between transformed IMT and a geometric parameter, z. The z-value expresses the vertical distance of the patch in which IMT was measured to the bifurcation point.

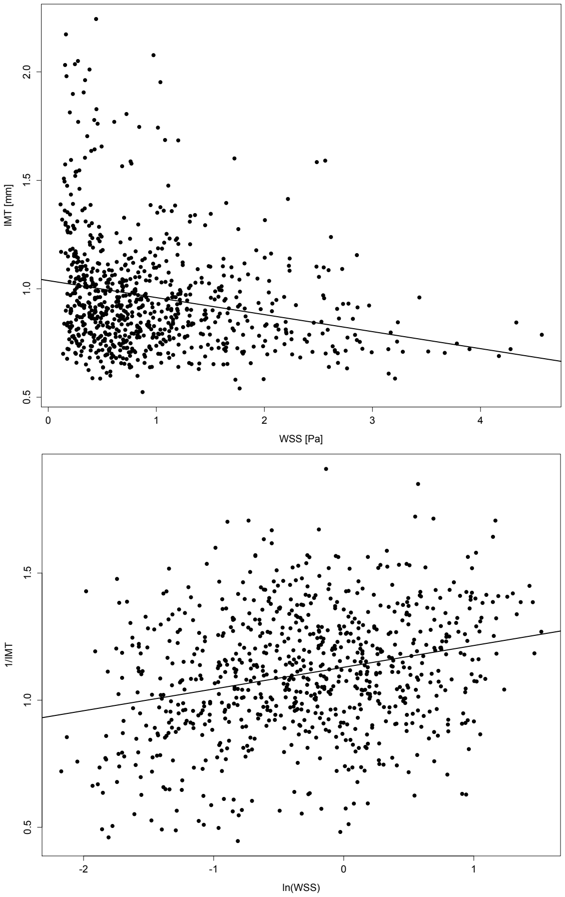

FIGURE 3.5: Top: Scatter plot of IMT versus WSS. Bottom: scatter plot of $\frac{1}{IMT}$ versus $ln(WSS)$

The larger the absolute value of z, the further the IMT value is measured from the bifurcation. The results of the regression analysis of $\frac{1}{IMT}$ versus $abs(z)$ are illustrated in figure 3.7 on page 46. A significant relationship between IMT and z was found, with higher IMT values near the bifurcation (R= 0.47 and 0.46 for CCA and ICA, respectively, P<0.001).

For each of the WSS parameters, both for CCA and ICA, the z-parameter was then included in a forward stepwise regression analysis. For multiple predictors, the forward stepwise regression procedure selects those parameters which significantly improve model performance, while discarding those which do not significantly contribute to

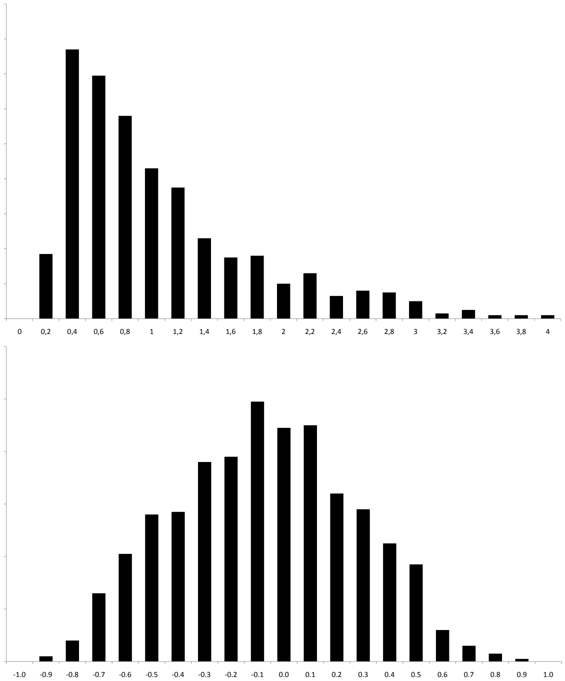

FIGURE 3.6: Distribution of WSS before (top) and after (bottom) transformation

the model. The most important predictor (i.e. with the highest bivariate correlation) is chosen first. The results of these forward stepwise regression analyses are summarized in table 3.4 on page 47. For all of the WSS related parameters, the z-parameter has the most predictive value for IMT. In some cases, the addition of the WSS relation parameter did not significantly improve model performance after inclusion of the geometry-related z-parameter.

3.4 DISCUSSION

The pathogenesis of atherosclerosis has been linked to the occurrence of 'abnormal' wall shear stress, with those arterial locations with low or oscillatory shear stress having been identified as preferential locations for thickening of the intima-media layer, itself a proven marker for the early onset of cardiovascular disease. The carotid artery location, with its bifurcation is one of these areas in which low and oscillatory shear stresses are commonly observed and is given its superficial location commonly examined in routine practice to detect early onset of carotid artery plaque.

Table 3.3: Summary of regression analysis of transformed IMT and WSS parameters in the common and internal carotid arteries

	$\frac{1}{IMT}$ versus	R	F	P
CCA	$ln(WSS)$	0.27	60.1	<0.001
	$ln(OSI)$	0.25	54.2	<0.001
	$ln(WSSGs)$	0.18	27.3	<0.001
	$ln(WSSGt)$	0.20	32.6	<0.001
	$ln(WSSAG)$	0.26	56.8	<0.001
ICA	$ln(WSS)$	0.16	18.9	<0.001
	$ln(OSI)$	0.22	37.5	<0.001
	$ln(WSSGs)$	0.14	14.0	<0.001
	$ln(WSSGt)$	0.16	19.2	<0.001
	$ln(WSSAG)$	0.19	26.9	<0.001

The subjects in the present study, having previously had their carotid artery bifurcations reconstructed based on BB MRI images, form an interesting dataset to investigate whether a relationship can be observed between WSS and WSS related parameters and carotid artery IMT, as determined from the same BB MRI images. Though BB MRI images inherently have a much lower resolution than carotid artery ultrasound, which is the gold standard method for IMT determination in the carotid artery, it is possible to manually delineate the intima and media interfaces on BB MRI images.

Despite the low resolution of the images, the intra- and inter-observer variability of the manual delineation method using the custom-built software interface developed for the present analysis is surprisingly good. The very small differences in IMT values are lower than the actual resolution of the images, and unlikely to be of clinical importance. The spread on the difference, on the other hand, is quite high, up to 20% of measured IMT values. It should however be pointed out that these results may be overly optimistic. Operator 2 had previously been trained in the manual IMT delineation by operator 1 on the same dataset. Though the measurements reported in the present study were redone on a separate occasion and operator 2 was blinded to the results of operator 1 on that occasion, it is not unlikely inter-observer variability would be higher had both operators performed the manual measurements on a third set of data. Due to the limited amount of data available, this was however not possible. Likewise, the small set of data and the fact that manual measurements for the intra-observer

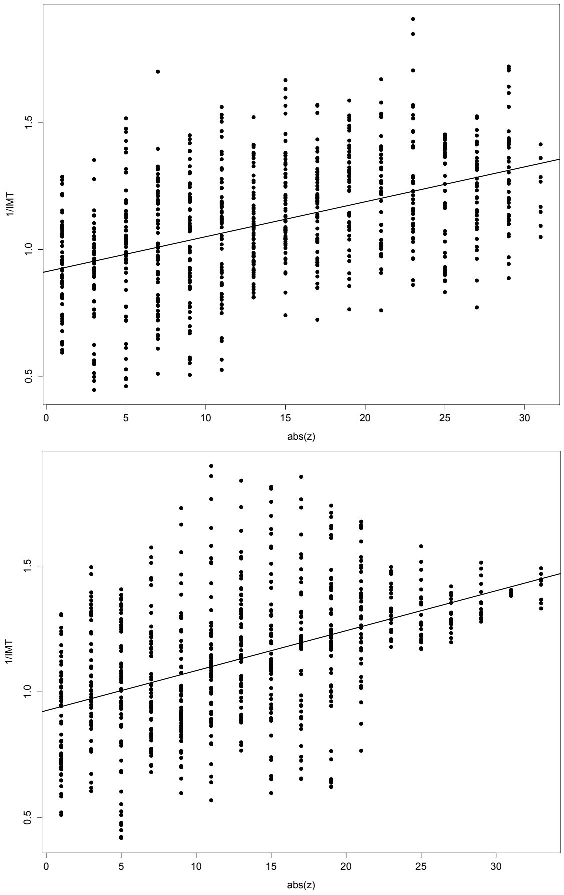

Figure 3.7: Regression analysis of $\frac{1}{IMT}$ vs $abs(z)$ in the CCA (top) and ICA (bottom)

variability study were performed within a very short timeframe may have improved intra-observer variability.

The relationship found between IMT and WSS related parameters in the present analysis, though significant, was quite weak. One of the reasons for this might be the limited resolution of the data available. The patching technique, which is required to match the calculated WSS parameters to the measured IMT values, averages out both the IMT values and the calculated WSS parameters. Also, IMT values were interpolated from the measurements performed by the operator in each slice. While the operators were instructed to discard slices (i.e. not make measurements) if they were unable to visually identify the intima-media interface evenly across the entire section of artery, the interpolation will undoubtedly smooth over small changes in IMT.

Table 3.4: Summary of the stepwise forward linear regression for $\frac{1}{IMT}$ versus each of the WSS parameters in the CCA and ICA

	parameter	Regression model	Included	R
CCA	WSS	$abs(z)$	✓	0.445
		$ln(WSS)$	✓	0.454
	OSI	$abs(z)$	✓	0.445
		$ln(OSI)$	✓	0.453
	WSSGs	$abs(z)$	✓	0.445
		$ln(WSSGs)$	—	—
	WSSGt	$abs(z)$	✓	0.445
		$ln(WSSgt)$	—	—
	WSSAG	$abs(z)$	✓	0.445
		$ln(WSSAG)$	✓	0.458
ICA	WSS	$abs(z)$	✓	0.462
		$ln(WSS)$	—	—
	OSI	$abs(z)$	✓	0.463
		$ln(OSI)$	✓	0.468
	WSSGs	$abs(z)$	✓	0.462
		$ln(WSSGs)$	—	—
	WSSGt	$abs(z)$	✓	0.462
		$ln(WSSGt)$	—	—
	WSSAG	$abs(z)$	✓	0.462
		$ln(WSSAG)$	—	0.462

The observation that IMT was not related to age in our study population is surprising, as IMT is generally known to increase with age. The lack of age-related increase in our study population may be related to the limited population size and age spread.

The main conclusion of the present study is that accounting for a simple geometric parameter like the distance to the bifurcation, in our dataset at least, has more predictive power than taking into account any of the calculated wall shear stress parameters. Though the distance to the bifurcation is not completely unrelated to the WSS parameters (low, oscillatory wall shear stress is mostly found around the bifurcation), the fact that including the calculated WSS in addition to the geometric parameter hardly improves the model does illustrate that in our population sample, simply looking at the geometry is probably more efficient than taking the time to calculate all of the WSS parameters.

The present study does have several important limitations. First and foremost, the quality of the BB MRI images were only barely sufficient to manually determine IMT. It is clear that using an ultrasound-based approach would have yielded more reliable IMT measures. The limited set of data available and the loss of resolution due to the patching further reduces the power of comparing measured IMT to calculated WSS on a point-to-point basis. One advantage of the use of transversal MRI images however, is that it does allow to examine IMT in the circumferential direction, which is important to match IMT to calculated WSS as it does not assume the IMT to be constant (circumferentially) in each section.

3.5 CONCLUSIONS

The manual delineation using the custom-developed tool for manual delineation on BB MRI images shows good intra- and inter-observer variability. Nevertheless, image quality in general is only barely acceptable for the purpose of defining IMT. BB MRI images cannot compete with the superior resolution and accessibility of ultrasound. In spite of this, the tentative results of the present analysis show that in the study population a weak, but significant correlation is found between IMT and measured WSS. The relationship between IMT and WSS related parameters was stronger in the CCA than in the ICA regardless of the WSS parameter under consideration. In contrast, measured IMT values were strongly correlated to the site of measurement; taking the distance to the carotid bifurcation into account has more predictive power than any of the investigated WSS related parameters. Furthermore, including WSS related parameters in a model taking into account the distance to the carotid bifurcation did not significantly improve model performance.

Chapter 4

Validation of an automated ultrasound-based IMT detection tool

4.1 Introduction

An increase in carotid artery intima media thickness (IMT) is considered an early marker of atherosclerosis. Several large scale studies have confirmed that IMT measurements accurately identify cardiovascular risk [11, 13, 37–41]. Over the past few years there has been a growing interest in validated, clinically applicable tools for automated IMT measurements. This study aims to validate a novel semi-automated IMT detector supplied by GE Healthcare, Cardiovascular Ultrasound.

4.2 Methods

4.2.1 Ultrasonography

For the purpose of this study 150 subjects were randomly selected from the Asklepios study database. The Asklepios study is a large scale, longitudinal population study focusing on the interplay between aging, cardiovascular hemodynamics and inflammation in (pre-clinical) cardiovascular disease [42]. The Asklepios study protocol was approved by the ethics committee of the Ghent University Hospital and all subjects gave written informed consent.

As part of the Asklepios protocol all subjects underwent a resting ultrasound scan of the left and right carotid arteries performed by a single observer using a commercially available ultrasound system (GE Vingmed Ultrasound Vivid7) equipped with a vascular transducer (12L linear array transducer set at 10 MHz). For the purpose of carotid artery imaging, subjects were examined in recumbent position with the neck in slight hyperextension and turned approximately 30 degrees contralateral to the examined carotid artery. All measurements consisted of cine loops of at least 5 cardiac cycles during normal breathing. Images were stored in Vivid7 raw data format to magneto-optical disk and an image server for subsequent off-line analysis. Images had been successfully obtained from all participating subjects.

4.2.2 Manual IMT assessment

Manual IMT measurements were performed off-line within GE Healthcare Ultrasound Echopac version 2.0.1 software on a dedicated workstation.

From each of the available cine loops a single frame at end diastole was selected using electronic calipers. End-diastole was determined by the R-top of the synchronized ECG. Both for left and right carotid artery 12 IMT measurements were performed by placing boundary points on the lumen-intima and intima-media interfaces in a 15 mm long segment 1-2 cm before the bifurcation in the last segment where parallelism of near and far walls was maintained prior to the dilatation of the bulb. The largest magnification which still displayed both near and far walls of the vessel was used for IMT measurement and obtained values were averaged per segment as IMT_{man}, i.e. for each segment a value of IMT_{man} was assessed for the left and right common carotid artery.

4.2.3 Automated IMT assessment

The same cine loop images used for manual measurement of IMT were also used for off-line (semi-)automatic assessment of IMT within EchoPac SWOnly 5.0.1B184 which included the automated IMT delineation application. In each of the available cine loops a single frame was selected near end-diastole at the peak of the R wave. The choice of frame was left free to the operator, no special consideration was made that the same frame as used for manual IMT delineation was chosen. The operator selected a region of interest in the same general area where manual IMT measurements were performed by drawing a box in the software application. The automated detection algorithm then finds the lumen-intima and intima-media interface resulting in an averaged IMT$_{aut}$ across the region of interest. Manual intervention in lumen-intima interface delineation is possible by way of a slider provided in the software interface. An example of what the operator sees in the ultrasound image is shown in figure 4.1.

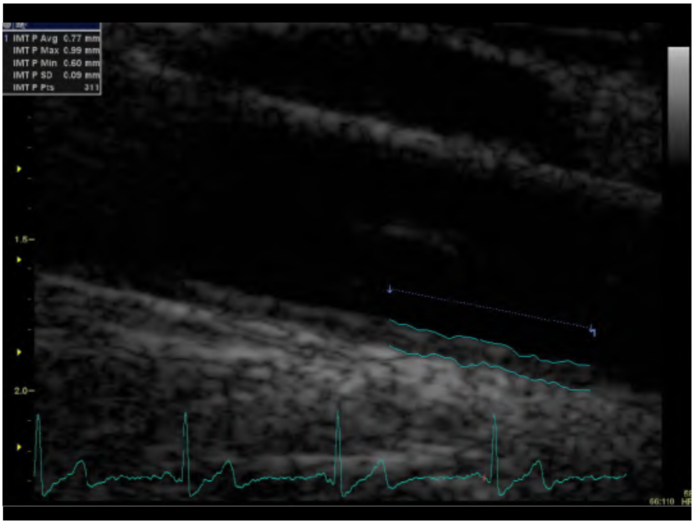

FIGURE 4.1: Example of IMT detection using the new IMT detection algorithm

4.2.4 Study protocol

The complete dataset comprises 150 subjects of which both left and right carotid arteries were imaged for a total of 300 images. Our goal was to compare inter- and intra-observer variability of the manual and automated IMT delineation methods and compare automated to manual measurements. In order to eliminate variability introduced by the imaging procedure the same cine loops were used for manual and automated processing thus ensuring reported variabilities are due to the different measuring techniques and not due to variability introduced by imaging the vessel at different times.

The data were processed by three operators (ER (1), SV (2), PS (3)) using the manual and/or automated measurement protocol. Operator 1 is a well trained expert reader in IMT measurements having performed several thousands of manual IMT measurements using the aforementioned protocol. Operators 2 and 3 are novice readers. Operator 1 manually processed the entire dataset and on a separate occasion redid the manual measurements on a subset of 50 subjects. Operators 2 and 3 both processed a different subset of 100 subjects using the automated method, resulting in an overlap of 50 subjects. Additionally, operator 2 on a different occasion, redid the automated measurements and performed the manual measurements in a subset of 50 subjects randomly chosen from the first set he had previously processed.

Intra-observer variability analysis for the manual measurements was performed by comparing the two sets of manual IMT measurements performed by operator 1; for the automated measurements the two sets of automated measurements performed by operator 2 were used. Inter-observer variability analysis was performed by comparing the subjects which had been processed manually by operators 1 and 2 and, for the automated measurements, by comparing the subjects which had been processed using the automated algorithm by operators 2 and 3. Finally in order to compare manual to automated IMT measurements the automated measurements performed by operators 2 and 3 were pooled and compared to the full set of manual measurements performed by operator 1. Operators were blinded to results from other operators or previous measurements. Table 4.1 on the facing page gives an overview of the datasets used for the analysis (top) and the way they were used in the intra- and inter-operator variability studies and comparison of manual to automated IMT measurements.

4.2.5 Data analysis and statistics

Data are reported as mean values (standard deviations), Pearson correlation coefficients between measurements and results of paired *t*-tests and visually displayed in the form of Bland-Altman plots. For the intra- and inter-observer variability study additionally the coefficient of variation (CV) and repeatability coefficient (RC) are calculated. The CV is the average of the variation coefficient of all individual measurements x_1 and x_2 and is expressed as a percentage:

$$CV = mean\left(\frac{SD\left(x_1, x_2\right)}{mean\left(x_1, x_2\right)}\right) \quad [\%] \tag{4.1}$$

The RC is 2 times the standard deviation of all individual differences between individual measurements and is expressed in mm.

$$RC = 2 \cdot SD\left(x_1 - x_2\right) \quad [mm] \tag{4.2}$$

Table 4.1: Available datasets (top) and protocol for the intra- and inter-operator variability study and comparison of manual to automated measurements (bottom). Each block represents a set of 50 subjects.

operator	visit	(m)anual or (a)automated	measurements	code
1	1	m	▨▨▨	01v1.m
	2	m	▨□□	01v2.m
2	1	a	▧▧□	02v1.a
	2	a	▧□□	02v2.a
	2	m	▨□□	02v2.m
1	1	a	□▧▧	03v1.a

study	operator	measurements	dataset used
Intra-observer manual	1	▨░░	o1v1.m
	1	▨□□	o1v2.m
Intra-observer automated	2	▧░□	o2v1.a
	2	▧□□	o2v2.a
Inter-observer manual	1	▨░░	o1v1.m
	2	▨□□	o2v2.m
Inter-observer automated	2	░▧□	o2v1.a
	3	□▧░	03v1.a
Manual versus automated	1	▨▨▨	o1v1.m
	2	▧▧□	02v1.a
	3	□░▧	03v1.a

To assess operator or vessel dependence of the agreement between manual and automated IMT values a multiple linear regression model was designed of the form

$$IMT_{man} = a_1 + a_2\,IMT_{auto} + a_3\,operator + a_4\,vessel \qquad (4.3)$$

and significance of a_1–a_4 coefficients was tested. All statistical analyses were performed using SPSS release 12.0 (SPSS inc., Chicago, IL).

4.3 RESULTS

4.3.1 Manual IMT assessment

Table 4.2 summarizes the results of the manual IMT measurement intra-observer variability study. Correlation between the two measurement series was excellent ($r=0.92$, $p<0.001$). Bland-Altman analysis [43] (figure 4.2 on the facing page (top)) showed no significant (*t*-test, $p<0.05$) bias between measurements and limits of agreement were [-0.110 0.126] mm. Coefficient of variation and repeatability coefficient were 5.23 % and 0.118 mm, respectively.

The results of the inter-observer variability study are shown in table 4.2. There was good correlation between the two measurement series ($r=0.89$, $p<0.001$) and Bland-Altman analysis (figure 4.3 on page 56 (top)) showed a small (0.040 mm) but significant (*t*-test, $p<0.001$) measurement bias and limits of agreement ranging [-0.181 0.100] mm. Coefficient of variation and repeatability coefficient were 7.57 % and 0.140 mm respectively.

TABLE 4.2: Intra- and inter-observer variability study for manual and automated measurements. *: $P<0.05$.

		Manual	Automated
Intra-observer	IMT_1 [mm]	0.620 (0.132)	0.615 (0.151)
	IMT_2 [mm]	0.612 (0.151)	0.625 (0.151)
	R	0.92^*	0.95^*
	mean Δ [mm]	0.008 (0.059)	0.010 (0.046)
	CV [%]	5.23	4.02
	RC [mm]	0.118	0.091
Inter-observer	IMT_1 [mm]	0.612 (0.151)	0.624 (0.134)
	IMT_2 [mm]	0.653 (0.138)	0.614 (0.127)
	R	0.89^*	0.90^*
	mean Δ [mm]	$0.040 (0.070)^*$	0.024 (0.110)
	CV [%]	7.57	5.10
	RC [mm]	0.140	0.118

4.3.2 Automated IMT assessment

Intra-observer variability results are represented in table 4.2. Correlation between repeated measurements was excellent ($r=0.95$, $p<0.001$)

and Bland-Altman analysis (figure 4.2 (bottom)) showed no significant bias (t-test, $p<0.05$) with limits of agreement [-0.101 0.081] mm. Coefficient of variation and repeatability coefficient were 4.02 % and 0.091 mm, respectively.

Results of inter-observer variability analysis is shown in table 4.2. Correlation again was excellent ($r=0.95$, $p<0.001$) while Bland-Altman analysis (figure 4.3 (bottom)) showed no significant bias (t-test, $p<0.05$) and limits of agreement [-0.126 0.109] mm. Coefficient of variation and repeatability coefficient were 5.1 % and 0.118 mm respectively.

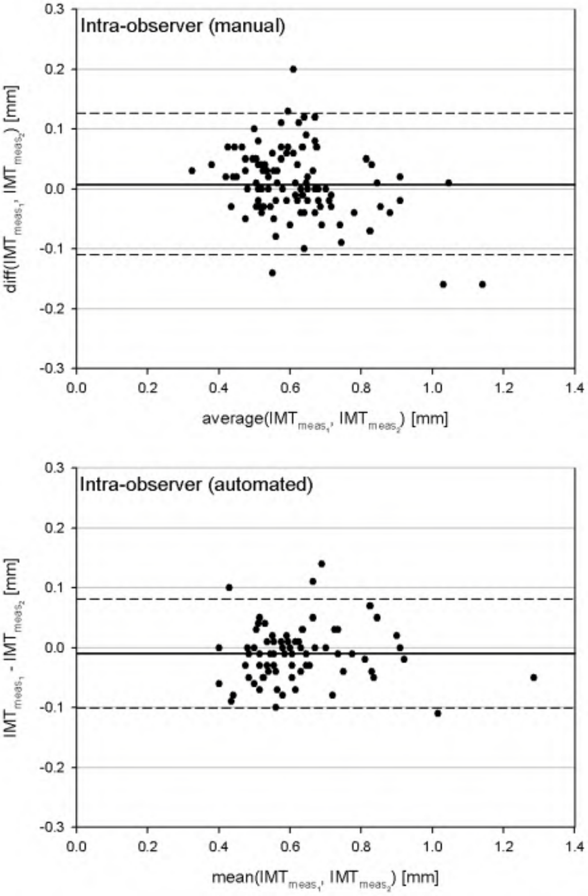

FIGURE 4.2: Bland-Altman plots of the intra-variability study for the manual (top) and automated (bottom) IMT detections.

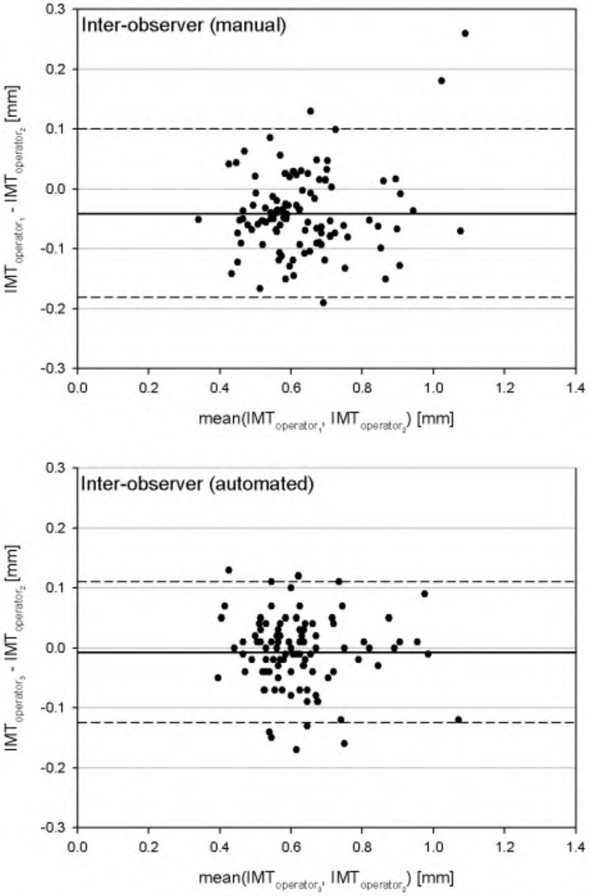

FIGURE 4.3: Bland-Altman plots of the inter-variability study for the manual (top) and automated (bottom) IMT detections.

4.3.3 Automated versus manual assessment

Since the interobserver variability study did not reveal a significant bias between operators, automated measurements from operator 2 and 3 were pooled and compared to manual assessments performed by operator 1. IMT_{man} and IMT_{aut} averaged 0.606 (0.151) mm and 0.629 (0.131) mm respectively. There was good correlation between manual and automated measurements (r=0.88, p<0.001).

Statistical analysis of the multilinear regression model proposed in equation 4.3 revealed that the factors 'vessel' (left CCA or right CCA) or 'operator' were not significant. Analysing the results with Bland-Altman analysis (figure 4.4 on the facing page) revealed a small (0.023

mm) but significant (t-test, $p<0.001$) difference between manual and automated IMT measurements with limits of agreement [-0.103 0.148] mm. Coefficient of variation and repeatability coefficient were 6.2 % and 0.125 mm, respectively.

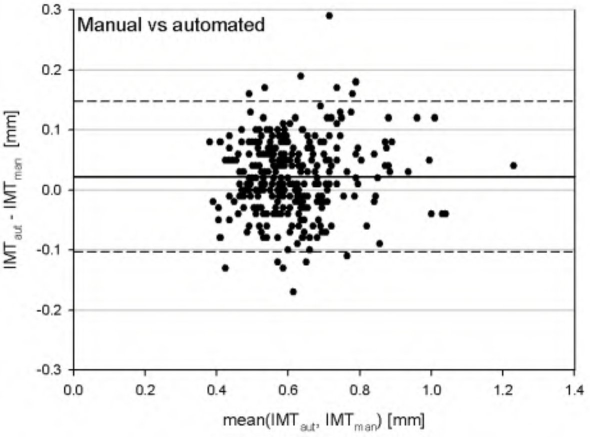

FIGURE 4.4: Bland-Altman plot of manual versus automated IMT

4.4 DISCUSSION

Carotid artery ultrasound provides an attractive means for screening of carotid artery IMT as an additional tool for the assessment of total cardiovascular risk. The manual delineation of intima and media boundaries however hampers its deployment in routine medical practice, in part due to its implied operator-dependence but more importantly because of the time-consuming nature of accurate measurements. An automated procedure could be the answer to both impediments.

Automated measurement protocols have already been proposed and authors found good correlation with manual measurements and an improvement in variability compared to suggested manual protocols, while decreasing reading time significantly [44–46]. These findings are in agreement with our results. Moreover in our study CV of repeated measurements were lower or similar to those reported or reviewed in literature both for manual and automated measurements [41, 44–47].

The automated intima media boundary detection used in this study was feasible on all recorded images. Despite the relative inexperience of the operators using the automated measurement tool, their measurements correlated extremely well with manual measurements. There was a tendency towards higher IMT values using the automated method, resulting in a small yet statistically significant bias of 0.023 mm. This value is 3.7 % of the mean IMT found in this study and 2.5 % of the threshold value of 0.9 mm considered indicative for elevated IMT. Its clinical relevance therefore, seems negligible.

Comparing the performance of manual and automated IMT assessments, the results of the automated measurements are excellent. Repeatability coefficients of the automated measurements were both for intra- and interobserver variability analysis slightly better than those of the current best practice manual measurement protocol. The values for intraobserver reliability are especially noteworthy since they reflect variability in manual IMT measurements performed by an expert reader compared to automated readings by novices without prior training.

4.5 CONCLUSIONS

Overall, the automated IMT measurement delivers a reliability at least as good as the manual measurements in a fraction of the time, without the need for extensive training of operators. Given these properties, the automated IMT detection algorithm tested in this study seems an excellent tool for routine assessment of IMT in clinical practice.

Three

Models of the arterial tree

CHAPTER 5

Outline

The second part of this manuscript is consecrated to modeling aspects of the arterial network. As evident from the mathematical background that came forward in the discussion of arterial physiology in chapter 1, pressure and flow in the arterial tree, like in any other tube network, obey a set of basic laws which can be used to gain knowledge of what makes the arterial system tick.

Arterial models are the theoreticist's tools for dissecting the inner workings of the arterial tree. From the simple to the extremely complex, models are used to understand what lies at the cause of certain observed behavior and what happens if the boundary conditions of the system change. Yet models also have real practical use. Only by a thorough understanding of how different properties of the arterial tree interact and how these properties influence the shape of the pressure and flow waveforms can approaches for treating unwanted behavior be defined without having to resort to random 'trial and error' testing. They are also, to a certain degree, required for the quantification of arterial stiffness, a topic that will be the subject of part 4 of this manuscript.

Chapter 6 therefore introduces the most important models of the arterial tree. The two basic paradigms of the arterial tree—its representation as a lumped parameter (windkessel) or wave system—are discussed, the latter both in the frequency and the time domain. The goal of this chapter is to familiarize the reader with the concepts that will be required for the quantification of arterial stiffness in part 3 of this manuscript.

Lumped parameter and wave (transmission line) models represent two contradictory, yet complementary views of how the arterial tree should be viewed. Both have their strengths and weaknesses, but neither is sufficiently superior over the other in all application domains. Recently, efforts have been made to marry the windkessel and wave reflection views of the arterial tree in 'hybrid' models by separating the pressure wave in the time domain in a reservoir and wave reflection component. This approach however seems to have a lot in common with the established three element windkessel model.

Chapter 7 investigates these similarities by applying both the 3-element windkessel and the reservoir-wave separation model to the Asklepios study population data. The main goals of this study were to (1) evaluate the performance and applicability of the reservoir-wave separation model in the Asklepios population; (2) compare reservoir pressure derived using the three element windkessel model to reservoir pressures derived using the reservoir-wave separation models to see to which extent they are different; and (3) examine the evolution of the three element windkessel and reservoir-wave separation reservoir pulse pressure with age and gender in the Asklepios population. The results from this study have been accepted for publication in:

S.J. Vermeersch, E.R. Rietzschel, M.L. De Buyzere, L.M. Van Bortel, T.C. Gillebert, P.R. Verdonck, P. Segers. The reservoir pressure concept: the 3-element windkessel model revisited? Application to the Asklepios population study. *J Eng Math*, in press.

CHAPTER 6

Modeling the arterial system

6.1 INTRODUCTION

6.1.1 On the use and limitations of models

The arterial system as a whole is a thoroughly complex network of interacting elements contributing to the homeostasis of the human organism. Studying the intricacies of such a tightly interwoven system in which a change in one constituent influences many others is a daunting task at best. To better understand the relationships between physical observations within the arterial system – such as pressure and flow propagation – and the properties of those arteries – such as stiffness, diameter, wall thickness and many others – the use of models can be of help.

As for any complex system, models are of use in two different ways. First, in the absence of a model, acquiring knowledge of the system is limited to making observations of the system in a given state. Studying the influence of a given change to the system's properties would imply making that change to the system and observing what, if any, changes are seen in its behavior. While this could be feasible in simple systems, especially in living, healthy subjects it is often impossible or at the very least unethical to make changes to the arterial system. Well established models allow one to 'simulate' the effect of a given change to the arterial network and predict the behavior of the modified system either to better understand the origins of certain observed effects in real life or to propose an approach for changing some unwanted behavior. Second, the use of models allows one to make an abstraction of the complexity of the real-life system. Most models offer but an approximation of the real-life behavior of a given system: to facilitate model construction and the interpretation of its parameters certain aspects of the complete system are omitted or simplified. For well-defined purposes the approximation offered by the model may be 'good enough' to warrant making conclusions on the real-life system, while at the same time offering a better way of grasping the impact of the most important system parameters by doing away with the burden of the often overly complicated complete system.

These two properties of any model have important implications to both the *usefulness* and *limitations* of model use. Different models offer different levels of abstraction and a different field of application depending on the choices made in their construction. For any given research question it is therefore of the utmost importance to select the model which is most appropriate for answering the given question *and* to verify whether the question to be answered lies within the scope and limitations of the model considered. For any obtained result it should always be verified whether it respects the limitations of the model's validity. These two points are paramount, especially in interpreting results obtained from a model and applying them back to the real-life system. Finally, to be able to confidently use results derived from any model, some sort of verification should always be considered to test whether the conclusions drawn from the model do not overstep its inherent boundaries and whether the model still corresponds to the real-life behavior of the system for the conditions under consideration. In cases where such validation is not evident, special care should be taken in the formulation and interpretation of results.

6.1.2 Models and the arterial system

Progress in model development is often related to the background of the person studying a given system and the technological or mathematical state of the art at the time the model was developed. The modeler's background comes into play in the selection of the model type, with the more successful modelers being able to apply well known modeling concepts from other disciplines to a new application domain previously not considered. Good models keep things as simple as possible. On the other hand, often times new information on the system's behavior, acquired through the advent of new measurement or analysis techniques, or the availability of new mathematical analysis tools, drives new models to be developed.

This continuous process of acquiring new information of a system's behavior, proposing a model for mimicking this observed behavior, testing and comparing the results from its application to measurements obtained from the real-life system and finally either refining or replacing the existing model is also evident when presenting an overview of the models of the arterial tree.

Over the course of the years, the arterial system has been modeled using a number of different approaches. These can broadly be categorized in two major categories: (i) lumped parameter 'windkessel' models in which the arterial tree is synthesized in a number of discrete elements representing different properties of the arterial tree and (ii) transmission line models in which the arterial tree is viewed as a wave system in which observed pressure and flow waves are the resultant of the interaction between forward waves emanating from the heart and backward waves reflected at different reflection sites situated along the arterial tree. Up to a certain point these different approaches are mutually exclusive: traditional windkessel models have no concept of wave reflections within the model and wave models do not allow for a discretization of their parameters into separate elements. As such, these form a perfect illustration of how models can seemingly contradict and yet both yield valuable information regarding the functioning of a system as they simply represent a different approach to investigating the functioning of the arterial system.

In what follows we will first briefly highlight the origins and properties of the models currently most often used in studying the behavior of the arterial tree, focussing on those approaches which will later return in our own investigations. First, the windkessel lumped parameter models will be discussed, followed by the wave transmission models which can be studied either in the frequency or time domain.

6.2 WINDKESSEL MODELS

Like much of the inner structures of the human body, the workings of the arterial system remained hidden for a long time. Up until the 17^{th} century it was assumed that venous and arterial blood flowed through two completely separate systems, venous (red) blood being produced in the liver and arterial (dark) blood in the heart, from where it was transported to all parts of the body where it was consumed. The concept of a circulation was unknown; blood was assumed to be single use and continuously produced in the liver and heart. This theory, believed to be first proposed by the ancient Greek Galen in the 2^{nd} century, was the basis for treatment by bloodletting which allowed excess blood to leave the body and was performed well into the 19^{th} century.

The existence of a pulmonary and systemic circulation was first described by the Arab scholar Ibn al-Nafis[1] and again in the 16th century by Servetus[2], but their works were either unknown or lost until the pulmonary and systemic circulation were rediscovered by Harvey[3] over two centuries later. It took another century before Hales[4] first measured and described the rise and fall of the arterial blood pressure by inserting a large glass tube in an artery of a horse. He already hypothesized the variations in pressure to be related to the elasticity of the arterial system. Supposedly, Weber[5] was the first to compare the functioning of the arterial tree in shaping the arterial pulse to the windkessel (an elastic reservoir) present in contemporary fire engines which regulated the outflow of water through a fire hose pumped by an intermittent pump.

The behavior of the arterial tree is of course wholly determined by its anatomical and physiological structure. These were discussed at length in chapter 1. Windkessel models especially attempt to link their elements to specific physiological functions of the arterial tree. It is therefore useful to keep the conceptual view of the physiology of the arterial tree in mind when delving into the mathematical background of the different windkessel models. For convenience, figure 6.1 summarizes the most important aspects of the arterial physiology in a schematic diagram.

6.2.1 Two-element windkessel model

The fire-engine like model proposed by Weber was first quantitatively formalized by Frank [48] as the so called two-element windkessel model. Schematically, this model consists of the combination of a resistance

---

[1] Ala al-Din Abu al-Hassan Ali ibn Abi-Hazm al-Qurashi al-Dimashqi (°1213 – †1288), Arab scholar who was born in Damascus, Syria and worked in Cairo, Egypt)

[2] Michael Servetus (°September 29, 1511 – †October 27, 1553), a Spanish scholar

[3] William Harvey (°April 1, 1578 – †June 3, 1657), an English physician

[4] Stephen Hales (°September 17, 1677 – †January 4, 1761), an English physician

[5] Ernst Heinrich Weber (°June 24, 1795 – †January 26, 1878), German physician considered to be one of the founders of experimental psychology. His brother Wilhelm Eduard Weber coincidentally lent his name to the SI unit for magnetic flux, Wb

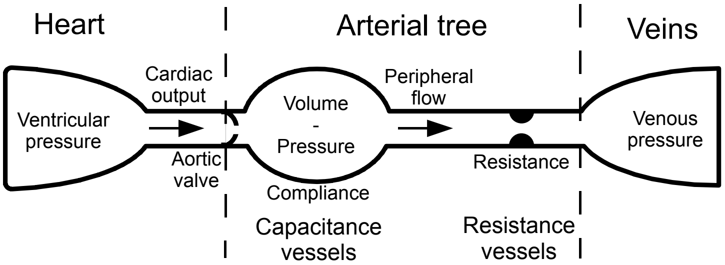

FIGURE 6.1: Schematic summary of the major elements of cardiovascular physiology playing a role in the windkessel models.

and a compliance element. The resistance element is mainly determined by the smaller arteries and arterioles of the peripheral arterial system as, according to the Hagen-Poiseuille equation (equation 1.3 on page 15) previously discussed in chapter 1, it is inversely proportional to the fourth power of the arterial diameter. The resistance element in the windkessel model is considered to be the summation of all parallel placed resistances in the vascular bed and is called the *total arterial resistance*. The compliance element on the other hand is mainly determined by the properties of the large elastic arteries. In a similar fashion to the total arterial resistance, the compliance element in the two-element windkessel model is considered to be the summation of all compliances of the complete arterial tree and is therefore called the *total arterial compliance*.

For the mathematical description of the 2-element windkessel model, it is useful to consider either the hydraulic or electric representation of the 2-element windkessel model represented in the top panel of figure 6.2. The properties of the 2-element windkessel can be fully described using basic hydraulic or electric circuit theory on the respective representation. The physiological counterparts of the various electrical terms and components used in the model description and analysis are summarized in table 6.1.

For the electrical models, the heart (or more precisely, the left ventricle of the heart) is considered to be a time-varying electrical potential element $P(t)$ connected to the arterial tree as represented by the models in right panels of figure 6.2.

Consider $I(t)$ to be the time-varying electrical current running into the system and $I_C(t)$ and $I_R(t)$ to be the currents running through

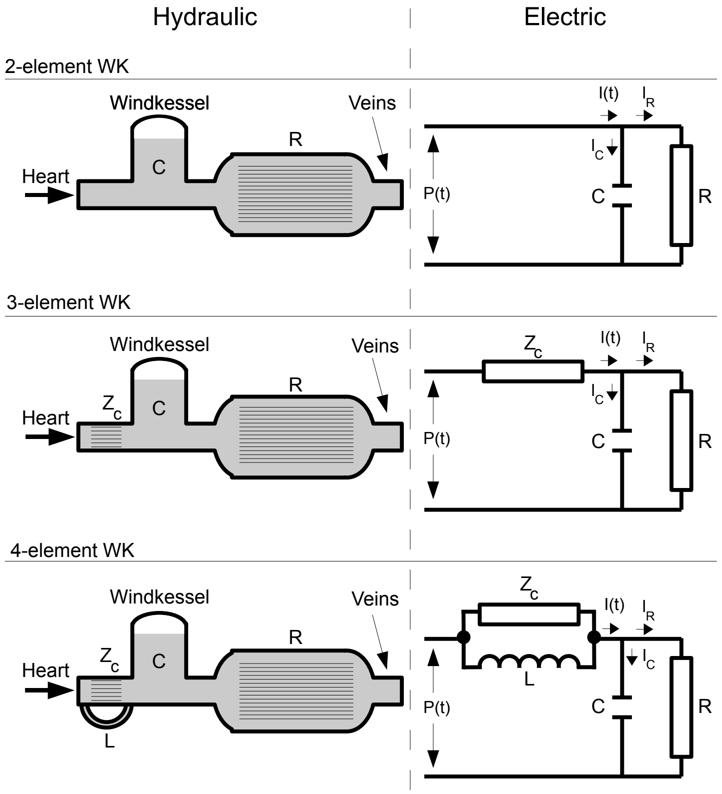
Hydraulic
Electric
2-element WK
Windkessel
Veins
Heart
C
R
I(t)
I_R
I_C
P(t)
C
R
3-element WK
Windkessel
Veins
Heart
Z_c
C
R
Z_c
I(t)
I_R
I_C
P(t)
C
R
4-element WK
Windkessel
Veins
Heart
Z_c
C
L
R
Z_c
I(t)
I_R
L
I_C
P(t)
C
R

FIGURE 6.2: Hydraulic and electric representations of the two-element (top), three-element (middle), and four-element (bottom) windkessel models. *R*: total peripheral resistance, *C*: total arterial compliance, Z_c: aortic characteristic impedance, *L*: arterial inertance, $P(t)$: potential difference (pressure) generated by the heart, *I*: current (flow) [49].

the branch with the capacitor *C* and resistor *R*, respectively. Then according to Ohm's[6] law:

$$I = \frac{U}{R} \tag{6.1}$$

where

I: current [A]
U: potential (difference) [V]
R: resistance [Ω]

---

[6] Georg Ohm (°March 16, 1789 – †July 6, 1854), German physicist

TABLE 6.1: Analogy between electrical circuit elements and physiological properties for the windkessel models

Symbol	Electrical component/quantity	Physiological counterpart
U/P	voltage/potential (difference) [V]	pressure [Pa]
I	current [A]	flow rate [m^2/s]
C	capacitance [F]	arterial compliance
R	resistance [Ω]	peripheral resistance

The potential drop over the resistor R is given by:

$$U_R = I_R \cdot R \tag{6.2}$$

The potential difference over the capacitor C is determined by its capacitance as:

$$U_C = \frac{Q}{C} \tag{6.3}$$

where

Q: Charge on the capacitor [C]
C: Capacitance of the capacitor [F]

and

$$I_C = \frac{dQ}{dt} \tag{6.4}$$

This simple electrical network can then be solved by alternately applying Kirchoff's current and voltage laws. Kirchoff's voltage law states that in any closed loop of the network, the sum of all potential differences must be zero. Applying this to the 2-element windkessel electrical network and using equations 6.2 and 6.3 gives:

$$U(t) = I_R \cdot R \tag{6.5}$$

and

$$U(t) = \frac{Q}{C} \tag{6.6}$$

Kirchoff's current law states that at any point in an electrical circuit that does not correspond to a capacitor plate, the sum of currents flowing towards that point must equal the sum of currents flowing away from that point. For the 2-element windkessel electrical model this implies:

$$I(t) = I_R + I_C \tag{6.7}$$

Substituting I_R and I_C from equations 6.2 and 6.4 into equation 6.7 finally yields the following differential equation which completely describes the behavior of the electrical 2-element windkessel model:

$$I(t) = \frac{P(t)}{R} + C\frac{dP(t)}{dt} \tag{6.8}$$

During diastole, blood flow from the heart ($I(t)$) is zero and equation 6.8 reduces to:

$$\frac{dP(t)}{dt} = -\frac{1}{RC} \cdot P(t) \tag{6.9}$$

In this case, the 2-element windkessel equation can be solved exactly for $P(t)$:

$$P_{dia}(t) = P(t_{es})e^{-\frac{t-t_{es}}{RC}} \tag{6.10}$$

with

t_{es}: Time at end systole [s]
$P(t_{es})$: End-systolic pressure [mmHg]

To examine to what extent the 2-element windkessel model accurately represents the actual arterial system, the input impedance of the model can be compared to the input impedance of the arterial system. Section 6.3.3 discusses the concept of input impedance. The input impedance of the 2-element windkessel model is, in complex notation (see section 6.3.1 for an explanation of the representation of arterial waveforms in the frequency domain):

$$Z_{in,2WK} = \frac{R}{1 + j\omega RC} \tag{6.11}$$

with

j: the complex constant
$\omega = 2\pi f$, with f: heart frequency

Equation 6.11 illustrates that the steady-state value of Z_{in} (at 0 Hz) for the 2-element windkessel model equals the resistance R. For high frequencies, the input impedance becomes zero. For low frequencies, the model input impedance compares well to measured impedance (figure 6.3 on the facing page), but for higher frequencies, the model clearly does not reflect reality [50, 51].

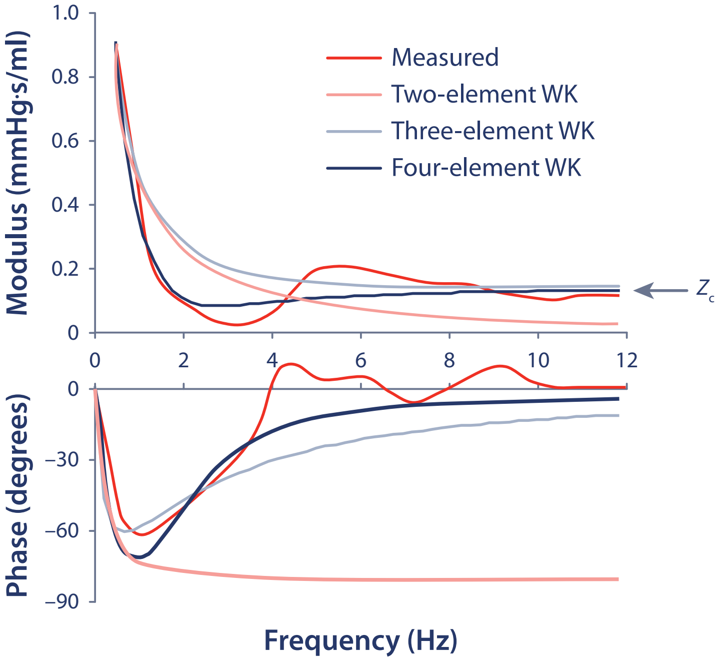

FIGURE 6.3: Example of aortic input impedance plotted with impedances predicted from a two-, three- and four element windkessel model [52].

6.2.2 Three- and four-element windkessel models

In order to improve the high-frequency behavior of the two-element windkessel model, Westerhof *et al.* [53] proposed adding a third resistive element to the model, accounting for the resistive-like behavior of the arterial tree in the high frequency range (figure 6.2). This third element represents the characteristic impedance of the ascending aorta. The input impedance of the three-element windkessel model is given by:

$$Z_{in,WK3} = Z_0 + \frac{R}{1 + j\omega RC} \tag{6.12}$$

The input impedance of the three-element windkessel is compared to measured arterial impedance in figure 6.3.

One problem with the three-element windkessel model is that Z_0, which represents the high-frequency behavior of the arterial tree, is added to the input impedance for all frequencies, resulting in a systematic overestimation of Z_{in} in the lower frequencies [51, 54]. To remedy this behavior, Stergiopulos *et al.* [55] introduced a fourth element to the windkessel model, representing an inertance (figure 6.2). For the steady-state component (at 0 Hz) and low frequencies, Z_c is bypassed through this new fourth inertial element. For high frequencies, the behavior is determined by Z_c. Figure 6.3 shows a graphical comparison of the 4-element model input impedance to measured arterial impedance.

6.3 The arterial tree as a wave system – frequency domain

6.3.1 Fourier decomposition of pressure and flow waves

The arterial pulse is a pulsatile signal, and not a periodic (sinusoidal oscillatory) one. Nevertheless, through the use of Fourier analysis, the pulsatile signal can be decomposed in a series of purely sinusoidal signals, each with a characteristic frequency which is a multiple of the heart rate frequency. The zeroth harmonic represents the steady state pressure, which corresponds to the mean arterial pressure, and should not be taken into account for wave reflection analysis. Assuming the original signal can be recomposed from the individual harmonics, any hemodynamic analysis can then be performed on each harmonic separately. Though a strict decomposition of the original signal according to the Fourier theory theoretically results in an infinite number of harmonics, in practice, an arterial pressure signal can reliably be reconstructed from the first 10–15 harmonics.

Figure 6.4 on the next page illustrates the decomposition of a pressure waveform into its harmonics.

Each individual sinusoidal wave, or harmonic, can be described by its amplitude and phase angle as a complex number. The n-th harmonic of the pressure and flow signal can thus be written as:

$$P_n = |P_n| e^{j(n\omega t + \Phi_{P_n})} \tag{6.13}$$

$$Q_n = |Q_n| e^{j(n\omega t + \Phi_{Q_n})} \tag{6.14}$$

where

$|P_n|$ and $|Q_n|$: amplitudes of the pressure and flow sine waves
Φ_{P_n} and Φ_{Q_n}: phase angles of the pressure and flow sine waves
ω: fundamental angular frequency

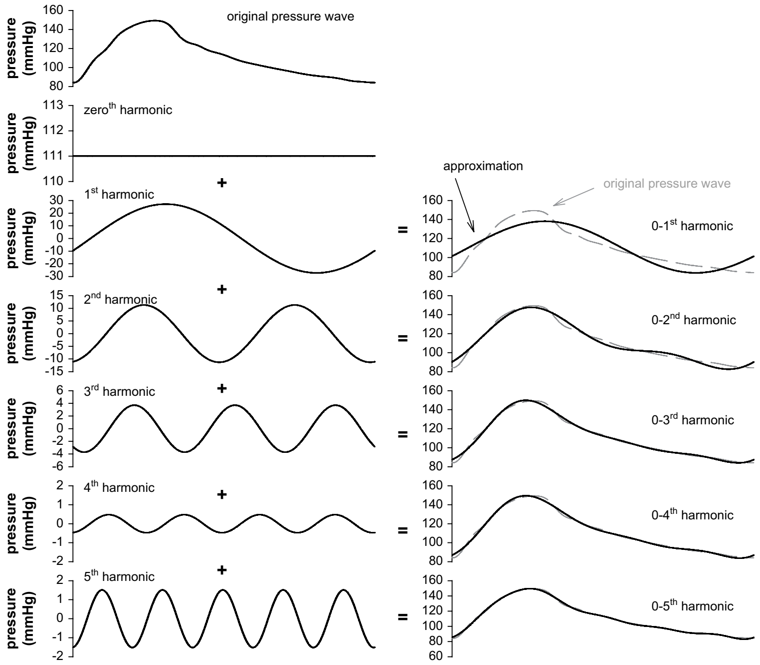

FIGURE 6.4: Decomposition of a pressure waveform into its harmonics [56].

As stated above, each harmonic of the decomposed pressure and flow signal has a characteristic frequency which is a multiple of the heart rate frequency. ω is thus related to the duration of a heart cycle (T) as:

$$\omega = \frac{2\pi}{T} \tag{6.15}$$

For a heart rate of 75 beats/min, ω is 7.85 rad/s.

6.3.2 Separation of pressure and flow in forward and backward waves

If the arterial tree is considered to be a uniform, visco-elastic tube, the pressure and flow waves in the tube at a given time (t) and position (z) can be written as a sum of forward (antegrade) and reflected (retrograde) waves:

$$P(z,t) = \sum_i B_i \left(P_{ant} e^{-\gamma z} + P_{ret} e^{\gamma z}\right) e^{j\omega t} \tag{6.16}$$

$$Q(z,t) = \sum_i B_i \left(Q_{ant} e^{-\gamma z} + Q_{ret} e^{\gamma z}\right) e^{j\omega t} \tag{6.17}$$

with

P_{ant}, Q_{ant}, P_{ret} and Q_{ret}: forward and backward pressure and flow waves at the entrance of the aorta
γ: wave propagation constant determined by the arterial properties (related to the stiffness of the vessel) and fluid properties
B_i: constants depending on the reflective and propagation properties of the arteries

If the relationship between pressure and flow is assumed to be linear for each harmonic, the ratio between pressure and flow is a constant defined as the characteristic impedance of the tube (Z_0):

$$\begin{aligned} Z_0 &= \frac{P_{ant}}{Q_{ant}} \\ &= -\frac{P_{ret}}{Q_{ret}} \end{aligned} \tag{6.18}$$

so equation 6.17 can be rewritten as:

$$Q(z,t) = \frac{1}{Z_0} \sum_i B_i \left(P_{ant} e^{-\gamma z} - P_{ret} e^{\gamma z} \right) e^{j\omega t} \tag{6.19}$$

Traditionally, the inlet of the arterial system is assumed to consist of a single input waveform consisting of one incident and one reflected wave. In that case, equations 6.16 and 6.19 can be simplified to:

$$P(z,t) = \left(P_f e^{-\gamma z} + P_b e^{\gamma z} \right) e^{j\omega t} \tag{6.20}$$

$$Q(z,t) = \frac{1}{Z_0} \left(P_f e^{-\gamma z} - P_b e^{\gamma z} \right) e^{j\omega t} \tag{6.21}$$

with P_f and P_b the forward and backward pressure wave seen at the root of the aorta (z=0):

$$P_{ao} = P_f + P_b \tag{6.22}$$

and thus:

$$Q_{ao} = Q_f + Q_b = \frac{1}{Z_0} \left(P_f - P_b \right) \tag{6.23}$$

Equations 6.22 and 6.23 can be solved for P_f and P_b, yielding [6]

$$P_f = \frac{P_{ao} + Z_0 Q_{ao}}{2} \tag{6.24}$$

$$P_b = \frac{P_{ao} - Z_0 Q_{ao}}{2} \tag{6.25}$$

Provided the characteristic impedance (Z_0) of the arterial tree is known, equations 6.24 and 6.25 can be used on each harmonic of the Fourier decomposed pressure and flow signal to obtain the individual harmonics of the forward and backward pressure and flow signal. The complete pressure and flow waves can then be reconstructed from these harmonics.

6.3.3 (Characteristic) impedance of the arterial tree

Impedance (Z) is defined as the ratio of (pulsatile) pressure and flow and represents the general 'resistance' of a system to flow. Impedance is calculated from the individual harmonics of P and Q and is thus a function of frequency. The modulus and phase of Z can be calculated as:

$$|Z_n| = \frac{|P_n|}{|Q_n|} \tag{6.26}$$

$$\Phi_{Z_n} = \Phi_{P_n} - \Phi_{Q_n} \tag{6.27}$$

If pressure and flow are measured simultaneously at the root of the aorta, the calculated impedance is called the 'input impedance' of the system, which fully captures the characteristics of the arterial tree.

$$Z_{in} = \frac{P_{ao}}{Q_{ao}} \tag{6.28}$$

The zeroth harmonic of the input impedance represents the ratio of steady-state (mean) pressure to flow, which corresponds to the total arterial resistance. For aortic pressure and flow, typically for higher frequencies, the phase angle of the input impedance oscillates around zero and the modulus remains virtually constant. This impedance value is the characteristic impedance which is required for the pressure and flow separation outlined in the previous section. It is defined as the ratio of pressure and flow in the absence of wave reflections. The value of the characteristic impedance can be estimated by averaging the modulus values of the third to tenth harmonics of the input impedance. For those high frequencies, reflected and incident waves interfere in a destructive way and the arterial system appears free from reflections. Alternatively, an approximation of the characteristic impedance can be determined in the time domain by the calculating the slope of the flow-pressure relationship during the first part of systole, as in general reflected waves did not yet have the time to return from the reflection sites at that time and the system again appears free from reflections.

6.3.4 Reflection coefficient

By calculating the characteristic impedance of the arterial tree, pressure and flow can be decomposed in their forward and backward constituents. The amount of reflection observed in a given system can be quantified by calculating the reflection coefficient (Γ) as:

$$\Gamma = \frac{P_b}{P_f} \tag{6.29}$$

which, given equations 6.24 and 6.25 equals

$$\Gamma = \frac{P_{ao} - Q_{ao}Z_0}{P_{ao} + Q_{ao}Z_0} \tag{6.30}$$

or, given equation 6.28:

$$\Gamma = \frac{Z_{in} - Z_0}{Z_{in} + Z_0} \tag{6.31}$$

Since the reflection coefficient is a complex number, often the reflected magnitude (Γ_M) is used to quantify wave reflection [50]:

$$\Gamma_M = \frac{|P_b|}{|P_f|} \tag{6.32}$$

Figure 6.5 illustrates the quantification of wave reflections in the frequency domain.

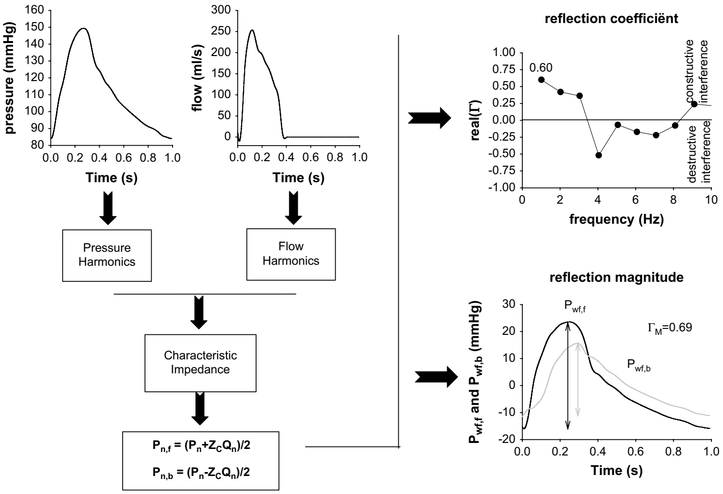
pressure (mmHg)
160
150
140
130
120
110
100
90
80
0.0 0.2 0.4 0.6 0.8 1.0
Time (s)
flow (ml/s)
300
250
200
150
100
50
0
0.0 0.2 0.4 0.6 0.8 1.0
Time (s)
Pressure Harmonics
Flow Harmonics
Characteristic Impedance
$P_{n,f} = (P_n+Z_cQ_n)/2$
$P_{n,b} = (P_n-Z_cQ_n)/2$
reflection coefficiënt
real(Γ)
1.00
0.75
0.50
0.25
0.00
-0.25
-0.50
-0.75
-1.00
0.60
constructive interference
destructive interference
0 2 4 6 8 10
frequency (Hz)
reflection magnitude
$P_{wf,f}$ and $P_{wf,b}$ (mmHg)
30
20
10
0
-10
-20
$P_{wf,f}$
Γ_M=0.69
$P_{wf,b}$
0.0 0.2 0.4 0.6 0.8 1.0
Time (s)

FIGURE 6.5: Schematic representation of the frequency domain method. Measured pressure and flow are decomposed in a series of harmonics, from which the characteristic impedance (Z_c) is calculated. For each harmonic, the forward and backward component is calculated, which can be used to display the (real part) of the reflection coefficient as a function of frequency. Alternatively, the reflection magnitude can be calculated from the ratio of the amplitudes of the reconstructed forward and backward waves [56].

6.4 THE ARTERIAL TREE AS A WAVE SYSTEM – TIME DOMAIN

6.4.1 Pressure and flow decomposition in wavefronts

Though the study of wave reflection in the frequency domain has proven to be very successful, it does have some drawbacks. It requires the decomposition of pressure and flow into its harmonics, necessitating the study of both their amplitude and phase angles to draw conclusions on the system, which is not very intuitive. As an alternative approach, Parker and Jones presented a different way of analyzing wave reflections in the time domain, called wave intensity analysis [57].

Rather than decompose the pressure and flow waveforms into sinusoidal components, wave intensity analysis considers the arterial pressure and flow waveforms to consist of a summation of infinitesimal ‘wavelets’ or ‘wavefronts’ [57, 58]. Each wavelet represents the change in arterial pressure (or flow velocity) during a given sampling period, i.e.

$$\begin{aligned} dP &= P(t+\Delta t) - P(t) \\ dU &= U(t+\Delta t) - U(t) \end{aligned} \tag{6.33}$$

Like for the decomposition of pressure and flow in their harmonics using Fourier-analysis, theoretically a signal can be perfectly reconstructed from its wavelets if the sampling period becomes infinitely small. In practice, a pressure and flow can be reconstructed reliably using some sufficiently small sampling period. Figure 6.6 on the next page illustrates the decomposition of a human aortic pressure waveform in sequential wavefronts.

Depending on the sign of dP and dU, four types of waves can be defined. To better understand the practical implications of the used terminology, it is useful to explain them considering a straight tube, in which the left to right direction has been defined as the forward direction. Depending on dP and dU, we can then discern:

Forward compression wave, which is characterized by $dP > 0$ and $dU > 0$. This is the type of wave you would get when *blowing* into the *left* side of the tube: pressure and flow velocity increase and the wavefront moves in the direction of the tube.

Backward compression wave, which is characterized by $dP > 0$ and $dU < 0$. This is the type of wave you would get when *blowing* into the *right* side of the tube: pressure increases, but velocity decreases and the wavefront moves from right to left.

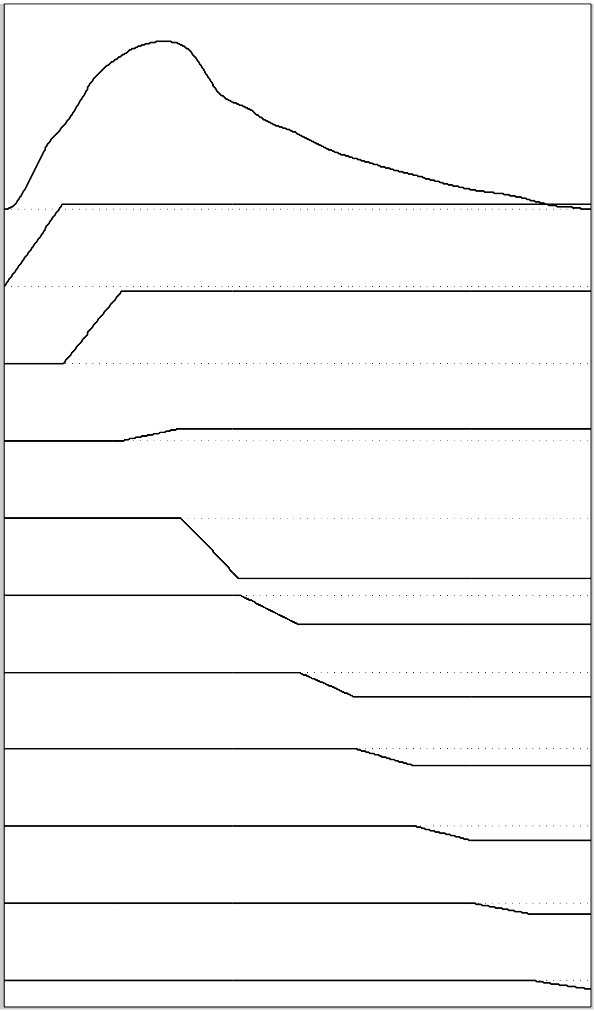

FIGURE 6.6: Separation of an aortic pressure waveform in sequential wavefronts

Forward expansion wave, which is characterized by $dP < 0$ and $dU < 0$. This is the type of wave you would get when *sucking* on the *left* side of the tube: both pressure and flow velocity decrease. The pressure decrease starts at the left side of the tube and moves to the right; the wavefront thus moves in the direction of the tube.

Backward expansion wave, which is characterized by $dP < 0$ and $dU > 0$. This is the type of wave you would get when *sucking* on the *right* side of the tube: pressure decreases, but velocity increases. The pressure drop starts at the right side of the tube and moves left, the wavefront thus moves from right to left.

Compression waves are thus characterized by an increase in pressure ($dP > 0$), while expansion waves are characterized by a decrease in pressure ($dP < 0$). By convention, forward and backward pressure and velocity waves are indicated by a subscripted '+' or '-' sign.

6.4.2 Wave intensity

The nature of a wave can best be described by its wave intensity, defined as

$$dI = dU\, dP \tag{6.34}$$

The wave intensity represents the energy flux carried by the wavefront, and is always positive for forward traveling wavefronts and always negative for backward wavefronts, regardless of whether the wavefront is a compression or expansion wave. If at any given time there are both forward and backward waves present in an artery, the wave intensity is given by the algebraic sum of the forward and backward wave components. If the resultant is positive, this indicates that forward waves are dominant, if it is negative, backward waves. The dominance of forward or backward waves is thus always visible by the sign of the net wave intensity. An example of the wave intensity derived from measured aortic pressure and flow velocity is shown in figure 6.7.

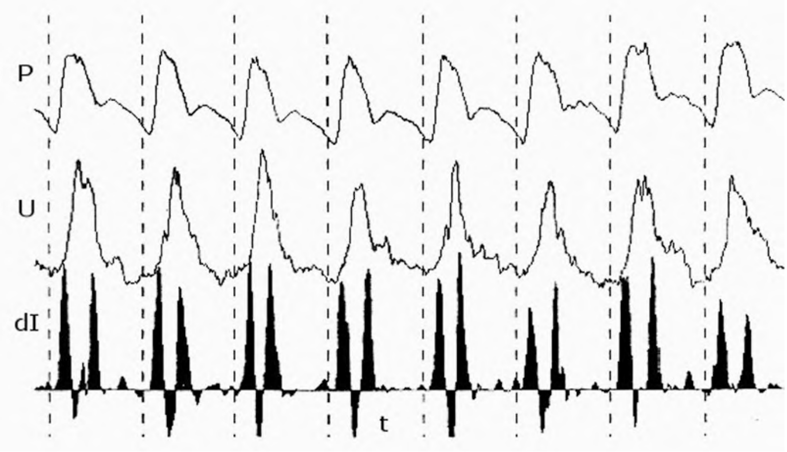

Figure 6.7: Measurement of wave intensity in the ascending aorta. The top trace is the pressure P, the middle trace the flow rate U, the bottom trace is the wave intensity dI calculated from P and U [57].

The definition of wave intensity given by equation 6.34 depends on the sampling interval over which dU and dP are measured, which makes comparison of wave intensities across studies performed using different sampling frequencies difficult. To overcome this problem, an alternative definition of wave intensity can be used:

$$dI' = \left(\frac{dP}{dt}\right)\left(\frac{dU}{dt}\right) \tag{6.35}$$

6.4.3 Separation of forward and backward waves in the time domain

According to the method of characteristics, any perturbation introduced in an artery will propagate with wave velocity $U \pm c$ in the forward (+) or backward (−) direction. The wave speed c is related to the stiffness of the artery by the Bramwel-Hill equation.

Assuming the wavefronts to be additive, the net pressure and wave velocity can be decomposed in their forward and backward components:

$$dP = dP_+ + dP_- \tag{6.36}$$

$$dU = dU_+ + dU_- \tag{6.37}$$

Taking into account the conservation of mass and momentum, dP and dU are related to each other by the water hammer equations:

$$dP_\pm = \pm\rho c \, dU_\pm \tag{6.38}$$

with ρ the density of blood.

Combining equations 6.36, 6.37 and the water hammer equations 6.38, the forward and backward pressure and flow velocity can be calculated in terms of the measured pressure and flow velocity:

$$\begin{aligned} dP_+ &= dP - dP_- \\ &= dP + \rho c \, dU_- \\ &= dP + \rho c \left(dU - dU_+\right) \\ &= dP + \rho c \, dU - \rho c \, dU_+ \\ &= \frac{dP + \rho c \, dU}{2} \end{aligned} \tag{6.39}$$

and likewise:

$$dP_- = \frac{dP - \rho c \, dU}{2} \tag{6.40}$$

The corresponding flow velocities can be found by applying the water hammer equations 6.38.

The total forward and backward pressure waveforms can then be obtained from these as:

$$P_+ = P_{dia} + \sum_{t=0}^{t} dP_+ \tag{6.41}$$

$$P_- = \sum_{t=0}^{t} dP_- \tag{6.42}$$

with P_{dia} the diastolic blood pressure.

Likewise:

$$U_+ = \sum_{t=0}^{t} dU_+ \tag{6.43}$$

$$U_- = \sum_{t=0}^{t} dU_- \tag{6.44}$$

The wave speed c can be determined from measured pressure and flow velocities using the water hammer equations (equation 6.38). In early systole, reflections are assumed to be minimal, so the slope of the P-U loop equals ρc.

Figure 6.8 on the next page shows an example of the separation of a measured aortic pressure (top panel) and flow velocity (bottom panel) waveform into its forward and backward constituents.

6.4.4 Reservoir-wave separation

Wave intensity analysis provides an attractive alternative to the classic analysis in the frequency domain. As it is entirely performed in the time domain, the interpretation of the results of wave separation with wave intensity analysis is far more intuitive. The wave separation theory as outlined in the previous section does however suffer from one problem. During diastole, the falling pressure coupled with small, nearly constant velocities, gives rise to the occurrence of relatively large, self-cancelling waves (see figure 6.8). These waves are a byproduct of the mathematical analysis, but are difficult to justify from a physiological point of view, as during diastole the arterial system is cut off from the left ventricle by the closure of the aortic valve.

To overcome this problem recently a new approach was proposed, combining elements of wave intensity analysis with the classic windkessel models [59, 60]. The reservoir-wave hypothesis assumes the

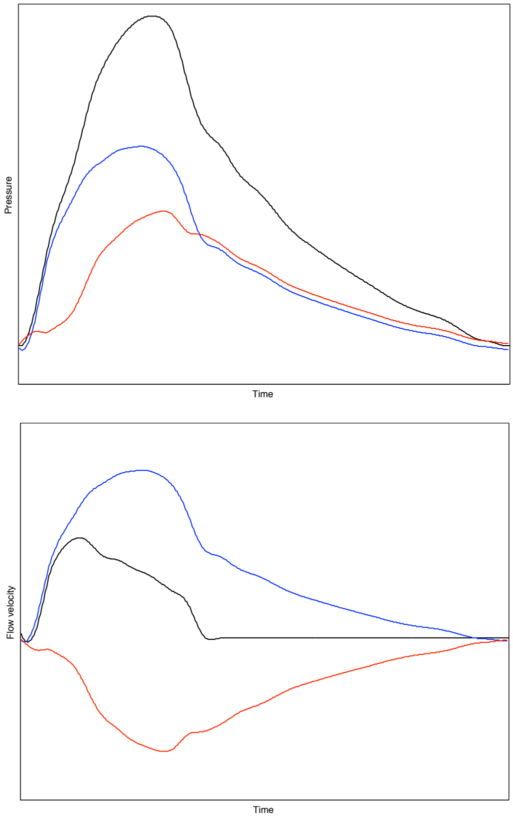

FIGURE 6.8: Separation of a measured pressure (top panel) and flow (bottom panel) into its forward and backward components. Top panel: black (top) line: measured pressure; blue (middle) line: forward pressure, red (bottom) line: backward pressure. Bottom panel: Blue (top) line: measured flow velocity; black (middle) line: forward flow velocity; red (bottom) line: backward flow velocity

observed pressure wave in the arterial system to be comprised of a static windkessel pressure (P_{res}), as defined by the 2-element windkessel model, and a wave pressure (P_{wave}) which drives the waves:

$$P(x,t) = P_{res}(t) + P_{wave}(x,t) \tag{6.45}$$

The reservoir pressure is derived from the measured pressure waveform by fitting an expression derived from a 2-element windkessel model to the fall-off of pressure during diastole [59, 60]. If the flow and pressure are simultaneously measured at the aortic inflow tract, it follows from the conservation of mass equations:

$$\frac{dV}{dt} = Q_{in} - Q_{out} \tag{6.46}$$

with Q_{in} and Q_{out} the flow into the arteries from the heart and from the arteries to the capillaries, respectively. Assuming the flow through the capillaries to be resistive, Q_{out} is given by:

$$Q_{out} = \frac{P - P_\infty}{R} \tag{6.47}$$

with R the resistance of the capillaries and P_∞ the pressure at which flow to the capillaries ceases.

With C, the total arterial compliance, as:

$$C = \frac{dV}{dP} \tag{6.48}$$

equation 6.47 can be rewritten as:

$$\frac{dP}{dt} + \frac{P - P_\infty}{RC} = \frac{Q_{in}}{C} \tag{6.49}$$

During diastole, when Q_{in} is zero, the solution of equation 6.49 is given by an exponential function:

$$P_{res} = P_{res,0}e^{-\frac{t}{\tau}} + P_{res,\infty} \tag{6.50}$$

with $\tau = RC$, the time constant of the exponential decay.

If the input flow has been measured simultaneously with pressure, the time constant τ can be determined from fitting an exponential equation to the pressure drop in diastole. Total arterial resistance can be determined from cardiac output (obtained by integrating the measured input flow) and mean blood pressure. Total arterial compliance can then be obtained from the fitted time constant τ and calculated total arterial resistance, and finally, P_{res} can be obtained from the solution of the differential equation 6.49. The wave pressure is obtained by subtracting the reservoir pressure from the measured pressure waveform.

Figure 6.9 on the following page shows the separation of an aortic pressure and flow waveform into its forward and backward constituents using the reservoir-wave hypothesis. This figure clearly shows that the large, self-cancelling waves found during diastole in figure 6.8 are no longer found using the reservoir-wave separation approach.

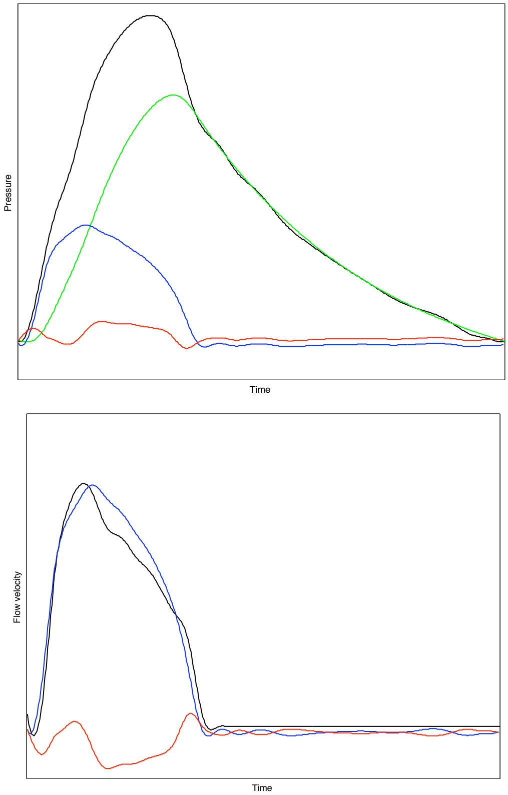

FIGURE 6.9: Separation of a measured pressure (top panel) and flow (bottom panel) into its forward and backward components using the reservoir-wave hypothesis. Top panel: (from top to bottom) black line: measured pressure; green line: calculated reservoir pressure, blue line: forward pressure, red line: backward pressure. Bottom panel: (from top to bottom) black line: forward flow velocity; blue line: measured flow velocity; red line: backward flow velocity

CHAPTER 7

The reservoir-wave pressure concept and the 3-element windkessel model

7.1 INTRODUCTION

Understanding the origin and nature of the pressure and flow waves generated by the heart pumping blood into the arterial system has always been of critical importance. To better understand the influence of arterial properties on these waveforms several models have been proposed. Two major, well-accepted ways of looking at the arterial system co-exist. The first approach, the so-called windkessel model of the arterial system, is the oldest. This model regards the arterial system as a lumped parameter model consisting of a resistance and compliance element placed in parallel, first mathematically described by Otto Frank [48]. The compliance represents the buffering capacity of the large elastic vessels, while the resistance represents the summed resistance residing in the small arteries and arterioles. The alternative model views the arterial system as a wave system in which arterial pressure and flow waveforms are the result of the interaction between forward travelling waves from the heart and backward reflected waves originating from points of impedance mismatch at the peripheral vessels and bifurcations.

Both models have their strengths and weaknesses and neither is significantly superior over the other in predicting all aspects of the arterial pressure and flow waveforms in all types of subjects. Moreover, recent studies indicate that the ideal way in which the arterial system should be regarded may change with age, with a wave system being more appropriate for younger subjects gradually evolving to a more windkessel like system with ageing [61].

This somewhat ambiguous behavior of the arterial system is confusing, and efforts have been made to construct models incorporating elements of both approaches to bridge the apparent differences between these models. One such model recently proposed regards the arterial system as a classic windkessel system which still allows for wave propagation and reflection by separating the pressure waveform into a reservoir and wave component [59, 60]. The major contributor to the pressure waveform in this approach is the reservoir pressure with the superimposed wave travel and reflection serving only to modulate this pressure. In essence, according to this model, the arterial pressure waveform can be regarded as the result of a combination of slow (~low frequency behavior in frequency domain) pressure changes due to loading and unloading of the pressure reservoir and fast acting (~high frequency behavior) changes due to forward and backward traveling waves.

The basis of this new approach appears similar to that of the three element windkessel model as first introduced by Westerhof *et al.* [53].This model builds upon the classic two element windkessel model proposed by Frank, which is able to accurately reproduce the low frequency behavior of the arterial system, by adding a third element: the characteristic impedance. This third element was added precisely to improve the high frequency behavior of the windkessel model.

The aims of this study are multiple. First, we want to apply the novel generalized wave separation approach proposed Aguado-Sierra *et al.* [59] based on the model previously proposed by Wang *et al.* [60] to non-invasively obtained pressure data from the Asklepios population and investigate the contribution of the reservoir pressure to pulse pressure with age and gender. Second, we will compare these results to the reservoir pressure obtained by applying a three element windkessel model to our data to study to what extent the wave separation approach is different from or provides added value to the classic three element windkessel model.

7.2 METHODS

7.2.1 Study population

Data for the present study were drawn from the first round of the Asklepios study, completed between October 2002 and September 2004. The Asklepios study is a large-scale, longitudinal population study designed to focus on the interplay between aging, cardiovascular disease and inflammation in (pre-clinical) cardiovascular disease. The complete database comprises 2,524 apparently healthy subjects (1,301 female, 1,223 male) constituting a representative cohort of 35–55 year old subjects randomly sampled from the twinned Belgian communities of Erpe-Mere and Nieuwerkerken. For the purpose of the present study, subjects were excluded if they were on current anti-hypertensive or lipid lowering therapy. A complete description of the rationale, methods and baseline characteristics of the Asklepios study population was previously published [42]. This section will briefly discuss the collection of basic clinical data and measurement of local carotid pressure and aortic outflow.

7.2.2 Basic clinical data

Basic clinical data was gathered by a study nurse. Subjects were allowed a 10-15 min period of rest in a temperature-controlled environment prior to all measurements. Blood pressure measurements were performed using a validated [62] oscillometric Omron HEM-907 blood pressure device with cuff sizes individually chosen based on arm circumference. Subjects were blinded to blood pressure results during measurements. Blood pressure values reported are distinct from baseline and were recorded before the tonometry measurements.

7.2.3 Measurement of local carotid pressure

Applanation tonometry was performed consecutively at the left brachial and carotid arteries using a Millar pen type tonometer (SPT-301, Millar Instruments, Houston, Texas, USA) and a custom-built hard- and software platform [63]. Applanation tonometry is a non-invasive approach for measuring local pressures that is performed by placing a micromanometer tipped probe (tonometer) on a superficial artery. By applying slight pressure to the artery, the arterial wall is flattened (applanated), allowing the micromanometer to record relative pressure changes in the artery. Absolute pressure changes are obtained by properly calibrating the measured pressure waveforms. A more detailed description of the setup, processing and calibration process used in the Asklepios study protocol was previously described [42]. Briefly, brachial artery tonometry readings were first calibrated by identifying the peak and trough of the waveform to oscillometric brachial artery systolic (SBP_{bra}) and diastolic (DBP_{bra}) blood pressure. These calibrated brachial artery waveforms were subsequently used to calibrate the carotid artery tonometry readings by identifying the mean and trough values of the carotid artery tonometry waveform to the calibrated brachial artery tonometry waveform. Mean values were determined by calculating the arithmetic mean of the tonometry waveforms. This approach is based on the validated [64, 65] assumption that mean and diastolic blood pressure remain relatively constant in the large arteries. In 417 subjects brachial artery waveforms could not be obtained with sufficient quality within a reasonable amount of time. For these subjects, the carotid tonometry reading was scaled using a calibrated radial artery waveform. The radial artery waveform was scaled using DBP_{bra} and an estimated value for the radial artery systolic blood pressure (SBP_{rad}) obtained from population based model:

$$SBP_{ra} = 4.974 + 1.11\ SBP_{bra} - 0.178\ DBP \tag{7.1}$$

This model was derived from a linear regression analysis on a subset of 1,863 subjects in the Asklepios study in which both brachial and radial artery tonometry readings were available (R^2=0.91). This approach was previously detailed and takes into account the brachial to radial amplification of systolic blood pressure [66].

7.2.4 Measurement of aortic outflow

Subjects underwent a resting echocardiographic examination using a commercially available ultrasound system (Vivid7, GE Vingmed Ultrasound, Horten, Norway) equipped with a cardiac (M3S) probe. Measurements were ECG gated and consisted of cineloops of at least five and up to 30 cardiac cycles during normal breathing. The internal diameter of the left ventricular outflow tract (LVOT) was measured and the LVOT area was calculated assuming circularity. Flow velocities were obtained in the LVOT. All images were exported for off-line processing within a dedicated software platform running in a Matlab environment (The Mathworks Inc, Natick, MA, USA) in order to determine the maximal velocities. The obtained maximal velocities were multiplied by the LVOT cross-sectional area to obtain the aorta outflow waveform (Q).

7.2.5 Determination of reservoir pressure by pressure wave separation ($P_{res,WS}$)

A mathematical framework for the separation of pressure and flow waves in a reservoir ($P_{res,WS}$) and wave component was recently published [59] based on the work of Wang *et al.* [60]. The latter was outlined in section 6.4.4 in chapter 6. Briefly, the reservoir pressure at an arbitrary location can be determined from:

$$\frac{dP_{res,WS}}{dt} = a\left(P - P_{res,WS}\right) - b\left(P_{res,WS} - P_v\right) \tag{7.2}$$

where

a, b: rate constants of the system

$P_{res,WS}$: reservoir pressure

The solution of equation 7.2 is given by:

$$P_{res,WS} - P_v = \left(P_{res,WS}(T_N) - P_v\right) \cdot e^{-b(t-T_N)},\ T_N \le t \le T \tag{7.3}$$

$$\begin{aligned} P_{res,WS} &= \frac{b}{a+b}P_v + e^{-(a+b)t}\dots \\ \dots&\left[\int_0^t aP(t')\, e^{(a+b)t'}dt' + P_{res,WS}(t=0) - \frac{b}{a+b}P_v\right], \\ &0 \le t \le T_N \end{aligned} \tag{7.4}$$

T: time when heart beat ends

T_N: time when aortic valve shuts at end of systole (dicrotic notch)

The venous pressure (P_v) was assumed to be zero. The dicrotic notch was visually identified on the carotid pressure waveforms.

$P_{res,WS}(T_N)$ was determined by fitting equation 7.3 to measured pressure during diastole; a and b were determined by fitting equation 7.4 and requiring continuity at $P_{res,WS}(T_N)$, both using an unconstrained non-linear optimization routine (fminsearch in Matlab), minimizing the sum of squares of the error between fitted and measured pressure data. Finally, $P_{res,WS}$ was determined for the entire period by combining equations 7.3 and 7.4. As free fitting of P_v resulted in unphysiological values for P_v in many cases, it was decided to set P_v to 0 mmHg for the entire dataset.

7.2.6 Determination of reservoir pressure using a 3-element windkessel model

We fitted the 3-element windkessel model to the available data. The analysis was performed in Matlab (version 7.0, The Mathworks, Natick, MA) using the fminsearch (Nelder-Mead simplex) algorithm with default convergence settings and without any constraints on the model parameter values [67]. We used measured flow, Q, as an input to the model, and minimized the difference between the model response (P_{model}) and the measured pressure, P.

The model response was calculated in the frequency domain through the impedance of the model (Z_{model}). As such, flow was decomposed into a Fourier series ($\sum Q_n$), the response for each harmonic (index n) was calculated, and these were recomposed ($\sum P_n$) to obtain P_{model}. For each harmonic, the following applies (see section 6.2.2 in chapter 6):

$$P_n = Z_{model} \cdot Q_n \tag{7.5}$$

For the 3-element windkessel model, Z_{model} becomes:

$$Z_{WK3} = Z_c + \frac{R}{i2\pi fRC} \tag{7.6}$$

with

f: frequency
i: the complex constant
R: vascular resistance
C: total arterial compliance
Z_c: characteristic impedance

Windkessel pressure in the 3-element windkessel model configuration, $P_{res,WK3}$ was calculated as

$$P_{res,WK3} = P_{model} - Q \cdot Z_c \tag{7.7}$$

Pressure and flow data obtained from the Asklepios study population were used to calculate reservoir pressures using the wave separation and windkessel models. The contribution of the reservoir pulse pressures obtained using either model to carotid pulse pressures was examined for men and women per age half-decade and differences between reservoir pulse pressures were examined. To quantify wave reflection, the reflection magnitude (the ratio of the amplitude of the backward to the forward pressure wave) was calculated from carotid pressure and aortic flow as previously described [61].

7.2.7 Statistical analysis

Subjects were divided into four age categories (35–40 years, 41–45 years, 46–50 years, 51–56 years). Comparison between groups was performed using t-tests. Influence of age and gender was evaluated using ANOVA analyses. All statistical analyses were performed in R 2.8.1 [68]. Values reported are mean (standard deviation). Statistical significance is indicated by P-values < 0.05 unless indicated otherwise.

7.3 RESULTS

7.3.1 Fitting performance

Table 7.1 on the next page summarizes the main descriptives of the study population. From the 2,524 Asklepios study subjects, 374 were excluded due to current antihypertensive or lipids treatment therapy. The required pressure and flow data were available in 2,019 subjects. The fitting procedure as outlined in [59] for determination of the wave separation model parameters was successful in 1,712 subjects (84.8%). For the remaining 307 subjects a modified fitting algorithm was used in which the diastolic part of the pressure waveform was defined as the last two thirds of the heart cycle past the occurrence of the dicrotic notch (as opposed to the part of the cycle from the dicrotic notch on). This modified algorithm was successful in determining the model parameters in an additional 227 subjects (11.2%). In 80 subjects (4.0%) the fitting algorithm did not converge to a solution. These subjects were discarded from further analyses. The parameters of the 3-element windkessel model were successfully determined in all subjects where the parameters of the wave separation model had been determined. Table 7.2 on the following page summarizes the average values for the fitted parameters for the wave separation and 3-element windkessel models. Figure 7.1 shows a representative example of the fittings using the reservoir pressure and windkessel model approach.

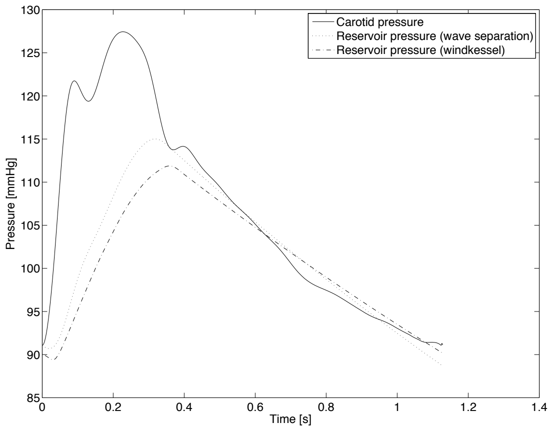

FIGURE 7.1: Representative example of the fittings to a carotid pressure waveform using the reservoir pressure and windkessel model approach

TABLE 7.1: Overview of general population parameters of the study population. Values are mean (SD).

Age (years)	45 (6)
Gender (F/M)	1,017 / 922
Weight (kg)	72.4 (13.7)
Height (cm)	169.3 (8.8)
SBP_{bra} (mmHg)	126 (8.8)
DBP_{bra} (mmHg)	126 (13)
PP_{bra}	46 (8)
Smoking (active/ex/never)	391 / 525 / 1,023
Total cholesterol (mg/dl)	216.3 (36.7)
HDL cholesterol (mg/dl)	64.8 (17.2)
LDL cholesterol (mg/dl)	130.5 (34.3)
Triglycerides (mg/dl)	104.5 (71.7)
Glycemia (mg/dl)	90.4 (8.9)

TABLE 7.2: Overview of fitting parameters for the reservoir-wave and three-element windkessel models obtained by fitting them to the measured carotid pressure data.

	Parameter	Mean (SD)
Reservoir pressure concept	a (s^{-1})	10.5 (22.3)
	b (s^{-1})	0.64 (0.15)
	$P_{res,WS}(T_N)$ (mmHg)	108 (14)
3-element windkessel model	R (mmHg/ml s)	1.18 (0.29)
	C (ml/mmHg)	1.66 (0.59)
	Z_c (mmHg/ml s)	0.10 (0.03)

7.3.2 Evolution of carotid pulse pressure and reservoir pressure with age in men and women and model comparisons

The change of carotid pulse pressure (PP_{car}) according to age quartiles for men and women is graphically represented in figure 7.2 on the facing page. Carotid pulse pressure increased with age regardless of gender (ANOVA, $P<0.001$), but did so in a more pronounced way for women. ANOVA analysis showed a significant age-gender interaction ($P<0.001$).

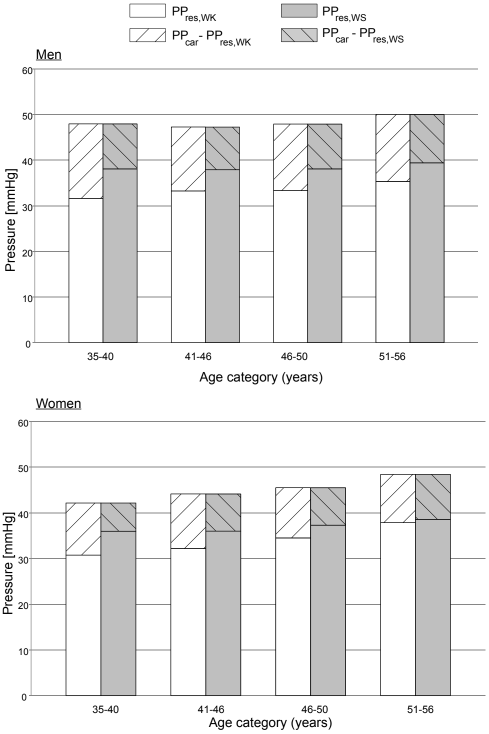

Figure 7.2: Stacked bar representation of the evolution of carotid pulse pressure and the contribution of the reservoir pressure determined by a wave separation model (white bars, $PP_{res,WS}$) and a three-element windkessel model (grey bars, $PP_{res,WK}$). Top: data for men; bottom: data for women. The difference between $PP_{res,WS}$ and $PP_{res,WK}$ is significant in men and women for all age groups, with exception of the 51-56 age group for women.

Figure 7.2 also shows the evolution of the reservoir pressure obtained from the wave separation model ($PP_{res,WS}$) and by applying a 3-element windkessel model ($PP_{res,WK}$). Reservoir pulse pressures increase with age ($P<0.001$), regardless of the model used for their determination. Both models show the evolution of PP_{res} with age to be different for men and women. Furthermore, figure 7.2 shows a good qualitative agreement between both models in the way in which the evolution with age differs. In both cases, PP_{res} increases more significantly in women. In men it only increases markedly in the oldest age group, whereas PP_{res} remains fairly constant in the first three age groups.

While there is certainly an agreement in the overall averaged tendencies in windkessel and reservoir pressure in men and women for both model approaches, figure 7.2 also reveals that the magnitude of PP_{res} in both differs, especially in the younger subjects, where $\mathrm{PP}_{res,WS}$ tends to higher values than does $\mathrm{PP}_{res,WK}$. These results are further illustrated in the top panel of figure 7.3 on the next page, showing a scatter plot of $\mathrm{PP}_{res,WS}$ and $\mathrm{PP}_{res,WK}$. While a relatively good correlation was found between $\mathrm{PP}_{res,WS}$ and $\mathrm{PP}_{res,WK}$ (R=0.76, P<0.001), as illustrated in the top panel of figure 7.3, there is a significant bias with $\mathrm{PP}_{res,WS}$ on average higher than $\mathrm{PP}_{res,WK}$, the difference being slightly more pronounced for higher PP values. The bottom panel of figure 7.3 finally, shows the Bland-Altman plot of $\mathrm{PP}_{res,WS}$ and $\mathrm{PP}_{res,WK}$.

7.4 DISCUSSION

The 2-element windkessel model as originally introduced by Frank [48] is probably still the most widely used model of the arterial system. Its elements are readily identified to physiological reality and it successfully explains the pressure drop in diastole as the uniformly decreasing outflow of a pressure reservoir in time. The 2-element windkessel model is virtually always the core element of more elaborate lumped parameter models [69] and the model is often the basis of methods used to determine total arterial compliance [51]. Nevertheless, it has its obvious shortcomings. It fails to accurately predict complete arterial waveforms, especially during systole, it does not take into account the wave propagation properties of the arterial tree and inherently assumes an infinite wave speed throughout the arteries [50, 70].

The value of considering the arterial tree as a wave system in which forward and backward travelling waves determine the shape of the arterial waveform in a complex interaction of constructive and destructive interference has long been demonstrated [6, 71, 72]. Models considering the arteries as a wave system have been proposed and yield relatively good predictions of arterial waveforms [53, 73–76]. They lack however the conceptual simplicity of linking a limited number of model parameters directly to physiological parameters as in the windkessel model. These models are most suitable to study 'forward' hemodynamic problems, i.e., the effect of changing arterial system properties on pressure and flow waves [74, 76], but they are too complex to be used in reverse engineering applications, i.e. estimating arterial properties from measured pressure and flow. Another potential problem

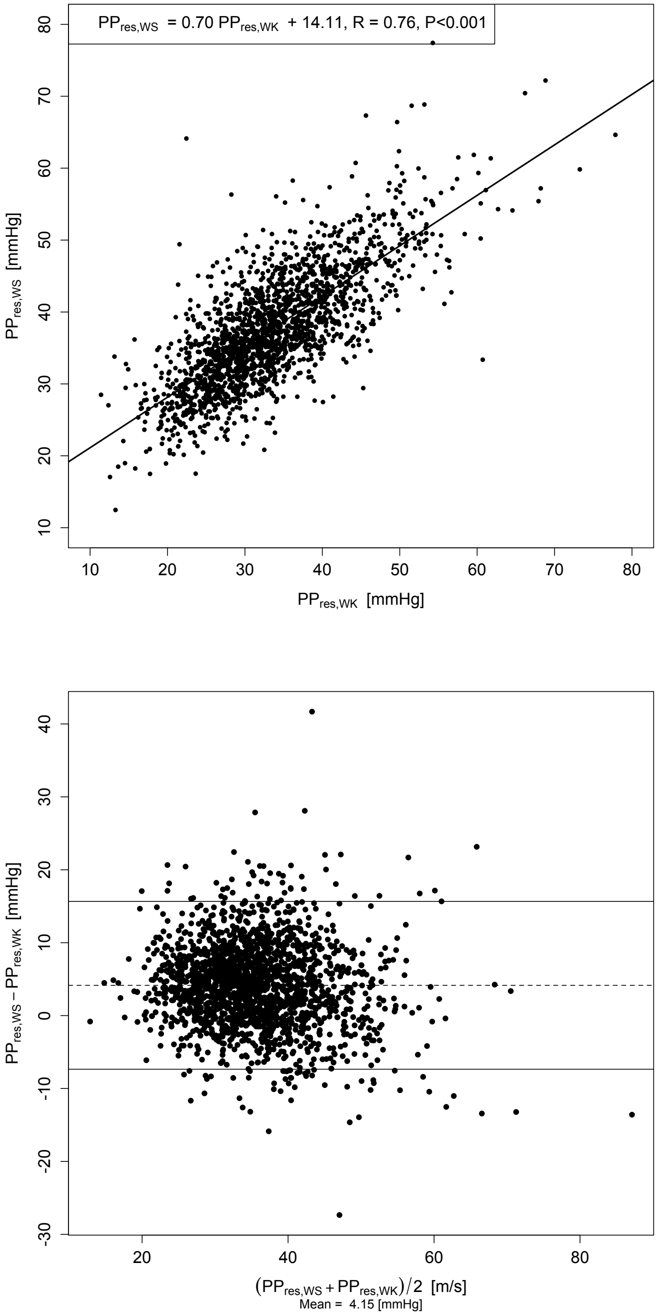

FIGURE 7.3: Top panel: regression of $PP_{res,WS}$ and $PP_{res,WK}$. Bottom panel: Bland-Altman plot of $PP_{res,WS}$ and $PP_{res,WK}$

with pure wave models is that the strict application of the wave separation theory to physiological pressure and flow profiles necessarily leads to the existence of relatively large, self-cancelling forward and backward waves during diastole. Though mathematically sound, these waves are difficult to explain from a physiological point of view as the arterial system is cut off from the left ventricle by the closure of the aortic valve during diastole [60].

Attempts have been made to improve both types of models. Westerhof *et al.* [50, 77] improved on the original windkessel model by adding a third component, the characteristic impedance, in an effort to improve the high frequency behaviour, most obvious in systole. Although this model is capable of closely mimicking arterial input impedance, it strictly does not take into account wave propagation and again implies an infinite wave speed through the arteries. Nevertheless, the introduction of the characteristic impedance can be seen as a link between the 2-element windkessel model, and the intrinsic wave system properties of the arterial tree [50, 77]. Quick *et al.* [78] further elaborated on reconciling the 3-element windkessel model and a wave model and introduced the concept of a frequency-dependent 'apparent arterial compliance', which allows to incorporate transmission line theory within the concept of the 3-element windkessel model.

The recently introduced hybrid conceptual model of the arterial system as a reservoir on top of which there is wave travel and reflection is another expression (in the time domain) of the urge to reconcile the two conceptual views of the arterial system [59, 60] and to solve the difficulty of the self-cancelling forward and backward waves during diastole found when applying a pure wave separation model.

The question is which of the two modelling approaches is most accurate. The description of the arterial tree as a branching network with wave travel and reflection is certainly the most general in nature. Based on measured patterns of input impedance in middle-aged subjects, Segers *et al.* [61] recently reported that treating the arterial tree as a wave system is probably more appropriate in younger subjects, while the arterial tree gradually evolves to a more windkessel like system with ageing. This observation is in accordance with the theoretical study of Mohiuddin *et al.* [79], who demonstrated that the systemic arterial tree degenerates into a windkessel with increasing pulse wavelength. With ageing and associated vessel stiffening, pulse wave velocity indeed increases, and so does the pulse wavelength, supporting our observations. Given these observations, the question as to which approach is the most appropriate is moot and hence the potential interest of hybrid models incorporating both windkessel and wave concepts. In theory, the hybrid reservoir-wave model might be able to capture both the windkessel-like arterial behavior of older subjects as well as the more wave-like aspects of the arterial tree in younger subjects.

In spite of its outward appearance, the wave separation model has a lot in common with the more established three-element windkessel model. Both view the arterial waveform as the result of an interaction between fast and slow acting phenomena, and both define a reservoir pressure driving the pressure drop during diastole. The main difference between the models lies in the way the fast acting phenomena are modelled: the 3-element windkessel adds a third component, disregarding wave phenomena, whereas the wave separation model seeks to model the fast acting phenomena by accounting for wave propagation effects. The former is applied in the frequency domain, while the latter is applied in the time domain. Nevertheless, in both models, the RC-element and the reservoir functionally act as filters, separating slow (low frequency) and fast (high frequency) wave phenomena. We therefore hypothesized that the reservoir pressures derived from either model should in theory agree relatively well. Our results indeed show that $PP_{res,WS}$ agrees well with $PP_{res,WK}$, with a relatively strong correlation between both (R=0.76). A further point of similarity between both models is found when examining the model parameters influencing the exponential decrease in diastole. For the wave separation model, the model parameter b is a measure of the exponential decrease in pressure in diastole. For the three-element windkessel model, the parameter 1/RC is indicative of the steepness of exponential decrease during diastole. A linear regression performed on 1/RC and b found an excellent correlation between both parameters (R=0.86, P<0.001), as illustrated in figure 7.4 on the following page. This further supports our view that the reservoir pressure concept is very similar to the concept of the arterial tree as a 3-element windkessel model.

The fitting of the wave separation model was, in our population, less evident than the fitting of the windkessel model parameters. For the calculation of our wave separation models we had to assume the venous pressure to be zero. In the fitting algorithm as outlined by Aguado-Sierra *et al.* [59], the venous pressure is a parameter, which is to be estimated in the optimization routine. We found that including the venous pressure as a parameter in the model however, yielded a large number of cases with values for the venous pressure that were not physiological. Even after assuming the venous pressure to be zero,

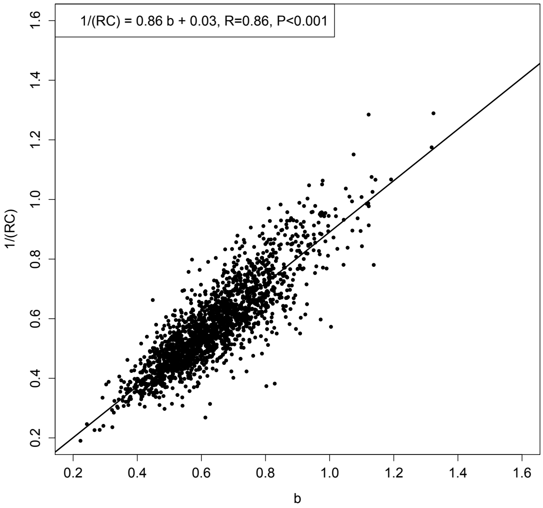

Figure 7.4: Regression of parameters b (from wave separation model) and 1/RC (from windkessel model)

which is a de facto simplification of the model, we found the original fitting procedure to yield unphysiological model parameters in 15% of our subjects, which we managed to decrease to 4% by slightly modifying the fitting algorithm. In contrast, we had no such problems in determining the model parameters for the 3-element windkessel model.

The problem associated with the fitting is related to the diastolic part of the waveform, which is not always a true exponential. To illustrate our case, we make use of two exemplary pressure waveforms (see figure 7.5 on the next page), which one may encounter in humans, one of the so-called A-type (left panel), and one of the C-type (right panel). As one might expect, the reflection magnitude (ratio of backward to forward pressure wave amplitude) was relatively high (0.68) for the A-type wave, while reflection magnitude was much lower for the C-type wave (0.33). The A-type waveform is characterized by an early return of the reflected wave (early inflection point). More importantly, the diastolic part shows a clear exponential decay, and this wave could be ascribed to a system with a high 'windkesselness'. The C-type wave, on the other hand, shows a late systolic inflection point and it can be appreciated that there is no clear exponential pressure decay in diastole. One could consider this system as having a low 'windkesselness'. This waveform is clearly more determined by wave phenomena, despite the fact that the reflection magnitude in itself is rather low. As one might expect, given the absence of the exponential decay in diastole, fitting the reservoir component to C-type waveforms is challenging. The fitting is relatively poor and a low reservoir pressure component is found, in contrast to the case of the A-type wave.

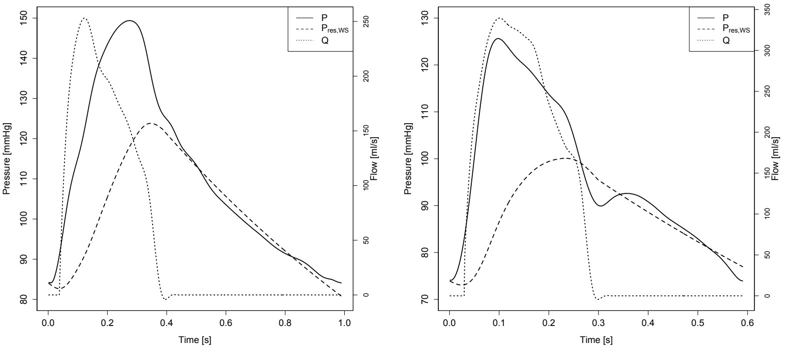

FIGURE 7.5: Case study for A-type (left panel) and C-type (right panel) waveform showing measured pressure (P; full line), flow (Q; dotted line) and reservoir pressure ($P_{res,WS}$, dashed line).

The result is also that, when plotting the excess pressure (P_{ex}; the difference between the total pressure and the reservoir pressure) as a function of flow, the relation between both much more adheres to a straight, linear relation for the A-type wave than for the C-type wave (figure 7.6 on the following page). This can be nicely illustrated when plotting the relation between the reflection magnitude and the area enclosed by the Q–P_{ex} loop (figure 7.7 on page 101, bottom panel). The finding that the relation between excess pressure and flow tends to linearize with increasing reflection magnitude is intriguing: in arterial hemodynamics, a linear relation between pressure and flow is indicative for a wave system free of reflected waves. Wang *et al.* [60] used this observation as an argument to state that, when subtracting the reservoir component, the excess pressure component is in phase with the aortic flow, suggesting that there is hardly any effect of reflected waves in systole. In our opinion, this interpretation might be too simplistic, as the flow waveform is not a single forward wave, but is in itself affected by reflected pressure waves [6] and is therefore a composite waveform.

It is our feeling that the fact that the relation between pressure and flow linearizes provides additional indirect evidence that the reservoir pressure concept is not (so) different from the 3-element windkessel model.

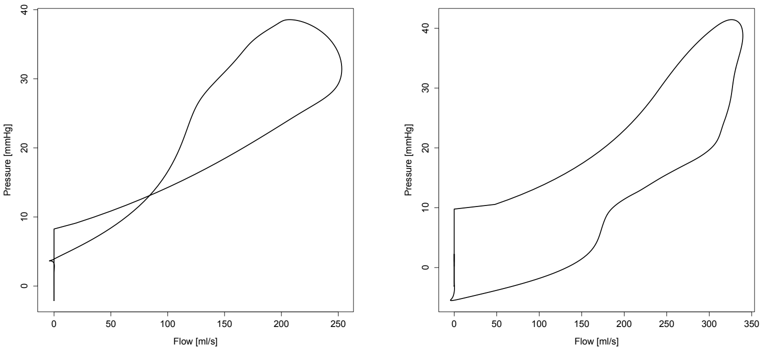

FIGURE 7.6: Case study for A-type (left panel) and C-type (right panel) waveform showing the relation between Q versus P_{ex} (excess pressure: the difference between measured pressure and $P_{res,WS}$).

These observations also imply that the greater the effect of wave reflection magnitude becomes, the better the reservoir pressure concept seems to hold. This is, in our opinion, due to the interplay between wave reflection and the 'windkesselness' of the system in the systemic circulation. In order to 'recruit' the buffer capacity of the arterial system and to load the windkessel, vascular resistance needs to be high enough, which leads to a greater effect of wave reflections and waveforms of the A-type exhibiting a clear exponential decay. When resistance is low (vasodilatation), the arterial buffer is far less recruited and there is no clear exponential decay (C-type waveform). As the reservoir component is more difficult to assess in these cases (without prolonging the diastolic phase), it becomes much more difficult to apply the reservoir pressure concept. As such, it is our feeling that the arterial system should display sufficient 'windkesselness' for the reservoir pressure concept to be applicable. This is to some extent counterintuitive, as the potential benefit of the reservoir pressure concept over windkessel models is that it aims to reconcile the windkessel and the co-existence of pressure waves.

In a different study performed in the Asklepios population (see chapter 13) it was found that local carotid stiffness indices, though grad-

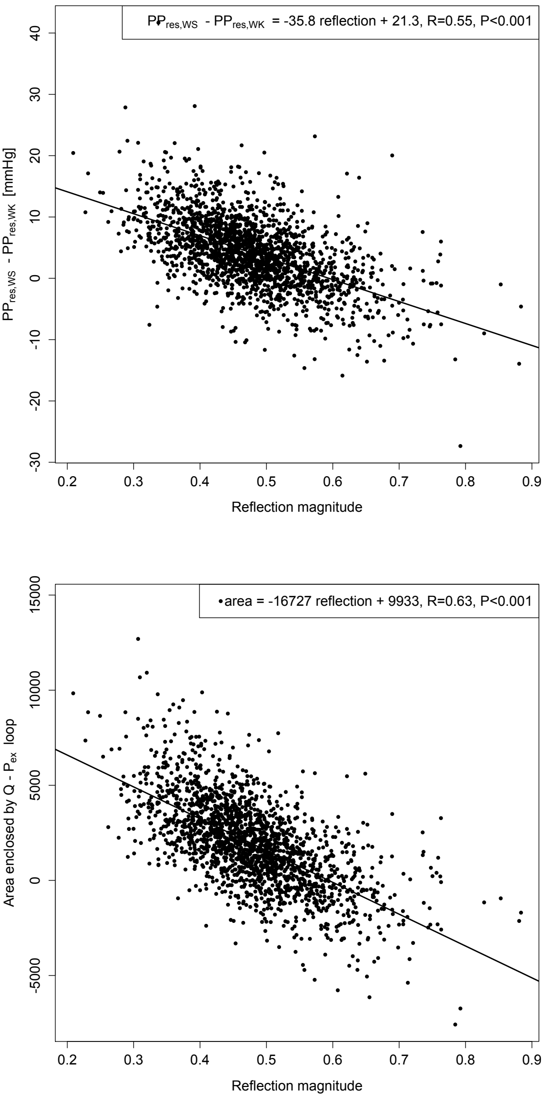

FIGURE 7.7: Top panel: Difference between reservoir pulse pressures derived using the wave separation ($PP_{res,WS}$) and windkessel ($PP_{res,WK}$) models versus reflection magnitude. Bottom panel: area enclosed by Q–P_{ex} versus reflection magnitude. P_{ex} (excess pressure) is found by subtracting the reservoir pressure ($P_{res,WS}$) from the measured pressure (P_{car}). Q: measured flow. The area is counted positive for loops running clockwise; negative for loops running counterclockwise, explaining the negative values in the graph.

ually increasing with age regardless of gender, increase differently in men and women [80]. Since pulse pressure levels are related, amongst other things, to arterial stiffness, the difference in behaviour of carotid pulse pressure with age is as expected. Our results show this increase in pulse pressure to be mostly due to the increase in reservoir pressure with age due to arterial stiffening of the vessels, and to a lesser extent due to the increase in reflections. When looking at the evolution of PP_{res} with age in men and women to a certain degree there is also a relatively good qualitative agreement between the wave separation and windkessel model approach. In both cases, reservoir pressure is fairly constant in men in the first three age quartiles, rising only in the fourth age group, whereas in women a constant, quicker increase in reservoir is found over all age quartiles. As anticipated, given the discussion above, the difference between both approaches is most clear in the younger age groups, where the contribution of reservoir pressure to total pressure is larger for the wave separation model than for the windkessel model. The difference gradually becomes smaller in the older age groups, which appears to be another reflection of the fact that with increasing age, the 'windkesselness' of the arterial system increases [61, 79]. These results are illustrated in figure 7.7 (top panel), which show the difference between $\text{PP}_{res,WS}$ and $\text{PP}_{res,WK}$ to decrease with increasing reflection magnitude.

Finally, it should be stressed that the data we used in this study were obtained non-invasively, implying some methodological limitations. We used hand-held carotid applanation tonometry recordings as surrogate for central pressure curves, and combined these with flow waveforms measured at the left ventricular outflow tract. Although both curves were carefully re-aligned in time, the contours of central and carotid pressure are not entirely equal. Also, the age range in our study is rather narrow. This has the advantage of focussed analysis over this specific age range, but precludes thorough analysis of effects of aging.

7.5 CONCLUSIONS

We have shown that the recently proposed (time domain) reservoir pressure concept shows large similarities to the classical (frequency domain) 3-element windkessel model, especially in subjects characterized by a high reflection magnitude and high 'windkesselness' of their arterial system. The more wave reflections are present in the system, and thus the more the arterial tree behaves like a windkessel, the better the reservoir pressure concept seems to hold. Hence, rather than unify the lumped parameter and wave reflection model views, the reservoir-wave concept thus seems to merely represent a time-domain wave propagation analogy of the classic three element windkessel model, albeit yielding slightly different quantitative results. When both models are applied to the Asklepios population, both show the increase of pulse pressure with age to be largely due to increasing reservoir pressures, rather than changes in wave pressures.

Four

Arterial stiffness

CHAPTER 8

Outline

The material in this section covers the bulk of the work performed during my PhD research. All of it is related in some way to different measures of arterial stiffness and tools for their assessment. The stiffness of the arteries is a critical parameter for the function of the cardiovascular system. Arterial stiffness has been shown to be predictive for clinical outcome in numerous populations and an elevated stiffness has been shown to be an independent predictor for all-cause and cardiovascular mortality. As such, measurements of arterial stiffness are increasingly used in clinical practice and have since long found their way in research and clinical trial settings.

Given the heterogeneity of the arterial system, with its wide range of differently sized arteries with differing structures, it should come as no surprise that arterial stiffness can be quantified using a similarly large set of different stiffness measures. Many arterial stiffness measures are related to certain models of the arterial network; these models were discussed in chapter 6.

Chapter 9 gives an overview of the most commonly used measures of arterial stiffness. These include systemic, regional and local measures and measures based on the quantification of wave reflections. Several of the arterial stiffness parameters discussed in this chapter require the measurement of central (aortic) pressure signals. Since true aortic pressure waveforms can only be obtained invasively through the use of catheters, alternatives have been developed to approximate central arterial pressure using some other waveform. Two main approaches exist: either pressures can be measured at the carotid artery, which due to its proximity to the aorta has pressure waveforms that match closely to invasively measured aortic pressures, or pressures measured at a different location—usually the radial artery—can be transformed into central pressures using a radial-to-aortic transfer function.

Both approaches have strengths and drawbacks. Carotid tonometry can be difficult to perform in the elderly, particularly obese subjects or in the presence of carotid artery plaques, and the transfer function is non-patient specific, being a population based function.

Chapter 10 examines another potential problem with the use of transfer functions. Over the course of the years, different transfer functions have been proposed, determined on different populations. Often, the type of transfer function used is tied to the device used to determine the central hemodynamics and arterial stiffness, and the impact of using different types of transfer functions is not always clear. The aim of this study was to investigate whether two established transfer functions could be used interchangeably for the calculation of central systolic blood pressure and augmentation index in a subset of the Asklepios population.

Chapter 11 investigates a possible alternative to carotid tonometry for measuring carotid artery pressures. Instead of determining carotid pressures directly from the tonometry readings, this study aims to ascertain whether calibrated diameter distension waveforms, obtained using ultrasound, could be used as a surrogate pressure signal. Depending on the assumed pressure-diameter relationship, different calibration schemes can be proposed. We investigated two calibration techniques, based on an assumed linear and exponential pressure-diameter relationship. For both relationships, the model parameters can be determined based on pressures obtained at a reference location (in our case, the brachial artery). The aim of the study was to compare systolic blood pressures and augmentation indices determined on linearly and exponentially scaled diameter waveforms to systolic blood pressures and augmentation indices determined on carotid artery tonometry readings in the Asklepios population. The results of this study have been published in:

S.J. Vermeersch, E.R. Rietzschel, M.L. De Buyzere, D. De Bacquer, G. De Backer, L.M. Van Bortel, T.C. Gillebert, P.R. Verdonck, P. Segers.

Determining carotid artery pressure from scaled diameter waveforms: comparison and validation of calibration techniques in 2,026 subjects. *Physiol Meas*, 29:1267–80, 2008.

Chapter 12 is a corollary to chapter 11. Both the exponential and linear pressure-diameter relationships are an approximation of the true pressure-diameter relationship that give good approximations of the true arterial pressure-diameter relationships in the largest part of the physiological pressure range. A far better approximation of the true arterial pressure-diameter relationship is given by the Langewouters relationship [81], determined by studying the diameter changes for a broad pressure range on excised human aortas. A second advantage to the sigmoidal langewouters pressure-diameter relationship is that it can be used to define a pressure dependent stiffness index. Most stiffness indices give some value of arterial stiffness which is either valid for a specific point in the cardiac cycle, or an average value over the complete cardiac cycle. As explained in chapter 1 however, the structure of the artery implies that its stiffness is inherently pressure dependent and thus changes over the course of the cardiac cycle. A pressure dependent index is thus a better representation of the real-life arterial behavior. The pressure dependent index proposed by Langewouters *et al.*, however, is geometry dependent, which makes comparing the stiffness index between subjects difficult. The goals of the study outlined in this chapter were (1) to propose a geometry independent, pressure dependent stiffness index based on the geometry dependent index proposed by Langewouters *et al.*; (2) to use this index to investigate the evolution of arterial stiffness with age and gender in the Asklepios population and (3) to compare this evolution with the evolution with age and gender of a different stiffness index, derived from the exponential pressure-diameter relationship.

Arterial stiffness indices measured at different locations do not necessarily match and may yield complementary information on the arterial system. *Chapter 13* investigates differences in age-gender interaction in local arterial stiffness determined on the carotid and femoral arteries and carotid-femoral pulse wave velocity in the Asklepios population. The results of this study were published in:

S.J. Vermeersch, E.R. Rietzschel, M.L. De Buyzere, D. De Bacquer, G. De Backer, L.M. Van Bortel, T.C. Gillebert, P.R. Verdonck, P. Segers. Age and gender related patterns in carotid-femoral PWV and carotid and femoral stiffness in a large healthy, middle-aged population. *J Hypertens*, 26:1411–19, 2008.

Despite its prognostic value and its growing use in clinical practice, the widespread use of arterial stiffness is hampered by the lack of reference values. The reference values for arterial stiffness' collaboration aims to remedy this issue by providing a large database to which participating centers contribute in order to obtain a representative and sufficiently large dataset on which reference values can be determined. During my PhD I performed the data collection and construction of the reference value database and performed the analysis leading to the reference values for pulse wave velocity.

Chapter 14 introduces the reference values for arterial stiffness' collaboration set-up and database.

In a first stage, the data from the reference value database were leveraged to investigate reference values for PWV, which is the current gold-standard method for assessing central arterial stiffness. PWV measures do however suffer from important methodological issues: a number of different definitions of PWV exist, and up to now no conversion factors between both had been investigated, making comparisons between or pooling of data from different centres impossible.

Chapter *15* presents a study in which an approach was investigated to convert between PWV definitions. In a subpopulation of the reference value database—consisting of the Asklepios and Hôpital Européen Georges Pompidou databases—in which all elements were available for the calculation of PWV according to either definitions, a population based statistical model is proposed which can be used for the conversion between definitions. The results of this study have been submitted for publication in:

S.J. Vermeersch, E.R. Rietzschel, M.L. De Buyzere, L.M. Van Bortel, T.C. Gillebert, P.R. Verdonck, S. Laurent, P. Segers, P. Boutouyrie. Influence of distance measurements on the assessment of carotid to femoral pulse wave velocity. Submitted to *J Hypertens*.

Using these conversion formulae, the PWV values in the reference value database were homogenized to a single PWV definition. In *Chapter 16* the influence of classic risk factors, age and blood pressure, on PWV is investigated in the reference value population and finally, reference values and normal values for PWV are presented.

Chapter 9

Arterial stiffness

9.1 Introduction

Over the past few years, there has been an increasing interest in the role of arterial stiffness in the development of cardiovascular disease. The term 'arterial stiffness' can be quantified by a number of different indices, depending on the scope and area of application in which the investigator is interested. Increasingly, arterial stiffness indices are included in the clinical assessment of patients, especially in large-scale clinical trials. One of these indices in particular, the measurement of carotid-femoral pulse wave velocity, has recently been recommended in the 2007 European Society of Cardiology / European Society of Hypertension guidelines for the management of hypertension [9] in order to assess arterial damage, evaluate the level of cardiovascular risk and adapt the therapeutic management of patients.

This chapter introduces the basic principles behind the most commonly reported measures of arterial stiffness. Indices will be categorized depending on their scope (systemic, regional or local) and clinical applications and limitations will be discussed. For a more thorough overview of the methodological issues and clinical applications on arterial stiffness measures, see [82].

9.2 ARTERIAL STIFFNESS AND MODELS OF THE ARTERIAL TREE

"Arterial stiffness" is a physical measure that often finds its basis in a specific conceptual modeling view of the arterial tree. To fully understand the use and limitations of the different types of these stiffness measures, a good working knowledge of the basic hemodynamics and modeling approaches of the arterial tree is required.

As outlined in chapter 6, there exist two basic views of the arterial system. One is the lumped parameter 'windkessel' view, the other the transmission line 'wave propagation' view. The most basic windkessel modeling approach separates the properties of the arterial tree in a resistive 'conduit' element and a capacitive 'cushioning' element [71, 83]. Following this approach, an increase in systemic resistance leads to an increase in mean arterial pressure, which translates to an equal increase in the difference between systolic and diastolic blood pressure. An additional decrease in arterial compliance leads to an increase in the amplitude of the oscillations in arterial pressure resulting in increased systolic pressures with little or no impact on diastolic blood pressures [83].

While the arterial windkessel provides useful insight in the physiology of the arterial tree, it does have two important limitations. First, the separate resistance and compliance elements modeled in the lumped parameter approach have no real-life counterparts. In reality, each vessel combines to some extent a conduit and cushioning function. The proportion of conduit and cushioning function the vessel exhibits depends largely on its location: while the large arteries in close proximity to the heart display a more 'elastic' behavior characterized by a predominant cushioning function, the more 'muscular' peripheral arteries have a predominant conduit function. A second problem is that the windkessel models inherently assumes wave travel through the arterial tree at infinite speed: at any given time the waveform is assumed to be the same in all locations of the arterial tree. This is clearly not the case in real life. On the contrary, due to the gradual increase in arterial stiffness from the central (elastic) to the peripheral (muscular) arteries, the amplitude of the pressure wave also gradually increases from the central arteries to the periphery, an effect which is referred to as the central to peripheral pressure amplification.

Wave propagation models inherently incorporate these issues. They assume the speed at which a wave travels through the arterial tree to be of finite value, as derived by Bramwell and Hill from the Moens-

Korteweg equation:

$$c_0 = \sqrt{\frac{Eh}{2R\rho}}\ [m/s] \tag{9.1}$$

with

c_0: wave speed [m]
E: Young's modulus [Pa]
h: wall thickness [m]
R: radius [m]
ρ: blood density [kg/m^3]

yielding:

$$c_0 = \sqrt{\frac{1}{\rho}\frac{V \cdot dP}{dV}} \tag{9.2}$$

with

dP: change in arterial pressure [Pa]
dV: change in arterial volume due to dP [m^3]

The Bramwell-Hill equation (equation 9.2) was the first to demonstrate the relationship between wave speed (c_0, commonly referred to as pulse wave velocity (PWV)) and stiffness ($dV/(V \cdot dP)$), showing wave speed to increase with increasing stiffness. Wave propagation models additionally assume the wave propagated from the heart to the peripheral arteries to reflect at sites of impedance mismatch, which include bifurcations and the termination of the arterial tree in the smaller muscular arteries. The reflected wave interferes with the propagated wave, resulting in a pressure amplification which can occur during the systolic phase if the wave is reflected with sufficient speed (i.e. in stiffer arteries).

A distinct advantage of the parameters derived from the wave propagation approach is that, contrary to those derived from lumped parameter models, which need to be estimated by applying the model to measured pressure and/or flow, they can be directly and non-invasively measured at different locations in the arterial tree.

Finally, it should be pointed out that arterial stiffness measures are always to some extent dependent on the operating environment in which they are determined. Some measures are directly affected by heart rate, vessel size or other confounding factors, others like pulse wave velocity are largely independent of these influences, but none can be completely separated from the conditions in which they are taken. From a physiological point of view, the stiffness of a vessel increases with increasing pressure, as with increasing vessel diameter more and more of the elastin fibers in the vessel wall are being recruited and increasingly the stiff collagen fibers come into play. The instantaneous stiffness of a vessel therefore even changes during each cardiac cycle. Most arterial stiffness measures offer some average value of stiffness over the complete cardiac cycle.

In what follows we will first briefly discuss how stiffness parameters can be derived by applying lumped parameter models to measured pressure and flow waveforms before delving more deeply into a number of stiffness parameters linked to the wave propagation view of the arterial tree. Since lumped parameter models, by assuming an infinite wave speed, are by default 0-dimensional models, they can only be used to derive systemic stiffness indices quantifying the stiffness of the entire arterial tree. Stiffness parameters based on the wave propagation view can be subdivided in 'direct' regional or local stiffness parameters, which offer a direct quantification of the intrinsic arterial stiffness over a segment (regional indices) or a specific location (local indices) of the arterial tree and indices which quantify wave reflections.

9.3 LUMPED PARAMETER VIEW — SYSTEMIC PARAMETERS

Total arterial resistance (R) is commonly determined from the ratio of mean aortic pressure to cardiac output (neglecting venous pressure), as previously outlined in chapter 6. For the determination of total arterial compliance in the time domain, different methods exist, all based on the windkessel model of the arterial system. Of these, the most commonly used are the time decay method, the area method and the pulse pressure method.

9.3.1 Time decay method [48]

According to the two-element windkessel method, during diastole, when flow is zero, the decrease of aortic pressure is governed by an exponential equation:

$$P(t) = P_0\, e^{\frac{-t}{RC}} \tag{9.3}$$

By fitting equation 9.3 to the diastolic part of a measured (aortic) pressure profile, and using the estimate of R obtained from the mean aortic pressure and the cardiac output, an estimate of the total arterial compliance can be obtained.

9.3.2 Area method [84]

The time decay constant RC can also be determined from the area underneath the diastolic part of the arterial pressure waveform. At any given point of the arterial tree, the change in volume is determined by the continuity equation:

$$\frac{dV}{dt} = Q_{in} - Q_{out} \tag{9.4}$$

with

Q_{in}: flow rate into the system
Q_{out}: flow rate out of the system

By definition, total arterial compliance is given by:

$$C = \frac{dV}{dP} \tag{9.5}$$

The relationship between blood flow and total arterial resistance is assumed to be linear:

$$Q_{out} = \frac{P - P_0}{R} \tag{9.6}$$

P_0 represents the venous pressure, which for the sake of simplicity, we can assume to be zero here. Combining equations 9.4, 9.5 and 9.6 yields:

$$Q_{in} = C\frac{dP}{dt} + \frac{P}{R} \tag{9.7}$$

During diastole, Q_{in} is zero, and equation 9.7 reduces to:

$$C\frac{dP}{dt} + \frac{P}{R} = 0 \tag{9.8}$$

The 2-element windkessel model assumes R and C to be constants. Equation 9.8 can thus be solved by direct integration during diastole. Assuming diastole to occur from t_1 to t_2 we get:

$$C\int_{t_1}^{t_2} \frac{dP}{dt}dt + \frac{1}{R}\int_{t_1}^{t_2} Pdt = 0 \tag{9.9}$$

or

$$RC = \int_{t_1}^{t_2} \frac{P}{P_1 - P_2}dt \tag{9.10}$$

The time decay can thus be determined from the area under the diastolic part of the pressure curve divided by the pressure difference between start and end points.

9.3.3 Pulse pressure method [85, 86]

As a final example, the total arterial compliance can also be determined by fitting the output of a two-element windkessel model to measured pressures. In order to do so, a measured flow waveform is entered into the windkessel model using an estimated value for total arterial resistance as outlined above and a guess for the value of total arterial compliance. The pulse pressure from the waveform thus obtained is compared to actually measured pulse pressure. If the difference between estimated and measured pulse pressure is larger than some threshold value, the procedure is repeated with a new guess for the total arterial compliance. Compliance adjustment is often performed through trial and error, taking into account that higher compliances lead to lower pulse pressures.

9.3.4 Clinical applications of systemic arterial stiffness parameters

Total arterial compliance and resistance obtained from the application of windkessel models to measured aortic pressure and flow can yield valuable information on the overall status of the cardiovascular system, but their use is mainly restricted to theoretical applications. One difficulty with the fitting of windkessel models is that ideally, they require pressure and flow to be measured simultaneously at the level of the ascending aorta. The measurement location is of importance as for most fitting approaches it is important the flow to be zero during a large segment of the diastolic phase to get stable results. While flow profiles can be obtained non-invasively using Doppler echography, aortic pressure measurements are invasive. Carotid tonometry can be used as a surrogate with good results, though its use does introduce the additional difficulty of properly aligning measured pressures and flows on their respective time scales.

The use of systemic stiffness parameters in a clinical setting has been investigated, but up to now, no evidence has been found to demonstrate total arterial compliance to have an independent predictive value for cardiovascular events [87].

9.4 DIRECT MEASURES OF ARTERIAL STIFFNESS — LOCAL PARAMETERS

9.4.1 Compliance and distensibility coefficient

The assessment of most local stiffness parameters is based on simultaneous pressure and diameter measurements at a given arterial location.

Pressures can be measured non-invasively by applanation tonometry [65], which is relatively easy to perform at most superficial arterial sites and is routinely performed at the carotid, femoral, brachial and radial arteries. Obtaining pressures and diameters simultaneously is often difficult, in which case sequential pressure and diameter tracings can be used. Pressure tracings obtained using tonometry then additionally require proper calibration to obtain absolute pressure readings.

A major advantage of these parameters is that they are direct estimates of arterial stiffness, which means they are directly obtained from measured pressure and diameter without having to fit model parameters which by default offer but an approximation of the true arterial behavior.

Two commonly reported local measures of arterial stiffness are the cross-sectional compliance and distensibility coefficients, representing the relative and absolute changes in lumen area during systole for a given pressure change. The arterial cross-section is calculated from the measured arterial diameter (d) by assuming the lumen to be circular:

$$A = \frac{\pi \cdot d^2}{4} \tag{9.11}$$

From this calculated area, the compliance (CC) and distensibility (DC) coefficients are calculated as:

$$CC = \frac{\Delta A}{\Delta P} \left[\frac{m^2}{kPa} \right] \tag{9.12}$$

$$DC = \frac{\Delta A}{A_{dia} \cdot \Delta P} \left[\frac{1}{kPa} \right] \tag{9.13}$$

with

ΔP: local pulse pressure

ΔA: local area change between systole and diastole

A_{dia}: local area at diastole

Note that the compliance coefficient is geometry dependent: the compliance coefficient of larger vessels will by definition almost always be higher than that of smaller vessels due to the larger absolute area increase from diastole to systole in the former. This implies that for instance comparing compliance coefficients of similar vessels in men and women is difficult, as men on average have larger vessels and thus larger compliance coefficients for similar vessels.

9.4.2 Clinical applications of local stiffness measures

While local diameter and pressure measurements are relatively easily performed and are non-invasive, their determination does require skilled operators, especially for local pressure determination by applanation tonometry. They also require specialized devices, proper calibration and are relatively time-consuming to perform correctly. For these reasons, the measurement of local stiffness is usually restricted to research settings rather than routine clinical practice.

9.5 DIRECT MEASURES OF ARTERIAL STIFFNESS — REGIONAL PARAMETERS

Regional stiffness measures rely on the measurement of the wave speed of the arterial pulse along a section of the arterial tree. Though pulse wave velocity (PWV) can be measured along any segment of the arterial tree, the major vessel of interest is the aorta, as it makes the largest contribution to the arterial buffering function and as it is what the left ventricle 'sees' being the first connection of the ventricle to the rest of the arterial system.

9.5.1 Pulse wave velocity definition

PWV is a measure of regional arterial stiffness of the arterial territory between the two measurement sites. This parameter is related not only to the elastic modulus (E) of the arterial wall (which represents the intrinsic stiffness of the wall), but also to the arterial geometry (thickness and radius) and blood density as illustrated by the Moens-Korteweg equation 9.1. Bramwell and Hill applied the Moens-Korteweg equation to arterial physiology and described the relationship in terms of relative change in volume and pressure during ex vivo experiments (equation 9.2), demonstrating that PWV is a direct measure of arterial stiffness since it is proportional to the square root of 1/distensibility:

$$PWV = \sqrt{\frac{1}{\rho}\frac{V\,dP}{dV}} \tag{9.14}$$

Assuming the lumen to be circular, and with the length of the artery L:

$$V = A \cdot L \tag{9.15}$$

this gives:

$$PWV = \sqrt{\frac{1}{\rho}\frac{A}{dA}dP} \tag{9.16}$$

which in terms of the distensibility (D) equals:

$$PWV = \sqrt{\frac{1}{\rho\, DC}} \tag{9.17}$$

The assessment of PWV involves measurement of the transit time of the arterial pulse along the analyzed arterial segment (Δt) and the distance on the skin between both recording sites (L) (figure 9.1).

$$PWV = \frac{L}{\Delta t} \tag{9.18}$$

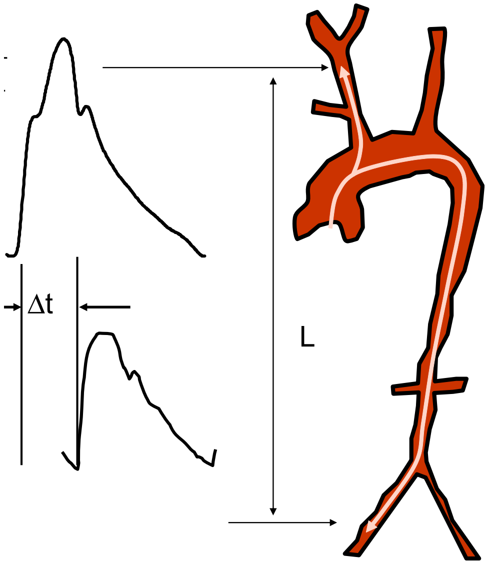

FIGURE 9.1: Measurement of carotid-femoral pulse wave velocity[88]

Pulse wave velocity can be assessed based on different types of waveforms, such as pressure waves, distension waves or flow waves. Although these waves are different in nature, they are theoretically in phase at the early phase of cardiac cycle, and therefore should be interchangeable for the calculation of PWV. The most often used signal is the pressure wave, although this choice may not be the best as it implies the application of a pressure transducer on the artery of interest, and inadequate application may result in distorted waves. Non or minimal contact techniques such as echotracking or Doppler may yield better results, with either high definition distension waves (at the cost of expensive equipment) or sharp systolic upstrokes for Doppler. The transit time is usually measured between the two different measurement sites. Both for the transit time and the distance used for the calculation of PWV differences in methodology exist, leading to differences in absolute PWV values of up to 30% between methodologies.

9.5.2 Transit time: detection of the foot of the waveform

The exact part of the waveform detected at the measurement sites from which the time delay is calculated is of crucial importance for the reliability and reproducibility of the technique. Since the instantaneous stiffness of any vessel is pressure-dependent, PWV varies during the cardiac cycle and choosing a reference point at end-systole will result in different values of PWV than if the reference point is placed at end-diastole. Moreover, the shape of the pressure waveform is different for different arterial sites, as it is influenced by the timing and amplitude of reflected waves which are dependent on the proximity of the arterial site to the reflection points. All this means that the humps and bumps of a waveform seen at one site do not necessarily correspond to the ones seen on other sites [89, 90].

An implicit consensus is to use the systolic upstroke as the reference point. Although this point seems to be well-defined, enlargements of foot of the wave exhibit a very mild transition from diastole to systole, especially at the carotid site [91]. Therefore, identification of the foot of the wave has to rely on algorithms. The three algorithms that are used are intersecting tangents, point of maximum upstroke of the wave by detection of the first or second derivative zero crossing and 10% of the pulse pressure (figure 9.2 on the next page). They have been compared by Millasseau *et al.* [90], who showed that the intersecting tangent method was the most reliable, although the other two methods were also consistent and not influenced by heart rate.

9.5.3 Measurement sites and distance measurements

Pulse wave velocity can be measured on any vessel. The theory underlying the relationship between PWV and stiffness assumes a homogeneous, isotropic material, with no curvature—essentially an infinitely long uniform tube—which is obviously not the case for arteries. The preferred site for the proximal measurement is the common carotid artery, and the femoral artery for the distal site. This introduces a conceptual problem in that the pressure waveform moves in

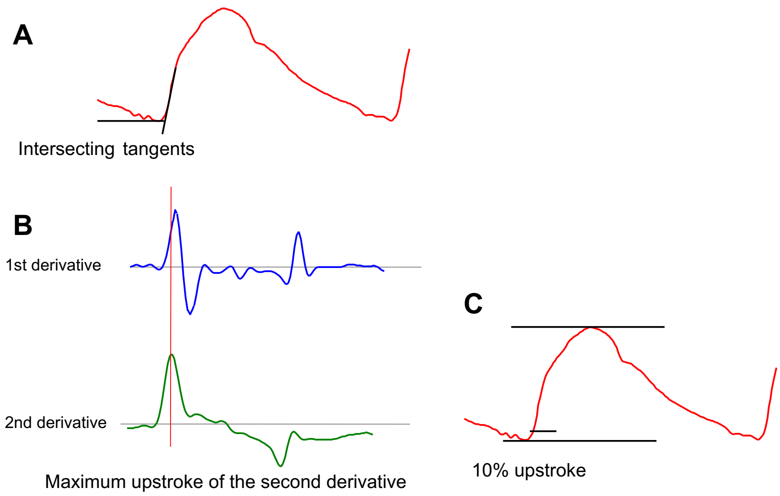

Figure 9.2: Different algorithms used to identify a specific reference point on a waveform (here a distension waveform of the carotid artery). Panel A: intersecting tangents; panel B: maximal upstroke by peak detection in the second derivative; panel C: percentage of the maximal amplitude of the waveform.[88]

opposite ways in both measurement sites. This is not a major issue assuming the stiffness of the common carotid artery to be identical to that of the thoracic aorta, which is a reasonable assumption in most cases. Nevertheless, the differing direction of wave propagation and the definition of the 'true' distance traveled by the detected waveform has given rise to a number of different path lengths which are commonly used to calculate carotid-femoral PWV. Different ways to define the path length travelled by the waveform are illustrated in figure 9.3 on the following page. The simplest approach is to measure the direct distance between the two measurement sites either transcutaneously or by use of a caliper. This approach leads to a systematic overestimation of PWV by about 30%. It is possible to correct this by using a path length defined by subtracting the distance from the carotid measurement site to the sternal notch from the distance between the sternal notch to femoral measurement site. This approach delivers PWV values which are closer (but not identical) to invasive measurements, but is more complicated and the multiple measurements required for the path length determination is a source of errors. Moreover, the direct (carotid-femoral) distance was used in nearly all epidemiological studies [82].

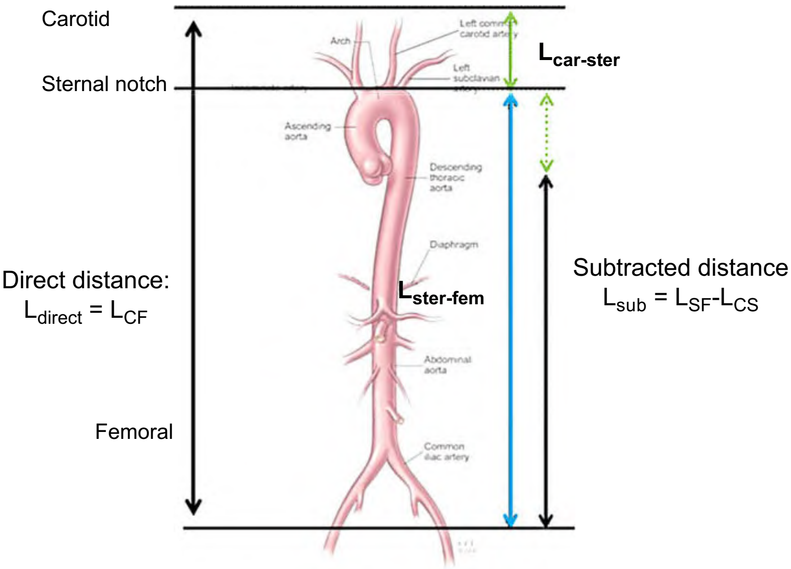
Carotid
Sternal notch
Direct distance:
$L_{direct} = L_{CF}$
Femoral
Arch
Left common carotid artery
Left subclavian artery
Ascending aorta
Descending thoracic aorta
Diaphragm
$L_{ster\text{-}fem}$
Abdominal aorta
Common iliac artery
$L_{car\text{-}ster}$
Subtracted distance
$L_{sub} = L_{SF}\text{-}L_{CS}$

FIGURE 9.3: Overview of different approaches for defining the path length for PWV calculation

The issues of the different transit time and path length definitions used for PWV calculations present a serious hurdle in the development of reference values for PWV, which will need to be dealt with if results from different studies are to be pooled or compared.

9.5.4 Clinical applications of PWV

Carotid-femoral PWV is at present the most widely used index of arterial stiffness, and has demonstrated its predictive value independent of, and above and beyond classical risk factors in more than 11 longitudinal follow-up studies, performed at different centers throughout the world and including various types of populations [82]. Pulse wave velocity also predicts cognitive decline [92–94] and further increase in systolic blood pressure [95]. The measurement of carotid-femoral pulse wave velocity has been considered as the 'gold standard' measurement of arterial stiffness in a recent expert consensus document [82] and is generally accepted as the most simple, robust and reproducible method to determine aortic stiffness.

9.6 INDICES QUANTIFYING WAVE REFLECTIONS

9.6.1 Central pressure wave analysis

As described in section 9.1, the wave propagation models of the arterial tree consider the arterial pressure waveform to be the resultant of the interference between a forward pressure wave generated by the left ventricle and a reflected wave originating from the different points of impedance mismatch along the arterial tree. For elastic vessels, in which the pulse wave velocity is low, the reflected wave arrives back at the aortic root sometime during late systole, which in some cases is visible by the appearance of a second peak in the pressure waveform. For stiffer arteries, the reflected wave returns faster, and in some cases arrives during the early systolic phase, where it adds to the systolic pressure. This pressure augmentation due to the increased speed at which waves return in stiffer arteries is one of the reasons why systolic blood pressure increases with age, as arterial stiffness also increases with age.

The timing of the return of the reflected wave, and the resulting augmentation of arterial pressure, is thus an indirect index of arterial stiffness, which can be quantified through the augmentation index (AIx), defined as the difference between the second and first systolic peaks expressed as a percentage of the pulse pressure (figure 9.4 on the next page) [96, 97]. AIx is sometimes used as an indirect index of arterial stiffness, but is influenced by a number of other factors, most importantly those which have an influence on the location of the reflection sites, such as height and DBP, next to heart rate. For these reasons, AIx should not be used as an independent measure of arterial stiffness.

Though the augmentation index can be calculated from waveforms obtained at any arterial location, ideally it should be derived from central (aortic) pressures. Non-invasive approximations of central pressures can either be obtained by carotid artery tonometry or by applying a so-called transfer function [99–101] on waveforms obtained at the radial artery. Carotid tonometry is more difficult to perform than radial artery tonometry, requiring a more experienced operator and being more difficult in particularly obese subjects, but does not require the use of a transfer function as the carotid artery is anatomically located in close proximity to the aorta and carotid artery waveforms have been found to be very similar to aortic waveforms [99].

Next to the augmentation index, central pulse pressure is also sometimes used as an indirect index of arterial stiffness. Pulse pressure is

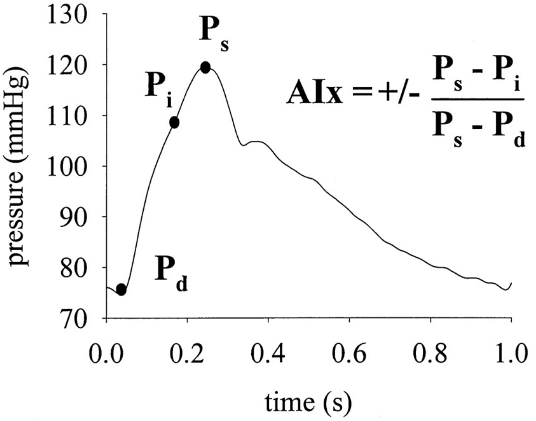

FIGURE 9.4: Carotid pressure waveform recorded by applanation tonometry and definition of augmentation index.[98]

co-determined by different non-stiffness related parameters, like heart rate and stroke volume, and should thus—like augmentation index—never be used as a single independent measure of arterial stiffness. Estimating central pulse pressures from carotid artery tonometry introduces an additional difficulty: the pressure waveforms obtained by applanation tonometry give only relative pressure information. To transform these into absolute pressures, some sort of calibration is required. An often performed calibration technique was proposed by Van Bortel *et al.*, [65] based on the observation that mean and diastolic blood pressures remain fairly constant throughout the large arteries. In practice, mean arterial pressure and diastolic blood pressure are obtained at a reference artery, usually the brachial artery, and subsequently used to calibrate the carotid tonometry readings (figure 9.5 on the facing page).

9.6.2 Clinical applications of pressure wave analysis

Central augmentation index and pulse pressure have been linked to all-cause mortality in end-stage renal disease patients [102, 103], as well as for cardiovascular events in patients of the CAFÉ study [104]. At other arterial sites, like the carotid artery, the evidence is less clear or inconclusive.

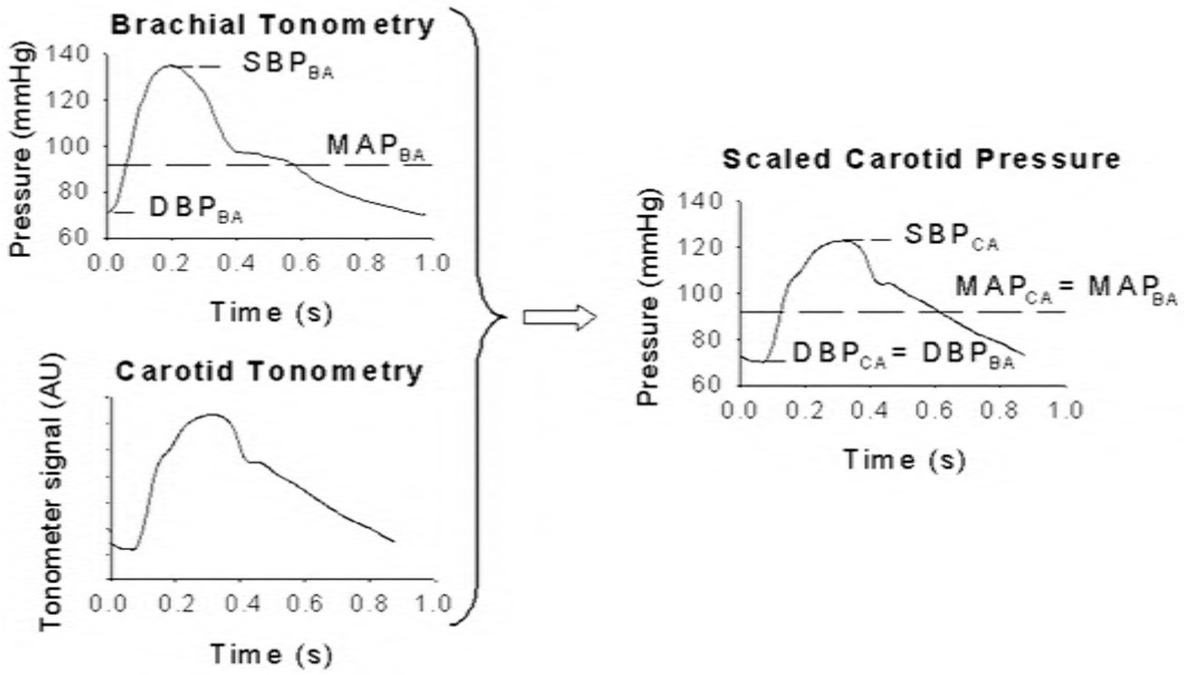

FIGURE 9.5: Calibration method to obtain central pressure waveforms from carotid tonometry readings.[66]

Chapter 10

Comparison of two transfer functions for the assessment of central systolic blood pressure and augmentation index

10.1 Introduction

As discussed in chapter 9, there is significant interest in quantifying the augmentation index and pulse pressure from pressure waveforms. Ideally, these indices should be derived from central pressure waveforms. Augmentation index or pulse pressures determined on waveforms obtained at peripheral locations do not convey the same information due to the pressure amplification which occurs from the heart to the peripheral arteries (for pulse pressure) and the different distances to the peripheral reflection sites which influence the timing of the reflected waves (for augmentation index).

However, since central (aortic) pressures cannot be obtained non-invasively, different approaches have been developed to approximate central arterial pressure waveforms. Two approaches are possible. Pressures can be obtained (non-invasively) at the level of the carotid artery by applanation tonometry, or central pressures can be calculated by use of a radial-to-central transfer function (TFF) on radial artery tonometry recordings.

The carotid artery is anatomically speaking located in close proximity to the heart, and pressure waveforms obtained at the carotid artery show good correspondence to invasively obtained central pressures. Tonometry waveforms by themselves however, only relate relative pressure changes. To transform these into absolute pressure values, some sort of calibration is required. A commonly used approach, based on the validated assumption that mean and diastolic blood pressure do not change appreciable throughout the large arteries, is to calibrate the carotid artery tonometries using mean and diastolic pressure obtained at a reference artery, usually the brachial artery. Carotid tonometry readings which have been calibrated using this approach show good agreement with invasively obtained pressures [99]. A second problem is that carotid tonometry can sometimes be difficult to perform, especially in the elderly or in particularly obese subjects. Also, there is some concern that the pressure exerted on the carotid artery, which is required to perform the measurement, might dislodge vulnerable plaques in subjects with severe atherosclerosis, though to our knowledge there are no known cases of this actually happening.

The use of a radial-to-central transfer function circumvents these issues. Radial artery tonometry is more easy to perform due to the presence of an underlying bony structure against which the artery can be flattened, and tonometry readings obtained at the radial artery can easily be calibrated by local sphygmomanometry. In recent literature, however, the use of synthesized aortic pressure waveforms has been the subject of debate [105–112]. A recent study from our group found that while systolic pressures derived from synthesized aortic pressure waveforms showed good agreement to systolic pressures (SBP) derived from carotid tonometry, the correlation between AIx determined on both waveforms was poor [63]. In addition, there is no single standard transfer function. Different transfer functions have been derived on different populations and it is not entirely clear what the effect of using a different transfer function is on derived parameters like systolic blood pressure and augmentation index.

It is the aim of the present study to compare the use of two different established transfer functions [100, 113] on a subset of the Asklepios population [42]. To this extent, we will investigate differences in estimated SBP and AIx from synthesized aortic pressure waveforms using these well established TFF and compare them to SBP and AIx estimated on carotid artery tonometry readings.

10.2 METHODS

10.2.1 Study population

A total of 268 subjects free from overt cardiovascular disease (174 male, 94 female, age 45.5 (5.7) years (mean (SD)) were included in the study. All subjects were examined in supine position in a quiet room (temperature 21-23 °C). After a resting period of 10 minutes, brachial systolic and diastolic blood pressure was measured using a validated [62] blood pressure monitor (Omron HEM-907, Omron Matsusaka Co. Ltd. Japan).

10.2.2 Measurement of carotid, radial and central pressures

In what follows, $P_{wf,xx}$ denotes a complete pressure waveform at site xx (ba for brachial artery; ca for carotid artery, sao,1 and sao,2 for synthesized aortic waveform using the transfer function proposed by Karamanoglu *et al.* [113] and Chen *et al.* [100], respectively.) The maximum, minimum and mean pressure at site xx are respectively denoted as SBP_{xx}, DBP_{xx} and MAP_{xx}.

Applanation tonometry was performed using a Millar pen-type tonometer (SPT 301, Millar Instruments, Houston, Texas, USA) using a custom-built hard- and software platform [63]. The obtained tonometry waveforms were calibrated using a scheme as proposed by Kelly and Fitchett [64] and validated by Van Bortel *et al.* [65]. Tonometry was first performed at the level of the brachial artery, and the tonometric recording was calibrated by designating the peak and trough of the curve the value of SBP_{ba} and DBP_{ba}, respectively, yielding a scaled brachial artery pressure tracing, $P_{wf,ba}$. Numerical averaging of $P_{wf,ba}$ yielded mean arterial pressure, MAP_{ba}.

Next, tonometry was performed at the *radial* artery. For the calibration of the averaged radial artery tonometric recording, we used the validated assumption that diastolic pressure and mean pressure remain fairly constant in the large arteries. As such, the trough and mean of all tonometric recordings were assigned the values of DBP_{ba} and MAP_{ba} giving scaled radial artery pressure ($P_{wf,ra}$) and carotid artery pressure ($P_{wf,ca}$). The maximum of the radial and carotid pressure curves was respectively radial systolic pressure, SBP_{ra} and carotid systolic pressure SBP_{ca}. The difference between systolic and diastolic pressure at radial, brachial and carotid artery sites are respectively indicated as PP_{ba}, PP_{ra} and PP_{ca}.

We also synthesized central aortic pressure waveforms, $P_{wf,sao,1}$ and $P_{wf,sao,2}$, from P_{ra} using the generalized radial-to-aorta pressure transfer functions derived by Karamanoglu *et al.* (TFF_1) and Chen *et al.* (TFF_2). $SBP_{sao,1}$ and $SBP_{sao,2}$ were derived. The characteristics of both transfer functions are visually represented in figure 10.1

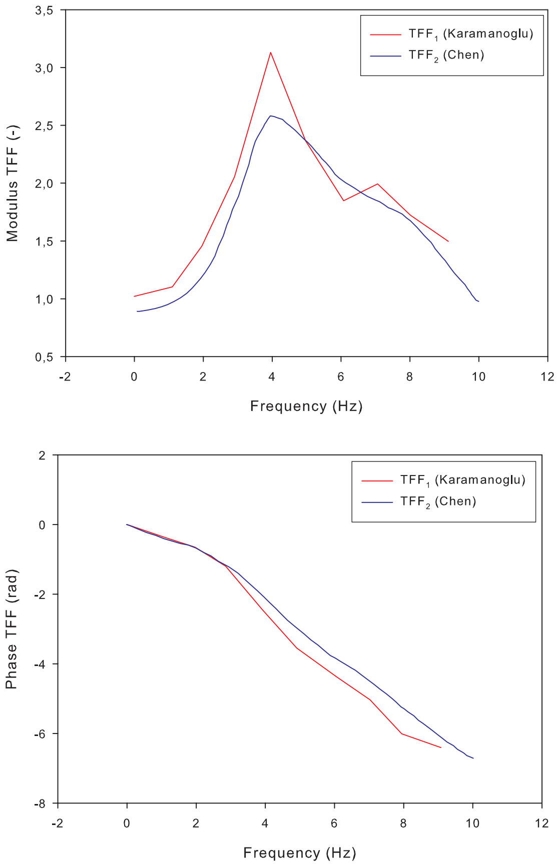

Figure 10.1: Graphical representation of the transfer functions of Karamanoglu (TFF_1) and Chen (TFF_2).

10.2.3 Augmentation index

The augmentation index was defined as

$$AIx = 100\frac{P_2 - P_1}{PP} \tag{10.1}$$

For waves with a shoulder preceding systolic pressure (so-called A-type waves, typically seen in aged subjects), P_1 is a pressure value characteristic for the shoulder, while P_2 is systolic pressure (figure 10.2).

AIx values are positive. For C-type waves (typically seen in young subjects), the shoulder follows systolic pressure, and P_1 is systolic pressure, while P_2 is a pressure value characteristic for the shoulder, thus yielding negative values for AIx (figure 10.2) (see chapter 9). AIx was automatically derived using an algorithm based on the detection of changes in the fourth derivative of the pressure signal [63, 114].

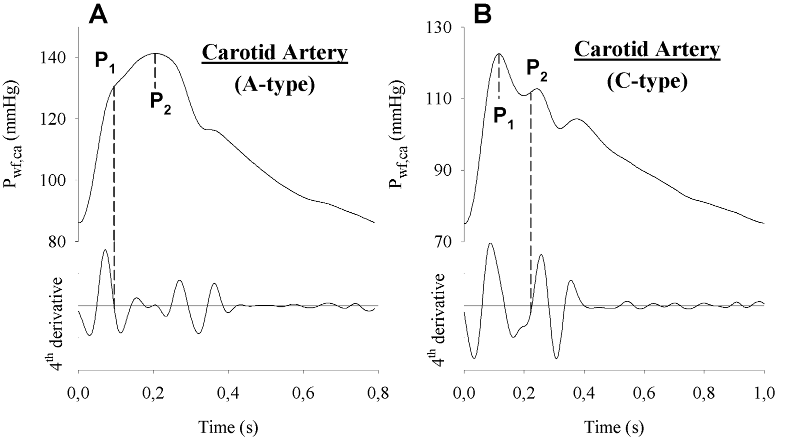

Figure 10.2: Principle behind the automated detection of the shoulder point based on the 4th derivative of the pressure signal (bottom row). Top panels show a carotid recording of an A-type (panel A) and C-type (panel B) wave profile [63].

10.2.4 Statistical analysis

Data are reported as mean (standard deviation). Relations between AIx and systolic blood pressure derived from carotid tonometry and central calibrated waveforms were assessed using linear regression analysis and Bland-Altman plots. All analyses were done in SPSS 11.5.1 (SPSS Inc., Chicago, Il, USA).

10.3 RESULTS

10.3.1 Blood pressures

Brachial systolic and diastolic blood pressures were 132.4 (15.3) and 80.9 (10.3) mmHg, respectively. SBP_{ca} was 130.0 (16.3) while $SBP_{sao,1}$ and $SBP_{sao,2}$ were 127.9 (15.8) and 131.4 (16.6), respectively.

SBP_{ca} correlated well to both $SBP_{sao,1}$ and $SBP_{sao,2}$, as illustrated in figure 10.3 (top panel) and table 10.1 on the following page. Figure 10.4

shows the Bland-Altman plots comparing systolic blood pressures determined from carotid tonometry to systolic blood pressures obtained from synthesized aortic waveforms using TFF_1 (top panel) and TFF_2 (bottom panel). Figure 10.5 (top panel) additionally shows the comparison of systolic blood pressures derived using both transfer functions. Differences between pressures are summarized in table 10.2 on the next page.

10.3.2 Augmentation index

AIx_{ca} correlated well to both $\text{AIx}_{sao,1}$ and $\text{AIx}_{sao,2}$, as illustrated in figure 10.3 (bottom panel) and table 10.1. Figure 10.6 on page 136 shows the Bland-Altman plots comparing augmentation indices determined from carotid tonometry to systolic blood pressures obtained from synthesized aortic waveforms using TFF_1 (top panel) and TFF_2 (bottom panel). Figure 10.5 (bottom panel) additionally shows the comparison of the augmentation indices derived using both transfer functions. Differences between AIx are summarized in table 10.2.

10.4 Discussion

The quantification of the contribution of reflected waves in the arterial system through the calculation of pulse pressure and augmentation index is thought to have potential prognostic power. Although there is a general consensus that for this purpose, the pulse pressure and augmentation index should ideally be determined from central arterial waveforms, there is some debate as to how these central waveforms are best obtained non-invasively.

Table 10.1: Results of regression analysis of SBP and AIx derived from synthesized aortic pressure waves and carotid tonometry

	R	P
SBP_{ca} vs $\text{SBP}_{sao,1}$	0.966	< 0.001
SBP_{ca} vs $\text{SBP}_{sao,2}$	0.971	< 0.001
$\text{SBP}_{sao,1}$ vs $\text{SBP}_{sao,2}$	0.995	< 0.001
AIx_{ca} vs $\text{AIx}_{sao,1}$	0.686	< 0.001
AIx_{ca} vs $\text{AIx}_{sao,2}$	0.700	< 0.001
$\text{AIx}_{sao,1}$ vs $\text{AIx}_{sao,2}$	0.847	< 0.001

TABLE 10.2: Mean differences between SBP and AIx derived from synthesized aortic pressure waves and carotid tonometry.

	Mean	SD	P
SBP_{ca} - $SBP_{sao,1}$	2.14	3.95	< 0.001
SBP_{ca} - $SBP_{sao,2}$	-1.35	4.23	< 0.001
$SBP_{sao,1}$ - $SBP_{sao,2}$	-3.49	1.86	< 0.001
AIx_{ca} - $AIx_{sao,1}$	-12.76	10.04	< 0.001
AIx_{ca} - $AIx_{sao,2}$	-3.41	10.58	< 0.001
$AIx_{sao,1}$ - $AIx_{sao,2}$	9.43	7.03	< 0.001

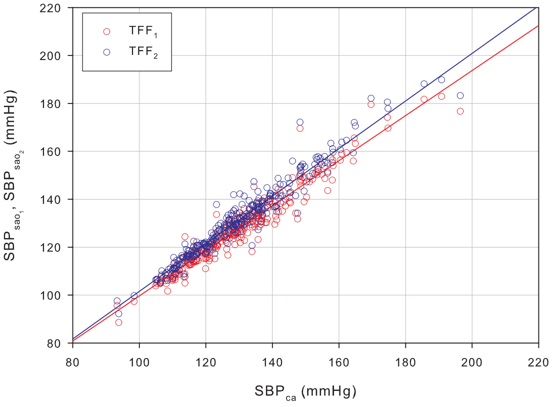

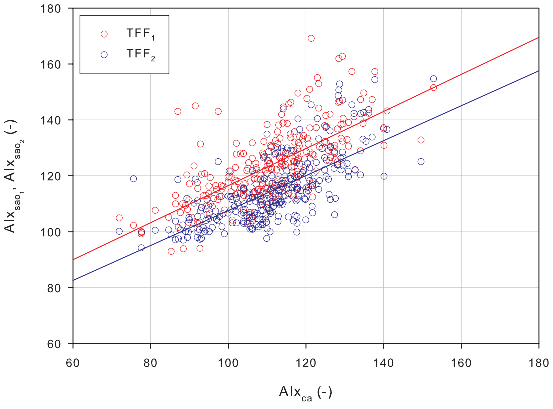

FIGURE 10.3: Regression analysis of $SBP_{sao,1}$ and $SBP_{sao,2}$ versus SBP_{ca} (top) and $AIx_{sao,1}$ and $AIx_{sao,2}$ versus AIx_{ca} (bottom)

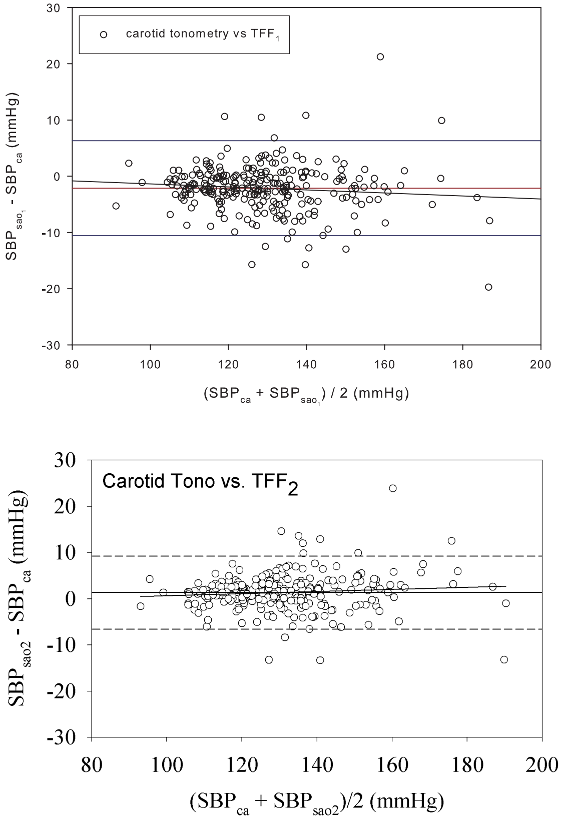

Figure 10.4: Bland-Altman plot of SBP$_{sao,1}$ versus SBP$_{ca}$ (top) and SBP$_{sao,2}$ versus SBP$_{ca}$ (bottom)

The most direct approach is to measure waveforms as close to the heart as possible, with the carotid arterial site being an obvious candidate. Alternatively, central pressure wavefoms can be calculated from radial artery waveforms by the use of generalized radial-to-aorta transfer functions. Although the application of generalized transfer functions has been the object of discussion [107, 115, 116], there are indications that for the estimation of central systolic and pulse pressure, synthesized central pressures correspond well to true aortic pressures [100, 101]. For AIx, there is considerably more debate. Chen *et al.* [100], in their transfer function validation study, reported that synthesized aortic pressure waveforms underestimated AIx obtained from invasively measured pressures by 7%. A recent study from our group,

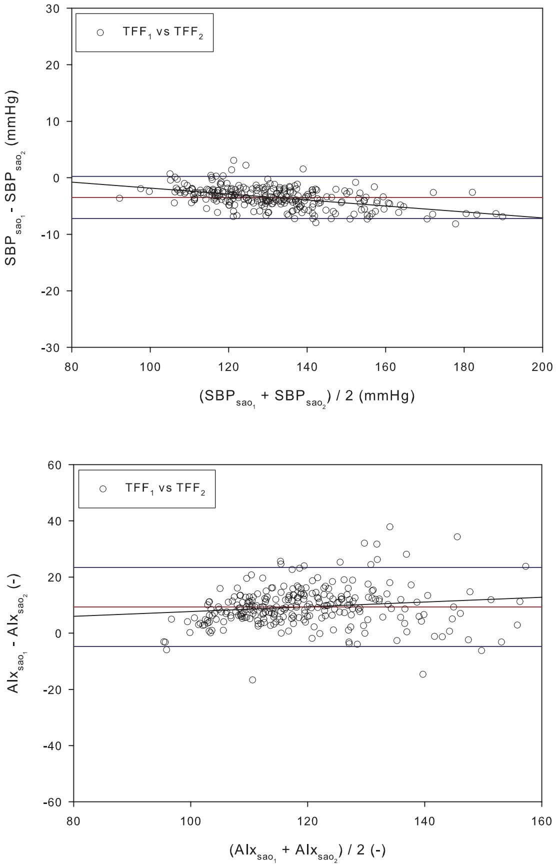

Figure 10.5: Bland-Altman plot of SBP$_{sao,1}$ versus SBP$_{sao,2}$ (top panel) and AIx$_{sao,1}$ versus AIx$_{sao,2}$ (bottom panel).

comparing results from applying the same transfer function to carotid tonometry readings obtained in the Asklepios population found augmentation indices obtained from both pressure curves to correlate rather poorly (R=0.75) with a bias of 11.0 (14)% between both [63].

This study shows that systolic pressures and augmentation indices are also dependent on the type of transfer function used to transform radial pressures into central pressures, with especially for AIx important differences depending on exact transfer function used. For the determination of AIx, the exact shape of the pressure waveform is of great importance, as the detection of the inflection points is sensitive to small changes in the waveform shape. As illustrated in figure 10.1,

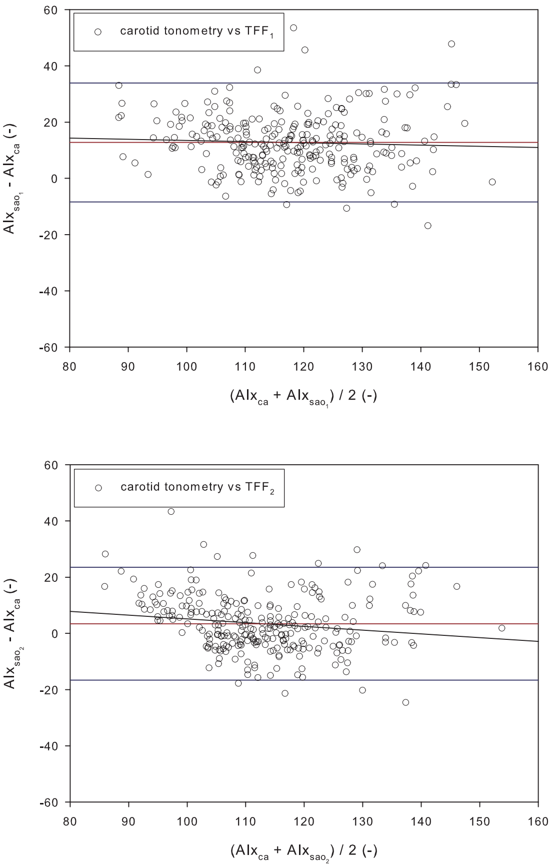

FIGURE 10.6: Bland-Altman plot of $AIx_{sao,1}$ versus AIx_{ca} (top) and $AIx_{sao,2}$ versus AIx_{ca} (bottom)

though both transfer functions are similar, there are substantial differences, especially in amplitude, for certain frequency components of the transfer function. These differences result in small changes in the synthesized aortic pressure waveform which change the location of the detected reference points for the calculation of AIx. As the systolic blood pressure is less sensitive to these changes, the influence of the differences in transfer function on estimated systolic pressures is smaller, yet still significant. The higher amplitude of TFF_1 reflects more important central-to-peripheral pressure-pulse-amplification and yields lower SBP and higher AIx than TFF_2.

The major limitation of our study is the absence of invasive central pressure recordings, which would have allowed to make more decisive conclusions. This makes it difficult to determine which of the pressures or augmentation indices more closely resembles the true aortic pressure and augmentation index. Also, we calculated $P_{wf,sao,2}$ using the TFF as published by Chen *et al.* [100] without, however, transforming mean arterial blood pressure (amplitude TFF at 0 Hz was assumed 1), and thus neglecting viscous pressure losses along the radial-aorta pathway. This may be the reason that $SBP_{sao,2}$ was, on average, slightly higher than SBP_{ca}, while it is anticipated that, with peripheral amplification, SBP_{sao} would be slightly lower.

10.5 Conclusions

Central systolic blood pressure and augmentation index differ depending on the transfer function used to calculate the central pressure waveform from the measured peripheral waveform. Data obtained with different TFF are not interchangeable: derived parameter values are determined by the specifics of the TFF, especially for AIx.

CHAPTER 11

Carotid diameter distension versus applanation tonometry

11.1 INTRODUCTION

Measurements of central pressure and central pressure waveform features (such as the augmentation index) have gained increased attention over the past few years. These central arterial pressure waveforms differ from those at peripheral locations like the brachial artery [71] and evidence has been found that they may change differently in response to drug treatment [117] and that these differences may have an influence on outcome in large trial studies [117, 118]. Central augmentation index (AIx) and pulse pressure (PP) were also found to be independent predictors of all-cause mortality in end-stage renal disease patients [103, 119] and in hypertensive patients in the CAFE study [104] and the Strong Heart Study [120].

The central pressure waveforms can be determined non-invasively either by properly calibrated applanation tonometry measurements at the carotid site [65] or by applying a transfer function to radial artery pressure waveforms [100]. Though good correlations were found between invasively measured aortic pressures and transformed radial pressures [100, 101, 121], the transfer function still remains an average over a given population and its use might not be valid in all populations. Furthermore, its use might result in a loss of individual information

[115]. Correctly performed tonometry readings on the other hand, require a well-trained operator and are difficult to perform in elderly or particularly obese subjects [71], especially for the carotid or brachial arteries. They require a lean skin to avoid cushioning of the waveform and the presence of a stiff or bony underlying structure, as found for instance for the radial artery, helps to flatten the arterial wall.

A possible alternative approach is to derive pressure waveforms from diameter waveforms by appropriate calibration. Arterial diameter can be determined very accurately by ultrasound [122, 123], a procedure which is in general easier to perform correctly than tonometry and is not limited by obesity of subjects. Though several calibration schemes to convert diameter distensions to pressure waveforms have previously been reported [65, 124], data on their applicability and performance in a general population are still lacking. If properly calibrated, diameter distension waveforms allow for accurate assessment of local arterial pressure, this method may provide an alternative way for pressure assessment applicable to a wider range of subjects and potentially at more arterial sites than applanation tonometry.

It is the aim of this paper to investigate and validate the use of pressure waveforms obtained by linear and exponential scaling of carotid diameter measurements by comparing them to waveforms measured by applanation tonometry in a general population. Performance will be quantified by comparing systolic blood pressures (SBP) and augmentation indices (AIx) derived from calibrated diameter waveforms to those calculated from tonometry readings. To this extent, data were used from the Asklepios population study, comprising 2,524 apparently healthy 35–55 year old subjects from a general population.

11.2 MATERIALS AND METHODS

11.2.1 Study population

The Asklepios study is a longitudinal population study designed to focus on the interplay between ageing, cardiovascular hemodynamics and inflammation in (pre-clinical) cardiovascular disease [42]. Data were available from the first round of the study, completed between October 2002 and September 2004. The complete study database contains 2,524 subjects (1,301 female/1,223 male) constituting a representative cohort of 35–55 year old subjects randomly sampled from the twinned Belgian communities of Erpe-Mere and Nieuwerkerken. The required carotid pressure and diameter data required for this study were available in a total of 2,026 subjects (989 females/1,037 males).

A thorough description of the design, baseline characteristics, and methodological details of the Asklepios study can be found elsewhere [42]. This section will briefly describe the basic clinical data and the assessment of local diameter and pressure.

11.2.2 Basic clinical data

Measurements were performed after a 10–15 minute rest period in a temperature controlled environment. Blood pressures were taken using a validated [62] oscillometric Omron HEM-907 device with cuff sized individually chosen based on arm circumference. Subjects were blinded to the blood pressure results during measurement. Blood pressure values reported are distinct from the baseline measurements and were recorded between the echographic (diameter) and tonometer measurements.

11.2.3 Measurement of local pressure by tonometry

Local arterial pressure waveforms were consecutively obtained at the left brachial and left carotid arteries by applanation tonometry using a Millar pen type tonometer (SPT 301, Millar Instruments, Houston, Texas, USA) and a dedicated hard- and software platform. The set-up, processing and calibration process used were previously described [63, 66]. Tonometry waveforms were recorded at 200 Hz. A time sequence of 20 seconds was registered, and an ensemble averaged waveform was constructed of at least 10 beats. Signals were filtered using a Savitsky-Golay filter of the third order with a 15 sample frame width (Matlab, The Mathworks Inc., Natick, MA, USA). This filters the signal using a third-order polynomial over a 15 sample sliding point window. This filter was chosen for its better preservation of the relevant high-frequency components of a signal than more traditional low-pass filters.

The waveforms obtained at the brachial artery were calibrated by identifying the peak and trough of the waveform with oscillometric systolic (SBP_{bra}) and diastolic (DBP_{bra}) brachial pressures. For calibration of the carotid artery waveforms the validated assumption was used that the difference between diastolic and mean blood pressures remains fairly constant throughout the large arteries [64, 65]. Mean arterial pressure (MAP) was calculated as the average value of the calibrated brachial artery waveform and carotid pressure waveforms were calibrated by assigning the trough and mean values to values of DBP_{bra} and MAP.

Brachial artery waveforms could not be obtained with sufficient quality within a reasonable time in 417 subjects. For these subjects a scaled radial artery waveform was used to calculate MAP, which was calibrated using oscillometric brachial DBP and an estimated value for radial artery systolic blood pressure (SBP_{rad}) obtained using a regression equation based on a subset of 1863 subjects in the Asklepios study in which both brachial and radial artery tonometry readings were available. This approach was described in detail in [66] and takes into account the brachial to radial amplification of systolic blood pressure.

11.2.4 Measurement of local arterial diameter

Arterial diameter distension waveforms were obtained at the left common carotid artery, approximately 2 cm proximal to the carotid bulb, using a commercially available ultrasound system (Vivid7, GE Vingmed, Horten, Norway) equipped with a vascular transducer (12L) set at 10 MHz and dedicated acquisition software. All measurements were ECG gated.

For diameter measurements the operator selects a region of interest during B-mode vascular imaging containing both the anterior and posterior vessel wall. Radio-frequency (RF) data are acquired at 209 frames/sec along 8 evenly distributed beams within this region of interest. A sequence of 4 to 5 cycles was recorded for each measurement. These RF data are stored together with the B-mode cineloops for offline analysis in a dedicated Matlab environment (The Mathworks Inc., Natick, MA, USA). A single beam is selected along which the stored RF-data are presented as an RF M-mode image in conjunction with a 4 mm wide section of the B-mode image around the selected beam. The vessel boundary is then manually selected in the intima-media interface and its movement is automatically tracked using a modified autocorrelation estimator [125, 126]. The result is a diameter distension waveform containing 4 to 5 cycles. These waveforms were filtered using the same filter settings as for the tonometry recordings, and an ensemble average was constructed (from at least 3 cycles).

11.2.5 Calibration of diameter waveforms

Diameter waveforms were calibrated using a linear and an exponential calibration scheme. The linear calibration scheme is similar to the scheme used to calibrate tonometry readings: the diameter waveform is treated as being a pressure waveform and is calibrated by assigning the waveform's trough and mean values the values of diastolic and mean brachial pressure [65].

For the exponential calibration, a modified procedure based on the scheme proposed by Meinders *et al.* [124] was used. The relationship between pressure and diameter is assumed to be exponential [127]:

$$p(t) = p_d \exp\left[\alpha\left(\frac{A(t)}{A_d} - 1\right)\right] \tag{11.1}$$

with

$$A(t) = \frac{\pi d^2(t)}{4} \tag{11.2}$$

$$\alpha = \frac{A_d \, ln\left(\frac{p_s}{p_d}\right)}{A_s - A_d} \tag{11.3}$$

where

$p(t)$: blood pressure waveform
$d(t)$: diameter waveform
$A(t)$: arterial cross-section waveform
p_d: end-diastolic blood pressure
p_s: end-systolic blood pressure
A_d: end-diastolic arterial cross-section
A_s: end-systolic arterial cross-section
α: wall rigidity coefficient

The wall rigidity coefficient α, is pressure-independent [124]. To use equation 11.1 to calculate the pressure waveform from a given diameter waveform, the systolic and diastolic pressures must be known at the same time and location as the arterial cross-section. By again assuming diastolic and mean arterial pressure to remain constant throughout the large arteries, the iterative scheme proposed by Meinders *et al.* [124] can be used to determine α based on diastolic and mean brachial artery pressure. However, in contrast to Meinders *et al.*, who calculated MAP from MAP = DBP + (SBP-DBP)/3, we calculated MAP as the average of the brachial pressure waveform, as before.

11.2.6 Comparison of scaled diameter and pressure waveforms

In order to properly assess whether scaled diameter waveforms can be used as surrogates for tonometry waveforms and to determine the impact of the different diameter scaling techniques, three parameters will be investigated: one 'morphological' parameter and two 'functional' parameters. The purpose of the morphological parameter is to quantify the *overall correspondence* of the scaled diameter waveform to the tonometry waveform, whereas the functional parameters serve to quantify the *usefulness* of the scaled diameter waveform as a replacement for the corresponding tonometry waveform.

As the morphological parameter, the root mean squared error (RMSE) was chosen:

$$RMSE = \left[\frac{\sum_{i=1}^{n} \left(p_{tono,i} - p_{diam,i}\right)^2}{n} \right]^{1/2} \tag{11.4}$$

where

$p_{tono,i}$: tonometry pressure at a given point of the waveform

$p_{diam,i}$: linearly or exponentially scaled diameter pressure at a given point of the waveform

n: number of points over which both pressures were compared

The RMSE is a measure of the absolute difference between the scaled diameter and tonometry waveforms and as such allows to quantify how closely the values of the waveforms match across the entire waveform. Pressure and scaled diameter waveforms were aligned on the trough of the curves.

The functional parameters used in the present study are systolic blood pressure, determined as the maximum of the scaled diameter or tonometry waveform, and augmentation index (AIx):

$$AIx = 100\frac{P_2 - P_1}{PP} \tag{11.5}$$

with

P_1, P_2: first and second systolic peaks of the pressure waveform

PP: pulse pressure; $PP = SBP - DBP$

The augmentation index aims to quantify the contribution of the reflected wave to the pressure wave and is included in the present study to ascertain to which degree calibrated diameter waveforms are able to capture the details (shoulder point) of the tonometry waveform. The shoulder point was detected automatically based on an algorithm proposed by Takazawa *et al.*, which is based on the fourth derivative of the pressure signal [61, 114].

11.2.7 Statistical analysis

Data are reported as mean values (standard deviation). Comparisons between parameters derived using different scaling techniques are performed using paired Wilcoxon tests and are graphically represented by Bland-Altman plots [43]. Statistical significance is indicated by P-values smaller than 0.05 unless stated otherwise. All statistical analyses were performed in SPSS 15.0 software (SPSS Inc., Chicago, IL, USA).

11.3 RESULTS

General population parameters are summarized in table 11.1.

11.3.1 Root mean squared error

Linearly scaled diameters in general compared well to actual tonometry pressures with an average RMSE of 5.2 (3.3) mmHg. Exponential calibration significantly (P<0.001) improved RMSE values by 12% to an average of 4.6 (3.6) mmHg.

TABLE 11.1: General description of the study population. Values are mean (SD).

Age (years)	45.8 (6.0)
Gender (M/F)	1037/989
Weight (kg)	73.2 (13.9)
Height (cm)	169.5 (8.9)
Body mass index (kg/m^2)	25.3 (3.8)
SBP_{bra} (mmHg)	132.5 (15.4)
DBP_{bra} (mmHg)	77.1 (10.8)
MAP_{bra} (mmHg)	100.4 (12.0)
PP_{bra} (mmHg)	56.2 (10.8)
Smoking (active/ex/never)	401/580/1,045
Total cholesterol (mg/dl)	216.1 (36.7)
HDL cholesterol (mg/dl)	63.7 (17.2)
Triglycerides (mg/dl)	109.0 (82.9)
Glycemia (mg/dl)	90.9 (9.4)

11.3.2 Carotid systolic blood pressure

Figure 11.1 (a) shows a graphical representation of average carotid systolic blood pressures as determined by carotid artery tonometry ($SBP_{car,tono}$) and derived from linearly ($SBP_{car,lin}$) and exponentially ($SBP_{car,exp}$) calibrated diameter waveforms. Linear scaling of distension waveforms underestimated systolic blood pressure by on average 4.9% or 6.4 (4.1) mmHg compared to scaling of pressure waveforms by tonometry, exponential scaling of distension waveforms underestimated systolic blood pressure by 1.5% or 1.9 (3.9) mmHg.

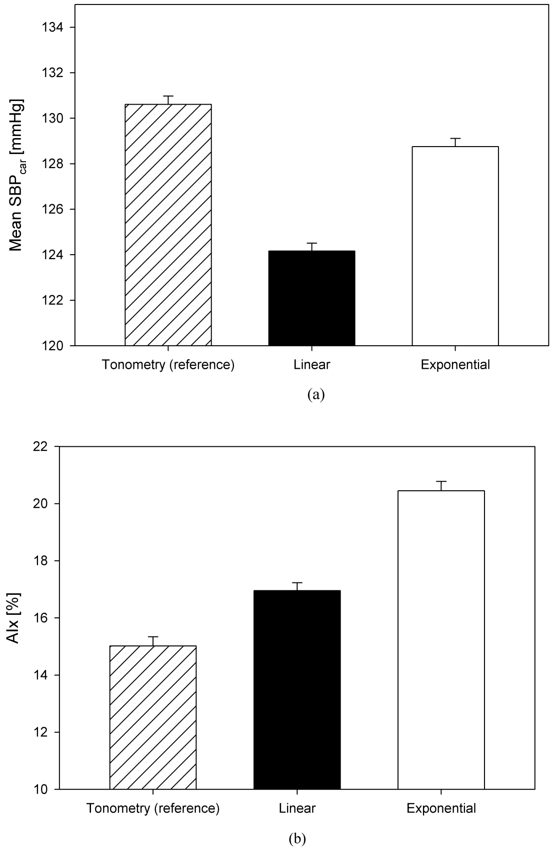

Figure 11.1: (a) Average systolic blood pressure in the carotid artery (SBP_{car}) estimated from linearly and exponentially calibrated diameter waveforms compared to pressure measured by carotid artery tonometry. (b) Average carotid artery augmentation index (AIx) estimated from linearly and exponentially calibrated diameter waveforms compared to pressure measured by carotid artery tonometry.

Bland-Altman analysis of $SBP_{car,tono}$ and $SBP_{car,lin}$ (figure 11.2 on the next page, (a)) furthermore shows a relatively small (R=0.29) but pronounced increase of the difference between $SBP_{car,tono}$ and $SBP_{car,lin}$ with increasing systolic blood pressure (P<0.001). The same analysis for $SBP_{car,tono}$ and $SBP_{car,exp}$ (figure 11.2 (b)) shows this dependency to be greatly reduced (R=0.06), though it remains statistically significant (P=0.004).

To investigate the determinants of these trends in the Bland-Altman plots and quantify the impact of the different scaling techniques on its importance, we examined the correlation between ($SBP_{car,tono}$ - $SBP_{car,lin}$) and ($SBP_{car,tono}$ - $SBP_{car,exp}$) and the factors age, gender, smoking, hypercholesterolemia, body mass index (BMI) and brachial pulse pressure (PP_{bra}). First the correlation with each factor was determined in a univariate regression analysis after which all significantly related factors were included in a multivariate regression model. For ($SBP_{car,tono}$ - $SBP_{car,lin}$), only BMI (R=0.09) and PP_{bra} (R=0.4) were significantly (P<0.05) related to the pressure difference between measured and estimated systolic blood pressure. Multivariate analysis showed inclusion of BMI to only marginally increase the model performance (R=0.41; P<0.05). For ($SBP_{car,tono}$ - $SBP_{car,exp}$) on the other hand, PP_{bra} was not significantly related to the pressure difference and from the other risk factors again only BMI showed a weak correlation (R=0.07, P<0.05). Figure 11.3 on page 149 shows the results of the univariate regression analysis of ($SBP_{car,tono}$ - $SBP_{car,lin}$) and ($SBP_{car,tono}$ - $SBP_{car,exp}$) with PP_{bra}.

11.3.3 Carotid augmentation index

Average values for carotid AIx are graphically represented in figure 11.1 (b). AIx derived from linearly scaled diameter waveforms overestimated AIx calculated from tonometry readings by 1.9 (10.1) % in absolute values. Exponential calibration performed slightly worse, overestimating AIx by 5.4 (10.6) % in absolute values. Figure 11.4 on page 150 shows the Bland-Altman analysis comparing AIx derived from linear and exponential calibration to AIx calculated from tonometry. A small but significant (P<0.001) and clear increase in the difference between AIx_{tono} and AIx_{lin} with increasing average AIx is found (R = 0.25; P<0.001; figure 11.4 (a)). For exponentially calibrated AIx there is no significant correlation between the difference between AIx_{tono} and AIx_{exp} and average AIx (P=0.70; figure 11.4 (b)).

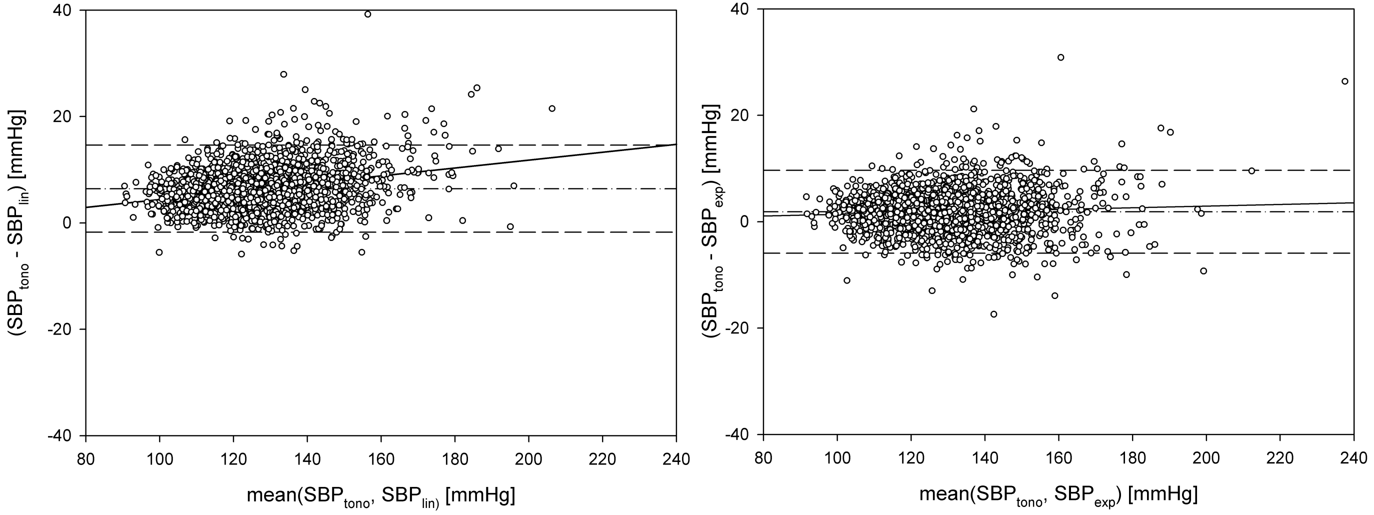

(a)

(b)

FIGURE 11.2: Bland-Altman plots comparing carotid artery systolic blood pressure derived from linearly (SBP$_{car,lin}$ (a)) and exponentially (SBP$_{car,exp}$ (b)) calibrated diameter distension waveforms to pressures measured by tonometry (SBP$_{car,tono}$)

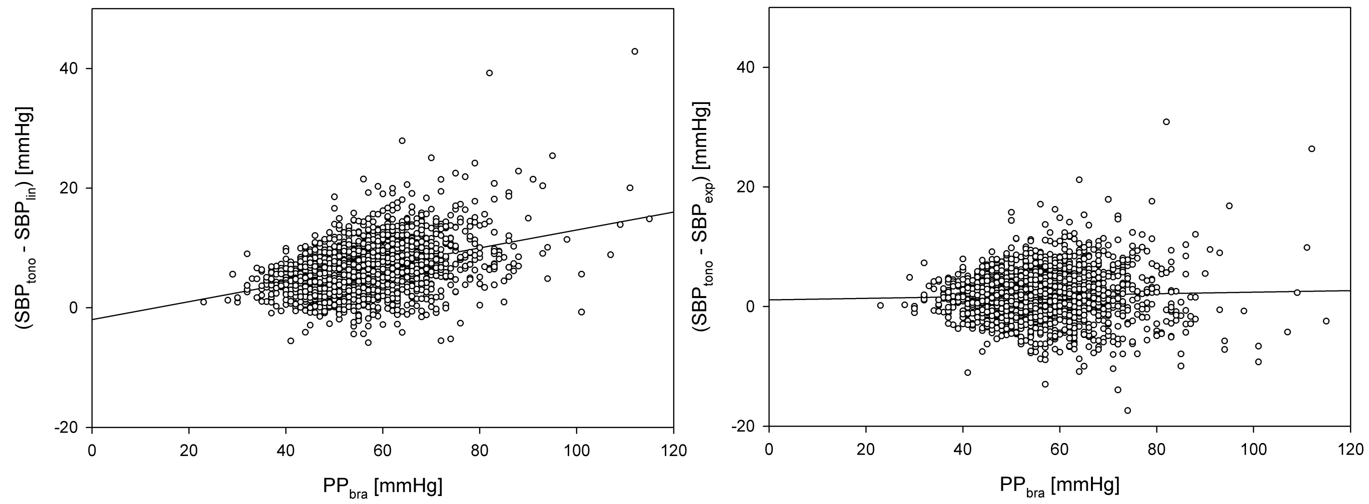

(a)

(b)

FIGURE 11.3: Influence of brachial artery pulse pressure (PP$_{bra}$) on the estimation of carotid systolic blood pressure by linear ((a) SBP$_{car,lin}$) and exponential ((b) SBP$_{car,exp}$ calibration of carotid artery diameter waveforms. The indicated trend in the right hand panel is not significant ($P > 0.05$)

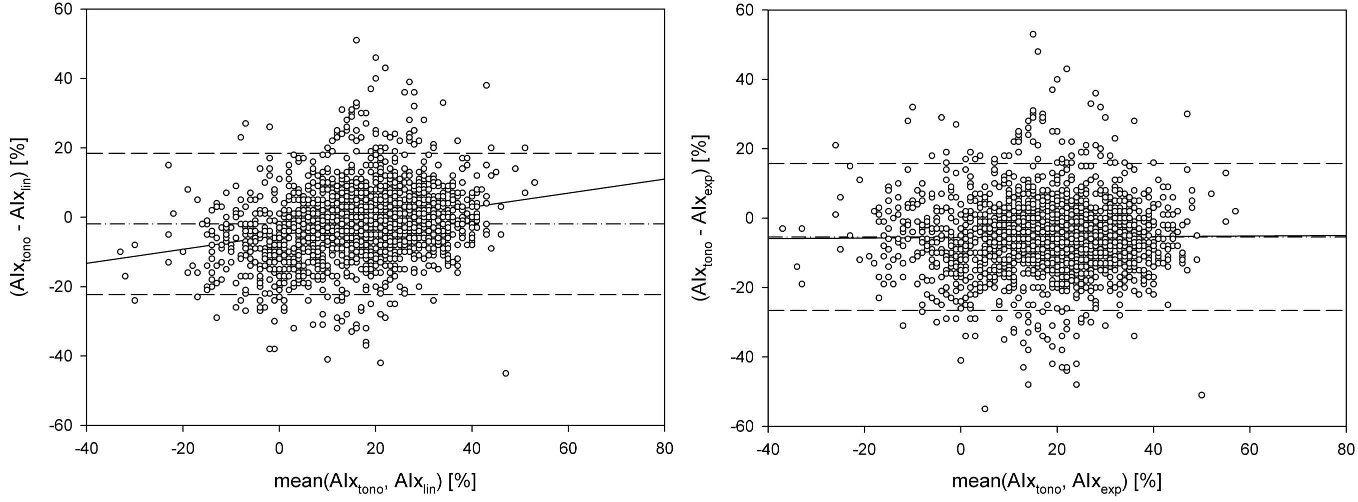

(a)

(b)

FIGURE 11.4: Bland-Altman plots comparing carotid augmentation index derived from linearly (AIx$_{lin}$ (a)) and exponentially (AIx$_{exp}$ (b)) calibrated diameter distension waveforms to pressures measured by tonometry (AIx$_{tono}$)

11.4 DISCUSSION

Nowadays ultrasound echo-tracking devices are available which allow one to track arterial wall distension with a resolution of less than 3 μm [122]. In spite of this, there has been little research into the potential of calibrated diameter waveforms for local arterial pressure estimation. Two different calibration schemes have previously been described in literature. Van Bortel *et al.* [65] compared the pressures obtained from carotid tonometry curves calibrated using mean and diastolic brachial pressures to pressures obtained invasively at the ascending aorta. Subsequently, the same calibration was applied to diameter distension waveforms obtained at the carotid artery and compared to the tonometry readings. Pulse pressures obtained by this linear calibration differed by 3.4 mmHg from pressures obtained by tonometry, but the accuracy of the method was dependent on pulse pressure, with the difference being more pronounced for subjects having higher pulse pressures [65]. Meinders *et al.* [124] assumed an exponential relationship between pressure and diameter but they did not validate their calibration scheme, only comparing the pressures obtained from calibrated diameter waveforms to conventionally measured brachial blood pressure. The present study is the first to combine the linear and (modified) exponential calibration schemes and compare the resulting pressure waveforms to pressures obtained by applanation tonometry in order to validate and quantify their performance in a large, general population sample.

The mean RMSE values underline the added value of the exponential model. RMSE values represent how well a model fits to reality. The use of an exponential model improves the overall fit to the actual data by 28% compared to a linear model. RMSE values however, though *useful*, are not the most *useable* parameter for assessing scaling performance. The overall agreement between waveforms is of little importance as most clinical interest lies in the parameters derived from the actual waveforms.

Given that mean arterial and diastolic pressure are assumed to be constant throughout the large arteries, systolic blood pressure (or pulse pressure) is most likely the most important parameter to be assessed from the scaled diameter waveforms. We found linear calibration of distension waveforms to underestimate tonometry pressure by 6.4 (4.1) mmHg, which is a larger value than reported in the study of Van Bortel *et al.* [65] which was performed in a smaller population sample (n=100) and, more importantly, also a younger population (mean age of 37 years) with lower BMI and brachial pulse pressure. Exponential calibration significantly reduced the underestimation. Bland-Altman analysis shows a statistically significant trend for both calibration methods to further underestimate systolic blood pressure for higher systolic blood pressures, though the trend is far more pronounced for the linearly calibrated curves than for the exponentially calibrated curves.

The discrepancies between estimated and actual systolic blood pressure, especially evident for the linear calibration, could be due to limitations inherent to the model in calibrating pressure waves with high systolic blood pressures. The distension of arteries at high operating pressures is mainly determined by the collagen and levels off as collagen fibres progressively stretch out. However, since elevated systolic blood pressure is usually associated with subjects displaying one or more cardiovascular risk factors, these discrepancies could also be due to changes in the intrinsic properties of the carotid artery due to risk exposure which the linear model fails to completely account for. To investigate the risk hypothesis, we performed a univariate regression analysis taking the most common risk factors (age, gender, BMI, smoking, hypercholesterolemia) into account. We found the difference between estimated and actual systolic blood pressure, both for linear and exponential calibration, to be independent of all risk factors with the exception of BMI, which showed a very weak correlation. This indicates that the source of the discrepancies should be sought in the inability of the model to correctly scale for high systolic blood pressure rather than its inability to account for changes in carotid artery structure with risk.

Accurate pressure-diameter relationships have previously been investigated. Langewouters *et al.* performed *in vitro* diameter measurements on excised aortas which were inflated from 0 to 200 mmHg and they proposed a three parameter sigmoidal pressure-diameter relationship [81]. Though the model was proposed for the aorta, it may be valid for the carotid as well, especially since both are in essence large elastic arteries. Unfortunately, the parameters of the sigmoidal model cannot always be approximated accurately non-invasively (the operating pressure range is too narrow to reveal the sigmoidal features), so the model's use in clinical practice is limited. The linear and exponential model are both approximations of this sigmoidal relationship with easier to estimate parameters. Since the physiological pressure range is mostly situated in the quasi-linear part of the sigmoidal curve, the linear model performs well in a majority of cases.

For subjects with high systolic or low diastolic pressure (or in general, high pulse pressure) however, the pressure-diameter relationship enters the curved part of the sigmoidal curve and for those subjects an exponential model significantly improves the approximation of the actual pressure-diameter relationship. Figure 11.5 on page 156 illustrates the calibration process and compares the performance of the different pressure-area or models. Panels (a) and (b) show measured pressure (tonometry) and diameter (ultrasound) waveforms. The upstroke of the pressure and diameter waveforms are displayed in panel (c), along with the fitted Langewouters, exponential and linear models in the physiological pressure range. The parameters of the Langewouters model for this figure were obtained by fitting the model to pressure-diameter curves. Panel (e) finally shows the result of applying the different models for pressure estimation from measured diameter and their comparison to measured pressure. The benefit of the Langewouters relationship which most closely resembles reality is illustrated more fully in panel (d). It clearly shows that, depending on the pulse pressure levels, the exponential model can yield a significant improvement in fitting to the actual pressure-area relationships over a linear model.

The regression analysis shown in figure 11.3 further illustrates the dependence of the pressure discrepancy between linearly scaled diameter and tonometry waveforms on pulse pressure and how the use of an exponential model removes this dependence. This also explains why our linearly calibrated diameter waveforms perform worse than reported in the study of Van Bortel *et al.* [65]. Average brachial pulse pressure in the Van Bortel *et al.* study was 45 mmHg compared to 56.2 mmHg in the present study. The relatively large increase in underestimation between the studies (6.4 mmHg to 3.4 mmHg) could be an indication that the discrepancy between measured and estimated pressures using a linear calibration scheme rises quickly for rising pulse pressure.

The results for the augmentation index show a mixed message. Looking strictly at the average AIx values (figure 11.1, right) it appears that linearly calibrated diameter curves allow for more exact estimation of carotid AIx than exponential calibration. On the other hand, Bland-Altman analysis of AIx derived from linearly calibrated diameters versus actual pressure waveforms shows a significant and important trend for an increasing discrepancy with rising values of AIx. This trend is completely absent for the exponentially calibrated diameters, indicating that although the absolute value of the bias is bigger with exponential calibration, the bias itself is systematic and is as such easily corrected for. Standard deviations remain relatively large regardless of the calibration scheme used. Calculation of the augmentation index involves the determination of a shoulder point on the waveform [61] and as such the augmentation index is highly dependent on the actual shape of the waveform. Though diameter waveforms resemble the corresponding pressure waveforms relatively well, as illustrated by the relatively low RMSE values, there are usually still significant differences between them which may mean that (scaled) diameter waveforms are less suitable for the determination of AIx than for the assessment of systolic blood pressure. It should however be pointed out that though tonometry currently constitutes the best possible way for non-invasive investigation, only a direct comparison of both techniques with invasively measured high-fidelity data can unequivocally resolve which technique delivers the most accurate AIx estimates.

It is worth noting that both for linear and exponential calibration, the value of mean arterial pressure that is used in the calibration scheme is of vital importance. In the present study, we calculated mean arterial pressure as the true mean of the brachial artery waveform. The original exponential calibration scheme proposed by Meinders *et al.* used an approximate measure for mean arterial pressure defined as MAP = DBP + (SBP - DBP)/3. Though this approximation is often used, it differs significantly from MAP calculated as the true mean of the arterial waveform [128, 129]. When using the approximated value for MAP, the exponential calibration procedure underestimates SBP by 13.2 (5.7) mmHg, the difference being mostly due to the different estimation of MAP used for calibration. (MAP-DBP) was 23.3 (4.4) mmHg for MAP calculated from tonometry and 18.5 (3.5) mmHg for MAP calculated with the approximative formula.

One important limitation of the present study is the absence of invasive pressure data to compare the results of applanation tonometry as well as the different calibration schemes to the actual pressures found in the carotid artery. In the absence of these data, carotid artery applanation pressures were used as pressure reference values. Though applanation tonometry is widely used in clinical practice as a tool for assessment of local pressures and good correspondence has been found between tonometry performed at the carotid artery and invasively measured pressures in the ascending aorta [65], true carotid artery pressure might still be over- or underestimated. Similarly, while excellent correlations were found between augmentation indices derived from carotid tonometry and invasively obtained central arterial pressure waveforms, true augmentation index might be underestimated from carotid tonometry waveforms [99]. Finally, given the limited age-range covered and the inclusion criteria of the Asklepios study, the full effect of age and cardiovascular disease on our findings cannot be judged. Although the dataset did contain a substantial number of hypertensive subjects, the performance of linear and exponential calibration might differ in severely hypertensive patients or patients with overt cardiovascular disease.

11.5 Conclusions

Exponentially calibrated diameter waveforms offer a valid alternative for local pressure assessment at the carotid artery. Unlike linearly calibrated waveforms, systolic blood pressure assessed by exponential diameter calibration is independent of the level of pulse pressure. Systolic blood pressure derived from exponentially calibrated diameter curves underestimate pressures obtained by carotid tonometry by 1.90 mmHg. AIx determined from exponentially calibrated diameter waveforms yields values which differ more from AIx derived from tonometry waveforms than when linear calibration is used, though in contrast to the linear calibration, the bias is systematic and should thus easily be corrected for. Nevertheless, the use of scaled carotid diameter waveforms for the assessment of AIx might be less appropriate as a direct alternative for carotid applanation tonometry.

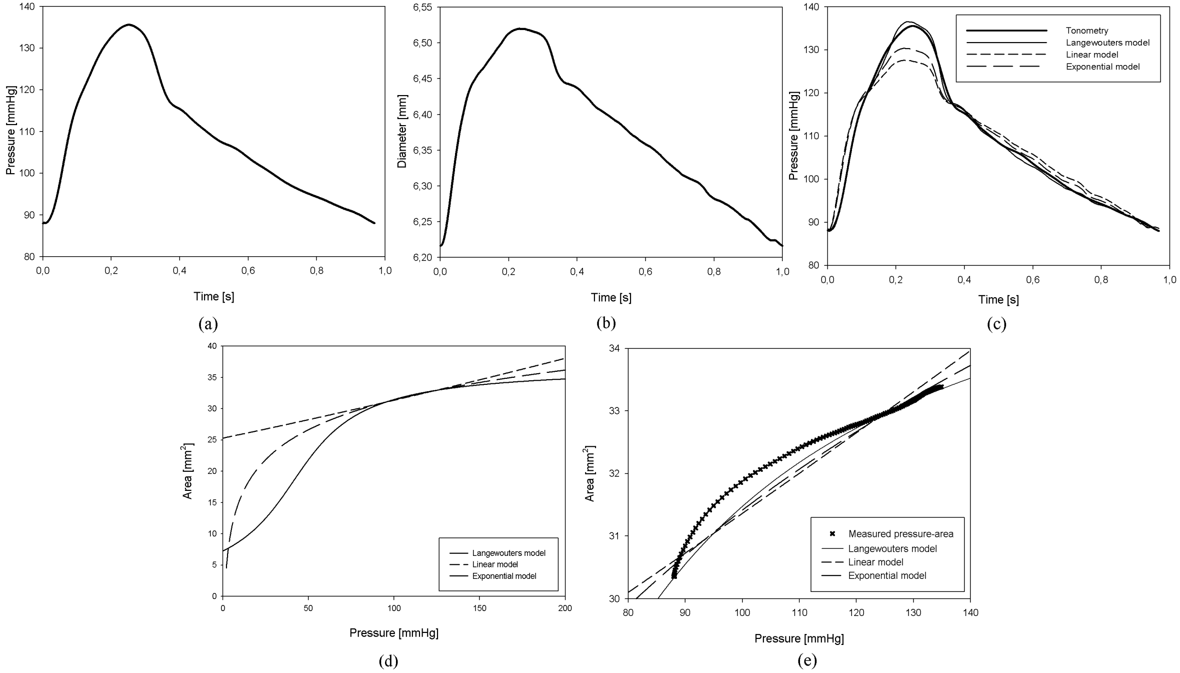

FIGURE 11.5: Measured pressure (a) and diameter (b) at the carotid artery; different pressure-area relationships (c) and their performance in comparison to measured data in the physiological pressure range (d); comparison of different diameter to pressure scaling techniques with carotid tonometry (e).

CHAPTER 12

A new pressure dependent, geometry independent stiffness index?

12.1 INTRODUCTION

The stiffness of the arterial wall is a reflection of the structural and functional properties of the vessel wall. Several cross-sectional population studies have shown associations between measures of arterial stiffness and cardiovascular risk factors like hypertension, diabetes mellitus, hypercholesterolemia and myocardial infarction [130]. In recent years, arterial stiffness and more specifically central arterial stiffness has been demonstrated to be both an independent risk factor for cardiovascular disease as well as a predictor for cardiovascular events.

Most arterial stiffness measures offer an integrated value which is assumed to be constant during the complete cardiac cycle. Structurally, the arterial wall is composed of a combination of elastic elastin and stiff collagen fibres which are gradually recruited when the arterial diameter increases due to an increase in pressure. The arterial stiffness of an artery therefore, changes with pressure during the cardiac cycle. Based on pressure-diameter measurements performed ex-vivo on excised aortas, Langewouters *et al.* [81] proposed a sigmoidal pressure-area relationship from which a pressure dependent compliance was derived.

Compliances are by definition however, geometry dependent: for similar arterial properties, a larger vessel will always have a larger compliance than a smaller vessel due to the larger absolute increase in arterial diameter for similar pressure changes. Compliances are therefore difficult to compare between individuals. For this reason, comparing compliances between men and women is also difficult, as men on average have larger vessels than women.

It is the aim of the present study to propose a new, pressure dependent, geometry independent stiffness index based on the pressure dependent, geometry dependent compliance proposed by Langewouters *et al.* [81]. This new index will be used to investigate potential differences in age-related central arterial stiffening between men and women and compared in that respect to the α stiffness index proposed in chapter 11.

12.2 METHODS

12.2.1 Arterial stiffness indices

Arterial stiffness can be quantified using different stiffness parameters. One way of characterizing local arterial stiffness is by studying pressure-area (P-A) relationships at a given location in the arterial tree. For a stiffer artery a given change in pressure will result in a smaller change in diameter compared to the change in diameter of a more compliant artery. From these P-A relationships stiffness indices can be derived by fitting different pressure-area models to measured pressure-area curves.

The exponential model proposed by Meinders *et al.* [124] is a commonly used pressure-area model:

$$p(t) = p_d \exp\left[\alpha\left(\frac{A(t)}{A_d} - 1\right)\right] \tag{12.1}$$

The α parameter in this model is an established geometry and pressure independent stiffness index. Though arterial stiffness is generally pressure dependent, the exponential model is a good approximation in the physiological pressure range.

A more correct approximation of the real arterial pressure-area relationship is obtained by fitting a sigmoidal (Langewouters) model to the P-A curves:

$$p = p_1 \tan\left[\pi\left(\frac{A}{A_m} - \frac{1}{2}\right)\right] + p_0 \tag{12.2}$$

in which p_0, p_1 and A_m are model parameters to be estimated by fitting the proposed relationship to measured pressure and area at a given arterial location.

From this equation, Langewouters *et al.* [81] derived a pressure dependent compliance:

$$C(p) = \frac{C_m}{1 + \left(\frac{p-p_0}{p_1}\right)^2} \tag{12.3}$$

with

$$C_m = \frac{A_m}{\pi p_1} \tag{12.4}$$

By normalizing the fitted pressure-area curves for vessel size using the calculated maximal area (A_m) obtained from the fittings, we derived a geometry independent distensibility coefficient:

$$D(p) = \frac{C(p)}{A_m} = \frac{D_m}{1 + \left(\frac{p-p_0}{p_1}\right)^2} \tag{12.5}$$

with

$$D_m = \frac{C_m}{A_m} = \frac{1}{\pi p_1} \tag{12.6}$$

12.2.2 Study population

For the purpose of this study data were drawn from the Asklepios Study database. The Asklepios Study is a large-scale longitudinal population study designed to focus on the interplay between hemodynamics, cardiovascular disease (i.e. atherosclerosis, heart failure) and ageing [42].

12.2.3 Data acquisition and signal processing

Pressure and diameter waveforms were acquired at the left carotid artery as part of the Asklepios Study protocol.

For assessment of the local pressure waveforms, applanation tonometry was performed at the left brachial and carotid arteries with a Millar pen-type tonometer (SPT 301, Millar Instruments, Houston, Texas, USA). Averaged brachial artery waveforms were calibrated using systolic and diastolic blood pressures obtained from conventional oscillometric recording. The averaged carotid artery waveform was calibrated based on the validated assumption [64] that diastolic and mean arterial pressure remain fairly constant throughout the large arteries. Hence, the carotid artery waveform was calibrated from the measured diastolic brachial pressure and mean arterial pressure calculated from the calibrated brachial artery waveform.

Local diameter waveforms were obtained from B-mode images obtained at the left carotid artery using a commercially available ultrasonographic system (Vivid 7, GE Vingmed Ultrasound, Horton, Norway). During measurements RF data are stored along 8 evenly distributed beams across an operator selected region of interest. These data are stored together with the B-mode cineloops for off-line analysis within a Matlab (The Mathworks Inc., Natick, MA, USA) environment. After manual selection of the vessel boundary at a given moment in time, its movement is automatically tracked using a modified autocorrelation estimator. After exclusion of artifact cycles, an averaged diameter waveform was constructed.

The exponential and Langewouters models were fitted to the obtained P-A loops using a Marquardt fitting algorithm. Subsequently, the α stiffness index and static distensibility were calculated for each subject. In order to compare the performance of the newly proposed pressure dependent static distensibility index to the pressure independent α stiffness index, the static distensibility was evaluated at the local mean arterial pressure as an approximation of local working pressure. Both indices were averaged over 4 age quartiles (Q_1: 35-40, Q_2: 41-45, Q_3: 46-50, Q_4: 51-55 years).

12.3 RESULTS

The fitting was successful in 2007 subjects. In cases the fitting failed this was either because of unavailability of the data due to poor measurements or because of the limited physiological pressure range available for the fitting.

Figure 12.1 on the next page shows the comparison of the evolution with age and gender of the α stiffness index (top panel) and static distensibility evaluated at mean arterial pressure (bottom panel). Figure 12.2 on page 162 additionally shows differences in evolution with age of the static distensibility index evaluated over a broad pressure range for men and women.

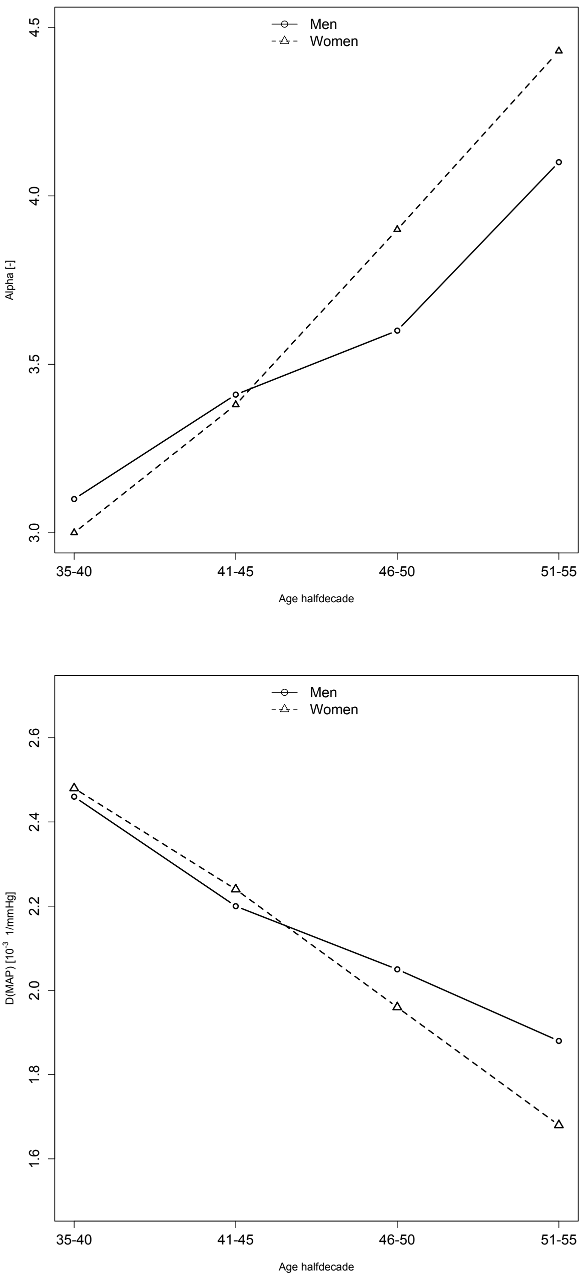

FIGURE 12.1: α stiffness index (left) and static distensibility evaluated at mean arterial pressure (right) per age quartile for men and women. (*): $P < 0.05$

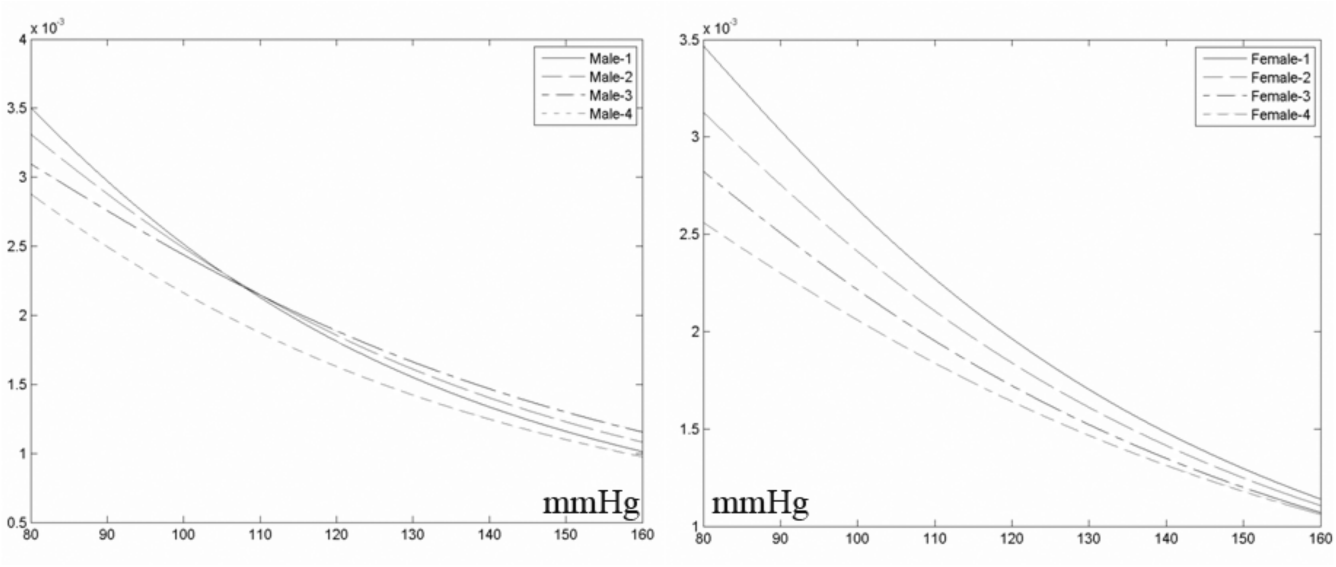

Figure 12.2: Static distensibility evaluated over a broad pressure range per age quartile for men (left panel) and women (right panel). Male-1 to Male-4 and Female-1 to Female-4 represent the four age quartiles (1: 43–40, 2:41–45, 3:46–50, 4:51–55) for men and women, respectively.

12.4 DISCUSSION

Both the static distensibility evaluated at mean arterial pressure and the α stiffness index show similar trends. Whereas in the younger age quartiles, women generally seem to have more compliant vessels then men, this is no longer true from around the age of 45 years on, with women having statistically significantly stiffer vessels than men in the older age groups. This indicates that there is indeed some form of age-gender interaction in the stiffening of the carotid artery in our study population. The pivotal role of the third age quartile could suggest a possible role for menopausal hormonal changes.

The newly proposed static distensibility coefficient yields similar information to the established α stiffness index when evaluated at mean arterial pressure. The difference in stiffness changes with age in men and women is further confirmed when evaluating this distensibility index at different pressure levels. Whether more clinically relevant information can be extracted from this evaluation remains however to be investigated.

12.5 CONCLUSIONS

The proposed static distensibility derived from a geometry-normalized Langewouters P-A relationship shows results in good agreement with the α stiffness index. Both indices demonstrate that over the studied age-range, the carotid artery becomes stiffer in women than in men around the age of 45.

CHAPTER 13

Age, sex and local versus regional arterial stiffness in the Asklepios population

13.1 INTRODUCTION

Aortic stiffness has been shown to be an independent predictor of all-cause and cardiovascular mortality. Several studies have demonstrated the prognostic value of pulse wave velocity (PWV) as a measure of aortic stiffness beyond all known classical risk factors, that is, increased aortic pulse wave velocity (PWV_{ao}) is associated with increased incidence of cardiovascular events [131–139]. At present, PWV_{ao} measurements are generally considered as the 'gold standard' method for evaluating aortic stiffness, commonly measured between the carotid and femoral artery [82, 140, 141]. As it is a direct and relatively robust measure of central arterial stiffness, it has been widely used in large-scale clinical studies. In recent work from our group [61] however, it was found that the well known age-related arterial stiffening independent of gender demonstrated by PWV_{ao} was not fully paralleled by (global) stiffness parameters derived from aorta pressure and flow. These discrepancies in behaviour of different measures of central arterial stiffness are at present not fully resolved.

Aortic PWV reflects the properties of the complete aorta, which gradually evolves from a large, elastic artery in the ascending and descending thoracic part to a more muscular vessel in the abdomen and the iliac bifurcation. It can thus not simply be categorized as either an elastic or a muscular artery and its behaviour likely reflects a mix of properties related to both arterial types. As a consequence, there is no clear-cut relationship between aortic PWV and locally measured stiffness indices obtained at the carotid artery, which behaves mostly as an elastic artery, nor at the muscular femoral artery.

The Asklepios study [42] offers a unique integrated perspective on arterial stiffness in a sizeable population of healthy individuals aged 35–55 years. The study protocol includes both central arterial stiffness measures as well as stiffness indices assessed locally at the carotid and femoral arteries. It offers a valuable dataset for examining the evolution of arterial stiffness at different sites and possible discrepancies between different stiffness parameters commonly used in literature in a single, well documented population. The aims of the present study are to compare the evolution with age and gender of central arterial stiffness to carotid and femoral arterial stiffness and to investigate discrepancies between arterial stiffness parameters in the Asklepios population.

13.2 METHODS

13.2.1 Study population

Data used in the present study were drawn from the Asklepios study database. The Asklepios study is a longitudinal population study designed to focus on the interplay between aging, cardiovascular hemodynamics and inflammation in (preclinical) cardiovascular disease [42]. In this study, the data from the first round of the Asklepios study, completed between October 2002 and September 2004, were used for a cross-sectional analysis of arterial stiffness in a representative cohort of 35–55 year-old subjects free from overt cardiovascular disease.

Of a total cohort of 2,524 subjects (1,301 women, 1,223 men), 2,195 (1,131 women, 1,064 men) were eligible for inclusion in this study. Two hundred and fifty-nine (259) subjects (10.3%) were excluded because of current antihypertensive treatment and an additional 70 datasets (3%) were incomplete due to missing PWV_{ao} measurements. A complete description of the design, baseline characteristics, and methodological details of the Asklepios study can be found elsewhere [42]. This section focuses on assessment of local pressure, local diameter and PWV_{ao}.

All data were collected by a single individual: basic clinical data were gathered by a study nurse, vascular echography and applanation tonometry by an expert operator. All measurements were single centre, single device and single operator. The study protocol was approved by the ethics committee of the Ghent University Hospital and all subjects gave written informed consent.

13.2.2 Basic clinical data

Body-size parameters were measured (weight, height, distances from sternal notch to carotid and femoral arteries) after which the subjects were allowed 10–15 min of rest in a temperature-controlled environment before further examinations. BMI was calculated as weight/height^2 (kg/m^2).

The blood pressure (BP) values reported were distinct from the baseline measurements, and recorded in between the echographic and tonometer measurements using a validated [62] oscillometric Omron HEM-907 device (Omron Matsusaka Co. Ltd., Japan). Cuff sizes were individually chosen based on arm circumference (<22 cm, 22–32 cm, >32 cm) and subjects were blinded to the BP results during measurement.

13.2.3 Measurement of local blood pressure

Local arterial pressure waveforms were assessed using applanation tonometry with a Millar pen type tonometer (SPT 301, Millar Instruments, Houston, Texas, USA) using a dedicated hardware and software platform. A detailed description of the set-up, processing and calibration process was previously published [63, 66]. Tonometry was first performed at the level of the left brachial artery. This tonometric reading was calibrated by identifying oscillometric systolic (SBP_{ba}) and diastolic (DBP_{ba}) BPs with the peak and trough of the pressure curve. Next, tonometry was performed consecutively at the left carotid and femoral arteries. These waveforms were calibrated using the validated assumption that diastolic and mean BPs remain fairly constant throughout the large arteries [64, 65]. Mean arterial pressure was calculated as the average value of the calibrated brachial artery waveforms (MAP). Both carotid and femoral pressure waveforms were then calibrated by assigning the trough and mean values of all recordings the values of DBP and MAP.

In 417 subjects brachial artery waveforms could not be recorded with satisfactory quality within a reasonable amount of time. For these subjects, MAP was calculated from a scaled radial artery waveform. The radial artery waveform was scaled using DBP and an estimated value for the radial systolic blood pressure (SBP_{ra}) obtained from a population based generalized model:

$$SBP_{ra} = 4.974 + 1.11 \cdot SBP_{bra} - 0.178 \cdot DBP \qquad (13.1)$$

This expression was derived from a linear regression analysis on a subset of 1,863 subjects in the Asklepios study where both brachial and radial artery tonometry recordings were available ($r^2 = 0.91$). By use of this approach, we accounted for the brachial-to-radial amplification of SBP [66].

13.2.4 Measurement of local arterial diameter

Arterial diameter distension waveforms were obtained by ultrasound echo wall tracking performed at the left common carotid artery, 2 cm proximal to the carotid bulb and at the left common femoral artery using a commercially available ultrasonographic system (Vivid7; GE Vingmed, Horten, Norway) equipped with a vascular transducer (12L) set at 10 MHz. Subjects were examined in the recumbent position with the neck in slight hyperextension and turned approximately 30 degrees contralateral to the examined carotid artery and with the legs slightly parted and exorotated for the femoral arteries. All measurements were ECG gated and consisted of cineloops of at least five and up to 30 cardiac cycles during normal breathing.

In order to obtain the diameter distension waveforms, the operator selects a region of interest during B-mode vascular imaging containing both the anterior and posterior walls. Within this region of interest, radio-frequency data are acquired at 209 frames/s along eight evenly distributed beams. These radio-frequency data are stored together with B-mode cineloops for offline analysis within a Matlab environment (The Mathworks Inc., Natick, Massachusetts, USA). After manual selection of the vessel boundary at a given moment in time, its movement is automatically tracked using a modified autocorrelation estimator [125, 126]. For this study, the vessel wall boundary was chosen on the intima-media interface.

13.2.5 Carotid-femoral pulse wave velocity

Aortic pulse wave velocity was estimated as

$$PWV = \frac{\Delta L_{S-F} - \Delta L_{S-C}}{\Delta T_{Q-F} - \Delta T_{Q-C}} \left[\frac{m}{s}\right] \tag{13.2}$$

with

ΔL_{S-F}: distance from sternal notch to femoral measurement site
ΔL_{S-C}: distance from sternal notch to carotid measurement site
ΔT_{Q-F}: time delay between start of QRS complex and upstroke of flow in femoral artery
ΔT_{Q-C}: time delay between start of QRS complex and upstroke of flow in carotid artery

13.2.6 Local arterial stiffness

Assuming the lumen to be circular, the carotid and femoral compliance (CC) and distensibility coefficients (DC) were assessed from the measured pressure and diameter waveforms at the level of the carotid and femoral arteries [82]:

$$CC = \frac{\Delta A}{\Delta P} = \frac{\pi}{4} \frac{D_s^2 - D_d^2}{\Delta P} \left[\frac{m^2}{Pa}\right] \tag{13.3}$$

$$DC = \frac{\Delta A / A_d}{\Delta P} = \frac{D_s^2 - D_d^2}{D_d^2 \Delta P} \left[\frac{1}{Pa}\right] \tag{13.4}$$

where

ΔA: systolic-diastolic change in arterial cross-section at a given location
ΔP: local pulse pressure (PP) at that given location
D_s: arterial diameter at end-systole
D_d: arterial diameter at end-diastole
A_d: arterial cross-section at end-diastole

13.2.7 Local arterial stiffness: derived parameters

Local carotid and femoral PWV (m/s) can be obtained from the distensibility coefficient using the Bramwell - Hill equation:

$$PWV = \sqrt{\frac{1}{\rho \cdot DC}} \left[\frac{m}{s}\right] \tag{13.5}$$

where ρ is the density of blood, assumed to be 1050 kg/m^3.

Finally, the characteristic impedance of an artery is given by

$$Z_c = \rho \frac{PWV}{A} \left[\frac{Pa \cdot s}{m^3} \right] \tag{13.6}$$

where A is the (diastolic) cross-sectional area of the vessel.

The subscripts 'ao', 'cca' and 'cfa' will be used for measurements related to the aorta, the common carotid and femoral artery, respectively.

13.2.8 Statistical analyses

Data are presented as mean values (standard deviation – SD) in the text and tables. In the figures, error bars denote SEM (standard error on the mean). Subjects were subdivided by gender into four half decades of age (Q_1–Q_4) for further analysis, defined as follows: Q_1:35–40,Q_2: 41–45, Q_3:46–50, Q_4: 51–56 years.

Effects of age and gender were assessed using analysis of variance techniques (ANOVA) with gender and age as fixed factors. Parameters depending on body size were adjusted for weight and height by including these confounding factors as covariants in the statistical analysis (ANCOVA). Further adjustments for MAP were performed where appropriate. Differences in gender were assessed by checking for overlap of the 95% confidence intervals of the estimated marginal means. Nonoverlapping intervals indicated significant differences ($P < 0.05$). All statistical analyses were performed using SPSS 12.0 (SPSS Inc., Chicago, Illinois, USA).

13.3 RESULTS

13.3.1 Basic clinical data and hemodynamics

Population and general hemodynamic data are displayed in table 13.1 on page 174. Mean age within each half decade was not different between men and women. The mean age difference between Q_1 and Q_4 was about 15 years. Men were taller and heavier than women, as expected. Body height decreased with age, the subjects in Q_1 being on average about 3 cm taller than the subjects in Q_4,both for men and women. Even though there was no significant change of weight with age, due to the differences in height the BMI increased significantly with age in both genders.

Brachial artery pressures increased with age. DBP and MAP were not different between men and women. For SBP_{ba} there was a difference between men and women in the first three age quartiles. The evolution with age and gender of carotid and femoral systolic pressure and MAPs are reported in table 13.2 on page 175.

13.3.2 Carotid-femoral pulse wave velocity (PWV_{ao})

Figure 13.1 shows the evolution of PWV_{ao} with age and gender. There was an increase of PWV_{ao} with age ($P < 0.001$) regardless of gender and PWV_{ao} increased at the same rate in men and women. PWV_{ao} did not differ between men and women in any of the age groups.

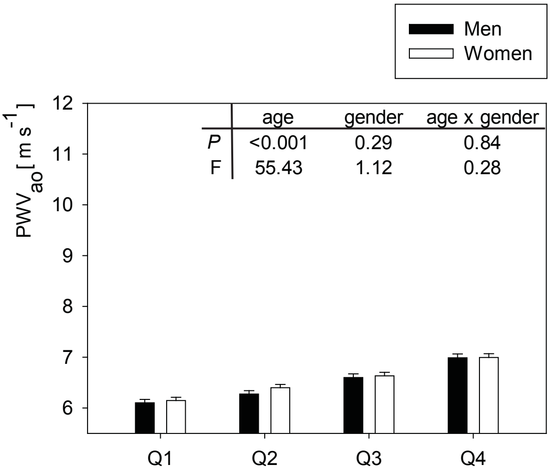

	age	gender	age x gender
P	<0.001	0.29	0.84
F	55.43	1.12	0.28

FIGURE 13.1: Evolution of carotid-femoral PWV with age and gender in the Asklepios population. The F and P values indicate the statistical significance of the factors age and gender and their interaction in the ANCOVA analysis. PWV was adjusted for mean arterial pressure. Error bars are SEMs. *: $P < 0.05$, men versus women

13.3.3 Local arterial stiffness - carotid artery

Changes in carotid stiffness are displayed in the left hand panels of figure 13.2 on page 173 [panels (c), (e), (g)]. Parameters CC_{cca},DC_{cca} and $Z_{c,cca}$ showed a significant change with age (all $P < 0.001$) indicating a progressive arterial stiffening. All but CC_{cca} showed a significant age-gender interaction ($P < 0.001$), with the rate of vessel stiffening being higher in women than in men over the studied age range. While there was no global systematic difference in DC_{cca} between men and women, CC_{cca} and $Z_{c,cca}$ did show a significant gender effect ($P < 0.001$). PWV_{car} derived from DC_{car} revealed a similar pattern as this parameter: a progressive increase with age regardless of gender, no significant differences between men and women and a more rapid age-related increase in women than in men (figure 13.2 (a)).

13.3.4 Local arterial stiffness - femoral artery

The right-hand panels of figure 13.2 display changes with age and gender of the different stiffness measures obtained at the femoral artery [panels (d), (f), (h)]. No age effects were found for DC_{cfa}, whereas $Z_{c,cfa}$ and CC_{cfa} did change with age, the former decreasing and the latter increasing with age. There were significant differences between men and women in all age groups for all parameters but CC_{cfa}. None of the parameters revealed an age-gender interaction. Derived femoral PWV_{cfa} was higher in men than in women, but did not change with age in men or in women (figure 13.2 (b)).

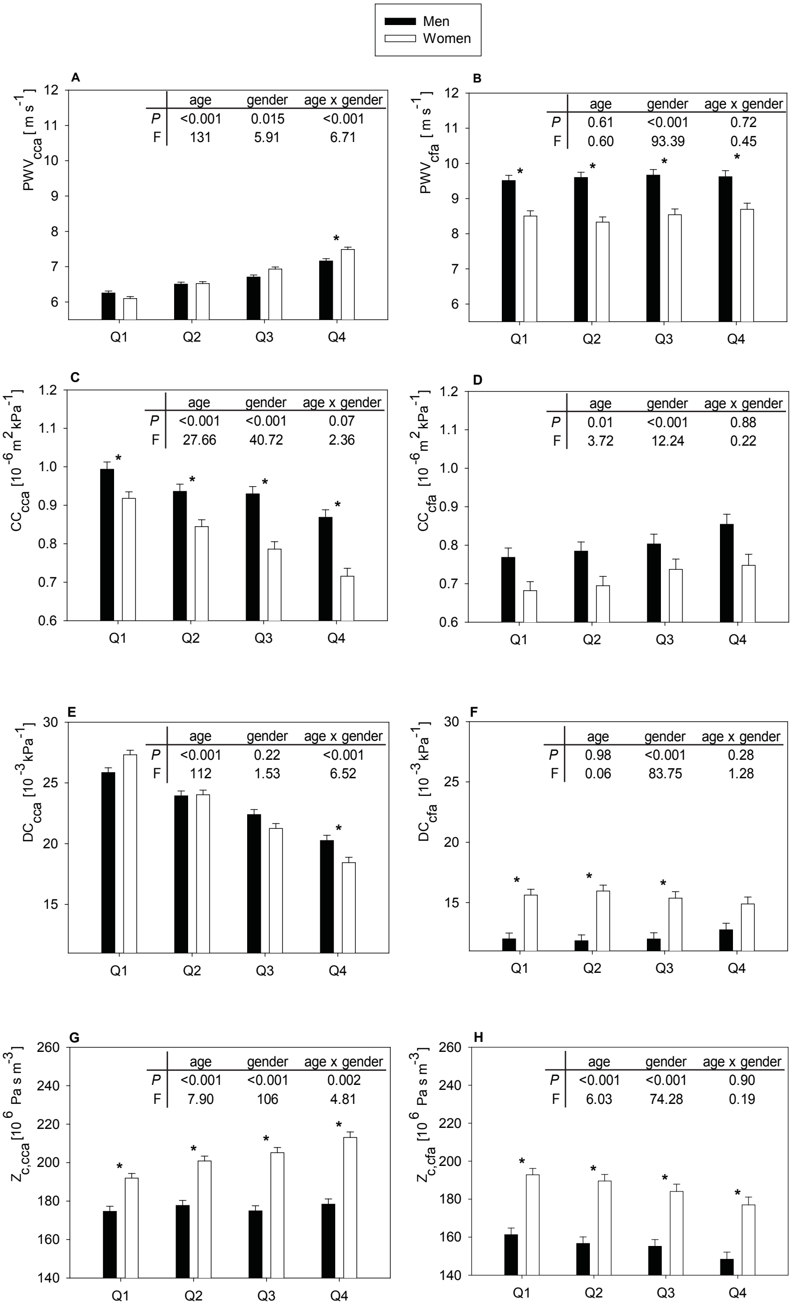

A

	age	gender	age x gender
P	<0.001	0.015	<0.001
F	131	5.91	6.71

B

	age	gender	age x gender
P	0.61	<0.001	0.72
F	0.60	93.39	0.45

C

	age	gender	age x gender
P	<0.001	<0.001	0.07
F	27.66	40.72	2.36

D

	age	gender	age x gender
P	0.01	<0.001	0.88
F	3.72	12.24	0.22

E

	age	gender	age x gender
P	<0.001	0.22	<0.001
F	112	1.53	6.52

F

	age	gender	age x gender
P	0.98	<0.001	0.28
F	0.06	83.75	1.28

G

	age	gender	age x gender
P	<0.001	<0.001	0.002
F	7.90	106	4.81

H

	age	gender	age x gender
P	<0.001	<0.001	0.90
F	6.03	74.28	0.19

FIGURE 13.2: Evolution of carotid and femoral stiffness indices with age and gender in the Asklepios population. (a) and (b): PWV; (c) and (d) compliance coefficient (CC), (e) and (f): distensibility coefficient (DC), (g) and (h): characteristic impedance (Z_c). The F and P values indicate the statistical significance of the factors age and gender and their interaction in the ANCOVA analysis. PWV, CC, DC and Z_c were adjusted for mean arterial pressure; Z_c and CC additionally for weight and height. Error bars are SEMs. *: $P < 0.05$, men versus women.

TABLE 13.1: Basic clinical data of the study population (mean (SD)). The P and F values of the factors age, gender and their interaction term are given in the last three columns. Additionally, per category it was verified whether the difference between men and women was statistically significiant. *: P<0.05.

Parameter		Q_1	Q_2	Q_3	Q_4	Variable	Age	Gender	Age × gender
No.	Men	276	284	257	247				
	Women	319	296	266	250				
Age (years)	Men	37.8 (1.7)	43.1 (1.4)	47.9 (1.4)	53.3 (2.0)				
	Women	37.7 (1.8)	42.9 (1.5)	47.8 (1.4)	53.2 (1.7)				
Height (cm)	Men	177.7 (6.6)	176.2 (6.3)	175.1 (6.4)	174.1 (6.2)	*P*	<0.001	<0.001	0.66
	Women	164.7 (6.0)*	164.1 (6.0)*	162.6 (5.7)*	161.3 (5.7)*	*F*	33.66	2,312	0.53
Weight (kg)	Men	81.3 (12.3)	80.8 (12.4)	82.0 (12.1)	80.9 (12.1)	*P*	0.12	<0.001	0.65
	Women	65.3 (11.6)*	64.7 (11.5)*	67.0 (12.9)*	66.3 (11.3)*	*F*	1.95	899	0.56
BMI (kg/m^2)	Men	25.7 (3.5)	25.9 (3.5)	26.6 (3.5)	26.7 (3.9)	*P*	<0.001	<0.001	0.37
	Women	24.0 (4.1)*	23.9 (3.9)*	25.3 (4.7)*	25.4 (4.2)*	*F*	14.31	85.47	1.04
SBP_{ba} (mmHg)	Men	131.0 (10.8)	132.9 (12.4)	134.0 (12.6)	136.9 (16.9)	*P*	<0.001	<0.001	0.005
	Women	123.9 (13.1)*	126.9 (14.9)*	130.4 (15.2)*	135.6 (17.8)	*F*	34.60	51.34	4.24
DBP (mmHg)	Men	74.4 (9.5)	77.7 (10.6)	79.1 (9.4)	79.6 (11.8)	*P*	<0.001	<0.001	0.43
	Women	73.8 (10.6)	75.4 (10.6)	76.5 (10.3)	77.6 (11.0)	*F*	18.36	16.31	0.92
MAP (mmHg)	Men	97.2 (9.5)	100.5 (11.2)	101.9 (10.2)	103.4 (13.3)	*P*	<0.001	<0.001	0.57
	Women	95.8 (11.3)	98.0 (11.8)	100.3 (11.9)	103.0 (13.0)	*F*	30.94	8.37	0.67
Glycemia (mg/dl)	Men	91.0 (7.8)	91.8 (9.4)	93.3 (9.6)	95.2 (9.3)	*P*	<0.001	<0.001	0.95
	Women	86.6 (7.4)*	87.1 (7.8)*	89.1 (8.6)*	91.1 (8.1)*	*F*	27.85	141	0.12
Total cholesterol (mg/dl)	Men	211 (2)	216 (2)	223 (2)	226 (2)	*P*	<0.001	0.001	0.12
	Women	203 (2)	209 (2)	216 (2)	227 (2)	*F*	30.04	10.89	1.94
HDL cholesterol (mg/dl)	Men	55.6 (13.6)	56.7 (13.8)	56.9 (13.3)	56.6 (13.1)	*P*	0.46	<0.001	0.26
	Women	71.6 (16.4)*	71.0 (17.7)*	70.1 (17.6)*	73.2 (16.4)*	*F*	0.87	516	1.34
Current smokers (%)	Men	24.3	19.7	20.6	20.7				
	Women	16.9	20.3	19.9	15.9				

TABLE 13.2: Hemodynamic and arterial parameters (mean (SD)). The P and F values of the factors age, gender and their interaction term are given in the last three columns. Additionally, per category it was verified whether the difference between men and women was statistically significiant. *: P<0.05.

Parameter		Q_1	Q_2	Q_3	Q_4	Variable	Age	Gender	Age × gender
SBP_{cca}	Men	126.5 (11.7)	129.7 (14.0)	131.2 (13.4)	134.8 (17.8)	*P*	<0.001	0.08	0.03
	Women	123.0 (14.3)	126.7 (16.2)	131.2 (16.9)	136.4 (19.5)	*F*	44.84	3.09	3.10
PP_{cca}	Men	52.0 (9.8)	51.9 (9.2)	51.9 (9.5)	55.2 (11.9)	*P*	<0.001	0.14	<0.001
	Women	49.1 (9.0)*	51.2 (10.9)	54.7 (12.8)*	58.8 (14.8)*	*F*	32.59	2.16	9.77
SBP_{cfa}	Men	132.3 (12.2)	135.9 (13.9)	137.5 (14.4)	141.0 (18.1)	*P*	<0.001	<0.001	0.36
	Women	126.5 (14.0)*	129.3 (14.8)*	132.2 (16.2)*	138.2 (19.0)	*F*	29.94	43.29	1.07
PP_{cfa}	Men	58.9 (10.8)	58.8 (9.4)	59.4 (10.6)	62.1 (12.7)	*P*	<0.001	<0.001	0.01
	Women	53.7 (9.6)*	55.4 (9.8)*	57.6 (12.7)	62.0 (15.0)	*F*	19.29	20.97	3.74
D_{cca}	Men	7.18 (0.62)	7.26 (0.61)	7.46 (0.81)	7.63 (0.82)	*P*	<0.001	<0.001	0.79
	Women	6.41 (0.54)*	6.51 (0.62)*	6.67 (0.62)*	6.80 (0.63)*	*F*	42.71	768	0.36
D_{cfa}	Men	9.43 (0.96)	9.61 (0.98)	9.67 (1.19)	9.81 (1.33)	*P*	<0.001	<0.001	0.35
	Women	7.48 (0.84)*	7.45 (0.88)*	7.70 (0.96)*	7.86 (1.02)*	*F*	11.95	1,722	1.09
ΔD_{cca}	Men	0.609 (0.141)	0.557 (0.144)	0.527 (0.144)	0.504 (0.158)	*P*	<0.001	<0.001	0.72
	Women	0.547 (0.111)*	0.502 (0.120)*	0.473 (0.114)*	0.432 (0.118)*	*F*	67.39	113	0.45
ΔD_{cfa}	Men	0.402 (0.155)	0.383 (0.145)	0.391 (0.142)	0.414 (0.172)	*P*	0.25	0.21	0.40
	Women	0.376 (0.147	0.389 (0.146)	0.390 (0.164)	0.398 (0.156)	*F*	1.37	1.61	0.98

13.4 DISCUSSION

The effect of age on arterial stiffening has been the subject of many different studies both for central (aortic) arterial stiffening as well as for the stiffening of more peripheral arteries like the carotid and femoral arteries [142–144]. Likewise, in recent years, there has been a growing interest in studying the effect of gender on cardiovascular risk factors, such as arterial stiffening [143–145].

Though aortic PWV is currently considered the gold standard method for assessment of central arterial stiffness and several large-scale studies have shown that aortic PWV can be considered both a risk factor for the development of cardiovascular disease as well as predictive for outcome [131–139], the assessment of arterial stiffness is still a rapidly evolving field. Recently, guidelines were published attempting to standardize the way stiffness is measured. Nevertheless a great many types of indices and parameters can be and still are used to evaluate stiffness at different arterial locations. The differences between these parameters are not always fully elaborated, nor are the potential influences of these differences on the interpretation of the results always clear. This study offers a new perspective by combining an integrated assessment of central arterial stiffness and peripheral stiffness evaluated at elastic and muscular arteries on a large representative middle-aged population.

To compare the evolution with age and gender of central arterial stiffness as expressed by PWV_{ao} to the evolution of local stiffness at the carotid and femoral arteries, an approach similar to the one used in a study by Paini *et al.* [146] was used. By converting the distensibility coefficients to a PWV using the Bramwell–Hill equation, a direct comparison of stiffness in a single unit is possible at these arterial sites. In terms of correlation coefficients, the correspondence of the stiffness indices is, at best, fairly moderate ($r^2 = 0.38$ between PWV_{ao} and PWV_{cca}, $r^2 = 0.22$ between PWV_{ao} and PWV_{cfa}, $r^2 = 0.33$ between PWV_{cca} and PWV_{cfa}; all $P < 0.001$). The correlation between PWV_{ao} and PWV_{cca} is somewhat lower than the values reported by Paini *et al.* [146] in a mixed population of healthy normotensives and diabetic and nondiabetic hypertensives.

The weak direct association between the parameters is also reflected in their different global patterns in relation with age and gender. For carotid–femoral PWV, no significant gender difference was found in any of the age quartiles, or a general gender difference over the studied age range (figure 13.1). These results are in agreement with other literature [147–149]. PWV assessed at the carotid and femoral arteries shows different behaviors. For the muscular femoral artery there seems to be little or no effect of aging on stiffness. There are significant differences between men and women in each of the studied age groups (men on general having stiffer arteries than women), but no age-gender interaction is evident from the present data (figure 13.2 (b)). These findings are in agreement with previously published studies on local femoral stiffness [150]. Other peripheral muscular arteries like the brachial artery show a similar behaviour [151]. It should be noted that Filipovsky *et al.* [148] did report an increase in PWV in the lower limb with age in women (but not in men, where PWV was overall higher) over the age range 25–65. The carotid artery on the other hand, showed stiffening with age in men and women and a significant age-gender interaction was found (figure 13.2 (a)) indicating that stiffening occurred at a faster pace in women.

The observed differences between aortic and femoral stiffness are as expected. Femoral stiffness indices are well accepted to be indicative of the muscular nature of the femoral artery, whereas aortic and carotid stiffness measures are considered to be indicative of more elastic arteries. It is known that muscular arteries can compensate for the decrease in stiffness found in more elastic arteries with aging [151], which is also reflected in figure 13.2 panels (d) and (h), showing an increase in compliance and decrease in characteristic impedance, respectively, with age in the femoral artery.

Aortic and carotid stiffness are usually both accepted as indicative for large elastic artery stiffness. Even so, the carotid artery is a first-to-second order daughter branch of the aorta and their structure and composition, though similar, are not the same. The observed differences in the relation between age and stiffness – mainly the absence of age-gender interaction in aortic PWV – could be the result of intrinsic differences between the aorta and the carotid artery, or a different response in time to exposure to risk factors. A recent study investigating the differences between carotid and aortic arterial stiffening found that the relationship between both was dependent on the presence of other risk factors like hypertension and type 2 diabetes mellitus [146].

These differences between aortic and carotid stiffness expressed by PWV could however also be at least partially explained by the intrinsic nature of carotid–femoral PWV. The distance over which carotid–femoral PWV is measured comprises the elastic proximal aorta as well as the more muscular abdominal aorta and iliac arteries. As such, PWV_{ao} likely yields a value reflecting the composite nature of the arterial segment over which it is measured. If this is the case, it becomes interesting to consider the behaviour of other established indices of central arterial stiffness which are unaffected by this possible 'blurring' effect. In a recent study from our group [61] input and characteristic impedance and global arterial parameters were assessed in the same Asklepios population. In women, $Z_{c,ao}$ remained approximately constant over the age range 35–55 years, while it decreased in men. Similarly, total arterial compliance also showed an age-gender interaction, decreasing in women while remaining constant in men. Since aortic PWV increased similarly in men and women, these findings were explained by assuming a differential modulation of effective aortic size, which was estimated to increase by 15% in women, and by 30% in men over the studied age range [61].

To allow comparison between the data, we calculated local characteristic impedance from local pulse wave velocity and local diameter. Interestingly, the characteristic impedance of the carotid artery, $Z_{c,cca}$, remained virtually constant in men, while it increased in women. These data demonstrate that the different tendencies found in men and women at the carotid artery are also found at the level of the aorta, at least when its properties are quantified in terms of characteristic impedance or volume compliance. Common carotid diameters, given in table 13.2, increased with age, but there was no difference in evolution between men and women. Hence, where we previously assumed a similar increase in aortic PWV and explained the observations through differences in effective aortic cross-sectional area in men and women, our data measured directly at the carotid artery now demonstrate that the explanation may also be sought in a more rapid stiffening of the proximal, elastic arteries in women than in men in this age group (reflected in steeper slopes for $Z_{c,cca}$, PWV_{cca} and DC_{cca}), rather than in differences in evolution of arterial diameters. This age-gender effect was also described in a study by Waddell *et al.* [152] who, equally based on impedance analysis, also found women to have a more compliant proximal aorta than men in the younger age group (mean age 23), and vice versa for the older age group (mean age 62 years). Similarly, in a previous study Laogun and Gosling [153] found a more rapid decrease in aortic compliance in women than in men after the age of 45 years.

These data all suggest that the age-gender effect observed in our study at the carotid artery is in fact also found at the (elastic section of the) aorta. We hypothesize that the reason these patterns are not reflected in the conventionally measured PWV$_{ao}$ is due to the blurring' effect of measuring PWV over a large arterial segment with differing properties. It be noted that even though carotid-femoral PWV seems to 'average' out the age-gender effects observed either at the carotid artery or using different central arterial stiffness parameters, this does not necessarily indicate that picking up these differences is also of importance. Within the Asklepios study, having only finished the first round of screening, no outcome data are available to investigate the relation between the different stiffness measures and cardiovascular events. Furthermore, whereas there are many different studies linking carotid-femoral PWV to cardiovascular risk and outcome, the evidence of the same for carotid artery stiffness is far more scarce or inconclusive [154, 155].

The observation that local and global arterial stiffness parameters may show different tendencies does, however, complicate the debate on which arterial stiffness parameter should be used for the assessment of an individual's cardiovascular risk. We nevertheless believe that with our study, we can positively contribute to this debate. With the Asklepios study we chose to assess large artery function in a broad perspective [42], using a multitude of techniques to assess local and global parameters, allowing for direct comparison between parameters. Given the size of our database and the well defined population and age range, our data could also contribute to the assessment of reference values for these parameters. The latter will be an absolute requirement if one wishes to identify subjects at increased cardiovascular risk based on abnormal stiffness values.

On the other hand, the present study has several limitations. Although the size of our population is large, the age range that it covers is fairly limited. Even though we found the age range typically associated with the onset of menopause (45.7 ± 10.6 years in our population) to be the pivotal age point in our age-gender interaction studies, a broader range would allow the trends seen in our analyses to be confirmed. The effect of menopause on arterial stiffness should be investigated on a larger population and in proven menopause. Furthermore, all subjects included in the study were free from overt cardiovascular disease. In a population including diseased subjects, the age-gender interactions found might be less obvious. Finally, women have higher resting heart rates than men, and if the vessel were to show visco-elastic behavior, it could be anticipated that for the same intrinsic vessel properties, a vessel would appear as more rigid in women than in men. As such, heart rate is a potential confounding factor in our study. Adding heart rate (HR) as a covariant in the analysis did decrease the statistical significance of the factor 'gender', but it did not have an impact on the more rapid increase in carotid stiffness in women compared to men over the considered age range. This is coherent with the fact that there is no effect of age on HR in men or women, so that it does not interfere with the interaction term. One might also think of height as a potential covariant, but stiffness parameters such as distensibility coefficients and PWV are intrinsically height independent, and height was already taken into account for those parameters depending on body size (characteristic impedance and compliance coefficient).

13.5 CONCLUSIONS

Increasingly, arterial stiffness is being considered as an important element for assessment of cardiovascular risk. Although some efforts towards standardized arterial stiffness measures have been made [82], their widespread use is still lacking. Several methods have been proposed, including measurement of carotid–femoral (aortic) PWV (considered as gold standard) and local stiffness measured at the level of the common carotid artery. Our data demonstrate that, in an apparently healthy middle-aged population, the evolution with age of these parameters is not the same in men and women. While carotid stiffness shows a more rapid increase with age in women than in men (over the measured age range of 35–55 years), this pattern is not reflected in aortic PWV, which increases to a similar extent in men and women. Other central arterial stiffness parameters do show an age-gender effect similar to the one observed at the carotid artery. Though the differences in evolution of different stiffness parameters with age and gender have not yet proven to be of clinical significance, the fact that these differences exist is important to keep in mind when analysing or interpreting results from arterial stiffness investigations. Special care is needed when different parameters are compared, especially in a field where proposed measurement standards are not yet widely adopted and reference values are lacking.

Chapter 14

The Reference Values for Arterial Stiffness' Collaboration

14.1 The reference value project

Carotid-femoral pulse wave velocity is now listed as a measure of target organ damage in the recent guidelines of the European Society of Hypertension (ESH) [9]. Despite the existence of a consensus on the gold standard for measuring arterial stiffness [82] no recent reference values based on a European population obtained using modern equipment are available. Providing these reference values is essential not only to set a threshold for normality, but also to help stratify the level of arterial abnormalities detected. This is the aim of the Reference Values for Arterial Stiffness' Collaboration.

With financing from the French ministry of health and under the endorsement of the European Network for Non-Invasive Investigation of Large Arteries, the Artery Society and the European Society of Hypertension Working Group on Large Arteries, a research proposal was launched aiming to investigate normal and reference values of arterial stiffness in a European population. The ultimate goal of the project is to promote the use of arterial stiffness as a standard tool both for screening and stratification of CV risk and its use as a surrogate endpoint for clinical management of patients. Appendix A.1 lists the research proposal on which the reference values for arterial stiffness' collaboration was based.

The European reference value project includes data from 13 European centers selected on their recognized expertise in arterial measurements. The centers at present participating in the reference value project are (figure 14.1):

Plzen Second department of Internal Medicine, School of medicine, Charles University, Plzen, Czech Republic.

Brescia Dept. of Clinical Medicine, Spedali Civili di Brescia, Il Medicina, Brescia, Italy

Manchester University of Manchester, Dept. of Medicine, Royal Infirmiry, Manchester, UK

Fleury-Mérogis Service d'Hémodialyse, Hôpital F.H. Manhès, Fleury-Mérogis, France

Paris Nutritional Epidemiology Research Unit, Paris 13, Paris, France

Amsterdam/Maastricht EMGO institute, VU University Medical center, Amsterdam, The Netherlands; Depts. of Clinical Epidemiology and Medical Technology Assessment, AZM Maastricht, Maastricht, The Netherlands

Nancy Centre de Gériatrie, CHU Nancy and INSERM U684, Nancy, France

Athens Cardiovascular Diseases and Sexual Health Unit, 1st Dept. of Cardiology, Athens Medical School, Hippokration Hospital, Athens, Greece

Gent Dept. Cardiovascular Diseases, Ghent University Hospital, Gent and IBiTech - bioMMeda, Ghent University, Gent, Belgium

Copenhagen Research Center for Prevention and Health, Copenhagen, Denmark

Paris (HEGP) Dept. of Pharmacology, Hôpital Européen Georges Pompidou and INSERM UMRS872, Université Paris Descartes, Paris, France

Cambridge/Cardiff Clinical Pharmacology Unit, University of Cambridge, Addenbrooke's Hospital, Cambridge, UK and Dept. of Cardiology, Wales Heart Research Institute, Cardiff, UK

Rotterdam Dept. of Epidemiology and Biostatistics, Erasmus Medical Center, Rotterdam, The Netherlands

Subjects included in the database require a minimal set of available data and documentation. The requirements for inclusion in the reference value project are listed in appendix A.2. Measurements required include a measurement of either aortic stiffness through carotid-femoral

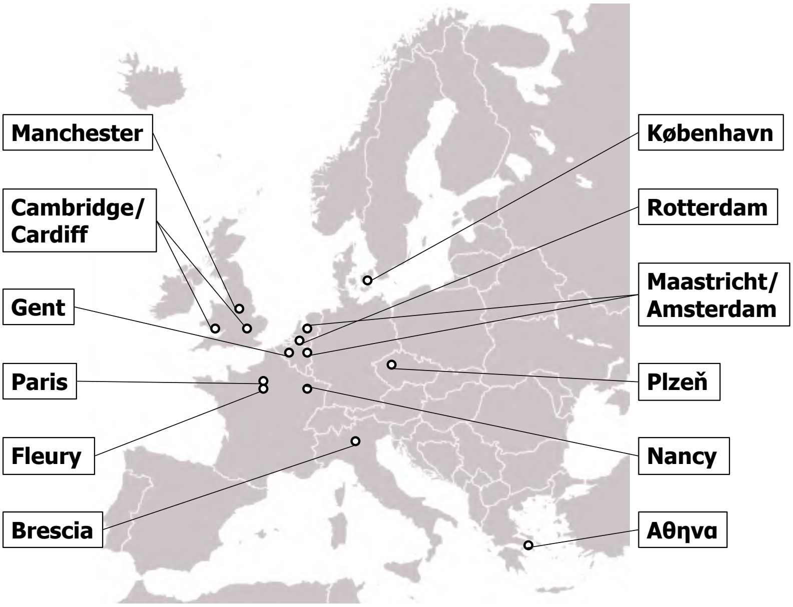

FIGURE 14.1: Geographic distribution of the centers participating in the reference value project

PWV, carotid stiffness determined from echotracking measurements, or measurements of central pulse pressure and wave reflection. In addition, for each subject, medical history, vital parameters, blood pressure, presence of classical risk factors and relevant treatments must have been assessed at the time of stiffness measurement. Most importantly, inclusion criteria concern also the documentation of techniques and measurement conditions in order to palliate for heterogeneities within studies.

14.2 OVERVIEW OF THE REFERENCE VALUE DATABASE

The reference value database currently contains data of over 24,000 subjects. Table 14.1 lists the number of subjects currently included per center.

The reference value database contains a large number of parameters, with differing levels of availability. Figure 14.3 illustrates the percentage of subjects in which a particular parameter is available for most parameters included in the reference value database. The percentage completeness values were calculated from a database snapshot taken in March 2008.

Table 14.1: Subjects included per center in the reference value database

Center	Included subjects
Plzen	256
Brescia	377
Manchester	579
Fleury-Mérogis	883
Paris	937
Amsterdam/Maastricht	1,102
Nancy	1,107
Athens	1,311
Gent	2,524
Copenhagen	2,592
Paris (HEGP)	3,400
Cambridge/Cardiff	4,687
Rotterdam	4,729
Total	*24,484*

The reference value database represents a sizable, European population, which is sufficiently large to perform meaningful analyses even after fine-grained categorization of subjects according to, for instance, risk or age categories. Average values and standard deviations for certain important population variables are illustrated in figure 14.2 on the next page. To illustrate differences between centers for these parameters, figure 14.2 also lists per parameter the average values for each center in comparison to the average population variables.

Given its size and the wealth of available data, the reference values for arterial stiffness' collaboration database provides a unique platform for the determination of reference and normal values valid in a European population. Though the database as of yet contains little or no outcome data, for each subject included in the database a unique link is maintained to the original center databases, making the future addition of such data trivial.

Finally, as is often the case, things that take the most effort and time to complete are often those things taken for granted later on, getting no more than a cursory mention. I would therefor be amiss were I not to emphasize one important aspect not mentioned in further detail in this manuscript. The construction and initial exploration of the reference value database was performed over the course of a nearly two year stay

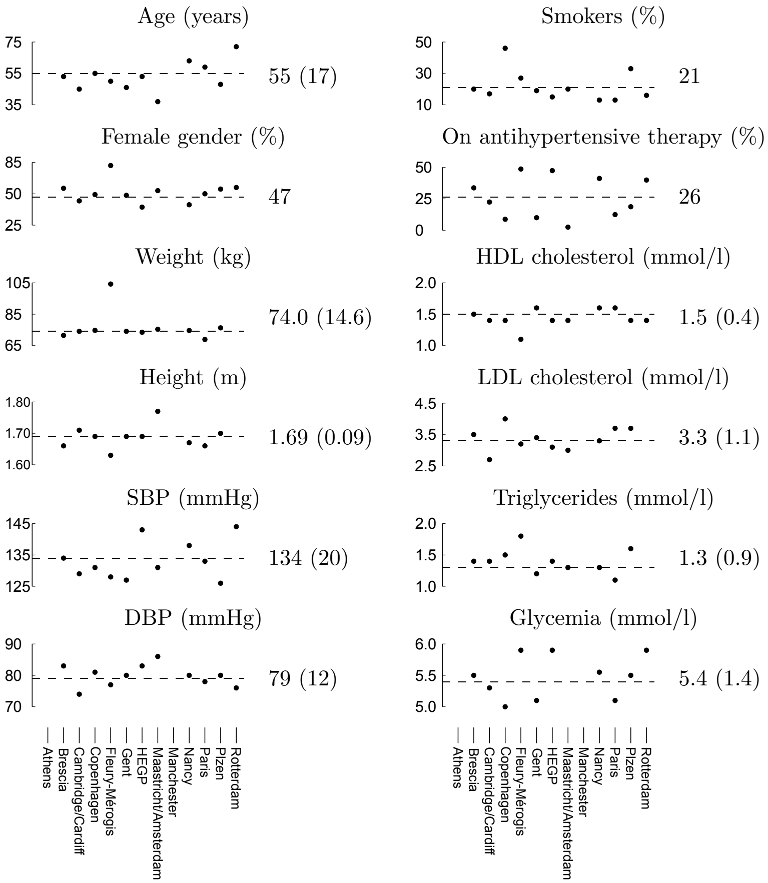

Figure 14.2: Overal mean (SD) of key subject characteristics in the reference value database and distribution of average values per center

at the HEGP and Université Paris Descartes in Paris. Throughout that period, easily the most time was spent on the actual construction of the database: communicating with centers interested in contributing, sometimes even visiting these centers to discuss or acquire the data, organizing and facilitating the data transfer, smoothing out technical differences, streamlining communication and procedures, working out protocols regarding the amount of required documentation and generally being a pain in the ass to the people I had to work with in the different centers across Europe. Though time-consuming, painstaking and often tedious, this particular part of the work was also sometimes the most rewarding, as the initial goals set out in the reference value project by others, were slowly getting realizable with every subject and center added by me. By far, getting the database to be actually exploitable represents the bulk of time spent on the project, yet it will not be mentioned again, favoring the actual exploitation of the database in the following chapters.

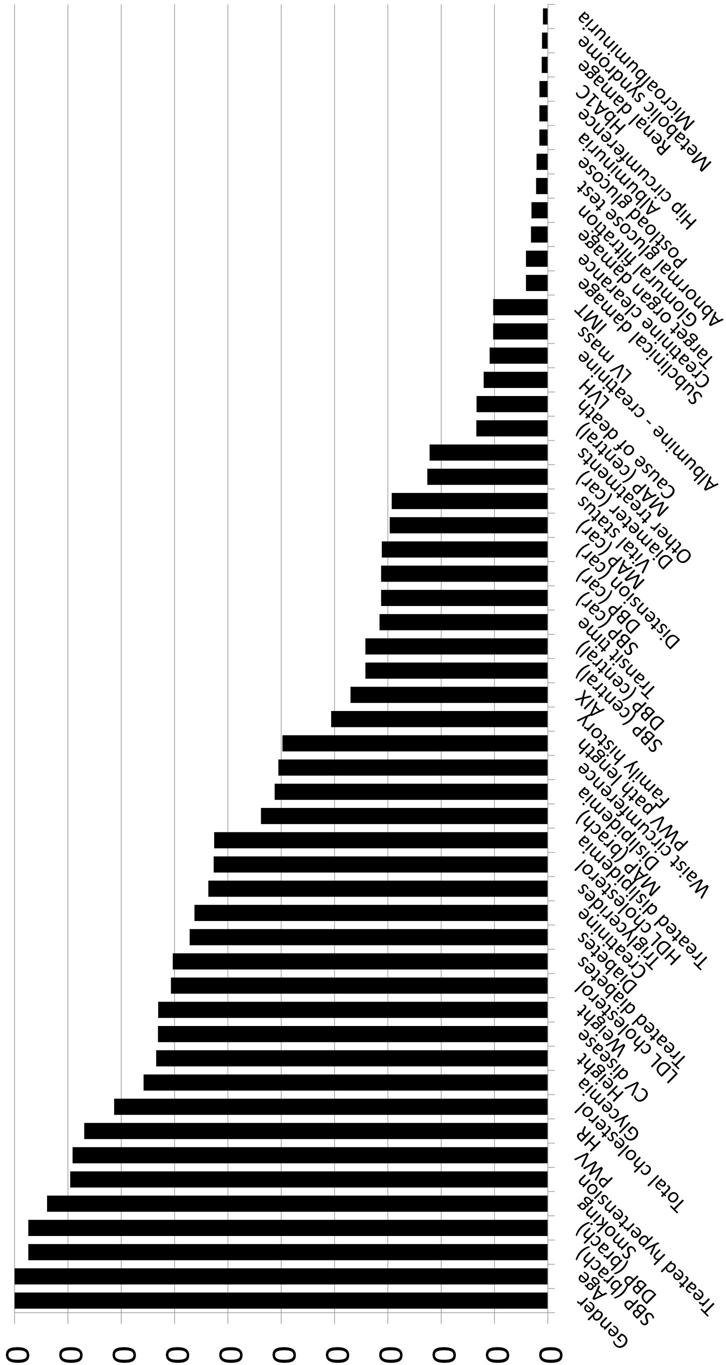

FIGURE 14.3: Percentage of subjects in which the listed parameters were available in March 2008

CHAPTER 15

Distance conversion for PWV calculation

15.1 INTRODUCTION

In recent years, there has been a growing interest in the assessment of arterial stiffness and its role in the evaluation of an individual's total cardiovascular risk [156]. Arterial stiffness can be quantified in a number of different ways [156], using either local [141], regional [151, 157] or systemic [158] stiffness parameters or by studying arterial wave reflections [101]. A thorough overview of the various approaches for arterial stiffness assessment and its clinical implications is outlined in [156].

Of all these approaches, the use of carotid-femoral pulse wave velocity (PWV) has become popular, as it has been demonstrated to be predictive for clinical outcome in numerous studies [132, 133, 154, 159–161]. Carotid-femoral PWV is a direct measure of aortic stiffness and can be measured in a sufficiently simple and accurate way to be used as a diagnostic test for assessment of target organ damage, as outlined in the latest 2007 European Society of Cardiology / European Society of Hypertension guidelines for the management of hypertension [9, 156]. These guidelines provide a threshold value for PWV of 12 m/s, which was derived from epidemiological studies. The absolute threshold value however, has been challenged due to its dependence on both the distance measurement used for its calculation [162, 163] and the device dependent algorithm used for detection of the waveform [90]. The carotid-femoral pathway used to calculate PWV can either be the direct distance between the measurement sites (DD), or the distance obtained by subtracting the carotid-sternal notch distance from the sternal notch-femoral distance (SD). The use of different distance definitions can result in differences in absolute PWV values of up to 30% while differences due to the wave detection algorithm used can account for differences of 5-10% [90]. These methodological issues have hampered the clinical applicability of PWV measures. Up to now, no large population based study was available to investigate these issues.

The aim of the present study was to propose and validate a model-based approach for the conversion between distance definitions based on data from two large populations in which all types of distance measurements are available. As corollary, the second aim was to propose equations for conversion between direct and subtracted distance based on these models.

15.2 METHODS

15.2.1 Study population

Data for the present study were drawn from the Asklepios study [42] and HEGP (Hôpital Européen Georges Pompidou) [133] databases. The Asklepios study is a large-scale longitudinal population study focusing on the interplay between ageing, cardiovascular hemodynamics and inflammation in cardiovascular disease. Data for the present study were drawn from the first round of the Asklepios study, completed between October 2002 and September 2004. A detailed description of the rationale, goals and methods of the Asklepios study has previously been described [42]. Briefly, pulse wave velocity was measured using a dedicated device based on flow waveforms obtained with pulsed-Doppler under bidimensional scan control. The Ghent University Hospital ethics committee approved the Asklepios study protocol and all subjects gave written informed consent. The HEGP database contains subject data from patients attending the clinical pharmacology unit at the HEGP. Subjects were selected based on the availability of required distance measurements and PWV measurements using the same version of the Complior device, previously validated [157]. The local ethics committee approved all HEGP protocols and all subjects gave written informed consent.

For model development and validation, the complete study population (n=3116) was subdivided into a model and a validation population. The model population is constituted of 10% (n=311) of all subjects available in the entire population sampled by random selection. The remaining subjects (n=2805) constitute the validation population.

15.2.2 Basic clinical data and PWV measurements

Subjects entering the Asklepios study and HEGP database underwent similar basic clinical examinations. Patients and subjects had their body size parameters and blood pressure measured after a 10–15 minute period of rest in a temperature-controlled environment. Blood pressures were recorded using validated measurement devices. Distances were measured with a tape measure.

For the Asklepios study subjects, PWV was determined from the difference in time delays between the start of the QRS complex on an ECG and the upstroke of flow in the femoral and carotid arteries determined by Doppler echography. Distances between carotid and femoral site and the sternal notch were measured. From these, the PWV distance was calculated in two ways corresponding to the DD and SD path length definitions:

$$DD = x_{ster-fem} + x_{car-ster}[m] \tag{15.1}$$

$$SD = x_{ster-fem} - x_{car-ster}[m] \tag{15.2}$$

In the HEGP patients, the direct distance and carotid to sternal notch distance were measured. PWV path length was then again determined in two ways, using either the direct or subtracted distance definitions:

$$DD = x_{car-fem}[m] \tag{15.3}$$

$$SD = x_{car-fem} - 2 \cdot x_{car-ster}[m] \tag{15.4}$$

15.2.3 Statistical analyses, model development and validation

Statistical analyses were performed using R version 2.8.0 [68]. Values reported are mean (standard deviation). The threshold for statistical significance was chosen as P = 0.05 unless indicated otherwise. Inter-population comparisons of continuous parameters were performed using Welsh two-sample t-tests; intra-population comparisons of estimated and measured distances using paired t-tests. The agreement between estimated and measured distances was evaluated through the construction of several multiple linear regression models with stepwise selection of covariates. Covariates considered for inclusion were age, gender, weight, height, body mass index (BMI) and waist circumference. Results of these analyses were additionally graphically represented by Bland-Altman plots. Model parameter selection was performed on the model population.

For accurate two-way conversion between distances definitions, two models were developed, one for each conversion sense. For each of these, the model yielding the best agreement between measured and estimated distances as determined from the multiple linear regression analysis mentioned earlier was selected. These models represent the optimal equations for converting between distance definitions. To validate the constructed models and to test their robustness, the conversion equations are first established in the model population and compared to a different set of equations using the same parameters issued from the entire population. The two sets of equations are then applied to the validation population to investigate the influence of sample size on the determination of the model parameters.

15.3 RESULTS

15.3.1 Population

The basic clinical data of the Asklepios and HEGP populations and the model and validation populations are summarized in table 15.2 on page 195. A total of 3,116 subjects were included, (1,505 women and 1,611 men) of which 2,510 (1,294 women and 1,216 men) come from the Asklepios and 606 (211 women and 395 men) from the HEGP databases. The HEGP population was on average 11 years older than the Asklepios population and covered a broader age range. Basic body size and clinical parameters were otherwise similar between populations, with the notable exception of the carotid to sternal notch distance, which differed on average 1.6 cm, between the Asklepios and HEGP populations.

15.3.2 Model development

Table 15.1 on the next page summarizes the stepwise forward selection process used for determining the relevant model parameters for conversion from subtracted to direct distance in the model population. Only the inclusion of height significantly improved R^2 by more than 20% (from R^2: 0.53 to 0.74). Other combinations of adjustments did not improve model prediction. Note that estimating DD from height by itself performs only slightly worse than estimating DD from SD only. (R^2: 0.51 and 0.53, respectively).

Based on these results, the following model emerged as the best compromise for the estimation of DD from SD:

$$DD = 0.45 \cdot SD + 0.21 \cdot height + 0.08[m] \tag{15.5}$$

A similar analysis was performed for the inverse conversion sense with similar results, yielding the following model for the estimation of SD from DD :

$$SD = 1.04 \cdot DD - 0.11 \cdot height - 0.02[m] \tag{15.6}$$

15.3.3 Model validation

The conversion equations are now applied to the validation population. Estimated direct and subtracted distances obtained by applying equations 15.5 and 15.6 in the validation population are compared to actually measured distances (figures 15.1 and 15.2 on page 197). Regression analyses (left hand panels) show a good agreement between

Table 15.1: Results of the forward stepwise regression analysis for the selection of model parameters for the subtracted to direct conversion sense (DD: direct distance, SD: subtracted distance).

Model	R^2
DD~SD + c^{te}	0.53
DD~SD + age + c^{te}	0.56
DD~SD + gender + c^{te}	0.59
DD~SD + weight + c^{te}	0.61
DD~SD + height + c^{te}	0.74
DD~SD + bmi + c^{te}	0.53
DD~SD + waist circumference + c^{te}	0.56
DD~height + c^{te}	0.51
DD~SD + height + age + c^{te}	0.74
DD~SD + height + gender + c^{te}	0.74
DD~SD + height + weight + c^{te}	0.75
DD~SD + height + bmi + c^{te}	0.75
DD~SD + height + waist circumference + c^{te}	0.75

measured and estimated values of both direct and subtracted distances. The subtracted to direct conversion performs better than the inverse conversion (R^2: 0.73 and 0.57, respectively). These results are echoed in the Bland-Altman plots (right hand panels). Mean differences are very small (<0.002 m); standard deviations are 0.01 and 0.02 m, for DD and SD, respectively, (i.e. less than 1.5% and 4.5%, of the actual distance, respectively). The average difference is for both conversion senses not significantly different from zero. In both cases however, there is a significant linear trend in bias. Again the subtracted to direct conversion outperforms the inverse conversion, with a slightly less important trend in bias.

To test the robustness of the proposed model, the coefficients of the conversion equations were re-determined on the complete population. This resulted in the following equations:

$$DD = 0.49 \cdot SD + 0.19 \cdot height + 0.08[m] \tag{15.7}$$

$$SD = 0.98 \cdot DD - 0.09 \cdot height - 0.02[m] \tag{15.8}$$

These results show that a tenfold increase in subjects available for determination of the conversion formulae has only a very limited impact on the value of coefficients. Applying the conversion equations separately in the HEGP and Asklepios populations leads to predictions of identical quality.

Finally, to illustrate the performance of using estimated distances for the conversion between PWV, figures 15.3 and 15.4 on page 199 show the results of comparing PWV values calculated from converted distances to PWV values calculated from measured distances, both for the direct and subtracted distance definitions. They show that the different models are suitable for use in converting between PWV definitions, with mean differences and standard deviations of 0.02 (0.32) m/s for the subtracted to direct conversion and 0.005 (0.47) m/s for the direct to subtracted conversion sense.

Table 15.2: Basic body size and clinical parameters of the Asklepios, HEGP, model and validation populations. Values are mean (SD)

	Asklepios	HEGP	All	Model	Validation
No.	2,510	606	3,116	311	2,805
(Asklepios + HEGP)				(251 + 60)	(2,259 + 546)
Age (years)	46 (6)	57 (16)	48 (10)	49 (10)	48 (10)
Age range	31–60	18–89	18–89	22–84	18–89
Gender (F/M)	1,294/1,216	211/395	1,505/1,611	144/167	1,361/1,444
Weight (kg)	74.1 (14.7)	73.7 (15.4)	74.1 (14.8)	74.2 (14.2)	74.0 (14.9)
height (m)	1.69 (0.09)	1.70 (0.09)	1.69 (0.09)	1.70 (0.09)	1.69 (0.09)
bmi (kg/m^2)	25.8 (4.3)	25.3 (4.0)	25.7 (4.2)	25.6 (4.1)	25.7 (4.2)
waist circumference (cm)	0.87 (0.13)	0.89 (0.13)	0.87 (0.13)	0.87 (0.12)	0.87 (0.13)
SBP (mmHg)	127 (14)	129 (20)	127 (15)	127 (15)	127 (15)
DBP (mmHg)	80 (10)	72 (10)	79 (10)	79 (11)	79 (10)
HR (beats/min)	70 (11)	64 (10)	69 (11)	69 (11)	69 (11)
Smoking (active/ex/never)	493/729/1,288	103/371/132	596/1,100/1,420	56/126/129	540/974/1,291
Total cholesterol (mmol/l)	5.61 (0.95)	4.89 (1.10)	5.57 (0.97)	5.54 (0.93)	5.57 (0.98)
HDL cholesterol (mmol/l)	1.65 (0.45)	1.21 (0.38)	1.62 (0.45)	1.58 (0.43)	1.63 (0.46)
LDL cholesterol (mmol/l)	3.39 (0.88)	3.05 (0.99)	3.37 (0.89)	3.37 (0.85)	3.37 (0.90)
Triglycerides (mmol/l)	1.25 (0.84)	1.54 (1.91)	1.26 (0.93)	1.31 (0.99)	1.25 (0.92)
Glycemia (mmol/l)	5.05 (0.53)	5.70 (1.48)	5.08 (0.62)	5.10 (0.59)	5.08 (0.63)
Direct distance (cm)	63 (4)	63 (4)	63 (4)	63 (4)	63 (4)
Subtracted distance (cm)	44 (4)	47 (5)	44 (4)	44 (4)	44 (4)
Carotid-sternal notch distance (cm)	9 (1)	8 (2)	9 (1)	9 (2)	9 (1)

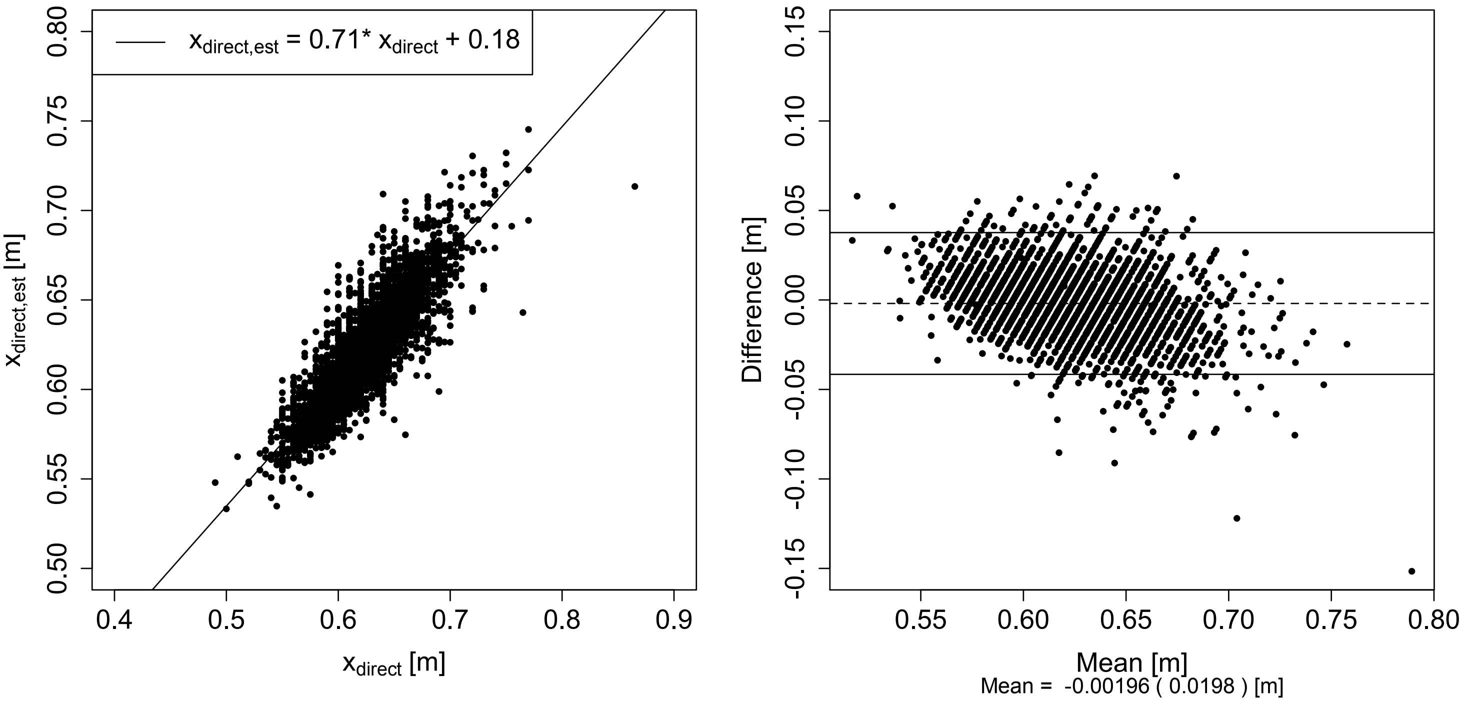

Figure 15.1: Comparison of estimated direct distance to measured direct distance. Left hand side: regression analysis. Right hand side: Bland-Altman plot

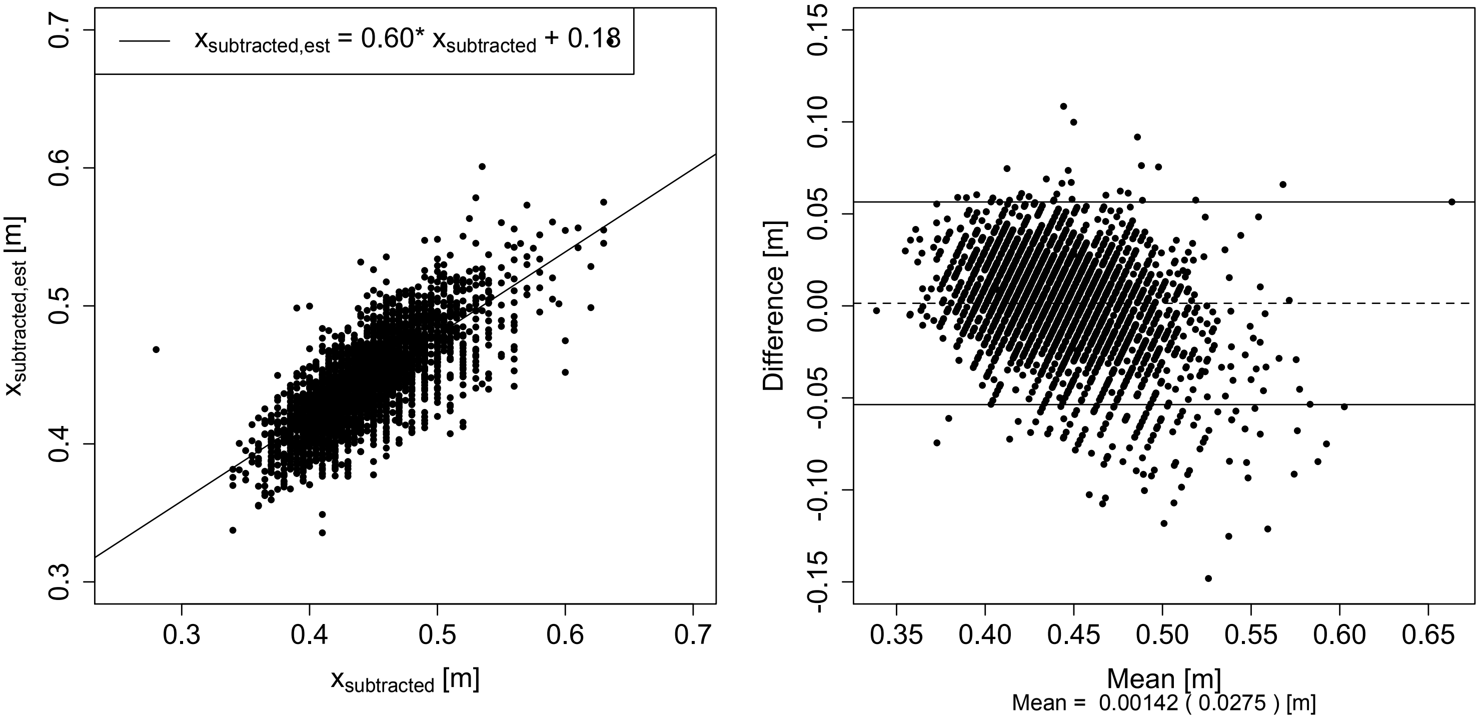

Figure 15.2: Comparison of estimated subtracted distance to measured subtracted distance. Left hand side: regression analysis. Right hand side: Bland-Altman plot

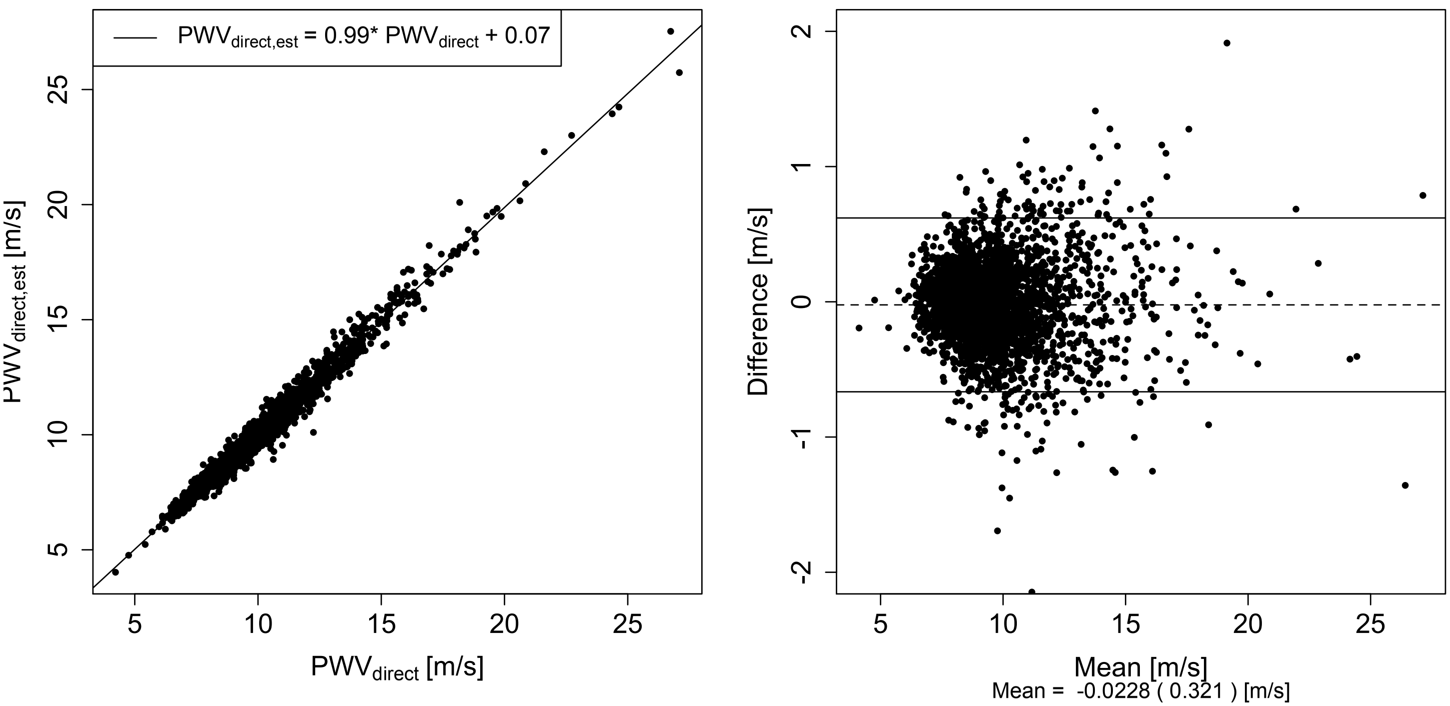

Figure 15.3: Comparison of estimated to measured pulse wave velocities for PWVs calculated using direct distance. Left hand side: regression analysis. Right hand side: Bland-Altman plot

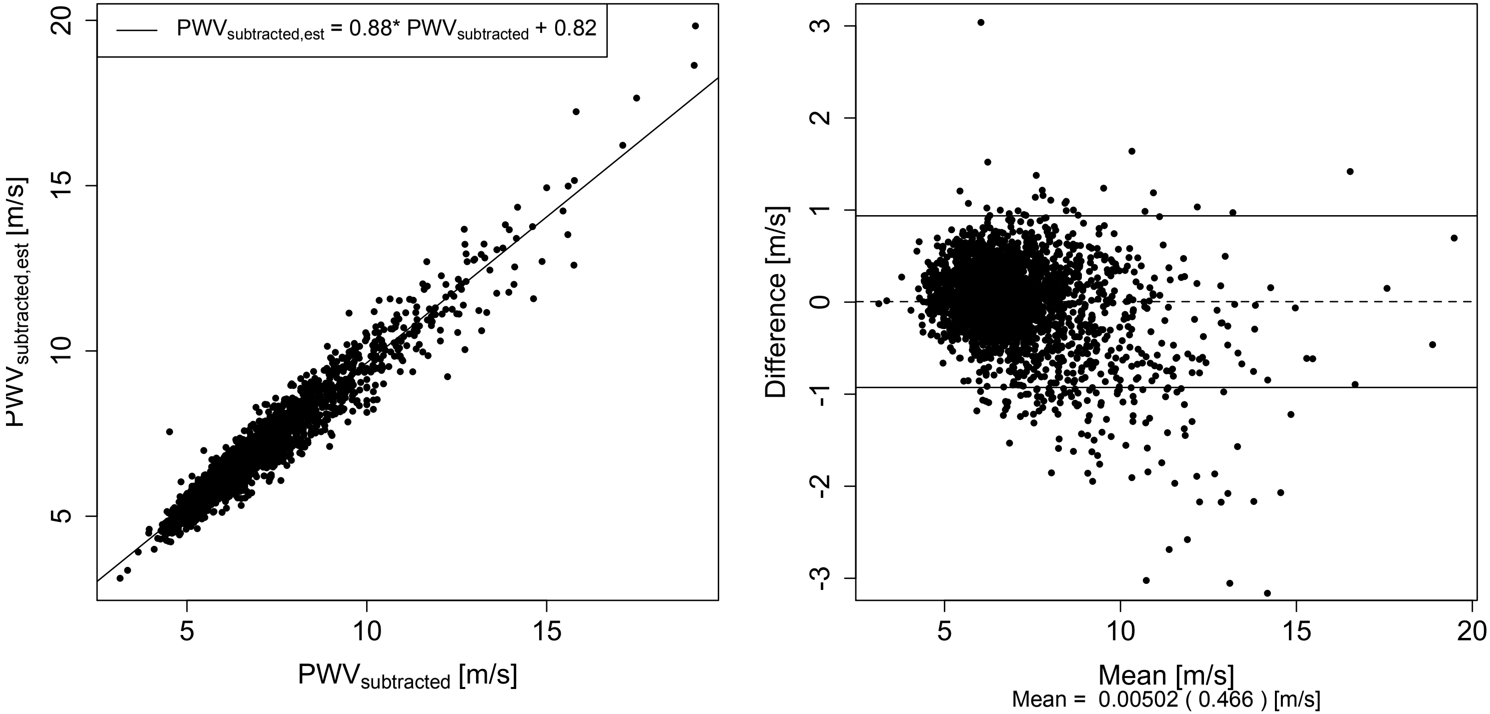

FIGURE 15.4: Comparison of estimated to measured pulse wave velocities for PWVs calculated using subtracted distance. Left hand side: regression analysis. Right hand side: Bland-Altman plot

15.4 Discussion

In the present study, we demonstrated in a large population based data set that the difference between direct and subtracted distance is partially dependent on body height. Taking body height into consideration through multivariate equations allowed improving the estimation of direct distance from subtracted distance and vice versa. Based on these observations, we presented a set of equations for the conversion between distance definitions.

The study leverages data from two large, independent databases in which all types of distance were measured. While the Asklepios study is the larger, subjects from the HEGP database covered a broader age range and allowed for the inclusion in the population of a number of real-life methodological differences, the two most important being a potential operator preference in choosing the measurement locations and differences in definitions of direct and subtracted distances between populations.

Since the HEGP and Asklepios populations were measured completely independently, differences in the exact location of the measurement site could not be excluded. Examination of the carotid-sternal distance, which was measured in both populations, showed a significant difference of 1.6 cm between populations, though other body size parameters were on average the same. Retrospectively, we could not identify any difference in methodology, other than a systematic difference in the way distances were measured in both populations. After correction for the systematic bias, we found no marked changes in the model equations, which suggests these small systematic differences are of no particular importance.

A second methodological difference issues from the exact definitions of distance used. As evident from equations 15.1, 15.2, 15.3 and 15.4, DD and SD were defined in different ways in both populations. These definitions represent the two most common approaches for determining direct and subtracted distances. It is not unlikely that model performance would be improved by eliminating this difference in distance definition. Unfortunately, the distance measurements required to do so were lacking in both populations. The fact that the model performs well despite ignoring these differences in definition likely indicates that the discrepancies between direct and subtracted distances derived using different definitions are too small to have an influence on the much larger difference between subtracted and direct distance.

The parameters considered for inclusion in the models covered the most important body size parameters. Since any distance is forcibly related to height, it comes as no surprise that including height as an extra parameter in the model significantly improves its performance, especially since the difference between direct and subtracted path corresponds to roughly twice the length of the neck, itself related to body height. Predicting either direct or subtracted distance directly from height however, is not an appropriate approach: though it performs about as well as the model containing only the distance to be converted, its performance is far inferior to the model which includes both height and the distance to be converted.

For both conversion senses, the models proposed perform very well in predicting the distance to be converted. Mean differences between measured and estimated values are below 0.002 m with standard deviations of 0.01 m (subtracted → direct) or 0.02 m (direct → subtracted). Though Bland-Altman analysis does reveal a significant trend in bias, its practical importance is small. The model for inverse conversion performs slightly worse: its trend evident in the Bland-Altman plot is more pronounced. Part of the decreased performance for the inverse conversion sense is due to the fact that subtracted distances are smaller than direct distances. Similar size errors are thus relatively more important for subtracted distances. In both cases, estimation errors remain within acceptable limits (<4.5%).

The results from the present study suggest that the conversion equations derived from the model population are very robust. Even when increasing the model population by a factor ten, the influence on the model parameter coefficients remains small, which suggest that in our population at least, the model is mature.

The conversion equations proposed in the present paper are meant to serve as a tool for converting between PWV values determined using either direct or subtracted distance in those cases where not all measurements are available. In the absence of gold standard, it is not in the scope of this paper to recommend one type of measurement over another. From a physiological point of view, PWV values obtained using the direct distance are higher than the values reported from invasive studies [71, 164], as the directly measured distance does not compensate for the fact that the pulse simultaneously travels both to the carotid and femoral arteries. From a methodological point of view, the precision obtained by using any distance definition is limited by both the precise identification of the measurement site (about 1 cm) and the precision of the tape measure (again about 1 cm). Since measurement errors are additive, for the direct measurement, the error is made only once whereas for subtracted distances, the error is made twice. As a consequence, the potential error on the actual distance is doubled. The maximal theoretical error made by measuring subtracted distance, reaches 4 cm, which is twice the size of the standard deviation of the largest difference between estimated and measured distance found in the present study.

Finally, distance measurement is only a means to convert transit time into velocity. As illustrated in figures 15.3 and 15.4, comparing PWV values calculated from distances estimated from our equations into PWV values calculated from actually measured distances, both approaches yielded close and acceptable results, with mean differences and standard deviations of 0.02 (0.32) m/s for the subtracted to direct conversion and 0.005 (0.47) m/s for the direct to subtracted conversion sense. These values are within the range of the inter-observer variability of common PWV techniques previously reported in literature [157, 165, 166] and are as such unlikely to be of major clinical importance.

15.5 CONCLUSIONS

Ideally all distances should be measured when measuring PWV so that exact conversion between the different distance definitions is always possible. For those cases in which only one type of measurement is available, the proposed conversions equations based on distance and body height offer a viable alternative, which can be used to convert between distance measurements—and thus PWV types.

Chapter 16

Reference values for carotid-femoral pulse wave velocity

16.1 Introduction

In the quest for early phenotypes of arterial disease, over the past few years, arterial stiffness has proven to be an important concept within the assessment of an individual's total cardiovascular risk profile. Among the different methods to assess arterial stiffness [82], carotid to femoral pulse wave velocity (PWV) has become the current gold standard method because of its relative ease in determination, its perceived reliability [9, 133] and most importantly, because of the large body of evidence demonstrating its predictive value above and beyond known classical risk factors in various populations [131–133, 135, 138, 139, 161, 167]. Increasingly, arterial stiffness measures, and PWV in particular, are included both in the routine clinical assessment of patients and within the framework of large scale clinical studies, as illustrated by their inclusion in the 2007 European Society of Hypertension / European Society of Cardiology guidelines for the management of hypertension [9].

In spite of its emergence as the gold standard method for assessment of central arterial stiffness, a wider implementation of PWV beyond clinical studies into clinical practice is still hampered by the lack of established reference values based on a large population and the absence of a standardized methodology for PWV assessment. Currently existing threshold values included in the 2007 ESH/ESC hypertension guidelines [9] were based on published epidemiological studies and do not take into account the multiple factors influencing PWV. Values recently published similarly lack broad applicability, since published in specific populations (elderly population [168]) or because they are based on a single methodology [149] — disregarding the important differences in absolute PWV values that exist between methodologies — or population specificity.

With financing from the French ministry of Health and under the endorsement of the European Network for Non-Invasive Investigation of Large Arteries, the Reference Values for Arterial Stiffness' Collaboration aims at building a very large database combining existing clinical and arterial stiffness data from the participating centers all over Europe. The present study has two primary goals: (1) establish reference and normal values for arterial stiffness measured with PWV taking into account the differences in methodology for PWV measurements and (2) investigate the influence of gender and common risk factors on observed PWV.

16.2 METHODS

16.2.1 Participating centers

Thirteen different centers distributed across eight European countries contributed to the reference value database. The contributing centers and the number of subjects they contributed are listed in chapter 14.

16.2.2 Study population

Subjects were eligible for inclusion in the Reference Values for Arterial Stiffness' Collaboration database if they had at least one of the following stiffness parameters measured: aortic stiffness by (carotid-femoral) PWV, carotid stiffness measures based on carotid diameter measurements obtained using echotracking devices (compliance and distensibility coefficient) or measurements of central pulse pressure and wave reflection. All subjects were required to have a full medical history. Subject data included vital parameters, blood pressure and the recording of any relevant risk factor, cardiovascular disease or treatment at the time of measurement. Finally, inclusion criteria included the availability of a full set of documentation regarding the protocol and measurement techniques used for assessment of the stiffness parameters.

Subjects were excluded from the present analysis if no PWV measurements were available, if they had an identified genetic cause of hypertension or secondary hypertension, or had overt cardiovascular disease. Subjects were further categorized (figure 16.1 on page 209) according to current treatment status (hypertension, dislipidemia or diabetes treatment) and the presence of additional cardiovascular risk factors (dislipidemia, smoking or diabetes) as defined by the 2007 European Society of Hypertension / European Society of Cardiology guidelines for hypertension management [9].

16.2.3 PWV: methodological considerations

PWV values depend on both the path length used for their calculation and the device dependent algorithm used for detection of the 'foot' of the waveform at the measurement sites. An overview of the different techniques was recently published [88] and was outlined in chapter 9. Briefly, the reference point chosen on the waveforms measured at the carotid and femoral measurement sites is dependent on the type of waveform measured (flow, pressure, diameter distension) and the algorithm used for its detection. Two of the most popular algorithms are the use of an intersecting tangents algorithm (as used on the Sphygmocor® system and recommended for manual identification) or detection of the point of maximal upstroke during systole (as used in the Complior® system). The use of different algorithms on the same waveforms can lead to differences in measured PWV values of 5-10% [90]. Since the point of maximal upstroke has been shown to underestimate PWV [90], especially when the rise time of the waveform is low, the intersecting tangent algorithm was chosen to express PWV values in the present study. If transit times had been determined using the maximal upstroke detection algorithm, an estimated value for the transit time determined from the intersecting tangent algorithm was calculated using the relationship previously found by Millasseau et al. [90]:

$$\Delta t_{intersecting\ tangent} = \frac{\Delta t_{maximal\ upstroke} - 14.96}{0.8486} [s] \qquad (16.1)$$

PWV values are also markedly dependent on the carotid-femoral pathway used for their calculation. This pathway can either be the direct distance measured between the carotid and femoral measurement sites, or the distance obtained by subtracting the carotid measurement site to sternal notch distance from the sternal notch to femoral measurement site distance. Differences in path length alone can lead to differences in PWV values of up to 30% [162, 163]. We recently investiaged an equation to convert from one pathway measurement to another with acceptable precision on those cases where exact conversion is not possible (see chapter 15):

$$x_{direct} = 0.45 \cdot x_{subtracted} + 0.21 \cdot height + 0.08[m] \qquad (16.2)$$

Due to these differences in absolute values, PWV values from different centers using different methodologies cannot be arbitrarily pooled without first converting them to a common definition. As the direct carotid-femoral distance, due to it only requiring a single distance measurement, is less prone to measurement error and since the intersecting tangent algorithm performs better for waveforms with low rising times, PWV values were expressed using directly measured distance and the intersecting tangent detection algorithm. Distance and transit times were converted using equations 16.1 and 16.2 if required.

16.2.4 Factors influencing PWV in the study population

Potential gender differences in PWV were assessed in the normal population, which excludes subjects on antihypertensive, lipids or diabetes treatment, smokers, diabetics and dislipidemics but included hypertensives. The influence of the presence of cardiovascular risk factors (smoking, dislipidemia, diabetes, hypertension and lipids treatment) on observed PWV values was evaluated by comparing PWV values in the normal (all blood pressure (BP)) population to PWV values in a population having the risk factor under consideration and excluding the presence of all other risk factors. This approach allows one to estimate the independent impact of each risk factor on observed PWV values. Dislipidemia was defined as total cholesterol > 5.0 mmol/l, hdl cholesterol < 1.0 mmol/l for men and < 1.2 mmol/l for women, ldl cholesterol > 3.0 mmol/l or triglycerides > 1.7 mmol/l). Diabetes was determined on blood glucose levels ≥ 7.0 mmol/l.

16.2.5 Reference and normal values in the study population

The reference value population was defined as the normal population (all BP) augmented with those subjects displaying risk factors which had been shown to have no influence on average observed PWV values after correction for mean age and blood pressure differences. For the presentation of the reference values, the study population was categorized according to age decade (<30, 30-39, 40-49, 50-59, 60-69, ≥70) and blood pressure category (optimal – <120/80, normal – <130/85, high normal – <140/90, grade I HT – <160/100 and grade II/III HT – ≥160/100 mmHg). Normal values were defined in the normal population having optimal or normal blood pressures and no additional cardiovascular risk factors.

16.2.6 Statistical analyses

All statistical analyses were performed using R version 2.8.1 [68]. Values reported are mean (standard deviation). The threshold for statistical significance was chosen to be $P<0.05$ unless stated otherwise. Average PWV values per category are represented as mean (standard deviation) and median (1st quartile – 3rd quartile). Influence of risk factors and gender is examined by comparing raw means and means corrected for age and systolic blood pressure (SBP) or pulse pressure (PP) where appropriate and multivariate analysis with age and blood pressure values as co-variates.

16.3 RESULTS

16.3.1 Study population

The complete reference value database contains data from 24,484 subjects and patients. The number of subjects included per center is listed in chapter 14. PWV and relevant clinical data were present in 12,053 subjects. Of those 1,037 were excluded due to the presence of overt cardiovascular disease, resulting in a study population of 11,016 subjects, which were included in the present analysis. The subdivision of the study population according to treatment, lipids and diabetic status is summarized in figure 16.1. Basic body size parameters and clinical data of the complete study population, reference value population and normal values population are summarized in table 16.1 on page 210.

16.3.2 Risk factors and observed PWV

Table 16.2 on page 211 summarizes the effects of different factors on average observed PWV values. After correction for age and SBP, there was no significant difference between men and women or smokers and non-smokers in average PWV values. Similarly, the PWV values in dislipidemic and normolipemic subjects did not differ significantly after correction for age and systolic blood pressure. On the other hand, significant differences were found between non-diabetic and diabetic subjects and subjects treated or untreated for hypertension and dislipidemia, even after correction for age and SBP. Additionally, we found there was no significant difference in average observed PWV values in controlled (treated) hypertensives and (untreated) normotensives, while there was a significant difference between uncontrolled (treated) hypertensives and (untreated) hypertensives, both after correction for age and SBP.

Since gender, smoking and lipid status have no influence on PWV after correction for age and blood pressure differences, the population used for determining the reference values was chosen to comprise all untreated (hypertension/lipids/diabetes) non-diabetic subjects. The normal value population consists of those subjects in the reference value population, which do not have any risk factors and optimal or normal blood pressure levels.

16.3.3 Reference and normal values for PWV

PWV increased both with increasing age and SBP levels in the reference value population. Both for age and SBP, the increase was more pronounced with increasing SBP and age respectively. Figures 16.2 on page 212 and 16.3 on page 213 show scatterplots of PWV versus age and SBP. For PWV versus age, the additional influence of rising SBP is illustrated graphically by plotting the regression line of PWV versus age for different blood pressure categories. For all BP categories, linear regression models on quadratic age offered the best fit to the observed data. Regression equations for each of the BP categories are summarized in table 16.3 on page 214 (top). Similarly, for PWV versus SBP, the additional influence of age is graphically illustrated by plotting the regression line of PWV versus SBP for different age categories. Regression equations for each of the age categories are summarized in table 16.3 (bottom). Figures 16.4 on page 215 and 16.5 on page 216 additionally illustrate the distribution of observed PWV values per age and BP category separately.

Reference values for PWV are illustrated in figure 16.6 on page 217, showing a graphical representation of average observed PWV according to age and BP. PWV distributions in each of the categories are additionally described in table 16.4 on page 218. The number of subjects included in each category is listed in table 16.5 on page 219. Finally, normal values are presented in figure 16.7 on page 220 and table 16.6 on page 222.

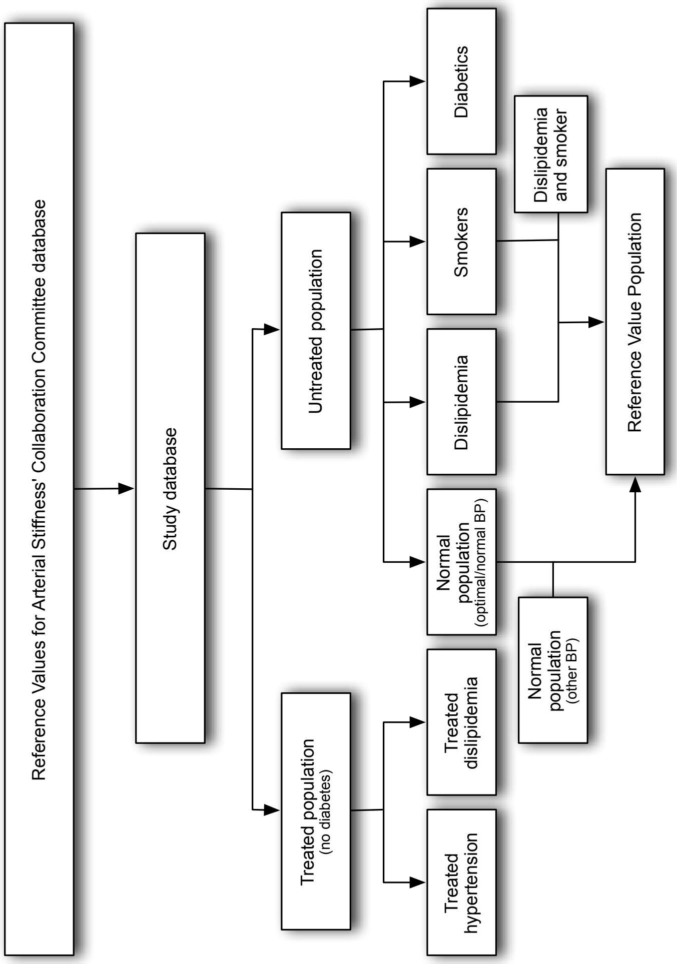
Reference Values for Arterial Stiffness' Collaboration Committee database
Study database
Treated population (no diabetes)
Untreated population
Treated hypertension
Treated dislipidemia
Normal population (optimal/normal BP)
Dislipidemia
Smokers
Diabetics
Normal population (other BP)
Dislipidemia and smoker
Reference Value Population

Figure 16.1: Flowchart illustrating the different subpopulations used throughout the study.

TABLE 16.1: Basic body size and general clinical parameters of the complete, reference value and normal value populations.

Parameter	Study population	Normal value population (optimal/normal BP)	Reference value population
	(N = 11,016)	(N = 1,344)	(N = 8,400)
Age (years)	49 (16)	30 (14)	45 (16)
Age range (years)	17–96	18–83	17–85
Gender (M/F)	5,817/5,199	541/803	4,296/4,104
Weight (kg)	74.3 (14.7)	66.8 (11.8)	73.1 (14.3)
Height (m)	1.70 (0.09)	1.71 (0.09)	1.70 (0.09)
SBP (mmHg)	131 (19)	114 (9)	127 (18)
DBP (mmHg)	79 (19)	69 (9)	78 (18)
PP (mmHg)	52 (13)	45 (8)	49 (12)
Total cholesterol (mmol/l)	5.5 (1.2)	4.1 (0.6)	5.4 (1.2)
HDL cholesterol (mmol/l)	1.5 (0.4)	1.6 (0.3)	1.5 (0.4)
LDL cholesterol (mmol/l)	3.3 (1.1)	2.2 (0.5)	3.3 (1.1)
Triglycerides (mmol/l)	1.3 (0.9)	0.8 (0.3)	1.3 (0.8)
Glycemia (mmol/l)	5.2 (1.2)	4.8 (0.6)	4.9 (0.6)
Smoking (# (%))	2,669 (24%)	—	2,136 (25%)
Dislipidemia (# (%))	8,338 (76%)	—	6,118 (73%)
Hypertension (# (%))	3,533 (32%)	—	2,118 (25%)
Diabetes (# (%))	566 (5%)	—	—
Treated hypertension (# (%))	1,781 (16%)	—	—
Treated lipids (# (%))	1,045 (9%)	—	—
Treated diabetes (# (%))	233 (2%)	—	—

Table 16.2: Influence of gender and risk on observed PWV values. Adjusted means are adjusted for age and SBP (gender, smoking, diabetes, hypertension treatment, lipids treatment) or age and PP (dislipidemia).

Factor	#subjects	Raw means [m/s]			Mean age [years] / SBP [mmHg]		Adjusted means			Adjusted at age [years] / SBP [mmHg]
		no	yes	P	no	yes	no	yes	P	
Gender (F/M)	1,000/905	8.7	9.4	<0.001	34/117	34/128	9.0	9.0	NS	34/122
Dislipidemia (no/yes)	1,905/4,359	9.0	10.6	<0.001	34/122	48/130	10.1	10.1	NS	44/127
Smoking (no/yes)	1,905/377	9.0	9.5	<0.001	34/122	40/123	9.1	9.1	NS	35/122
Diabetes (no/yes)	1,905/26	9.0	11.8	<0.01	34/122	51/131	9.0	10.0	<0.05	34/122
Treated hypertension (no/yes)	1,905/166	9.0	12.5	<0.001	34/122	60/137	9.2	9.8	<0.01	36/123
(Untreated) normotensives/ controlled hypertensives	1,627/91	8.5	11.8	<0.001	31/117	57/125	8.7	9.7	<0.001	33/118
(Untreated) hypertensives/ uncontrolled (treated) hypertensives	278/75	11.7	13.3	<0.001	46/150	63/150	12.1	11.9	NS	49/150
Treated dislipidemia (no/yes)	1,905/526	9.0	12.4	<0.001	34/122	55/142	9.6	10.1	<0.01	38/126

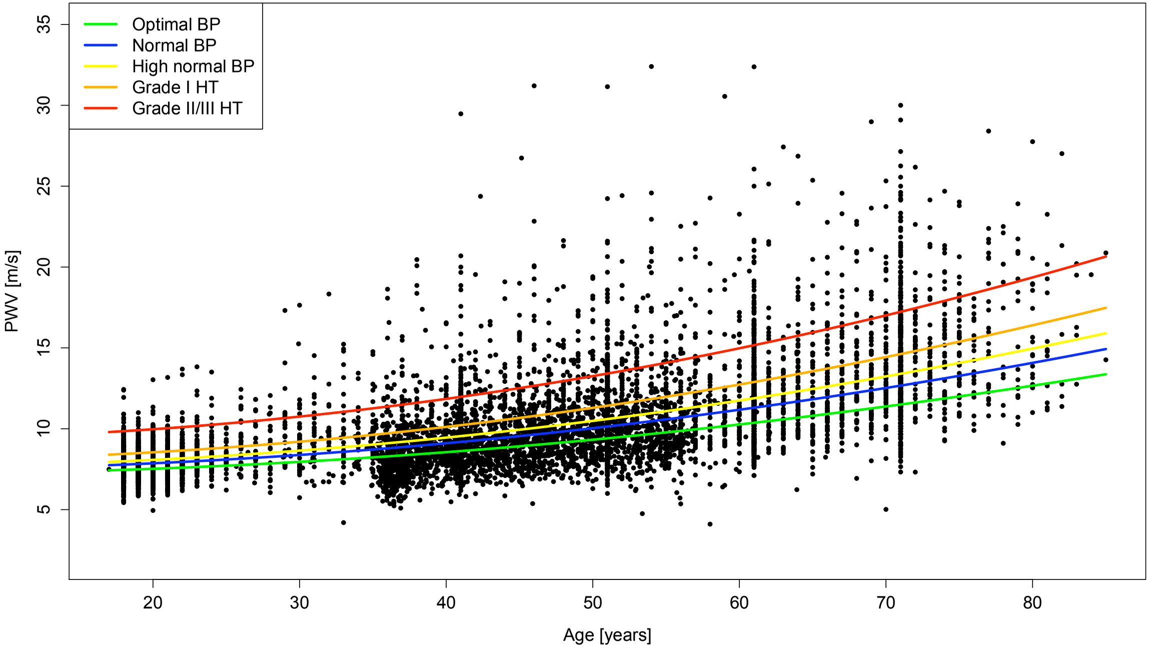

Figure 16.2: PWV versus age in the reference value population. Regression lines illustrate the linear regression lines on quadratic age for the different blood pressure categories.

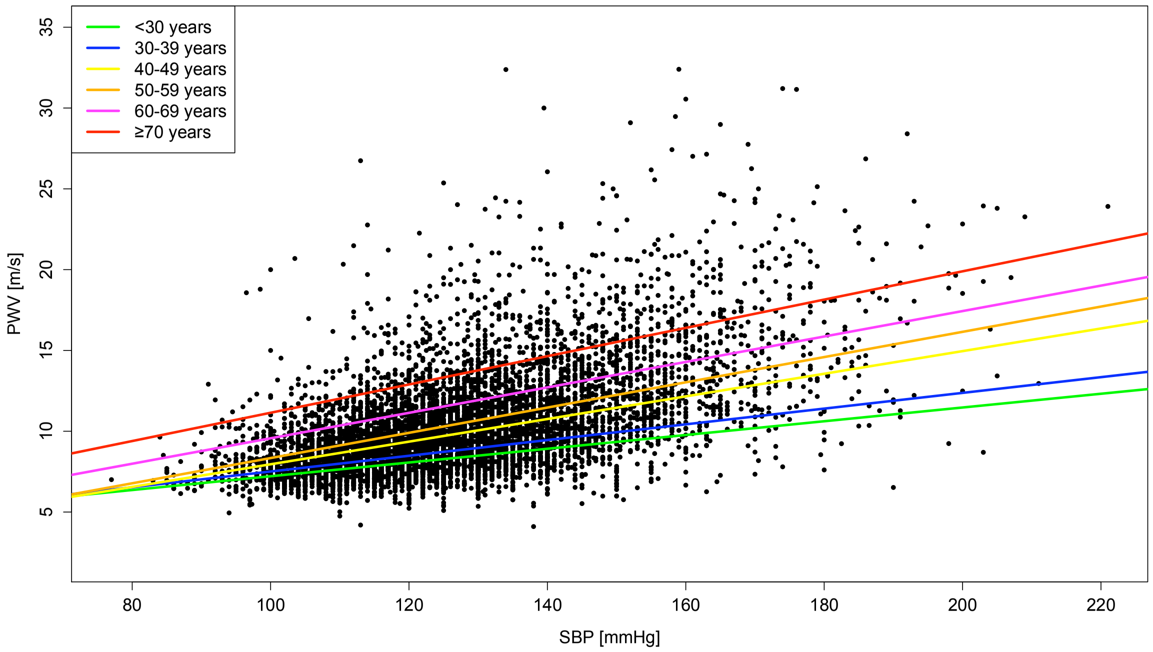

FIGURE 16.3: PWV versus SBP in the reference value population. Regression lines illustrate the linear regression lines on SBP for the different age categories.

TABLE 16.3: Regression equations for PWV [m/s] versus age (top) and SBP (bottom) according to blood pressure category (top) and age category (bottom) in the reference value population.

BP category	PWV~age	R^2
Optimal	$PWV = 0.856\ 10^{-3} \cdot age^2 + 7.18$	0.35
Normal	$PWV = 1.04\ 10^{-3} \cdot age^2 + 7.45$	0.40
High normal	$PWV = 1.15\ 10^{-3} \cdot age^2 + 7.62$	0.37
Grade I HT	$PWV = 1.31\ 10^{-3} \cdot age^2 + 8.02$	0.33
Grade II/III HT	$PWV = 1.56\ 10^{-3} \cdot age^2 + 9.35$	0.26
Age category	**PWV~SBP**	**R^2**
<30 years	$PWV = 0.0426 \cdot SBP + 2.96$	0.25
30-39 years	$PWV = 0.0487 \cdot SBP + 2.64$	0.15
40-49 years	$PWV = 0.0700 \cdot SBP + 0.96$	0.25
50-59 years	$PWV = 0.0781 \cdot SBP + 0.53$	0.26
60-69 years	$PWV = 0.0787 \cdot SBP + 1.69$	0.23
≥70 years	$PWV = 0.0875 \cdot SBP + 2.39$	0.17

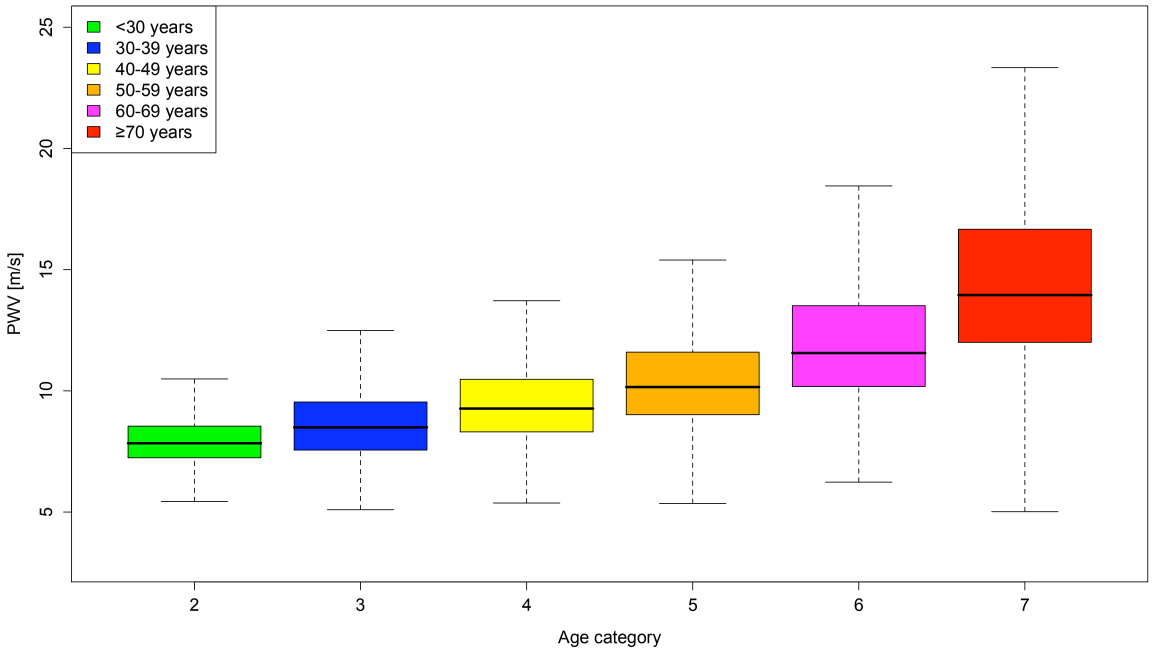

FIGURE 16.4: Boxplots showing the distribution of PWV per age decade in the reference value population. The box corresponds to the 25th and 75th percentile of the PWV distribution in each age group, the thick horizontal line is the group median. Whiskers extend to 1.5 times the interquartile range.

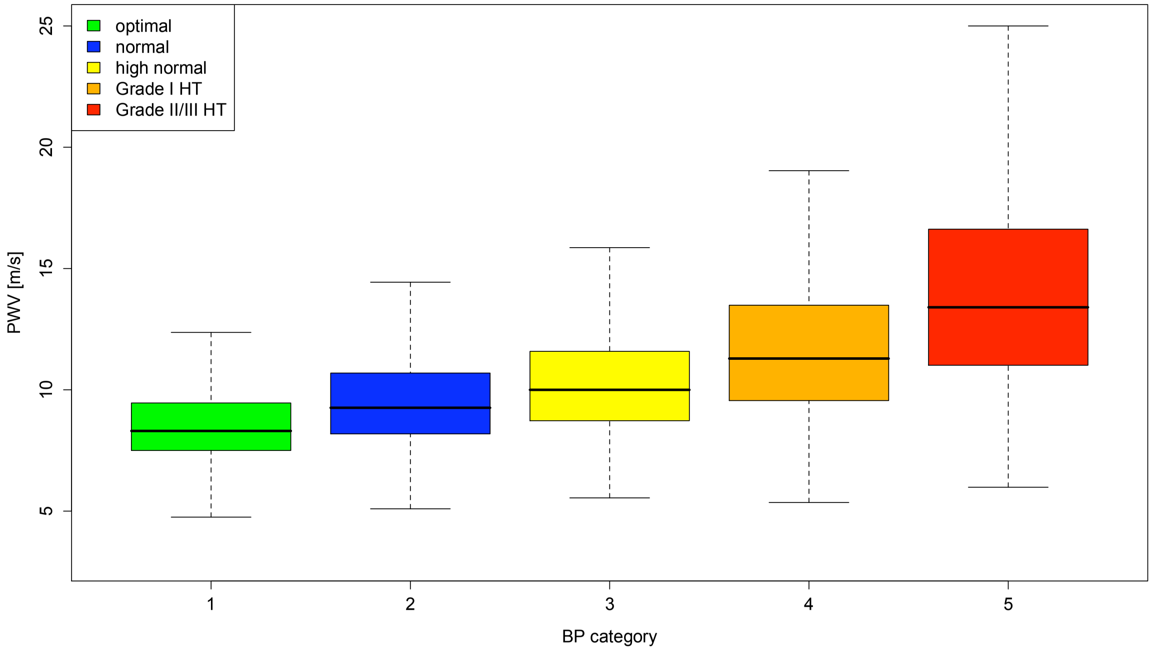

Figure 16.5: Boxplots showing the distribution of PWV per blood pressure category in the reference value population. The box corresponds to the 25th and 75th percentile of the PWV distribution in each blood pressure category, the thick horizontal line is the category median. Whiskers extend to 1.5 times the interquartile range.

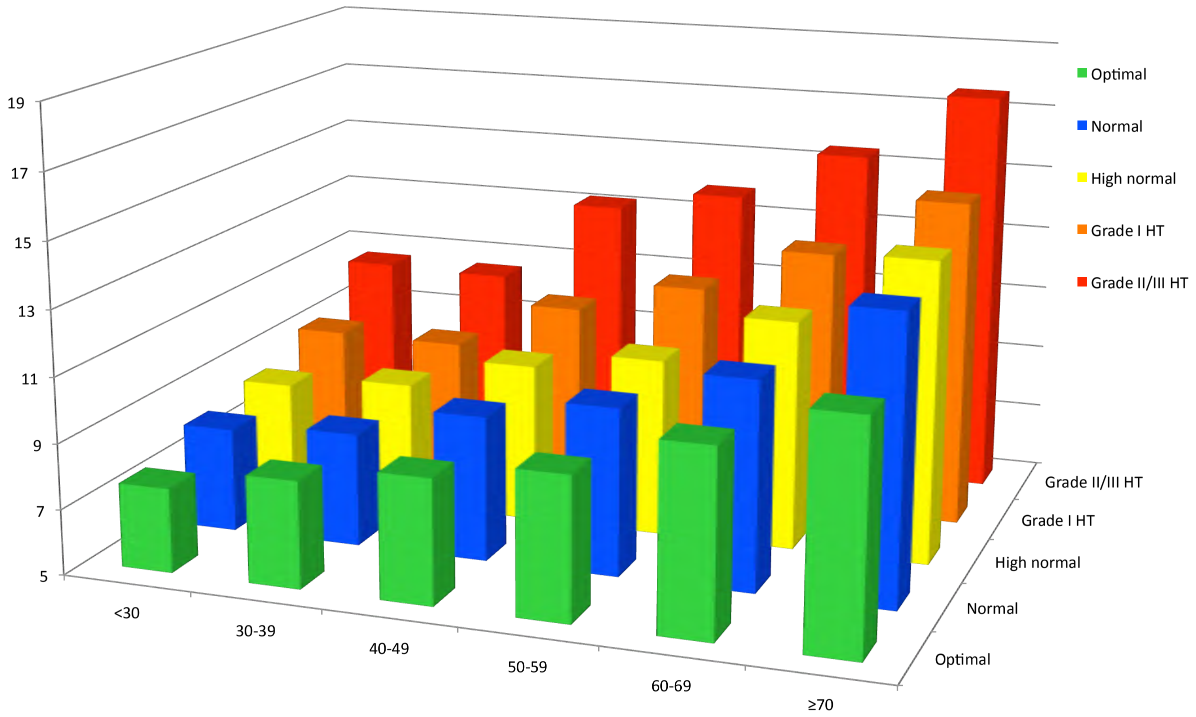

FIGURE 16.6: Average PWV [m/s] in the reference population according to age and blood pressure categories.

TABLE 16.4: Distribution of PWV values [m/s] in the reference value population according to age and blood pressure categories.

	Blood pressure category									
	Optimal		Normal		High normal		Grade I HT		Grade II/III HT	
Age category	Mean (SD)	Median (Q_1–Q_3)	Mean (SD)	Median (Q_1–Q_3)	Mean (SD)	Median (Q_1–Q_3)	Mean (SD)	Median (Q_1–Q_3)	Mean (SD)	Median (Q_1–Q_3)
<30	7.6	7.5	8.2	8.1	8.5	8.4	9.2	9.1	10.6	10.2
	(0.9)	(7.0 – 8.1)	(1.0)	(7.5 – 8.8)	(1.1)	(7.7 – 9.1)	(1.7)	(8.1 – 9.9)	(2.1)	(9.5 – 11.3)
30–39	8.3	8.1	8.5	8.3	8.9	8.7	9.2	8.9	10.5	9.9
	(1.4)	(7.4 – 9.0)	(1.6)	(7.5 – 9.4)	(1.6)	(7.9 – 9.9)	(2.1)	(7.7 – 10.1)	(3.3)	(8.3 – 11.8)
40–49	8.8	8.5	9.4	9.2	9.9	9.7	10.7	10.2	13.2	12.3
	(1.6)	(7.9 – 9.5)	(1.6)	(8.4 – 10.3)	(1.7)	(8.8 – 10.7)	(2.2)	(9.3 – 11.7)	(3.9)	(11.0 – 14.7)
50–59	9.4	9.2	10.1	9.8	10.5	10.2	11.7	11.3	13.9	12.9
	(1.6)	(8.3 – 10.2)	(1.7)	(9.0 – 11.0)	(1.9)	(9.2 – 11.5)	(2.9)	(10.0 – 12.9)	(4.2)	(10.9 – 15.7)
60–69	10.6	10.2	11.4	10.9	12.0	11.4	13.2	12.8	15.5	14.7
	(2.2)	(9.3 – 11.5)	(2.3)	(10.0 – 12.5)	(2.7)	(10.5 – 13.0)	(2.8)	(11.4 – 14.6)	(4.3)	(12.2 – 17.2)
≥70	11.9	11.8	13.7	13.0	14.2	13.3	15.1	14.7	17.6	16.8
	(2.5)	(9.9 – 13.3)	(3.0)	(11.8 – 14.9)	(4.1)	(11.7 – 15.7)	(3.5)	(12.4 – 16.9)	(4.4)	(14.9 – 19.7)

TABLE 16.5: Number of subjects included in each of the age and blood pressure categories used for determination of the reference values

	Blood pressure category				
Age category	Optimal	Normal	High normal	Grade I HT	Grade II/III HT
<30	896	413	220	95	23
30–39	314	243	184	189	83
40–49	821	559	385	325	117
50–59	446	396	327	366	154
60–69	228	247	217	294	112
≥70	77	122	187	233	127

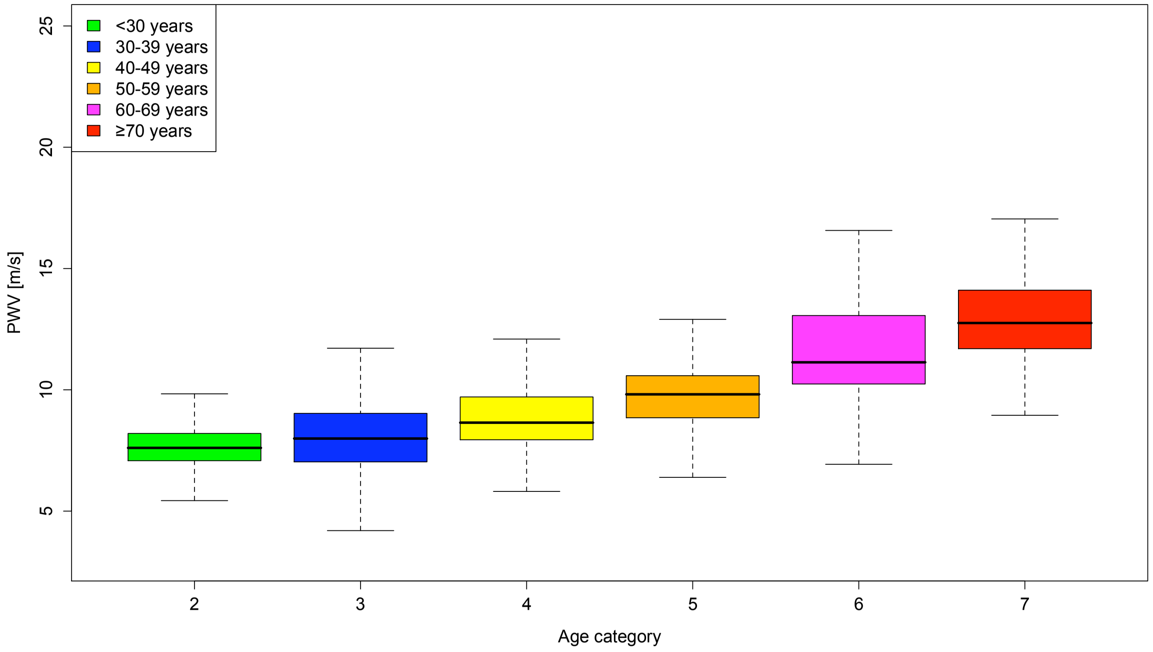

Figure 16.7: Average PWV per age decade in the normal values population.

16.4 DISCUSSION

The main result of this study is a set of reference and normal values for PWV based on an extensive dataset obtained from 13 centers distributed across Europe. It is the first study to reach out across different methodological approaches for the determination of PWV by applying previously established conversion equations for path lengths and transit times for those subjects in which exact conversion is not possible. Reference values are presented per age decade and BP category. These reference values present a critical step in the advance of the use of PWV as a clinical tool in routine patient assessment.

Though PWV has over the past few years emerged as a gold standard for the assessment of aortic stiffness and as such is to date widely reported in studies investigating arterial function, its widespread use has thus far been severely limited by the absence of a reliable set of reference values. The absence of standardization is a general problem for generalizing any test, be it biological [169] or morphological [170]. In the case of PWV, most of the standardization is purely methodological. PWV values obtained using different definitions, while yielding the same type of information for a group of patients, are not readily comparable between groups and impossible to compare to normal values. This has certainly hampered establishing reference values, as this typically requires the pooling of data across different centers in order to acquire a sufficiently large set of data. Efforts at establishing reference values have previously been made, but are usually limited by the size and specificity of the population, yielding results that are only valid in these specific populations. More importantly, values previously reported have always been limited to a single PWV methodology, restricting their applicability further to specific measurement protocols or devices.

The Reference Values for Arterial Stiffness' Collaboration's database contains data obtained using most of the currently used systems and approaches, and as such presents a unique opportunity to present reference values valid for each of these approaches. In the present paper, we have used previously published conversion equations for distance and transit time measurements to present the data in a uniform fashion. To simplify matters, PWV values reported in the present study are valid for direct path length measured between the carotid and femoral measurement site and transit times determined by detecting the foot of the waveform passing at these sites using an algorithm based on intersecting tangents. Though there is no scientific reason to choose one

TABLE 16.6: Distribution of PWV [m/s] according to age categories in the normal values population.

Age category	Mean (SD)	Median (Q_1–Q_3)
<30	7.7 (0.9)	7.6 (7.1 – 8.2)
30–39	8.2 (1.7)	8.0 (7.0 – 9.0)
40–49	9.0 (1.6)	8.6 (7.9 – 9.7)
50–59	9.9 (1.7)	9.8 (8.8 – 10.6)
60–69	11.7 (2.5)	11.1 (10.2 – 12.8)
≥70	13.0 (2.4)	12.8 (11.7 – 14.1)

PWV measurement approach over another, there are some arguments as to why this representation was chosen. Algorithms for transit time determination have previously been compared [90], and while all algorithms provide consistent results, the intersecting tangent algorithm was found to be the most reliable. For the distance measurements, from a physiological point of view, the use of a subtracted distance more closely resembles invasive PWV values [71, 164], as it takes into account the section of aorta traveled during the time it takes for the wave to move from the heart to the carotid measurement site. From a methodological point of view, the use of a subtracted distance requires two distance measurements as opposed to one for the direct measurement, which introduces extra inaccuracies linked to the precision of the measurement (typically performed by tape measure). Furthermore, the bulk of epidemiological data available has used direct distance for its calculation. It is not the intention of the present paper to defend one approach over the other, however, given the importance of standardization in measurements, we strongly encourage future investigators and device constructors to choose a single approach in presenting PWV values in research papers.

The PWV data present in the reference value database can be represented in different ways. If the reference values are to be used in practice, the presentations chosen needs to take into account certain pathophysiological realities associated with PWV and avoid the introduction of confounding factors. Arterial stiffness increases with age and blood pressure; it seemed thus natural to present PWV values according to age and blood pressure categories. To investigate which factors could potentially confound the presentation of the reference values, the influence of traditional risk factors such as gender, smoking, dislipidemia, diabetes and treatment on observed PWV values was investigated separately, each in the absence of the presence of other risk factors. Since PWV is dependent on age and SBP and given that average age and SBP tend to increase with increasing risk, PWV values were corrected for age and SBP before comparing the influence of the risk factor under consideration. These adjusted mean values allow one to correctly ascertain the influence of the risk factor under consideration if age and SBP were similar in both groups. To compare reported adjusted means for different risk factors, the mean age and SBP values used for calculating these adjusted means are also reported in table 16.2.

The adjusted means reported in table 16.2 show that while raw mean PWV values differ between men and women, smokers and nonsmokers and dislipidemic and normolipemic subjects, these differences were entirely accounted for by differences in age and blood pressure levels. After correction for age and blood pressure, these factors do not significantly influence average observed PWV, which means subjects can be included in the reference value population regardless of these factors, or put otherwise, that no separate tables are required depending on the values of these factors. Pharmacological treatment and diabetic status do however influence PWV beyond what is explained by age and pressure differences between categories, thus treated and diabetic subjects should be excluded from the population to serve as reference value population.

The relationships between PWV and age/SBP in the reference value population displayed in figures 16.2 and 16.3 clearly show that PWV is independently related to age and SBP. Average PWV values for any age are higher for subjects with higher blood pressures and vice versa. The increase of PWV with age is also more pronounced for subjects with higher blood pressures and vice versa. These results show the increase of PWV with SBP is not simply attributable to the increase of SBP with age. The gradual increase of average observed PWV with increasing age and BP levels is also evident from the categorical representation of the reference values in age and BP categories. Especially for this fine-grained representation, the large number of subjects available in the present study is of crucial importance. Finally, based on the representation of the reference values, normal values are defined by considering the normal population as the subset of the reference value population having optimal or normal BP and examining the differences in observed PWV with age.

It is important to consider the role of age in the presentation of reference values and normal values. Similarly as to what was done for blood pressure levels, it is questionable whether normality with respect to PWV should be defined according to age or not. For SBP, it proved to be an error to take for granted that SBP should increase with age. One important drawback of the use of a fixed threshold however is that, even if one would correct for normal ageing, at a certain level of BP or age, all subjects have elevated PWV values. Looking at figure 16.6 (table 16.4), using the 12 m/s threshold value from the ESC/ESH guidelines would mean that on average more than half of the subjects over 60 years are at risk. The usefulness of PWV as an added parameter for the assessment of an individual's cardiovascular risk would therefore be limited to subjects under 60. The observation that average PWV values increase with increasing risk could indicate that by using age-dependent threshold values, subjects might be identified as being at higher risk than others in a certain age group, even when PWV on average is already higher than the 12 m/s threshold in that group.

A final point worth mentioning is the interesting observation that while PWV is on average higher in controlled treated hypertensives than in normotensives, this is not the case when comparing uncontrolled treated hypertensives to untreated hypertensives in our study population. Though a more thorough analysis of these observations would require taking into account the length of time the treated subjects had been under treatment, these results seem to suggest that hypertension treatment by itself is insufficient for reducing average PWV values to those observed in untreated populations, while the stiffness of uncontrolled treated subjects roughly corresponds to that of untreated hypertensives.

16.4.1 Limitations of the study

This study is not longitudinal. While they are an accurate representation of the average PWV values found in a large European population, they do not give any information about the evolution along time of PWV in this population. Second, the reference value database at present does not contain any outcome data. While these data can always be added at a later stage, at present, the reference value database is unsuitable for determining prognosis threshold values for PWV. Based on the distribution of PWV within each of the categories, it is possible to provide information about where a PWV measured in an individual is situated in terms of percentiles of the reference population.

While these percentiles levels could be used as an incentive to intensify treatment in patients, there actually exists no outcome data to support such action. In contrast, the fixed cut-off value of 12 m/s set forward in the ESH/ESC 2007 hypertension guidelines was supported by outcome data. It should be stressed this 12 m/s threshold corresponds to directly measured distances.

16.5 Conclusions

The present study provides reference values for pulse wave velocity based on a large European population. Since absolute PWV values are dependent on the definition used for its determination, values are presented as valid for a specific approach, using direct carotid-femoral distance and transit times determined by the intersecting tangents algorithm. While the present dataset lacks outcome data to use the reference values as a basis for defining cut-off values for treatment, the data presented do allow for the identification of subjects in which PWV is abnormally elevated, which might warrant a more intensive follow-up.

Five

Conclusions

Chapter 17

Conclusions

All good things come to an end, and so does this manuscript. Tradition requires summarizing the main conclusions of the body of work presented in a PhD manuscript in a final chapter, and being a sucker for tradition, I will not disappoint. Since the work presented does not really culminate in a single (provisional) end-point, but rather represents a number of distinct studies, each with their proper conclusions, I will limit myself here to listing, per section, the different research questions I have strived to answer and summarizing how my research has contributed in providing an answer to these questions.

17.1 CAROTID ARTERY INTIMA-MEDIA THICKNESS

Can black-blood MRI images be used for reliable manual IMT delineation and can a relationship be found between cross-sectionally measured IMT values and WSS parameters calculated from MRI-based reconstruction through computational fluid dynamics?

The manual delineation using the custom-developed tool for manual delineation on BB MRI images presented in as outlined in chapter 3 shows good intra- and inter-observer variability. Nevertheless, image quality in general is only barely acceptable for the purpose of defining IMT. BB MRI images cannot compete with the superior resolution and accessibility of ultrasound.

In spite of this, the tentative results of the analysis performed in chapter 3 show that in the study population a weak, but significant inverse correlation is found between IMT and measured WSS. The relationship between IMT and WSS related parameters was stronger in the common carotid artery than in the internal carotid artery, regardless of the WSS parameter under consideration. In contrast, measured IMT values were strongly correlated to the site of measurement; taking the distance to the carotid bifurcation into account has more predictive power than any of the investigated WSS related parameters. Furthermore, including WSS related parameters in a model taking into account the distance to the carotid bifurcation did not significantly improve model performance.

Does the semi-automated ultrasound-based IMT detection algorithm supplied by GE Healthcare Ultrasound improve on manual IMT delineation?

Overall, the automated IMT measurement delivers a reliability at least as good as the manual measurements in a fraction of the time, without the need for extensive training of operators. Differences between manual and automated IMT measurements were negligible. Given these properties, the automated IMT detection algorithm tested in chapter 4 seems an excellent tool for routine assessment of IMT in clinical practice.

17.2 MODELS OF THE ARTERIAL TREE

Is the reservoir-wave separation modeling approach fundamentally different from the classic three element windkessel model and how do reservoir pressures derived from either model compare?

In chapter 7, we have shown that the recently proposed (time domain) reservoir pressure concept shows large similarities to the classical (frequency domain) 3-element windkessel model, especially in subjects characterized by a high reflection magnitude and high 'windkesselness' of their arterial system. The more the arterial tree behaves like a windkessel, the better the reservoir pressure concept seems to hold. Hence, rather than unify the lumped parameter and wave reflection model views, the reservoir-wave concept thus seems to merely represent a time-domain wave propagation analogy of the classic three element windkessel model, albeit yielding slightly different quantitative results. When both models are applied to the Asklepios population, both show the increase of pulse pressure with age to be largely due to increasing reservoir pressures, rather than solely due to increases in wave reflections.

17.3 ARTERIAL STIFFNESS

If a transfer function is used for the calculation of central pressures from peripheral pressure waveforms, how dependent are derived parameters like systolic blood pressure and augmentation index on the type of transfer function used?

The results presented in chapter 10 show that central systolic blood pressure and augmentation index differ depending on the transfer function used to calculate the central pressure waveform from the measured peripheral waveform. Data obtained with different transfer functions are not interchangeable: derived parameter values are determined by the specifics of the transfer function, especially for augmentation index (AIx).

Can calibrated carotid diameter distension waveforms be used as a surrogate for carotid tonometry waveforms for the determination of local systolic blood pressure and carotid augmentation index?

As chapter 11 details, exponentially calibrated diameter waveforms offer a valid alternative for local pressure assessment at the carotid artery. Unlike linearly calibrated waveforms, systolic blood pressure assessed by exponential diameter calibration is independent of the level of pulse pressure. Systolic blood pressure derived from exponentially calibrated diameter curves underestimate pressures obtained by carotid tonometry by 1.90 mmHg. AIx determined from exponentially calibrated diameter waveforms yields values which differ more from AIx derived from tonometry waveforms than when linear calibration is used, though in contrast to the linear calibration, the bias is systematic and should thus easily be corrected for. Nevertheless, the use of scaled carotid diameter waveforms for the assessment of AIx might be less appropriate as a direct alternative for carotid applanation tonometry.

Can a size independent, pressure dependent stiffness parameter be derived from the Langewouters pressure-area relationship and how does it compare to a a classic pressure independent stiffness parameter derived from an exponential pressure-area relationship?

The static distensibility proposed in chapter 12, which was derived from a geometry-normalized Langewouters P-A relationship shows results in good agreement with the α stiffness index derived from an exponential pressure-area relationship. Both indices demonstrate that over the age-range of 35-55 years, in the Asklepios population, the carotid artery becomes stiffer in women than in men around the age of 45.

Is there a difference in behavior of local carotid stiffness and carotid-femoral PWV with increasing age for men and women in the Asklepios population?

Increasingly, arterial stiffness is being considered as an important element for assessment of cardiovascular risk. Although some efforts towards standardized arterial stiffness measures have been made [82], their widespread use is still lacking. Several methods have been proposed, including measurement of carotid–femoral (aortic) PWV (considered as gold standard) and local stiffness measured at the level of the common carotid artery. The data presented in chapter 13 demonstrate that, in an apparently healthy middle-aged population, the evolution with age of these parameters is not the same in men and women. While carotid stiffness shows a more rapid increase with age in women than in men (over the measured age range of 35–55 years), this pattern is not reflected in aortic PWV, which increases to a similar extent in men and women.

The fact that though local carotid artery stiffness and carotid-femoral pulse wave velocity differ in behavior though both are assumed to be indicative of large elastic artery stiffness, could be due to the intrinsic nature of carotid-femoral PWV. The distance over which carotid-femoral PWV is measured comprises the elastic proximal aorta as well as the more muscular abdominal aorta and iliac arteries. As such, PWV likely yields a value reflecting the composite nature of the arterial segment over which it is measured. Other central arterial stiffness parameters do show an age-gender effect similar to the one observed at the carotid artery.

Though the differences in evolution of different stiffness parameters with age and gender have not yet proven to be of clinical significance, the fact that these differences exist is important to keep in mind when analysing or interpreting results from arterial stiffness investigations. Special care is needed when different parameters are compared, especially in a field where proposed measurement standards are not yet widely adopted and reference values are lacking.

Is there a way to convert between pulse wave velocities calculated using different distance measurements if not all distances required for exact conversion are available?

Ideally all distances should be measured when measuring PWV so that exact conversion between the different distance definitions is always possible. For those cases in which only one type of measurement is available, the conversions equations proposed in chapter 15, based on the distance to be converted and body height, offer a viable alternative, which can be used to convert between distance measurements—and thus PWV types.

What are the reference values for pulse wave velocity for a European population?

The study presented in chapter 16 provides reference values for pulse wave velocity based on a large European population. Since absolute PWV values are dependent on the definition used for its determination, values are presented as valid for a specific approach, using direct carotid-femoral distance and transit times determined by the intersecting tangents algorithm. While the presented dataset lacks outcome data to use the reference values as a basis for defining cut-off values for treatment, the data do allow for the identification of subjects in which PWV is abnormally elevated that might warrant a more intensive follow-up.

Appendices

Appendix A.1: Reference values for arterial stiffness research proposal

INTRODUCTION

We now have over 30 years of experience with the measurement of large artery properties. Over that period of time, several large scale studies have been performed demonstrating the prognostic value of pulse wave velocity in different populations around the world [131–139]. Similar findings have been reported, albeit to a lesser extent, for local arterial stiffness measurements in the carotid artery territory [154, 155]. For the purpose of the present project, arterial stiffness will from now on refer to either aortic or carotid artery stiffness.

One of the aims of the European Network for Non Invasive Investigation of Large Arteries is to promote the general use of arterial stiffness as a tool both for screening as well as risk stratification and a surrogate endpoint for clinical management of patients. It is therefore necessary to provide the clinician with a general framework to be used as a reference for evaluating the measurements he takes.

Despite the existence of a consensus on the gold standard for measuring arterial stiffness [82, 140, 141], no recent reference values based on a European population obtained using modern equipment are available. Several issues need to be addressed in order to create such a set of reference values. This is the object of the present project.

Population issues

Although arterial stiffness measurements have been published based on large population samples [147, 149], any such population study can only reflect the arterial properties of subjects of a given part of the world at the time they were collected. Moreover, even if these populations are qualified as 'normal' populations, this definition can be misleading since it usually means only patients devoid of patent cardiovascular disease at the time of measurement were included, which is far from normality. As a consequence, these so-called 'normal populations' are contaminated with patients with latent cardiovascular disease or prevalent risk factors which may ultimately lead to an underestimation of the extent of arterial stiffening in diseased subjects. These issues are even more obvious in populations selected on certain risk factors (e.g. hypertension, menopause, dyslipidemia, etc.)

Methodological issues — pulse wave velocity

There is a large heterogeneity in ways to measure arterial stiffness. For carotid to femoral pulse wave velocity (i.e. aortic stiffness), two major sources of inaccuracy are path length and the algorithm used for point recognition, but other factors can also play a role.

Signal used

Different types of signals can be used as a basis for calculating pulse wave velocity. Pressure applanation signals are used most commonly, but alternatively also Doppler signals can be used [132].

Path length

Path length is measured transcutaneously using a tape meter. In some protocols the site-to-site measurement method is used, others use the difference between carotid to sternal notch and carotid to femoral. Even though the measurement method used has a direct influence on the numerical value of the calculated pulse wave velocity, all of the techniques used are but an approximation of the true physiological distance covered by the observed pulse. Transit time is accurately measured, whereas distance is an approximation. Given this, we need to standardize the distance measurements for a correct scaling of PWV.

Algorithm

The influence of the algorithm for specific point recognition has been widely studied and has a profound influence on the absolute value of the pulse wave velocity [90]. It is therefore essential to know which device and which algorithm were used during measurements. One of the aims of this study is to investigate the differences between algorithms and attempt to compensate for them.

Methodological issues — Carotid artery stiffness

For carotid artery stiffness other methodological issues are raised. The gold standard method for assessing carotid artery stiffness is echotracking. Most of the measurements in large scale population studies are made with the Walltrack system. Over different studies, different generations of the Walltrack system were used with different data processing and handling. Moreover, different echo scanners were used, with significant difference in absolute values of measurements, even if identical software versions were used. Finally, the blood pressure values used for stiffness calculations could be (from worst to best) brachial pulse pressure, direct tonometry, rescaled tonometry (either using Sphygmocor or other dedicated methods) or rescaled diameter distension waveforms. Even when using the rescaling method, the waveform used to make the scaling could have significant influence on the result.

AIM OF THE STUDY AND OBJECTIVES

The aim of the present study is to assemble a very large database in order to derive a set of reference values for arterial stiffness. Data from different participating centers will be collected and added to the database. Only baseline (not follow-up) data will be used. Next to arterial stiffness data also an extensive set of related documentation will be gathered, ranging from general study descriptives, technical documentation regarding measurement techniques and devices and references to published papers.

Data will be analyzed separately for men and women and for both genders combined. Subjects will be stratified according to the ESH 2003 guidelines. Since classification of subjects as normal is difficult a priori, patients will be classified after data collection as having:

- No risk factors
- 1 to 2 risk factors
- 3 or more risk factors or diabetes or target organ damage
- Overt cardiovascular disease

The normal population will be constituted from those subjects with no risk factors and optimal blood pressure values. Other populations will serve to scale the stiffness abnormalities between populations.

PROJECT MANAGEMENT

Promoters and scientific head

The Pharmacology unit of the HEGP is hereafter designed as the promoter of the project, and is represented by its scientific head, Pr Pierre

Boutouyrie. The promoter has designed the study, defined its scientific objectives and funded the research through the ANR grant.

The promoter of the Reference Value project chairs the Research Committee. He manages the actual reference value database and is responsible for the constitution, implementation and maintenance of the reference value database.

The promoter is assigned the reference value project: establishment of reference values in the various populations and scaling of stiffness abnormalities between the populations.

Research committee

In order to resolve possible conflicts of interest with respect to access to the database a Research Committee will be constituted, whose will be to determine the priority in proposed research and the editorial policy of the reference value database. The Research Committee will be chaired by the promoters of the Reference Value Project. For each participating center, one representative will be member of the Research Committee.

The Research Committee is the owner of the Reference Value database in a system of co-ownership. For decisions requiring a regular or qualified majority, each member of the Research Committee will be given voting rights equal to the proportion of contributed subjects to the Reference Value database. In case of conflict and equality during the vote, the vote of the promoters of the Reference Value project will be decisive.

There will be at least one annual meeting of the Research Committee, coupled with the Artery meetings. Additional meetings will be preferentially held during international meetings.

Data access and benefits

Other research projects can be initiated by any participating research center. No preliminary authorization will be required. The project must be presented to and approved by the Research Committee before any query on the database is performed.

For researchers outside the participating centers, the unanimity of the Research Committee is required to allow access to the database. Access to the database will be limited to the parameters listed in the research project and charged according to the amount of work needed to execute the query.

If so desired, the participating center can limit the access to the data originating from their center for any new research project distinct from the reference value project. In this case, a new submission and approval form will be submitted to the owner of the participating center database. In case of refusal or absence of written agreement, the data of the participating center will be withdrawn for the analysis of the new project.

In case of benefits issued from the study (i.e. patents, industry,...) profits will be distributed between the various participating centers in proportion to the number of subjects included in the database.

DATA MANAGEMENT

Tentative list of parameters to be collected

The list of the main parameters of interest for the reference value database along with a description of the documentation required is summarized in appendix A.2. A complete list of parameters to be collected is to be agreed on with each individual center before data collection takes place.

Inclusion/exclusion criteria

Not all listed parameters need to be present for a subject to be eligible for inclusion in the Reference Value database. A subject will not be included if there is missing information regarding parameters listed in the 'required' column of the parameter overview or documentation requirements found in Appendix A. Subject data can be originating either from individual measurements or from the design/inclusion or exclusion criteria of the study (e.g. individual cholesterol measurements vs inclusion criterion 'only dislypidaemic subjects were included').

Confidentiality

All queries on the database will be performed anonymously. The main study database will not contain nominative data. For each participating center, a database file will be kept to allow linking the main study database to the individual center databases containing the nominative data. This database file will be stored at the participating center. This approach guarantees anonymity of the main database while still allowing for subject identification should the need arise. This file serves as a link between center and main database, and can thus also be used to add other data then those initially collected.

Security

The complete database file is to be kept on a dedicated machine located at HEGP and Université René Descartes Paris V. Access to this machine will be strictly restricted to the engineer in charge of database construction and maintenance and the promoters of the Reference Value project. Regular backups will be scheduled to include off-site storage in a secure environment.

Special care should be used when transferring parts of or the complete database to removable storage media. The use of USB keys to transfer database entries will be prohibited or strictly limited. All other forms of portable media, including but not limited to storage on laptop hard drives, should be properly encrypted and access restricted.

Database access

Access to the database will be determined by the Research Committee and limited to the parameters listed in the research project. Queries to the database will be performed by the engineer in charge of database maintenance.

Appendix A.2: Parameters for the reference value project

Tables 1 on the next page and 2 list the requirements for parameters and documentation to be included in the reference value project database. Both for the requested parameters and documentation, three levels of importance are discerned:

Level 1 parameters (required) are essential for the reference value project and are required for inclusion of a subject in the database, i.e. missing information for any of these parameters excludes the subject from analysis.

Level 2 parameters (recommended) are not essential for the database, but contain valuable information. If possible these should be included in the database

Level 3 parameters (optional) are parameters whose immediate importance for the reference value project is limited. Nevertheless, if available they will be included in the database for future reference.

TABLE 1: List of minimal and optional parameters for inclusion in the reference value database

Level 1 (required)	Level 2 (recommended)	Level 3 (optional)
Age (years)	Smoking (active/ex/never)	Heart rate (bpm)
Gender	Total cholesterol (mmol/l)	Abnormal glucose tolerance test
Brachial blood pressure (mmHg)	HDL cholesterol (mmol/l)	Family history of CV disease
Smoking (yes/no)	LDL cholesterol (mmol/l)	Plasma creatinine (μmol/l)
Dislipidemia (yes/no)	Triglycerides (mmol/l)	Glomural filtration rate
Diabetes (yes/no)	Fasting plasma glucose (mmol/l)	Creatinine clearance
Established CV disease (yes/no)	Postload plasma glucose (mmol/l)	Microalbuminuria (mg/24h)
Hypertension treatment (yes/no)	Waist circumference (cm)	Albumin–creatinine ratio (mg/g creatinine)
Lipids treatment (yes/no)	Subclinical organ damage (yes/no)	Cerebrovascular disease (yes/no)
Diabetes treatment (yes/no)	Left ventricular hypertrophy (yes/no)	Vital status
Carotid-femoral PWV (m/s) *or*	IMT (mm)	Cause of death
Carotid diameter and distension (mm)	Plaque (yes/no)	
	Renal organ damage (yes/no)	
	Metabolic syndrome (yes/no)	
	PWV transit time (s)	
	Carotid–femoral path length	
	Carotid–sternal notch path length	
	Sternal notch–femoral path length	
	Central pressure (mmHg)	
	Carotid AIx (%)	
	Central AIx (%)	

Table 2: List of minimal and optional documentation for inclusion in the reference value database

Level 1 (required)	Level 2 (recommended)	Level 3 (optional)
Aims/scope of study to be included	Study questionnaire	Dates of collection
Inclusion/exclusion criteria	References to published results	References to device validation studies
Population description	Devices used	
Measurement protocol		
Thresholds for lipids		
Thresholds for diabetes		
Definition of MS (if applicable)		

Bibliography

[1] Henry Gray and Warren H. Lewis. *Anatomy of the human body*. Lea & Febiger, Philadelphia and New York,, 20th edition, 1918.

[2] David E. Mohrman and Lois Jane Heller. *Cardiovascular physiology*. McGraw-Hill Professional, 6th edition, 2003.

[3] Elaine N. Marieb and Katja Hoehn. *Anatomy & Physiology*. Pearson/Benjamin Cummings, 3rd edition, 2008.

[4] K. Matthys and P. Verdonck. *Development and modelling of arterial applanation tonometry: a review*. Technol Health Care, 10(1):65–76, 2002.

[5] N. Stergiopulos and N. Westerhof. *Role of total arterial compliance and peripheral resistance in the determination of systolic and diastolic aortic pressure*. Pathol Biol (Paris), 47(6):641–7, 1999.

[6] N. Westerhof, P. Sipkema, G. C. van den Bos, and G. Elzinga. *Forward and backward waves in the arterial system*. Cardiovasc Res, 6(6):648–56, 1972.

[7] P. Segers and P. Verdonck. *Role of tapering in aortic wave reflection: hydraulic and mathematical model study*. J Biomech, 33(3):299–306, 2000.

[8] F. Y. Liang, S. Takagi, R. Himeno, and H. Liu. *Biomechanical characterization of ventricular-arterial coupling during aging: A multi-scale model study*. J Biomech, 2009.

[9] G. Mancia, G. De Backer, A. Dominiczak, R. Cifkova, R. Fagard, G. Germano, G. Grassi, A. M. Heagerty, S. E. Kjeldsen, S. Laurent, K. Narkiewicz, L. Ruilope, A. Rynkiewicz, R. E. Schmieder, H. A. Struijker Boudier, A. Zanchetti, A. Vahanian,

J. Camm, R. De Caterina, V. Dean, K. Dickstein, G. Filippatos, C. Funck-Brentano, I. Hellemans, S. D. Kristensen, K. McGregor, U. Sechtem, S. Silber, M. Tendera, P. Widimsky, J. L. Zamorano, S. Erdine, W. Kiowski, E. Agabiti-Rosei, E. Ambrosioni, L. H. Lindholm, A. Manolis, P. M. Nilsson, J. Redon, H. A. Struijker-Boudier, M. Viigimaa, S. Adamopoulos, V. Bertomeu, D. Clement, C. Farsang, D. Gaita, G. Lip, J. M. Mallion, A. J. Manolis, E. O'Brien, P. Ponikowski, F. Ruschitzka, J. Tamargo, P. van Zwieten, B. Waeber, B. Williams, Hypertension The task force for the management of arterial hypertension of the European Society of, and Cardiology The task force for the management of arterial hypertension of the European Society of. *2007 Guidelines for the management of arterial hypertension: The Task Force for the Management of Arterial Hypertension of the European Society of Hypertension (ESH) and of the European Society of Cardiology (ESC).* Eur Heart J, 28(12):1462–536, 2007.

[10] J. T. Salonen and R. Salonen. *Ultrasound B-mode imaging in observational studies of atherosclerotic progression.* Circulation, 87(3 Suppl):II56–65, 1993.

[11] M. L. Bots, A. W. Hoes, P. J. Koudstaal, A. Hofman, and D. E. Grobbee. *Common carotid intima-media thickness and risk of stroke and myocardial infarction: the Rotterdam Study.* Circulation, 96(5):1432–7, 1997.

[12] H. N. Hodis, W. J. Mack, L. LaBree, R. H. Selzer, C. R. Liu, C. H. Liu, and S. P. Azen. *The role of carotid arterial intima-media thickness in predicting clinical coronary events.* Ann Intern Med, 128(4):262–9, 1998.

[13] D. H. O'Leary, J. F. Polak, R. A. Kronmal, T. A. Manolio, G. L. Burke, and Jr. Wolfson, S. K. *Carotid-artery intima and media thickness as a risk factor for myocardial infarction and stroke in older adults. Cardiovascular Health Study Collaborative Research Group.* N Engl J Med, 340(1):14–22, 1999.

[14] C. K. Zarins, D. P. Giddens, B. K. Bharadvaj, V. S. Sottiurai, R. F. Mabon, and S. Glagov. *Carotid bifurcation atherosclerosis. Quantitative correlation of plaque localization with flow velocity profiles and wall shear stress.* Circ Res, 53(4):502–14, 1983.

[15] C. G. Caro, J. M. Fitz-Gerald, and R. C. Schroter. *Atheroma and arterial wall shear. Observation, correlation and proposal of a shear dependent mass transfer mechanism for atherogenesis.* Proc R Soc Lond B Biol Sci, 177(46):109–59, 1971.

[16] D. N. Ku, D. P. Giddens, C. K. Zarins, and S. Glagov. *Pulsatile flow and atherosclerosis in the human carotid bifurcation. Positive correlation between plaque location and low oscillating shear stress.* Arteriosclerosis, 5(3):293–302, 1985.

[17] C. K. Zarins, M. A. Zatina, D. P. Giddens, D. N. Ku, and S. Glagov. *Shear stress regulation of artery lumen diameter in experimental atherogenesis.* J Vasc Surg, 5(3):413–20, 1987.

[18] J. R. Buchanan, C. Kleinstreuer, S. Hyun, and G. A. Truskey. *Hemodynamics simulation and identification of susceptible sites of atherosclerotic lesion formation in a model abdominal aorta.* J Biomech, 36(8):1185–96, 2003.

[19] F. P. Glor. *Integrating medical imaging and computational fluid dynamics for measuring blood flow in carotid arteries.* PhD thesis, Ghent University, 2004.

[20] F. P. Glor, B. Ariff, A. D. Hughes, L. A. Crowe, P. R. Verdonck, D. C. Barratt, G. Thom S. A. Mc, D. N. Firmin, and X. Y. Xu. *Image-based carotid flow reconstruction: a comparison between MRI and ultrasound.* Physiol Meas, 25(6):1495–509, 2004.

[21] F. P. Glor, B. Ariff, L. A. Crowe, A. D. Hughes, P. L. Cheong, S. A. Thom, P. R. Verdonck, D. N. Firmin, D. C. Barratt, and X. Y. Xu. *Carotid geometry reconstruction: a comparison between MRI and ultrasound.* Med Phys, 30(12):3251–61, 2003.

[22] F. P. Glor, Q. Long, A. D. Hughes, A. D. Augst, B. Ariff, S. A. Thom, P. R. Verdonck, and X. Y. Xu. *Reproducibility study of magnetic resonance image-based computational fluid dynamics prediction of carotid bifurcation flow.* Ann Biomed Eng, 31(2):142–51, 2003.

[23] F. P. Glor, J. J. Westenberg, J. Vierendeels, M. Danilouchkine, and P. Verdonck. *Validation of the coupling of magnetic resonance imaging velocity measurements with computational fluid dynamics in a U bend.* Artif Organs, 26(7):622–35, 2002.

[24] D. E. Grobbee and M. L. Bots. *Carotid artery intima-media thickness as an indicator of generalized atherosclerosis.* J Intern Med, 236(5):567–73, 1994.

[25] J. Hulthe, J. Wikstrand, H. Emanuelsson, O. Wiklund, P. J. de Feyter, and I. Wendelhag. *Atherosclerotic changes in the carotid artery bulb as measured by B-mode ultrasound are associated with the extent of coronary atherosclerosis.* Stroke, 28(6):1189–94, 1997.

[26] J. P. Lekakis, C. M. Papamichael, A. T. Cimponeriu, K. S. Stamatelopoulos, T. G. Papaioannou, J. Kanakakis, M. K. Alevizaki, A. Papapanagiotou, A. T. Kalofoutis, and S. F. Stamatelopoulos. *Atherosclerotic changes of extracoronary arteries are associated with the extent of coronary atherosclerosis.* Am J Cardiol, 85(8):949–52, 2000.

[27] W. J. Mack, L. LaBree, C. Liu, R. H. Selzer, and H. N. Hodis. *Correlations between measures of atherosclerosis change using carotid ultrasonography and coronary angiography.* Atherosclerosis, 150(2):371–9, 2000.

[28] A. M. Malek, S. L. Alper, and S. Izumo. *Hemodynamic shear stress and its role in atherosclerosis.* JAMA, 282(21):2035–42, 1999.

[29] H. K. Song, A. C. Wright, R. L. Wolf, and F. W. Wehrli. *Multislice double inversion pulse sequence for efficient black-blood MRI.* Magn Reson Med, 47(3):616–20, 2002.

[30] F. P. Glor, B. Ariff, A. D. Hughes, L. A. Crowe, P. R. Verdonck, D. C. Barratt, G. Thom S. A. Mc, D. N. Firmin, and X. Y. Xu. *The integration of medical imaging and computational fluid dynamics for measuring wall shear stress in carotid arteries.* Conf Proc IEEE Eng Med Biol Soc, 2:1415–8, 2004.

[31] Q. Long, X. Y. Xu, M. W. Collins, M. Bourne, and T. M. Griffith. *Magnetic resonance image processing and structured grid generation of a human abdominal bifurcation.* Comput Methods Programs Biomed, 56(3):249–59, 1998.

[32] F. P. Glor, B. Ariff, A. D. Hughes, P. R. Verdonck, S. A. Thom, D. C. Barratt, and X. Y. Xu. *Operator dependence of 3-D ultrasound-based computational fluid dynamics for the carotid bifurcation.* IEEE Trans Med Imaging, 24(4):451–6, 2005.

[33] F. P. Glor, B. Ariff, A. D. Hughes, P. R. Verdonck, D. C. Barratt, A. D. Augst, S. A. Thom, and X. Y. Xu. *Influence of head position on carotid hemodynamics in young adults.* Am J Physiol Heart Circ Physiol, 287(4):H1670–81, 2004.

[34] A. D. Augst, D. C. Barratt, A. D. Hughes, F. P. Glor, G. Thom S. A. Mc, and X. Y. Xu. *Accuracy and reproducibility of CFD predicted wall shear stress using 3D ultrasound images.* J Biomech Eng, 125(2):218–22, 2003.

[35] J. B. Thomas, J. S. Milner, B. K. Rutt, and D. A. Steinman. *Reproducibility of image-based computational fluid dynamics models of the human carotid bifurcation.* Ann Biomed Eng, 31(2):132–41, 2003.

[36] G.E.P. Box and D.R. Cox. *An analysis of transformations.* Journal of the Royal Statistical Society, Series B, 26(2):211–52, 1964.

[37] G. L. Burke, G. W. Evans, W. A. Riley, A. R. Sharrett, G. Howard, R. W. Barnes, W. Rosamond, R. S. Crow, P. M. Rautaharju, and G. Heiss. *Arterial wall thickness is associated with prevalent cardiovascular disease in middle-aged adults. The Atherosclerosis Risk in Communities (ARIC) Study.* Stroke, 26(3):386–91, 1995.

[38] L. E. Chambless, G. Heiss, A. R. Folsom, W. Rosamond, M. Szklo, A. R. Sharrett, and L. X. Clegg. *Association of coronary heart disease incidence with carotid arterial wall thickness and major risk factors: the Atherosclerosis Risk in Communities (ARIC) Study, 1987-1993.* Am J Epidemiol, 146(6):483–94, 1997.

[39] O. T. Raitakari, M. Juonala, M. Kahonen, L. Taittonen, T. Laitinen, N. Maki-Torkko, M. J. Jarvisalo, M. Uhari, E. Jokinen, T. Ronnemaa, H. K. Akerblom, and J. S. Viikari. *Cardiovascular risk factors in childhood and carotid artery intima-media thickness in adulthood: the Cardiovascular Risk in Young Finns Study.* JAMA, 290(17):2277–83, 2003.

[40] J. T. Salonen and R. Salonen. *Ultrasonographically assessed carotid morphology and the risk of coronary heart disease.* Arterioscler Thromb, 11(5):1245–9, 1991.

[41] R. Salonen, A. Haapanen, and J. T. Salonen. *Measurement of intima-media thickness of common carotid arteries with high-resolution B-mode ultrasonography: inter- and intra-observer variability.* Ultrasound Med Biol, 17(3):225–30, 1991.

[42] E. R. Rietzschel, M. L. De Buyzere, S. Bekaert, P. Segers, D. De Bacquer, L. Cooman, P. Van Damme, P. Cassiman, M. Langlois, P. van Oostveldt, P. Verdonck, G. De Backer, and T. C. Gillebert. *Rationale, design, methods and baseline characteristics of the Asklepios Study.* Eur J Cardiovasc Prev Rehabil, 14(2):179–91, 2007.

[43] J. M. Bland and D. G. Altman. *Statistical methods for assessing agreement between two methods of clinical measurement.* Lancet, 1(8476):307–10, 1986.

[44] J. H. Stein, C. E. Korcarz, M. E. Mays, P. S. Douglas, M. Palta, H. Zhang, T. Lecaire, D. Paine, D. Gustafson, and L. Fan. *A semiautomated ultrasound border detection program that facilitates clinical measurement of ultrasound carotid intima-media thickness.* J Am Soc Echocardiogr, 18(3):244–51, 2005.

[45] I. Wendelhag, Q. Liang, T. Gustavsson, and J. Wikstrand. *A new automated computerized analyzing system simplifies readings and reduces the variability in ultrasound measurement of intima-media thickness.* Stroke, 28(11):2195–200, 1997.

[46] A. D. Gepner, C. E. Korcarz, S. E. Aeschlimann, T. J. LeCaire, M. Palta, W. S. Tzou, and J. H. Stein. *Validation of a carotid intima-media thickness border detection program for use in an office setting.* J Am Soc Echocardiogr, 19(2):223–8, 2006.

[47] S. D. Kanters, A. Algra, M. S. van Leeuwen, and J. D. Banga. *Reproducibility of in vivo carotid intima-media thickness measurements: a review.* Stroke, 28(3):665–71, 1997.

[48] O. Frank. *Die Grundform des arteriellen Pulses.* Z Biol, 37:483–526, 1899.

[49] N. Westerhof, J. W. Lankhaar, and B. E. Westerhof. *The arterial Windkessel.* Med Biol Eng Comput, 47(2):131–41, 2009.

[50] N. Westerhof, N. Stergiopulos, and M. Noble. *Snapshots of hemodynamics. An aid for clinical research and graduate education.* Springer Science + Business Media, New York, 2004.

[51] N. Stergiopulos, J. J. Meister, and N. Westerhof. *Evaluation of methods for estimation of total arterial compliance.* Am J Physiol, 268(4 Pt 2):H1540–8, 1995.

[52] J. W. Lankhaar. *Hemodynamics of pulmonary hypertension.* PhD thesis, Vrije Universiteit Amsterdam, 2008.

[53] N. Westerhof, F. Bosman, C. J. De Vries, and A. Noordergraaf. *Analog studies of the human systemic arterial tree.* J Biomech, 2(2):121–43, 1969.

[54] P. Segers, S. Brimioulle, N. Stergiopulos, N. Westerhof, R. Naeije, M. Maggiorini, and P. Verdonck. *Pulmonary arterial compliance in dogs and pigs: the three-element windkessel model revisited.* Am J Physiol, 277(2 Pt 2):H725–31, 1999.

[55] N. Stergiopulos, B. E. Westerhof, and N. Westerhof. *Total arterial inertance as the fourth element of the windkessel model.* Am J Physiol, 276(1 Pt 2):H81–8, 1999.

[56] A. Swillens and P. Segers. *Assessment of arterial pressure wave reflection: Methodological considerations.* Artery Res, 2:122–131, 2008.

[57] K. H. Parker and C. J. Jones. *Forward and backward running waves in the arteries: analysis using the method of characteristics.* J Biomech Eng, 112(3):322–6, 1990.

[58] R. A. Bleasdale, K. H. Parker, and C. J. Jones. *Chasing the wave. Unfashionable but important new concepts in arterial wave travel.* Am J Physiol Heart Circ Physiol, 284(6):H1879–85, 2003.

[59] J. Aguado-Sierra, J. Alastruey, J. J. Wang, N. Hadjiloizou, J. Davies, and K. H. Parker. *Separation of the reservoir and wave pressure and velocity from measurements at an arbitrary location in arteries.* Proc Inst Mech Eng [H], 222(4):403–16, 2008.

[60] J. J. Wang, A. B. O'Brien, N. G. Shrive, K. H. Parker, and J. V. Tyberg. *Time-domain representation of ventricular-arterial coupling as a windkessel and wave system.* Am J Physiol Heart Circ Physiol, 284(4):H1358–68, 2003.

[61] P. Segers, E. R. Rietzschel, M. L. De Buyzere, S. J. Vermeersch, D. De Bacquer, L. M. Van Bortel, G. De Backer, T. C. Gillebert, and P. R. Verdonck. *Noninvasive (input) impedance, pulse wave velocity, and wave reflection in healthy middle-aged men and women.* Hypertension, 49(6):1248–55, 2007.

[62] M. A. El Assaad, J. A. Topouchian, B. M. Darne, and R. G. Asmar. *Validation of the Omron HEM-907 device for blood pressure measurement.* Blood Press Monit, 7(4):237–41, 2002.

[63] P. Segers, E. Rietzschel, S. Heireman, M. De Buyzere, T. Gillebert, P. Verdonck, and L. Van Bortel. *Carotid tonometry versus synthesized aorta pressure waves for the estimation of central systolic blood pressure and augmentation index.* Am J Hypertens, 18(9 Pt 1):1168–73, 2005.

[64] R. Kelly, M. Karamanoglu, H. Gibbs, and A. P. Avolio. *Noninvasive carotid pressure wave registration as an indicator of ascending aortic pressure.* J Vasc Med Biol, 1:241–247, 1989.

[65] L. M. Van Bortel, E. J. Balkestein, J. J. van der Heijden-Spek, F. H. Vanmolkot, J. A. Staessen, J. A. Kragten, J. W. Vredeveld, M. E. Safar, H. A. Struijker Boudier, and A. P. Hoeks. *Non-invasive assessment of local arterial pulse pressure: comparison of applanation tonometry and echo-tracking.* J Hypertens, 19(6):1037–44, 2001.

[66] F. Verbeke, P. Segers, S. Heireman, R. Vanholder, P. Verdonck, and L. M. Van Bortel. *Noninvasive assessment of local pulse pressure: importance of brachial-to-radial pressure amplification.* Hypertension, 46(1):244–8, 2005.

[67] P. Segers, E. R. Rietzschel, M. L. De Buyzere, N. Stergiopulos, N. Westerhof, L. M. Van Bortel, T. Gillebert, and P. R. Verdonck. *Three- and four-element Windkessel models: assessment of their fitting performance in a large cohort of healthy middle-aged individuals.* Proc Inst Mech Eng [H], 222(4):417–28, 2008.

[68] R Development Core Team. *R: A Language and Environment for Statistical Computing.* Vienna, Austria: R foundation for Statistical Computing, 2008.

[69] S. M. Toy, J. Melbin, and A. Noordergraaf. *Reduced models of arterial systems.* IEEE Trans Biomed Eng, 32(2):174–6, 1985.

[70] P. Segers and P. Verdonck. *Principles of vascular physiology.* In P. Lanzer and E.J. Topol, editors, Pan vascular medicine. Integrated clinical management. Springer-Verlag, Heidelberg, 2002.

[71] Wilmer W. Nichols, Michael F. O'Rourke, and Donald A. McDonald. *McDonald's blood flow in arteries : theoretic, experimental, and clinical principles.* Hodder Arnold ; Distributed in the U.S.A. by Oxford University Press, London New York, 5th edition, 2005.

[72] M. F. O'Rourke. *Pressure and flow waves in systemic arteries and the anatomical design of the arterial system.* J Appl Physiol, 23(2):139–49, 1967.

[73] A. P. Avolio. *Multi-branched model of the human arterial system.* Med Biol Eng Comput, 18(6):709–18, 1980.

[74] M. Karamanoglu, D. E. Gallagher, A. P. Avolio, and M. F. O'Rourke. *Pressure wave propagation in a multibranched model of the human upper limb.* Am J Physiol, 269(4 Pt 2):H1363–9, 1995.

[75] P. Segers, N. Stergiopulos, P. Verdonck, and R. Verhoeven. *Assessment of distributed arterial network models.* Med Biol Eng Comput, 35(6):729–36, 1997.

[76] N. Stergiopulos, D. F. Young, and T. R. Rogge. *Computer simulation of arterial flow with applications to arterial and aortic stenoses.* J Biomech, 25(12):1477–88, 1992.

[77] N. Westerhof, G. Elzinga, and P. Sipkema. *An artificial arterial system for pumping hearts.* J Appl Physiol, 31(5):776–81, 1971.

[78] C. M. Quick, D. S. Berger, and A. Noordergraaf. *Apparent arterial compliance.* Am J Physiol, 274(4 Pt 2):H1393–403, 1998.

[79] M. W. Mohiuddin, G. A. Laine, and C. M. Quick. *Increase in pulse wavelength causes the systemic arterial tree to degenerate into a classical windkessel.* Am J Physiol Heart Circ Physiol, 293(2):H1164–71, 2007.

[80] S. J. Vermeersch, E. R. Rietzschel, M. L. De Buyzere, D. De Bacquer, G. De Backer, L. M. Van Bortel, T. C. Gillebert, P. R. Verdonck, and P. Segers. *Age and gender related patterns in carotid-femoral PWV and carotid and femoral stiffness in a large healthy, middle-aged population.* J Hypertens, 26(7):1411–9, 2008.

[81] G. J. Langewouters, K. H. Wesseling, and W. J. Goedhard. *The static elastic properties of 45 human thoracic and 20 abdominal aortas in vitro and the parameters of a new model.* J Biomech, 17(6):425–35, 1984.

[82] S. Laurent, J. Cockcroft, L. Van Bortel, P. Boutouyrie, C. Giannattasio, D. Hayoz, B. Pannier, C. Vlachopoulos, I. Wilkinson, and H. Struijker-Boudier. *Expert consensus document on arterial stiffness: methodological issues and clinical applications.* Eur Heart J, 27(21):2588–605, 2006.

[83] W. W. Nichols and D. A. McDonald. *Wave-velocity in the proximal aorta.* Med Biol Eng, 10(3):327–35, 1972.

[84] Z. Liu, K. P. Brin, and F. C. Yin. *Estimation of total arterial compliance: an improved method and evaluation of current methods.* Am J Physiol, 251(3 Pt 2):H588–600, 1986.

[85] N. Stergiopulos, J. J. Meister, and N. Westerhof. *Simple and accurate way for estimating total and segmental arterial compliance: the pulse pressure method.* Ann Biomed Eng, 22(4):392–397, 1994.

[86] N. Stergiopulos, P. Segers, and N. Westerhof. *Use of pulse pressure method for estimating total arterial compliance in vivo.* Am J Physiol, 276(2 Pt 2):H424–8, 1999.

[87] A. M. Dart, C. D. Gatzka, B. A. Kingwell, K. Willson, J. D. Cameron, Y. L. Liang, K. L. Berry, L. M. Wing, C. M. Reid, P. Ryan, L. J. Beilin, G. L. Jennings, C. I. Johnston, J. J. McNeil, G. J. Macdonald, T. O. Morgan, and M. J. West. *Brachial blood pressure but not carotid arterial waveforms predict cardiovascular*

events in elderly female hypertensives. Hypertension, 47(4):785–90, 2006.

[88] P. Boutouyrie, M. Briet, C. Collin, S. J. Vermeersch, and B. Pannier. *Assessment of pulse wave velocity.* Artery Res, doi:10.1016/j.artres.2008.11.002:(In press), 2009.

[89] G. E. McVeigh, P. K. Hamilton, and D. R. Morgan. *Evaluation of mechanical arterial properties: clinical, experimental and therapeutic aspects.* Clin Sci (Lond), 102(1):51–67, 2002.

[90] S. C. Millasseau, A. D. Stewart, S. J. Patel, S. R. Redwood, and P. J. Chowienczyk. *Evaluation of carotid-femoral pulse wave velocity: influence of timing algorithm and heart rate.* Hypertension, 45(2):222–6, 2005.

[91] E. Hermeling, K. D. Reesink, R. S. Reneman, and A. P. Hoeks. *Confluence of incident and reflected waves interferes with systolic foot detection of the carotid artery distension waveform.* J Hypertens, 26(12):2374–80, 2008.

[92] O. Hanon, S. Haulon, H. Lenoir, M. L. Seux, A. S. Rigaud, M. Safar, X. Girerd, and F. Forette. *Relationship between arterial stiffness and cognitive function in elderly subjects with complaints of memory loss.* Stroke, 36(10):2193–7, 2005.

[93] S. R. Waldstein, S. C. Rice, J. F. Thayer, S. S. Najjar, A. Scuteri, and A. B. Zonderman. *Pulse pressure and pulse wave velocity are related to cognitive decline in the Baltimore Longitudinal Study of Aging.* Hypertension, 51(1):99–104, 2008.

[94] A. Scuteri, A. M. Brancati, W. Gianni, A. Assisi, and M. Volpe. *Arterial stiffness is an independent risk factor for cognitive impairment in the elderly: a pilot study.* J Hypertens, 23(6):1211–6, 2005.

[95] S. S. Najjar, A. Scuteri, V. Shetty, J. G. Wright, D. C. Muller, J. L. Fleg, H. P. Spurgeon, L. Ferrucci, and E. G. Lakatta. *Pulse wave velocity is an independent predictor of the longitudinal increase in systolic blood pressure and of incident hypertension in the Baltimore Longitudinal Study of Aging.* J Am Coll Cardiol, 51(14):1377–83, 2008.

[96] I. S. Mackenzie, I. B. Wilkinson, and J. R. Cockcroft. *Assessment of arterial stiffness in clinical practice.* QJM, 95(2):67–74, 2002.

[97] G. London, A. Guerin, B. Pannier, S. Marchais, A. Benetos, and M. Safar. *Increased systolic pressure in chronic uremia. Role of arterial wave reflections.* Hypertension, 20(1):10–9, 1992.

[98] P. Segers, A. Qasem, T. De Backer, S. Carlier, P. Verdonck, and A. Avolio. *Peripheral "oscillatory" compliance is associated with aortic augmentation index.* Hypertension, 37(6):1434–9, 2001.

[99] C. H. Chen, C. T. Ting, A. Nussbacher, E. Nevo, D. A. Kass, P. Pak, S. P. Wang, M. S. Chang, and F. C. Yin. *Validation of carotid artery tonometry as a means of estimating augmentation index of ascending aortic pressure.* Hypertension, 27(2):168–75, 1996.

[100] C. H. Chen, E. Nevo, B. Fetics, P. H. Pak, F. C. Yin, W. L. Maughan, and D. A. Kass. *Estimation of central aortic pressure waveform by mathematical transformation of radial tonometry pressure. Validation of generalized transfer function.* Circulation, 95(7):1827–36, 1997.

[101] A. L. Pauca, M. F. O'Rourke, and N. D. Kon. *Prospective evaluation of a method for estimating ascending aortic pressure from the radial artery pressure waveform.* Hypertension, 38(4):932–7, 2001.

[102] G. M. London, J. Blacher, B. Pannier, A. P. Guerin, S. J. Marchais, and M. E. Safar. *Arterial wave reflections and survival in end-stage renal failure.* Hypertension, 38(3):434–8, 2001.

[103] M. E. Safar, J. Blacher, B. Pannier, A. P. Guerin, S. J. Marchais, P. M. Guyonvarc'h, and G. M. London. *Central pulse pressure and mortality in end-stage renal disease.* Hypertension, 39(3):735–8, 2002.

[104] B. Williams, P. S. Lacy, S. M. Thom, K. Cruickshank, A. Stanton, D. Collier, A. D. Hughes, H. Thurston, and M. O'Rourke. *Differential impact of blood pressure-lowering drugs on central aortic pressure and clinical outcomes: principal results of the Conduit Artery Function Evaluation (CAFE) study.* Circulation, 113(9):1213–25, 2006.

[105] E. D. Lehmann. *Where is the evidence that radial artery tonometry can be used to accurately and noninvasively predict central aortic blood pressure in patients with diabetes?* Diabetes Care, 23(6):869–71, 2000.

[106] S. C. Millasseau, S. J. Patel, S. R. Redwood, J. M. Ritter, and P. J. Chowienczyk. *Pressure wave reflection assessed from the peripheral pulse: is a transfer function necessary?* Hypertension, 41(5):1016–20, 2003.

[107] J. D. Cameron, B. P. McGrath, and A. M. Dart. *Use of radial artery applanation tonometry and a generalized transfer function to determine aortic pressure augmentation in subjects with treated hypertension.* J Am Coll Cardiol, 32(5):1214–20, 1998.

[108] A. P. Hoeks, J. M. Meinders, and R. Dammers. *Applicability and benefit of arterial transfer functions.* J Hypertens, 21(7):1241–3, 2003.

[109] S. A. Hope, I. T. Meredith, and J. D. Cameron. *Reliability of transfer functions in determining central pulse pressure and augmentation index.* J Am Coll Cardiol, 40(6):1196; author reply 1196–7, 2002.

[110] S. A. Hope, D. B. Tay, I. T. Meredith, and J. D. Cameron. *Use of arterial transfer functions for the derivation of aortic waveform characteristics.* J Hypertens, 21(7):1299–305, 2003.

[111] M. F. O'Rourke, A. Avolio, and A. Qasem. *Clinical assessment of wave reflection.* Hypertension, 42(5):e15–6; author reply e15–6, 2003.

[112] A. P. Avolio and M. F. O'Rourke. *Applicability and benefit of arterial transfer functions.* J Hypertens, 21(11):2199–200; author reply 2200–1, 2003.

[113] M. Karamanoglu, M. F. O'Rourke, A. P. Avolio, and R. P. Kelly. *An analysis of the relationship between central aortic and peripheral upper limb pressure waves in man.* Eur Heart J, 14(2):160–7, 1993.

[114] K. Takazawa, N. Tanaka, K. Takeda, F. Kurosu, and C. Ibukiyama. *Underestimation of vasodilator effects of nitroglycerin by upper limb blood pressure.* Hypertension, 26(3):520–3, 1995.

[115] P. Segers, S. Carlier, A. Pasquet, S. I. Rabben, L. R. Hellevik, E. Remme, T. De Backer, J. De Sutter, J. D. Thomas, and P. Verdonck. *Individualizing the aorto-radial pressure transfer function: feasibility of a model-based approach.* Am J Physiol Heart Circ Physiol, 279(2):H542–9, 2000.

[116] S. A. Hope, D. B. Tay, I. T. Meredith, and J. D. Cameron. *Comparison of generalized and gender-specific transfer functions for the derivation of aortic waveforms.* Am J Physiol Heart Circ Physiol, 283(3):H1150–6, 2002.

[117] T. Morgan, J. Lauri, D. Bertram, and A. Anderson. *Effect of different antihypertensive drug classes on central aortic pressure.* Am J Hypertens, 17(2):118–23, 2004.

[118] Z. Dhakam, C. M. McEniery, Yasmin, J. R. Cockcroft, M. J. Brown, and I. B. Wilkinson. *Atenolol and eprosartan: differential effects on central blood pressure and aortic pulse wave velocity.* Am J Hypertens, 19(2):214–9, 2006.

[119] G. M. London, S. J. Marchais, and A. P. Guerin. *Arterial stiffness and function in end-stage renal disease.* Adv Chronic Kidney Dis, 11(2):202–9, 2004.

[120] M. J. Roman, R. B. Devereux, J. R. Kizer, E. T. Lee, J. M. Galloway, T. Ali, J. G. Umans, and B. V. Howard. *Central pressure more strongly relates to vascular disease and outcome than does brachial pressure: the Strong Heart Study.* Hypertension, 50(1):197–203, 2007.

[121] S. Soderstrom, G. Nyberg, M. F. O'Rourke, J. Sellgren, and J. Ponten. *Can a clinically useful aortic pressure wave be derived from a radial pressure wave?* Br J Anaesth, 88(4):481–8, 2002.

[122] A. P. Hoeks, P. J. Brands, F. A. Smeets, and R. S. Reneman. *Assessment of the distensibility of superficial arteries.* Ultrasound Med Biol, 16(2):121–8, 1990.

[123] A. P. Hoeks, C. Willekes, P. Boutouyrie, P. J. Brands, J. M. Willigers, and R. S. Reneman. *Automated detection of local artery wall thickness based on M-line signal processing.* Ultrasound Med Biol, 23(7):1017–23, 1997.

[124] J. M. Meinders and A. P. Hoeks. *Simultaneous assessment of diameter and pressure waveforms in the carotid artery.* Ultrasound Med Biol, 30(2):147–54, 2004.

[125] S. I. Rabben, S. Baerum, V. Sorhus, and H. Torp. *Ultrasound-based vessel wall tracking: an auto-correlation technique with RF center frequency estimation.* Ultrasound Med Biol, 28(4):507–17, 2002.

[126] P. Segers, S. I. Rabben, J. De Backer, J. De Sutter, T. C. Gillebert, L. Van Bortel, and P. Verdonck. *Functional analysis of the common carotid artery: relative distension differences over the vessel wall measured in vivo.* J Hypertens, 22(5):973–81, 2004.

[127] K. Hayashi, H. Handa, S. Nagasawa, A. Okumura, and K. Moritake. *Stiffness and elastic behavior of human intracranial and extracranial arteries.* J Biomech, 13:175–184, 1980.

[128] W. J. Bos, E. Verrij, H. H. Vincent, B. E. Westerhof, G. Parati, and G. A. van Montfrans. *How to assess mean blood pressure properly at the brachial artery level.* J Hypertens, 25(4):751–5, 2007.

[129] E. A. Verrij, H. H. Vincent, and W. J. Bos. *Rule of thumb to calculate mean arterial pressure at the brachial artery level.* J Hypertens, 26(5):1043–5, 2008.

[130] P. C. Simons, A. Algra, M. L. Bots, D. E. Grobbee, and Y. van der Graaf. *Common carotid intima-media thickness and arterial stiffness: indicators of cardiovascular risk in high-risk patients. The SMART Study (Second Manifestations of ARTerial disease).* Circulation, 100(9):951–7, 1999.

[131] J. Blacher, A. P. Guerin, B. Pannier, S. J. Marchais, M. E. Safar, and G. M. London. *Impact of aortic stiffness on survival in end-stage renal disease.* Circulation, 99(18):2434–9, 1999.

[132] K. Cruickshank, L. Riste, S. G. Anderson, J. S. Wright, G. Dunn, and R. G. Gosling. *Aortic pulse-wave velocity and its relationship to mortality in diabetes and glucose intolerance: an integrated index of vascular function?* Circulation, 106(16):2085–90, 2002.

[133] S. Laurent, P. Boutouyrie, R. Asmar, I. Gautier, B. Laloux, L. Guize, P. Ducimetiere, and A. Benetos. *Aortic stiffness is an independent predictor of all-cause and cardiovascular mortality in hypertensive patients.* Hypertension, 37(5):1236–41, 2001.

[134] S. Laurent, S. Katsahian, C. Fassot, A. I. Tropeano, I. Gautier, B. Laloux, and P. Boutouyrie. *Aortic stiffness is an independent predictor of fatal stroke in essential hypertension.* Stroke, 34(5):1203–6, 2003.

[135] F. U. Mattace-Raso, T. J. van der Cammen, A. Hofman, N. M. van Popele, M. L. Bos, M. A. Schalekamp, R. Asmar, R. S. Reneman, A. P. Hoeks, M. M. Breteler, and J. C. Witteman. *Arterial stiffness and risk of coronary heart disease and stroke: the Rotterdam Study.* Circulation, 113(5):657–63, 2006.

[136] S. Meaume, A. Benetos, O. F. Henry, A. Rudnichi, and M. E. Safar. *Aortic pulse wave velocity predicts cardiovascular mortality in subjects >70 years of age.* Arterioscler Thromb Vasc Biol, 21(12):2046–50, 2001.

[137] T. Shoji, M. Emoto, K. Shinohara, R. Kakiya, Y. Tsujimoto, H. Kishimoto, E. Ishimura, T. Tabata, and Y. Nishizawa. *Diabetes mellitus, aortic stiffness, and cardiovascular mortality in end-stage renal disease.* J Am Soc Nephrol, 12(10):2117–24, 2001.

[138] T. Shokawa, M. Imazu, H. Yamamoto, M. Toyofuku, N. Tasaki, T. Okimoto, K. Yamane, and N. Kohno. *Pulse wave velocity predicts cardiovascular mortality: findings from the Hawaii-Los Angeles-Hiroshima study.* Circ J, 69(3):259–64, 2005.

[139] K. Sutton-Tyrrell, S. S. Najjar, R. M. Boudreau, L. Venkitachalam, V. Kupelian, E. M. Simonsick, R. Havlik, E. G. Lakatta, H. Spurgeon, S. Kritchevsky, M. Pahor, D. Bauer, and A. Newman. *Elevated aortic pulse wave velocity, a marker of arterial stiffness, predicts cardiovascular events in well-functioning older adults.* Circulation, 111(25):3384–90, 2005.

[140] R. Asmar, J. Topouchian, B. Pannier, A. Benetos, and M. Safar. *Pulse wave velocity as endpoint in large-scale intervention trial. The Complior study. Scientific, Quality Control, Coordination and Investigation Committees of the Complior Study.* J Hypertens, 19(4):813–8, 2001.

[141] B. M. Pannier, A. P. Avolio, A. Hoeks, G. Mancia, and K. Takazawa. *Methods and devices for measuring arterial compliance in humans.* Am J Hypertens, 15(8):743–53, 2002.

[142] M. F. O'Rourke and W. W. Nichols. *Aortic diameter, aortic stiffness, and wave reflection increase with age and isolated systolic hypertension.* Hypertension, 45(4):652–8, 2005.

[143] G. F. Mitchell, H. Parise, E. J. Benjamin, M. G. Larson, M. J. Keyes, J. A. Vita, R. S. Vasan, and D. Levy. *Changes in arterial stiffness and wave reflection with advancing age in healthy men and women: the Framingham Heart Study.* Hypertension, 43(6):1239–45, 2004.

[144] H. Smulyan, R. G. Asmar, A. Rudnicki, G. M. London, and M. E. Safar. *Comparative effects of aging in men and women on the properties of the arterial tree.* J Am Coll Cardiol, 37(5):1374–80, 2001.

[145] K. Narkiewicz, S. E. Kjeldsen, and T. Hedner. *Hypertension and cardiovascular disease in women: progress towards better understanding of gender-specific differences?* Blood Press, 15(2):68–70, 2006.

[146] A. Paini, P. Boutouyrie, D. Calvet, A. I. Tropeano, B. Laloux, and S. Laurent. *Carotid and aortic stiffness: determinants of discrepancies.* Hypertension, 47(3):371–6, 2006.

[147] A. P. Avolio, S. G. Chen, R. P. Wang, C. L. Zhang, M. F. Li, and M. F. O'Rourke. *Effects of aging on changing arterial compliance and left ventricular load in a northern Chinese urban community.* Circulation, 68(1):50–8, 1983.

[148] J. Filipovsky, M. Ticha, R. Cifkova, V. Lanska, V. Stastna, and P. Roucka. *Large artery stiffness and pulse wave reflection: results of a population-based study.* Blood Press, 14(1):45–52, 2005.

[149] C. M. McEniery, Yasmin, I. R. Hall, A. Qasem, I. B. Wilkinson, and J. R. Cockcroft. *Normal vascular aging: differential effects on wave reflection and aortic pulse wave velocity: the Anglo-Cardiff Collaborative Trial (ACCT).* J Am Coll Cardiol, 46(9):1753–60, 2005.

[150] A. Benetos, S. Laurent, A. P. Hoeks, P. H. Boutouyrie, and M. E. Safar. *Arterial alterations with aging and high blood pressure. A noninvasive study of carotid and femoral arteries.* Arterioscler Thromb, 13(1):90–7, 1993.

[151] J. J. van der Heijden-Spek, J. A. Staessen, R. H. Fagard, A. P. Hoeks, H. A. Boudier, and L. M. van Bortel. *Effect of age on brachial artery wall properties differs from the aorta and is gender dependent: a population study.* Hypertension, 35(2):637–42, 2000.

[152] T. K. Waddell, A. M. Dart, C. D. Gatzka, J. D. Cameron, and B. A. Kingwell. *Women exhibit a greater age-related increase in proximal aortic stiffness than men.* J Hypertens, 19(12):2205–12, 2001.

[153] A A Laogun and R G Gosling. *In vivo arterial compliance in man.* Clin Phys Physiol Meas, (3):201, 1982.

[154] J. Blacher, B. Pannier, A. P. Guerin, S. J. Marchais, M. E. Safar, and G. M. London. *Carotid arterial stiffness as a predictor of cardiovascular and all-cause mortality in end-stage renal disease.* Hypertension, 32(3):570–4, 1998.

[155] J. M. Dijk, A. Algra, Y. van der Graaf, D. E. Grobbee, and M. L. Bots. *Carotid stiffness and the risk of new vascular events in patients with manifest cardiovascular disease. The SMART study.* Eur Heart J, 26(12):1213–20, 2005.

[156] S. Laurent, J. Cockcroft, L. Van Bortel, P. Boutouyrie, C. Giannattasio, D. Hayoz, B. Pannier, C. Vlachopoulos, I. Wilkinson, and H. Struijker-Boudier. *Abridged version of the expert consensus document on arterial stiffness.* Artery Res, 1:2–12, 2007.

[157] R. Asmar, A. Benetos, J. Topouchian, P. Laurent, B. Pannier, A. M. Brisac, R. Target, and B. I. Levy. *Assessment of arterial distensibility by automatic pulse wave velocity measurement. Validation and clinical application studies.* Hypertension, 26(3):485–90, 1995.

[158] G. de Simone, M. J. Roman, M. J. Koren, G. A. Mensah, A. Ganau, and R. B. Devereux. *Stroke volume/pulse pressure ratio and cardiovascular risk in arterial hypertension.* Hypertension, 33(3):800–5, 1999.

[159] P. Boutouyrie, A. I. Tropeano, R. Asmar, I. Gautier, A. Benetos, P. Lacolley, and S. Laurent. *Aortic stiffness is an independent predictor of primary coronary events in hypertensive patients: a longitudinal study.* Hypertension, 39(1):10–5, 2002.

[160] C. Stefanadis, J. Dernellis, E. Tsiamis, C. Stratos, L. Diamantopoulos, A. Michaelides, and P. Toutouzas. *Aortic stiffness as a risk factor for recurrent acute coronary events in patients with ischaemic heart disease.* Eur Heart J, 21(5):390–6, 2000.

[161] T. Willum-Hansen, J. A. Staessen, C. Torp-Pedersen, S. Rasmussen, L. Thijs, H. Ibsen, and J. Jeppesen. *Prognostic value of aortic pulse wave velocity as index of arterial stiffness in the general population.* Circulation, 113(5):664–70, 2006.

[162] M. W. Rajzer, W. Wojciechowska, M. Klocek, I. Palka, M. Brzozowska-Kiszka, and K. Kawecka-Jaszcz. *Comparison of aortic pulse wave velocity measured by three techniques: Complior, SphygmoCor and Arteriograph.* J Hypertens, 26(10):2001–7, 2008.

[163] P. Salvi, E. Magnani, F. Valbusa, D. Agnoletti, C. Alecu, L. Joly, and A. Benetos. *Comparative study of methodologies for pulse wave velocity estimation.* J Hum Hypertens, 22(10):669–77, 2008.

[164] William R. Milnor. *Hemodynamics.* Williams & Wilkins, Baltimore, 2nd edition, 1989.

[165] K. Sutton-Tyrrell, R. H. Mackey, R. Holubkov, P. V. Vaitkevicius, H. A. Spurgeon, and E. G. Lakatta. *Measurement variation of aortic pulse wave velocity in the elderly.* Am J Hypertens, 14(5 Pt 1):463–8, 2001.

[166] I. B. Wilkinson, S. A. Fuchs, I. M. Jansen, J. C. Spratt, G. D. Murray, J. R. Cockcroft, and D. J. Webb. *Reproducibility of pulse wave velocity and augmentation index measured by pulse wave analysis.* J Hypertens, 16(12 Pt 2):2079–84, 1998.

[167] C. U. Choi, E. B. Park, S. Y. Suh, J. W. Kim, E. J. Kim, S. W. Rha, H. S. Seo, D. J. Oh, and C. G. Park. *Impact of aortic stiffness on cardiovascular disease in patients with chest pain: assessment with direct intra-arterial measurement.* Am J Hypertens, 20(11):1163–9, 2007.

[168] C. Alecu, C. Labat, A. Kearney-Schwartz, R. Fay, P. Salvi, L. Joly, P. Lacolley, H. Vespignani, and A. Benetos. *Reference values of aortic pulse wave velocity in the elderly.* J Hypertens, 26(11):2207–12, 2008.

[169] E. A. Loeliger, A. M. van den Besselaar, and S. M. Lewis. *Reliability and clinical impact of the normalization of the prothrombin times in oral anticoagulant control.* Thromb Haemost, 53(1):148–54, 1985.

[170] R. B. Devereux and N. Reichek. *Echocardiographic determination of left ventricular mass in man. Anatomic validation of the method.* Circulation, 55(4):613–8, 1977.